TG 1164
JULY 1971
Copy No. 8

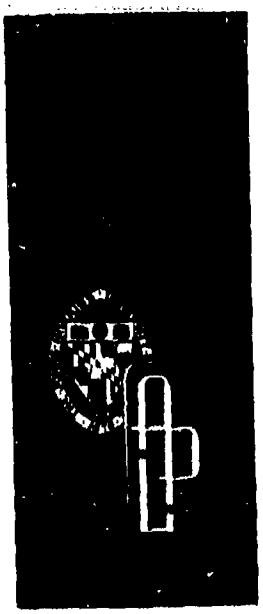

Technical Memorandum

THE MOTION OF BALLISTIC MISSILES

by L. S. GLOVER and J. C. HAGAN

THE JOHNS HOPKINS UNIVERSITY ▪ APPLIED PHYSICS LABORATORY

DISCLAIMER NOTICE

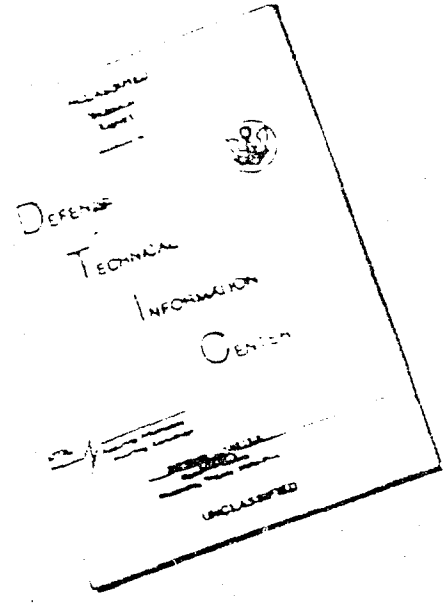

THIS DOCUMENT IS BEST QUALITY AVAILABLE. THE COPY FURNISHED TO DTIC CONTAINED A SIGNIFICANT NUMBER OF PAGES WHICH DO NOT REPRODUCE LEGIBLY.

UNCLASSIFIED
Security Classification

DOCUMENT CONTROL DATA - R & D

Security classification of title, body of abstract and indexing annotation must be entered when the overall report is classified)

1. ORIGINATING ACTIVITY (Corporate author)
The Johns Hopkins University Applied Physics Lab.
8621 Georgia Ave.
Silver Spring, Md. 20910

2a. REPORT SECURITY CLASSIFICATION
Unclassified

2b. GROUP
NA

3. REPORT TITLE
The Motion of Ballistic Missiles

4. DESCRIPTIVE NOTES (Type of report and inclusive dates)
Technical Memorandum

5. AUTHOR(S) (First name, middle initial, last name)
L. S. Glover and J. C. Hagen

6. REPORT DATE	7a. TOTAL NO. OF PAGES	7b. NO. OF REFS
July 1971	390	20

8a. CONTRACT OR GRANT NO.	9a. ORIGINATOR'S REPORT NUMBER(S)
N00017-62-C-0604	TG 1164
b. PROJECT NO.	
c.	9b. OTHER REPORT NO(S) (Any other numbers that may be assigned this report)
d.	

10. DISTRIBUTION STATEMENT
Approved for public release; distribution unlimited.

11. SUPPLEMENTARY NOTES	12. SPONSORING MILITARY ACTIVITY
	Strategic Systems Project Office

13. ABSTRACT

This handbook on the motion of ballistic missiles has been prepared primarily for use in training new personnel charged with the responsibility of evaluating the performance of reentry bodies. Aerodynamic fundamentals and characteristics of the atmosphere are reviewed briefly, followed by discussions of the effects on ballistic missile motion of gravity, earth rotation, the atmosphere, and initial body rates. The anomalous motion resulting from various types of mass and/or aerodynamic asymmetries is discussed in detail. Simple solutions are given for the impact dispersion resulting from asymmetries and nonstandard meteorological characteristics at the impact location. Various trajectory simulations and flight test analyses are also discussed. Numerical examples illustrate the material.

DD FORM 1 NOV 65 1473

UNCLASSIFIED
Security Classification

14. KEY WORDS

Ballistic missile
Ballistic flight test data
Trajectory simulation
Aerodynamic characteristics
Training manual
Impact dispersion
Missile trajectory
Numerical solution

12

TG 1164
JULY 1971

Technical Memorandum

THE MOTION OF BALLISTIC MISSILES

by L. S. GLOVER and J. C. HAGAN

THE JOHNS HOPKINS UNIVERSITY ■ APPLIED PHYSICS LABORATORY
8621 Georgia Avenue, Silver Spring, Maryland 20910
Operating under Contract N00017-62-C-0604 with the Department of the Navy

THE JOHNS HOPKINS UNIVERSITY
APPLIED PHYSICS LABORATORY
SILVER SPRING MARYLAND

ABSTRACT

This handbook on the motion of ballistic missiles has been prepared primarily for use in training new personnel charged with the responsibility of evaluating the performance of reentry bodies. Aerodynamic fundamentals and characteristics of the atmosphere are reviewed briefly, followed by discussions of the effects on ballistic missile motion of gravity, earth rotation, the atmosphere, and initial body rates. The anomalous motion resulting from various types of mass and/or aerodynamic asymmetries is discussed in detail. Simple solutions are given for the impact dispersion resulting from asymmetries and nonstandard meteorological characteristics at the impact location. Various trajectory simulations and flight test analyses are also discussed. Numerical examples illustrate the material.

THE JOHNS HOPKINS UNIVERSITY
APPLIED PHYSICS LABORATORY
SILVER SPRING MARYLAND

ABSTRACT

This handbook on the motion of ballistic missiles has been prepared primarily for use in training new personnel charged with the responsibility of evaluating the performance of reentry bodies. Aerodynamic fundamentals and characteristics of the atmosphere are reviewed briefly, followed by discussions of the effects on ballistic missile motion of gravity, earth rotation, the atmosphere, and initial body rates. The anomalous motion resulting from various types of mass and/or aerodynamic asymmetries is discussed in detail. Simple solutions are given for the impact dispersion resulting from asymmetries and nonstandard meteorological characteristics at the impact location. Various trajectory simulations and flight test analyses are also discussed. Numerical examples illustrate the material.

THE JOHNS HOPKINS UNIVERSITY
APPLIED PHYSICS LABORATORY
SILVER SPRING MARYLAND

CONTENTS

ILLUSTRATIONS

ILLUSTRATIONS (cont'd)

ILLUSTRATIONS (cont'd)

TABLES

THE JOHNS HOPKINS UNIVERSITY
APPLIED PHYSICS LABORATORY
SILVER SPRING, MARYLAND

1. INTRODUCTION

The term ballistic missile as used herein describes any body in motion that is unpowered and uncontrolled. The motion may occur in either the atmosphere or the exoatmosphere. However, most of the interesting motion phenomena occur within the atmosphere, and most of the discussions concern reentry-type vehicles entering the atmosphere at speeds from 10 000 to 25 000 ft/sec.

The primary purpose of this report is to present material suitable for training new personnel charged with the responsibility of evaluating the performance of reentry bodies; therefore, the subject matter is treated as simply as possible while retaining enough detail to explain the missile behavior. Although the material is written primarily for personnel unfamiliar with the details of missile motion, it provides experienced personnel with readily available equations suitable for estimating order-of-magnitude effects of phenomena frequently encountered in flight test analysis, performance, and preliminary design work.

A brief discussion of the aerodynamic characteristics of missiles and the nature of the atmosphere is followed by a discussion of vehicle motion as affected by gravity, earth rotation, the atmosphere, and initial body rates. Also included is a detailed discussion of the anomalous motion resulting from various types of mass and aerodynamic asymmetries. Simple solutions are given for the impact dispersion resulting from asymmetries and nonstandard meteorological characteristics at the impact location. Simulations required for various types of studies and flight test analysis complete the subjects discussed. Numerical examples illustrate the material presented.

In some sections (particularly parts of Section 4) the material is new and is given in considerable detail. Since some readers may not be interested in details, a summary of the material covered and the major conclusions derived is given at the beginning of each section (each subsection for Section 4).

An attempt was made to use symbols and units of measure currently used by specialists in the various fields covered in this report. As a result, a particular symbol may have different definitions in various sections. A complete list of symbols is given at the beginning of each section (each subsection for Section 4), and conversion factors for units of measure are given in Section 8.

2. AERODYNAMICS

SYMBOLS FOR SECTION 2

Symbol	Definition	Typical Units
A	axial force	pounds
C_A	axial force coefficient	-
C_{A_B}	base drag coefficient	-
C_{A_F}	friction drag coefficient	-
C_{A_P}	pressure drag coefficient	-
c. g.	refers to center of gravity	-
C_{ℓ_p}	rolling moment damping coefficient	-
C_m	pitching moment coefficient	-
C_{m_o}	pitching moment coefficient at $\bar{\alpha} = 0$	-
C_{m_q}	pitching moment damping coefficient	-
C_{m_α}	$dC_m/d\bar{\alpha}$ at $\bar{\alpha} = 0$	-
C_N	normal force coefficient	-
C_{N_α}	$dC_N/d\bar{\alpha}$ at $\bar{\alpha} = 0$	-
c. p.	refers to center of pressure	-
D	total drag	pounds
D_F	drag resulting from skin friction	pounds
d	reference diameter	feet
K	Knudsen number (see Eq. (2-7))	-
L	lift	pounds
	or	
	body length	feet

Preceding page blank

Symbol	Definition	Typical Units
$L(p)$	rolling moment resulting from roll rate (roll damping moment)	lb-ft
ℓ_1	moment arm for asymmetric force	feet
M	Mach number = $V/\sqrt{\gamma RT}$	-
	or	
	pitching moment	lb-ft
$M(q)$	pitching moment resulting from pitch rate (pitch damping moment)	lb-ft
N	normal force	pounds
N_{asy}	normal force resulting from an asymmetry	pounds
N_s	normal force for a symmetrical vehicle	pounds
P	ambient pressure	lb/ft^2
P_c	cone surface pressure	lb/ft^2
P_F	flap surface pressure	lb/ft^2
p	roll rate	rad/sec
q	pitch rate	rad/sec
$\bar{q}$	dynamic pressure, $(\gamma/2)PM^2$ or $(1/2)\rho V^2$	lb/ft^2
R	gas constant = 1716	$ft^2/sec^2 - °R$
R_e	Reynolds number, $\rho VL/\mu = VL/\nu$	-
S	reference area	ft^2
S.M.	static margin	-
S_w	surface area excluding the base area	ft^2
T	absolute ambient air temperature	°R
T_o	reference temperature for viscosity	°R
V	vehicle velocity	ft/sec

Symbol	Definition	Typical Units
X	distance from nose to a point on the body centerline	feet
$X_{c.g.}$	distance from vehicle nose to the c.g.	feet
$X_{c.p.}$	distance from vehicle nose to the c.p.	feet
ΔX	$X_{c.p.} - X_{c.g.}$	feet
Y	distance normal to the body surface	feet
$\bar{\alpha}$	vehicle total angle of attack	radians
α_l	local angle of attack	radians
γ	ratio of specific heats - 1.4	-
δ	cone half-angle	radians
ϵ	asymmetry deflection angle	radians
ρ	ambient air density	$slug/ft^3$
μ	dynamic viscosity	slug/ft-sec
μ_o	dynamic viscosity at T_o	slug/ft-sec
ν	kinematic viscosity	ft^2/sec
τ	shear stress	lb/ft^2
$\Delta\theta$	body bend angle	degrees

SUMMARY AND CONCLUSIONS

The aerodynamic forces of interest for reentry body studies are discussed. The significance of the aerodynamic coefficients is reviewed, and equations are presented for estimating the magnitude of the coefficients for a sharp-nosed conical body. Several types of asymmetric cones are also considered. Numerical examples are given for a 10° semiangle cone having a length of 10 feet.

The major conclusions are:

1. The following aerodynamic forces and moments are important in the analysis of motion of a typical reentry body:

- Force perpendicular to the body centerline (normal force) and resulting moment about the body center of gravity (pitching moment)
- Force parallel to the body centerline (axial force)
- Moments resulting by virtue of body pitch, yaw, or roll rotational rate (pitch, yaw, or roll damping moments)
- Forces and/or moments resulting from body asymmetries.

2. For uncontrolled vehicles, it is important that the normal force act through a point (center of pressure) aft of the center of gravity. In this case the vehicle is said to be statically stable. The ratio of the distance between the center of gravity and the center of pressure to some characteristic body dimension (for example, length) is called the stability margin and is usually expressed as a percentage of the characteristic length.

3. The aerodynamic forces and moments are represented by dimensionless coefficients, thereby facilitating evaluation of the forces and moments over a wide variation in environmental parameters (velocity, altitude, etc.).

4. In general, the coefficients are functions of vehicle angle of attack and the similarity factors, Mach number – an indication of the effect of compressibility of the air, Reynolds number – an indication of the nature of the boundary layer on the vehicle, and the Knudsen number – an indication of the size of the vehicle relative to the mean free path of the ambient air particles.

2.1 Aerodynamic Forces

A body moving through air experiences forces – aerodynamic forces – resulting from the motion. The aerodynamic forces of interest for a reentry vehicle are:

1. Axial force,
2. Normal force,
3. Pitch damping force,
4. Roll damping force.

The axial force (for a symmetrical vehicle) acts along the body centerline as shown in the sketch for a cone.

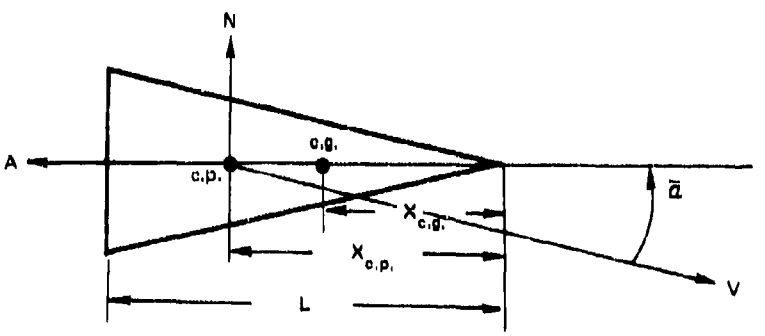

This force is produced primarily by relatively high pressure acting on the conical surface (pressure drag) and relatively low pressure acting on the cone base (base drag). In addition, a force produced by air viscosity (skin friction drag) exists on the conical surface.

A normal force (normal to the body centerline) exists when the body centerline is not directed along the

velocity vector. The angle between the velocity vector and the body centerline is called the angle of attack, $\bar{\alpha}$. The normal force results from high pressure acting on the windward side of the body compared to low pressure acting on the leeward side. The integration of this pressure difference over the cone surface is the normal force. The pressure differential across the body also produces a moment about the body center of gravity. For convenience in analysis, this aerodynamic moment is computed as the product of the normal force and a moment arm ($X_{c.p.} - X_{c.g.}$), where $X_{c.p.}$ is the longitudinal location at which the total normal force acts and is called the center of pressure and $X_{c.g.}$ is the longitudinal location of the center of gravity. Assume that a vehicle has its center of pressure forward of the center of gravity and that some disturbance causes an initial angle of attack. This angle of attack results in a normal force. Since the normal force is forward of the center of gravity, the aerodynamic moment produced is in a direction to increase the angle of attack. This process continues, and the missile eventually tumbles. Similar reasoning will show that, for a center of pressure located aft of the center of gravity, the aerodynamic moment will always tend to cancel a perturbation in $\bar{\alpha}$. Therefore, a vehicle having a center of pressure forward of the center of gravity is said to be statically unstable; a vehicle having a center of pressure aft of the center of gravity is said to be statically stable. The value of the ratio $(X_{c.p.} - X_{c.g.})/L = \Delta X/L$ is called the static margin. The margin must be positive for uncontrolled vehicles and for high performance vehicles is usually 3% to 5%.

The use of the word "normal" to define the force in the plane of $\bar{\alpha}$ and perpendicular to the body centerline is used here to be consistent with the usual terminology found in the literature. It is hoped that there will be no confusion with telemetry terminology where "normal" force and "lateral" force are the two components of the normal force as defined above. In an attempt to avoid confusion, in some sections of this report we have used

the term "transverse" force to mean the force in the plane of $\bar{\alpha}$ and perpendicular to the body centerline.

The pitch and roll damping forces exist by virtue of the body pitch and roll rates, respectively, and therefore are called dynamic forces. Consider a body pitching about its center of gravity with rotational velocity, q. The pitching motion produces a local velocity at X equal to $(X - X_{c.g.})q$. The distribution of velocity along the body is shown in the sketch.

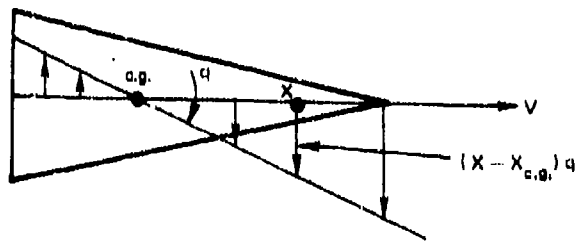

The local velocity distribution produces a local angle of attack, α_l, whose magnitude is given by the equation:

$$\tan \alpha_l = \frac{(X_{c.g.} - X)q}{V} \approx \alpha_l \quad . \qquad (2\text{-}1)$$

The local angle of attack results in a local normal force which, at all points along the body, tends to resist the pitching motion. The integral of the local forces (the damping force) is too small to be of significance in ballistic missile analyses. However, the damping moment, which is the integral of the local forces multiplied by their moment arms, is very important in some portions of the trajectory as will be shown later.

The example cited above is just one type of damping effect. Any force that exists by virtue of the pitch rate is a pitch damping force, and these forces do not always resist body pitch motion. The forces that do resist the pitch motion are said to be stable forces (or moments), and those that reinforce the pitch motion are said to be unstable forces (or moments).

The only roll damping force on a symmetrical body of revolution is the force produced by the viscosity of the air (skin friction). This force always tends to retard the roll rate.

Ideally, it would be desirable to calculate the aerodynamic forces accurately by theoretical means. However, this is not always possible, and it is necessary to measure the forces in ground tests by blowing air past a fixed body (wind tunnel), or by propelling the body through a stationary instrumented region (ballistic range), or sometimes by using a combination of both techniques. Economically it is not possible to obtain measurements on the actual vehicle for actual reentry conditions of ambient pressure, temperature, velocity, etc. To circumvent this difficulty, the aerodynamicist defines the forces and moments in terms of aerodynamic coefficients which apply over a wide range of environmental conditions. The following coefficients are of interest in the study of reentry body motion:

$$A = C_A \bar{q} S \tag{2-2}$$

$$N = C_N \bar{q} S \tag{2-3}$$

$$M(q) = C_{m_q} \left(\frac{qd}{V}\right) \bar{q} S d \tag{2-4}$$

$$L(p) = C_{\ell_p} \left(\frac{pd}{V}\right) \bar{q} S d \tag{2-5}$$

where $\bar{q} = (1/2)\rho V^2 = (\gamma/2)PM^2$ and is called dynamic pressure. The bar over the q is deleted in some sections of this report where there is no possible confusion between the symbols for pitch rate and dynamic pressure. The reference dimensions S and d may be any convenient dimensions. For a cone, they are usually taken as the base area and base diameter, and these reference dimensions will be used in the examples.

From dimensional analysis, it may be shown that for a given $\bar{\alpha}$ the aerodynamic coefficients C_A, C_N (and $X_{c.p.}$), C_{m_q}, and C_{ℓ_p} may be obtained from tests using a geometrically similar model (external shape) provided certain model similarity factors are the same as those for the actual vehicle. The major similarity factors of interest for the reentry body are:

Mach number,
Reynolds number,
Knudsen number.

The Mach number is the ratio of the vehicle velocity (V) to the velocity of a sound wave ($\sqrt{\gamma RT}$). There are four significant Mach number regimes. At subsonic speeds ($M \approx 0$ to 0.8), the aerodynamic coefficients are weakly dependent upon M. The transonic Mach number regime extends from the Mach number at which a local Mach number over the body first becomes sonic ($M_\ell = 1$) to the Mach number at which the flowfield over the body is predominantly supersonic. This Mach number range extends from about 0.8 to 1.5. The local supersonic speed results in the appearance of shock waves. The strength and location of the waves are highly sensitive to changes in Mach number. Therefore, in the transonic speed range, the aerodynamic coefficients are usually sensitive to change in M. In the supersonic speed range ($M \approx 1.5$ to 6), the shock wave strength is dependent upon Mach number but the shock location is somewhat insensitive to changes in Mach number so that the aerodynamic coefficients are moderately dependent upon M. The effect of

aerodynamic heating is moderate in the supersonic speed range. At hypersonic speeds (M > 6), the aerodynamic coefficients tend to be relatively insensitive to M and aerodynamic heating is severe.

The Reynolds number, $\rho VL/\mu = VL/\nu$, is indicative of the importance of the dynamic viscosity of the air, μ (or kinematic viscosity ν). As a result of viscous forces, a region of low velocity is produced in the vicinity of the body. In fact, for continuum flow (discussed below) the velocity of the air relative to the vehicle is zero at the vehicle surface. The region of degraded velocity is called the boundary layer. Since the layer of air adjacent to the body "sticks" to the surface, a shear stress, τ, or an element of friction drag, dD, results, tending to reduce the velocity of the vehicle.

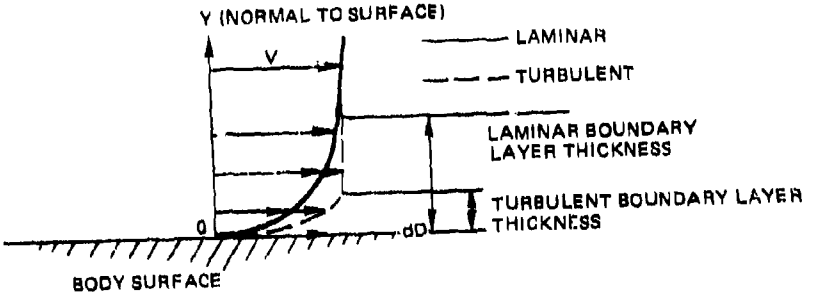

The total friction drag is given by:

$$D_F = \int \tau \, dS_w = \int \mu \left(\frac{dV}{dY} \right)_{Y=0} dS_w \, . \qquad (2\text{-}6)$$

Therefore, the viscous drag is proportional to the dynamic viscosity and the velocity gradient at the wall. The viscosity is very nearly a function of air temperature only

and is given by Sutherland's equation plotted in Figs. 2-1 and 2-2. The velocity gradient is a strong function of the Reynolds number. At very high Reynolds numbers, the flow in the boundary layer contains much eddy or vortical motion. As a result of mixing, the high energy air near the outer portion of the flow is transported in toward the surface. Since the layer of air adjacent to the wall sticks to the surface, this type of boundary layer has a very large velocity gradient at the surface and the skin friction is relatively high. This type of boundary layer is called a turbulent boundary layer. At sufficiently low Reynolds numbers, the eddy motion within the boundary layer disappears, and the velocity gradient at the wall and skin friction become much less than those for the turbulent case. This type of boundary layer is called a laminar boundary layer. At low Reynolds numbers the flow tends to be laminar; at high Reynolds numbers the flow tends to be turbulent. The Reynolds number at which transition from laminar to turbulent flow occurs varies with body shape and type of trajectory. A typical value of R_e at which transition begins to occur on a slender conical body is 10^7.

The surface heating rate is proportional to the skin friction and therefore is greater for turbulent flow than for laminar flow. In fact, the heating rate in turbulent flow may be nearly an order of magnitude greater than that for laminar flow.

The Knudsen number is the ratio of the mean free path of the ambient air particles to a characteristic dimension of the reentry vehicle. This ratio may be expressed in terms of R_e and M by the relation:

$$K = \frac{1.49\ M}{R_e} \quad . \tag{2-7}$$

For the very low values of density that exist early in the reentry phase, the particles of air are spaced at distances that are large compared to, say, the body length

or diameter. An air particle bouncing off the body is not likely to encounter another air particle. This region of flow is called the free molecular flow regime. At a somewhat lower altitude, the air particles have frequent collisions with other air particles in the vicinity of the reentry body. However, there are insufficient particles in the film of air adjacent to the body surface to cause it to stick to the surface. Therefore, although a boundary layer exists, the film of air adjacent to the wall "slides" along the body surface. This flow regime is called the slip flow regime. At still higher densities, the air particles at the surface stick to the surface. This flow regime is called the continuum flow regime.

The characteristics of the aerodynamic forces and surface heating depend upon the type of flow that exists on the body. There are no sharp boundaries between the various types of flow, but approximate boundaries are as follows:

Continuum to slip $\quad \dfrac{M}{\sqrt{R_e}} \approx 10^{-2}$

Slip to transition $\quad \dfrac{M}{\sqrt{R_e}} \approx 10^{-1}$

Transition to free molecular $\quad \dfrac{M}{R_e} \approx 10$.

The transition regime considered here is a transition in basic flow regimes which occurs at Knudsen numbers of approximately unity. This transition should not be confused with transition from laminar to turbulent flow in the boundary layer.

The Mach number, boundary layer, and basic fluid flow regimes are shown for a typical reentry body in Fig. 4-21, page 260. Note that practically all the reentry

phenomena for which aerodynamic data are required occur in the continuum flow regime; only this regime will be considered in the remainder of this report.

Sometimes the lift and drag components of the aerodynamic force are required for analysis. The relationship between the lift-drag system of forces and the normal force-axial force system is shown in the sketch.

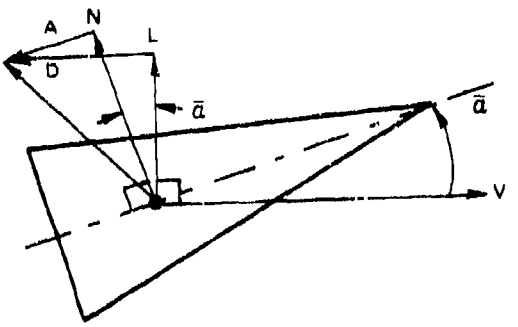

From this force diagram, the lift and drag coefficients may be obtained from the following equations:

$$C_L = C_N \cos \bar{\alpha} - C_A \sin \bar{\alpha} \qquad (2\text{-}8)$$

$$C_D = C_A \cos \bar{\alpha} + C_N \sin \bar{\alpha} \qquad (2\text{-}9)$$

Differentiating Eq. (2-8) with respect to $\bar{\alpha}$, and noting that the variation of C_A with $\bar{\alpha}$ is small, the slope of the lift curve at $\bar{\alpha} = 0$ is given by the equation:

$$C_{L_\alpha} = C_{N_\alpha} - C_A \qquad (2\text{-}10)$$

2.2 General Characteristics

It is beyond the scope of this report to provide procedures for estimating the aerodynamic coefficients for a body of arbitrary shape. However, a few remarks on the general behavior of the coefficients are given in this section, and approximate equations applicable to a sharp nosed cone are given in Section 2.3.

Axial Force. For most bodies of interest, the axial force coefficient is weakly dependent upon $\bar{\alpha}$ for small values of $\bar{\alpha}$ (1° to 2°), strongly dependent upon M, and moderately dependent upon R_e. For a sharp slender cone, the order of magnitude of C_A is 0.1.

Normal Force. The normal force coefficient is strongly dependent upon $\bar{\alpha}$ and M and nearly independent of R_e. For small values of $\bar{\alpha}$, C_N varies linearly with $\bar{\alpha}$ so that $C_N = C_{N_\alpha}\bar{\alpha}$. For a sharp slender cone, $C_{N_\alpha} \approx 2$ per radian.

Center of Pressure. In general, the center of pressure is strongly dependent upon $\bar{\alpha}$ and M and weakly dependent upon R_e. However, for small values of $\bar{\alpha}$, $X_{c.p.}$ is independent of $\bar{\alpha}$. For a sharp slender cone, $X_{c.p.} \approx (2/3)L$.

Pitch Damping. The pitch damping coefficient is strongly dependent upon M, weakly dependent upon $\bar{\alpha}$ for small values of $\bar{\alpha}$, and nearly independent of R_e. For a sharp slender cone, a typical value of C_{m_q} is -1 per radian. The negative value of C_{m_q} indicates a stable damping coefficient.

Roll Damping. The roll damping coefficient for a symmetrical vehicle is very small, negative, highly dependent upon R_e and M, and weakly dependent upon $\bar{\alpha}$ for small values of $\bar{\alpha}$. For a cone, a typical value of the roll damping coefficient is -0.003 per radian.

2.3 Approximate Equations for a Sharp Cone

For a major portion of the reentry trajectory, the Mach number is in the hypersonic regime. The aerodynamic coefficients are nearly independent of Mach number, and good approximations to the aerodynamic coefficients for sharp nosed cones are given by relatively simple equations.

The skin friction drag coefficient, C_{A_F}, is very sensitive to the cone surface temperature, to the type of boundary layer, and to surface roughness. To provide some idea of the order of magnitude of the coefficient, C_{A_F}, without becoming involved in details, equations are given below which apply to laminar flow with a cold wall (typical of early reentry conditions) and to a turbulent flow with a hot wall (typical of late reentry conditions). A smooth wall was assumed.

An estimate of C_{ℓ_p} is given in which it is assumed that the shear stress τ is directed along the vector $\vec{V} + \vec{pr}$ where $\vec{pr}$ is the circumferential velocity of a point on the cone surface. The circumferential component of τ is proportional to C_{ℓ_p}.

The following equations are applicable to a cone of half angle δ:

$$C_{N_\alpha} = 2 \cos^2 \delta \tag{2-11}$$

$$X_{c.p.} = \left[\frac{2}{3} \sec^2 \delta\right] L \tag{2-12}$$

$$C_A = C_{A_P} + C_{A_B} + C_{A_F} \tag{2-13}$$

$$C_{A_P} = 2 \sin^2 \delta \tag{2-14}$$

$$C_{A_B} = \frac{1}{M^2} \tag{2-15}$$

$$C_{A_F} = \frac{1.9}{\tan \delta} \left[\frac{(1 + \gamma M^2 \sin^2 \delta) \cos \delta}{R_e} \right]^{1/2} \qquad (2\text{-}16)$$

Laminar flow, cold wall

$$C_{A_F} = \frac{0.1}{\sqrt[5]{R_e}} \frac{(\cos \delta)^{0.8}}{\tan \delta} \frac{(1 + \gamma M^2 \sin^2 \delta)^{0.8}}{(1 + 0.17 M^2)^{0.7}} \qquad (2\text{-}17)$$

Turbulent flow, hot wall

$$C_{m_q} = \frac{1}{\tan^2 \delta} \left[\frac{2}{3} \frac{X_{c.g.}}{L} - \frac{1}{4}(1 + \tan^2 \delta) - \frac{1}{2} \cos^2 \delta \left(\frac{X_{c.g.}}{L} \right)^2 \right] \qquad (2\text{-}18)$$

$$C_{\ell_p} = - \left[\frac{1}{8} \cos^2 \delta \right] C_{A_F} \qquad (2\text{-}19)$$

2.4 Asymmetric Bodies

Bodies intended to be symmetrical are always asymmetrical to some extent as a result of manufacturing tolerances and various types of in-flight body distortion. The magnitude of the asymmetric force is usually very small. However, these small forces can have disastrous results on vehicle performance as will be shown later.

Consider a body for which the asymmetric force is produced by a small protuberance located near the aft end of the body, as shown in the sketch.

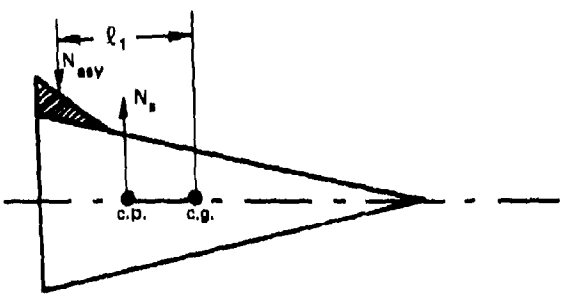

At $\bar{\alpha} = 0$, the protuberance results in a downward asymmetric normal force, N_{asy}. This force causes the nose to pitch up, producing an angle of attack. The angle of attack produces a normal force, N_s. The vehicle continues to pitch up until the moment about the center of gravity is zero. The zero moment condition is called the trim condition, and the values N and $\bar{\alpha}$ that exist at this condition are called the trim normal force and trim angle of attack, respectively.

It is convenient to define another dimensionless aerodynamic coefficient called the pitching moment coefficient, C_m, such that the moment about the center of gravity is given by:

$$M = C_m \bar{q} S d \quad . \tag{2-20}$$

From the above sketch (using a nose-up moment as positive):

$$M = N_{asy} \ell_1 - N_s (X_{c.p.} - X_{c.g.}) \quad . \tag{2-21}$$

The total normal force is given by:

$$N = N_s - N_{asy} \quad . \tag{2-22}$$

Writing Eqs. (2-21) and (2-22) in coefficient form:

$$C_m = \frac{N_{asy} \ell_1}{\bar{q} S d} - \frac{N_s}{\bar{q} S} \frac{(X_{c.p.} - X_{c.g.})}{d} \quad . \tag{2-23}$$

$$C_N = \frac{N_s}{\bar{q} S} - \frac{N_{asy}}{\bar{q} S} \quad . \tag{2-24}$$

The term, $N_s/\bar{q}S$, is the C_N for a symmetrical vehicle. The N_{asy} term is usually negligible compared to $N_s/\bar{q}S$

and may be ignored in Eq. (2-24). However, the effect of this term on C_m cannot be ignored. Let

$$\frac{N_{asy}\, \ell_1}{\bar{q}\, Sd} = C_{m_o} .$$

Then

$$C_m = C_{m_o} - C_N \frac{(X_{c.p.} - X_{c.g.})}{d} , \qquad (2\text{-}25)$$

If the body has a linear variation of C_N with $\bar{\alpha}$, then Eq. (2-25) may be written:

$$C_m = C_{m_o} - C_{N_\alpha} \frac{(X_{c.p.} - X_{c.g.})}{d} \bar{\alpha} , \qquad (2\text{-}26)$$

If C_{m_o} and $X_{c.p.}$ are independent of $\bar{\alpha}$, then C_m varies linearly with $\bar{\alpha}$.

Within the limitations imposed by the assumptions listed above, typical C_m characteristics for a stable symmetrical and a stable asymmetrical vehicle are shown in the sketch, page 27.

Note that C_{m_o} is the value of C_m at $\bar{\alpha} = 0$, and $\bar{\alpha}_{TR}$ is the value of $\bar{\alpha}$ at $C_m = 0$. The value of $\bar{\alpha}_{TR}$ is obtained from Eq. (2-26) as:

$$\bar{\alpha}_{TR} = \frac{C_{m_o}}{C_{N_\alpha} \frac{(X_{c.p.} - X_{c.g.})}{d}} = \frac{C_{m_o}}{C_{N_\alpha} \frac{\Delta X}{d}} , \qquad (2\text{-}27)$$

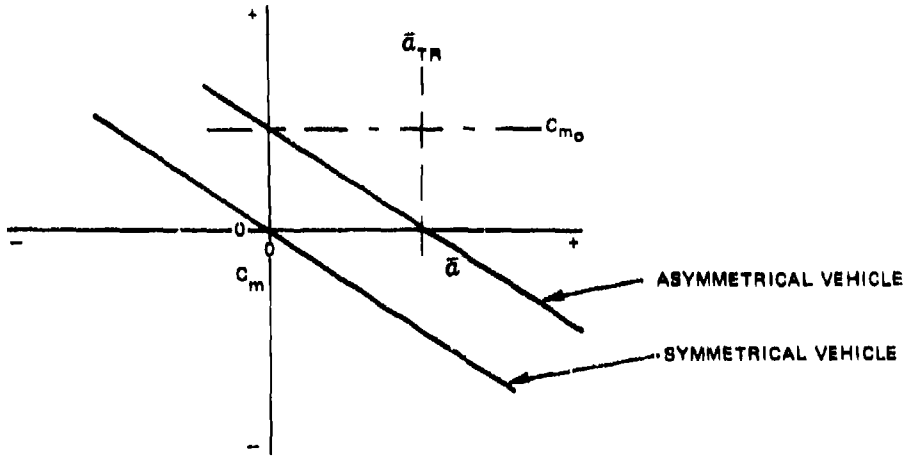

In terms of the static margin defined previously:

$$\bar{\alpha}_{TR} = \frac{C_{m_o}}{(L/d)C_{N_\alpha} S.M.} \quad , \tag{2-28}$$

In some reports the term C_{m_α} is used. An equation for C_{m_α} may be obtained by differentiating Eq. (2-26) with respect to $\bar{\alpha}$. Therefore:

$$C_{m_\alpha} = - C_{N_\alpha} \left(\frac{\Delta X}{d}\right) \quad . \tag{2-29}$$

To provide a feel for the magnitude of C_{m_o}, consider the flap-type protuberance discussed at the beginning of this section.

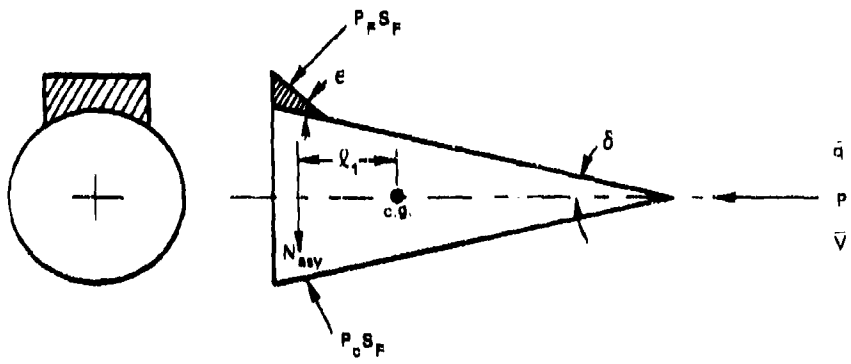

The pressure acting on the flap and cone surfaces may be estimated using Newtonian theory which, in the simplest form, states that (for zero angle of attack):

$$\frac{P_F - P}{\bar{q}} = 2 \sin^2 (\delta + \epsilon) \qquad (2\text{-}30)$$

$$\frac{P_c - P}{\bar{q}} = 2 \sin^2 \delta \ . \qquad (2\text{-}31)$$

The force resulting from the asymmetry may be divided into normal and axial force components. For small values of δ and ϵ, the axial component is small compared to the normal component. Neglecting the axial component, the total increment in normal force is:

$$N_{asy} = S_F (P_F - P_c) \ . \qquad (2\text{-}32)$$

Then:

$$C_{m_o} = \frac{M}{\bar{q}Sd} = \frac{N_{asy}\, \ell_1}{\bar{q}Sd} = \frac{S_F}{S} \frac{\ell_1}{d} \left[\frac{P_F}{\bar{q}} - \frac{P_c}{\bar{q}} \right] \ . \qquad (2\text{-}33)$$

Using Eqs. (2-30) and (2-31), and assuming δ and ϵ to be small:

$$C_{m_o} = 2 \frac{S_F}{S} \frac{\ell_1 \delta^2}{d} \left[2 \frac{\epsilon}{\delta} + \left(\frac{\epsilon}{\delta} \right)^2 \right] . \qquad (2\text{-}34)$$

As an example, let $\delta = 10°$, $\ell_1/d = 1$, $S_F/S = 0.1$, and $\epsilon = 2°$. For this asymmetry, Eq. (2-34) shows that $C_{m_o} = 0.0027$.

Another type of asymmetry for which C_{m_o} can be readily evaluated is one in which the body centerline is the arc of a circle. This type of asymmetry, for example, is an approximation to a distortion resulting from lateral loads or heating effects. For this asymmetry the moment is nearly a pure couple and C_{m_o} may be expressed in terms of the change in slope of the body centerline from nose to base.

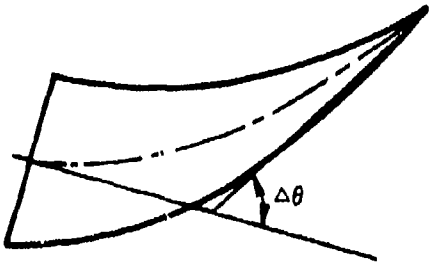

At high hypersonic Mach numbers:

$$C_{m_o} \approx 0.008 \, \Delta\theta \qquad (2\text{-}35)$$

where $\Delta\theta$ is in degrees.

2.5 Examples

A typical reentry body will be used in many examples in later sections of this report. To illustrate the material in the preceding subsections, the aerodynamic data required for subsequent examples will be computed.

The typical body is a 10-foot-long cone with a base diameter of 3.5 feet. These dimensions correspond to a cone semiangle of about 10°. The mass characteristics are assumed to be as follows:

Weight = 1000 pounds

$X_{c.g.}$ = 6.27 feet aft of the nose

Pitch moment of inertia about the center of gravity = 300 slug-ft^2

Roll moment of inertia = 30 slug-ft^2

We will use a reference length d of 3.5 feet and a reference area S of 9.65 ft^2.

At hypersonic speeds and for angles of attack close to zero, the aerodynamic coefficients are as follows:

$$X_{c.p.} = \left[\frac{2}{3}\sec^2 10°\right] 10 = 6.87 \text{ feet} \qquad (2\text{-}12)$$

$$C_{N_\alpha} = 2\cos^2 \delta = 1.94 \text{ per radian} \qquad (2\text{-}11)$$

It is observed from Eqs. (2-13) to (2-17) that C_A is a function of M, R_e, wall temperature, and type of boundary layer. The values of C_A for two combinations of wall temperature and boundary layer type are shown in Figs. 2-3 and 2-4. The laminar flow, cold wall case is typical of conditions that would exist early in the reentry flight, say above 100 000 feet; the turbulent flow, hot wall case is typical of conditions which would exist later in

flight, say below 100 000 feet. As will be shown later, most of the phenomena of interest occur for values of R_e from about 10^6 to 10^8. For these values of R_e:

$$C_A \approx 0.1 \ .$$

At M = 10 approximately 60% of C_A results from pressure drag (C_{A_P}), 30% from skin friction (C_{A_F}), and about 10% from base drag (C_{A_B}). The percentages vary somewhat with R_e, M, and type of boundary layer, but the given values are typical of the relative importance of the three sources of axial force for low-drag reentry bodies. For blunted bodies, the pressure drag may account for nearly 100% of the total drag.

Values of C_{m_q} (Eq. (2-18)) are shown as a function of $X_{c.g.}/L$ in Fig. 2-5, and values of C_{ℓ_p} (Eq. (2-19)) are shown in Figs. 2-6 and 2-7.

In the examples included in subsequent sections we will use typical values of the aerodynamic coefficients. The values of the mass and aerodynamic characteristics that will be used are shown in Table 2-1.

BIBLIOGRAPHY

2-1 S. A. Schaaf and L. Talbot, Handbook of Supersonic Aerodynamics, Section 16, "Mechanics of Rarefied Gases," NAVORDSYSCOM Report 1488 (Vol. 5), 1959.

2-2 M. Tobak and W. R. Wehrend, Stability Derivatives of Cones at Supersonic Speeds, NACA TN 3788, September 1956.

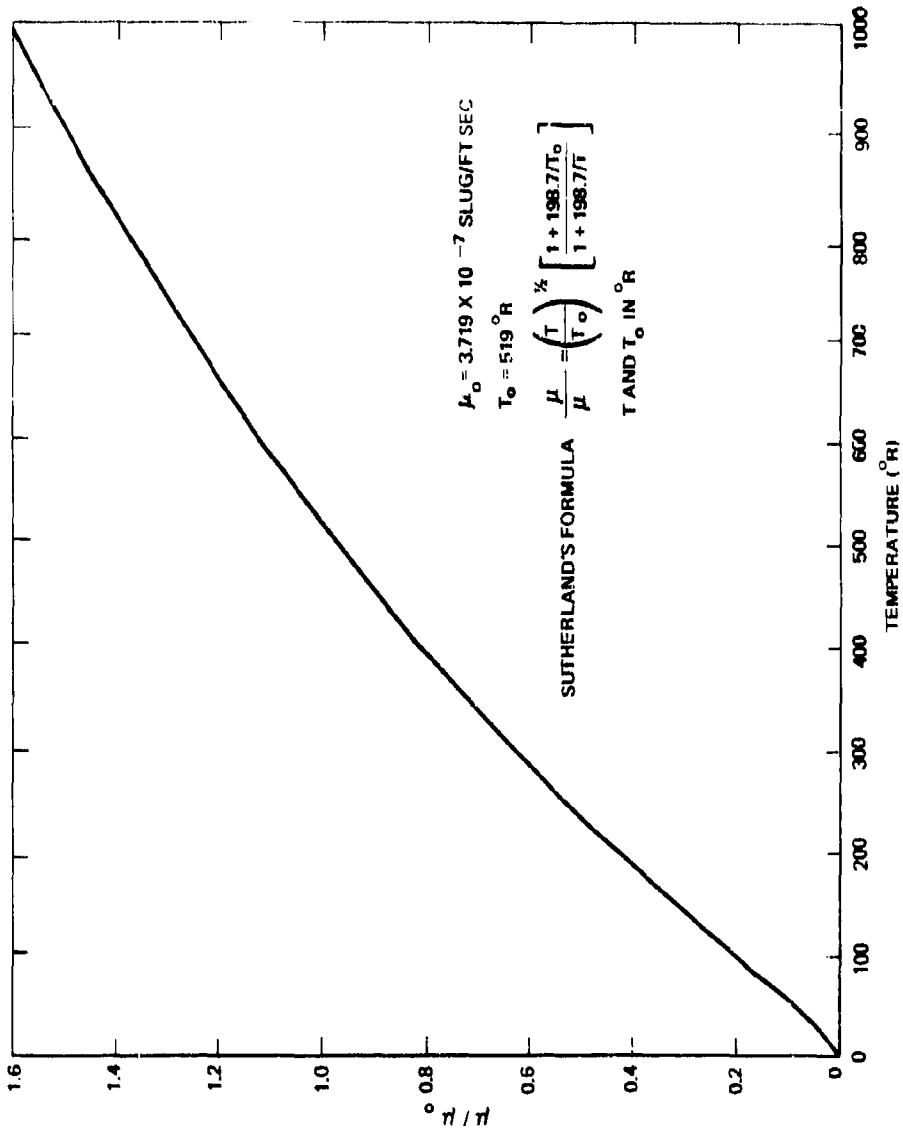

Fig. 2-1 VARIATION OF VISCOSITY WITH TEMPERATURE

Preceding page blank

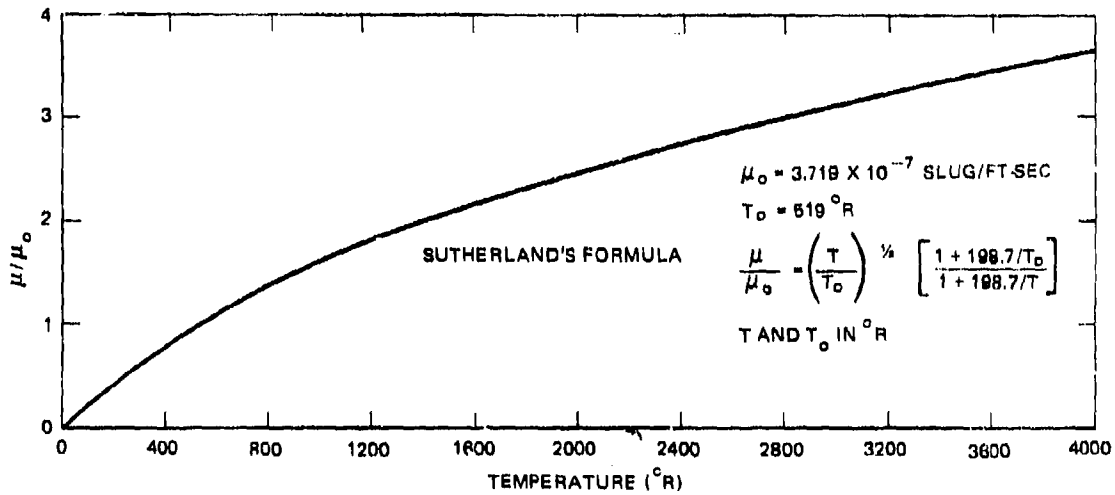

Fig. 2-2 VARIATION OF VISCOSITY WITH TEMPERATURE

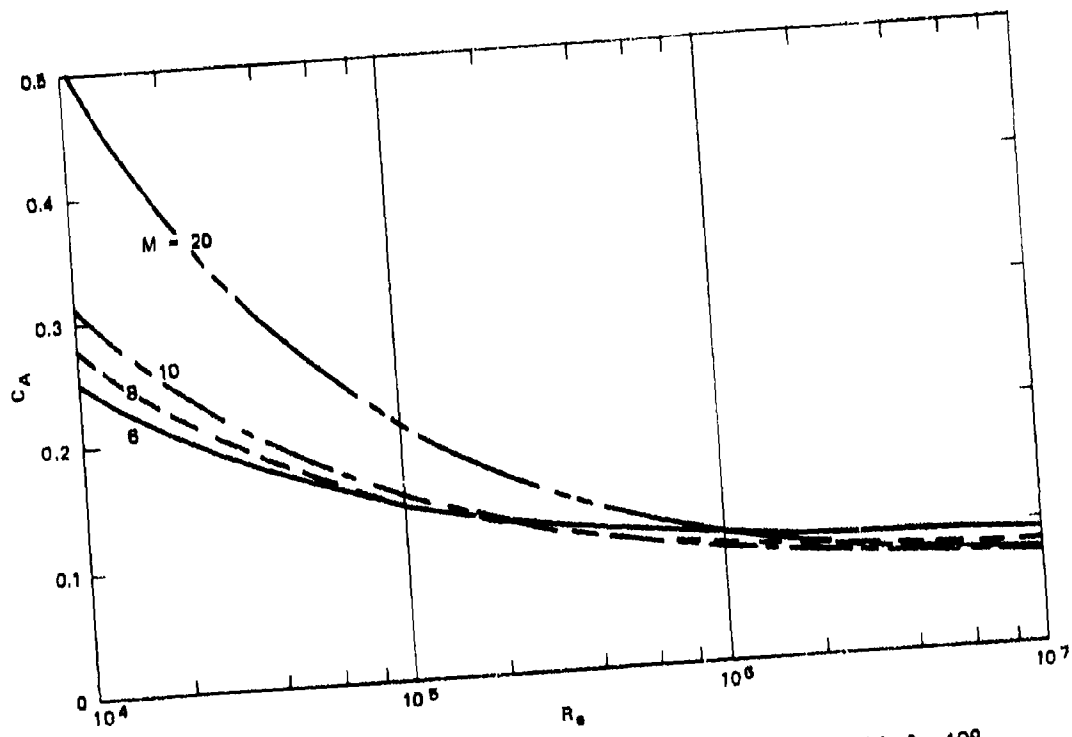

Fig. 2-3 CONE AXIAL FORCE COEFFICIENT, LAMINAR FLOW, COLD WALL, $\delta = 10^0$

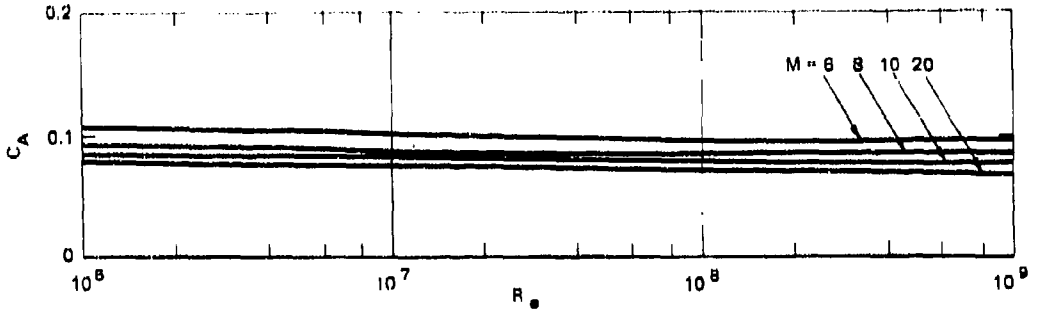

Fig. 2-4 CONE AXIAL FORCE COEFFICIENT, TURBULENT FLOW, HOT WALL, $\delta = 10^o$

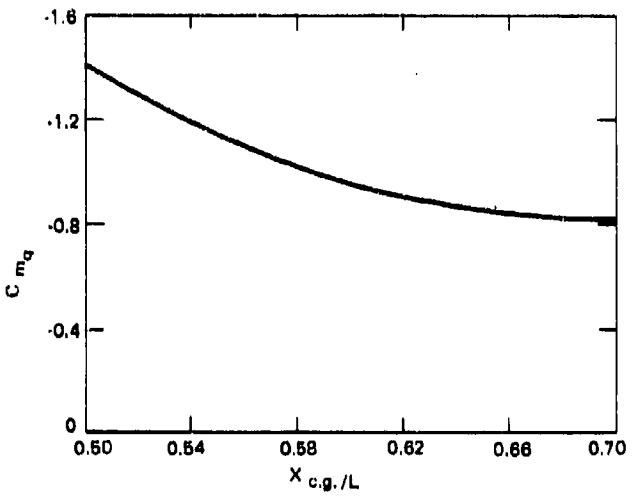

Fig. 2-5 PITCH DAMPING COEFFICIENT FOR 10° SEMIANGLE CONE

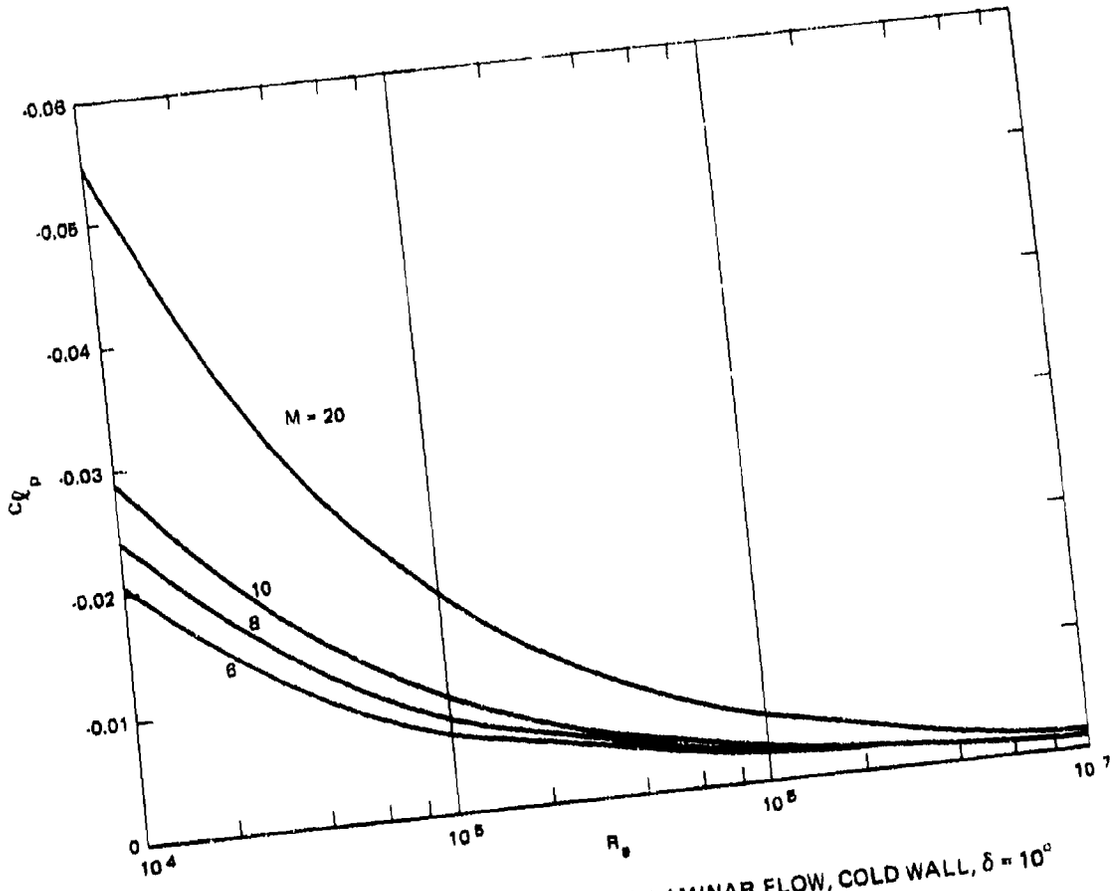

Fig. 2-6 ROLL DAMPING COEFFICIENT, LAMINAR FLOW, COLD WALL, $\delta = 10^\circ$

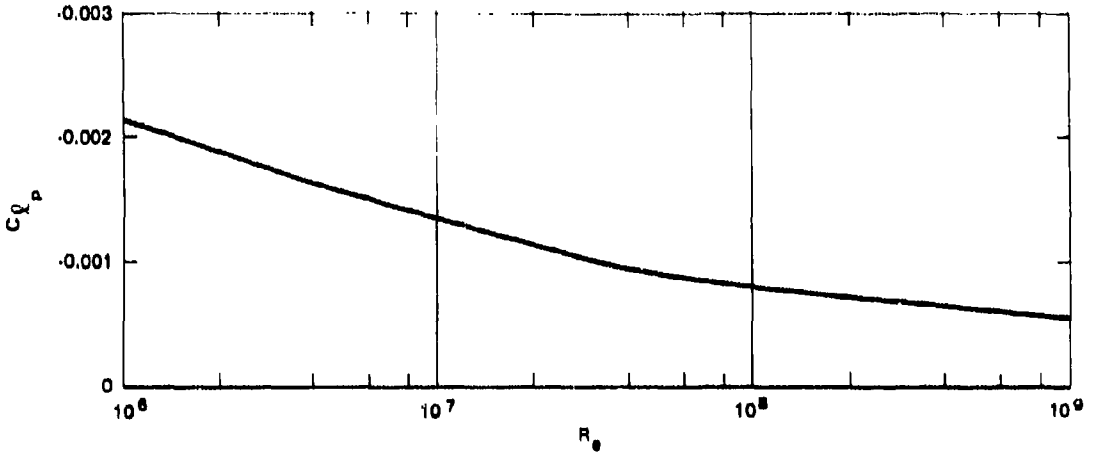

Fig. 2-7 ROLL DAMPING COEFFICIENT, TURBULENT FLOW, HOT WALL, $\delta = 10^\circ$

Table 2-1

Mass and Aerodynamic Characteristics

Mass Characteristics

$L = 10$ feet

$S = 9.65\ ft^2$

$d = 3.5$ feet

$X_{c.g.} = 6.27$ feet

Weight (W) = 1000 pounds

Mass (m) = 31.1 slugs

Roll moment of inertia (I_X) = 30 slug-ft^2

Pitch moment of inertia ($I_Y = I_Z$) = 300 slug-ft^2

$$\frac{I_Y}{md^2} = 0.79$$

$$\frac{I_X}{md^2} = 0.079$$

Aerodynamic Characteristics

$C_{N_\alpha} = 2$ per radian
$= 0.035$ per degree

$X_{c.p.} = 6.67$ feet

$C_A = 0.104$

$C_{m_q} = -1$ per radian

$C_{l_p} = -0.003$ per radian

Combined Parameters

$$\beta = \frac{W}{C_A S} = 1000\ lb/ft^2$$

$$S.M. = \frac{\Delta X}{L} = 4\%$$

$$\frac{\Delta X}{d} = 0.114$$

3. ATMOSPHERE

SYMBOLS FOR SECTION 3

Symbol	Definition	Typical Units
a	speed of sound $=\sqrt{\gamma RT}$	ft/sec
e	Napierian base	-
F_c	Coriolis force	pounds
F_P	horizontal force resulting from a pressure gradient	pounds
g	acceleration of gravity	ft/sec^2
H	scale height, RT/g_o	feet
h	geometric altitude	feet
h_G	geopotential altitude	feet
P	static pressure of dry or moist air	lb/ft^2
P_A	partial pressure of dry air	lb/ft^2
P_s	saturation pressure at T	lb/ft^2
P_w	partial pressure of water vapor	lb/ft^2
R	gas constant for dry air	$ft^2/sec^2 - °R$
R_o	radius of earth	feet
R_w	gas constant for water vapor	$ft^2/sec^2 - °R$
RAOB's	weather measurements in which a balloon is used as instrumentation carrier	-
ROCOB's	weather measurements in which a rocket is used as instrumentation carrier	-
S. L.	sea level	-
T	temperature of dry or moist air	°R
T_D	dew point temperature	°R

Symbol	Definition	Typical Units
t	time	seconds
V	missile velocity	ft/sec
V_w	wind speed	ft/sec
W	weight of an elementary volume of air	pounds
dx, dy, dh	dimensions of an elementary volume of air	feet
Z	refers to time at the zero meridian	-
ϵ	change in density defined by Eq. (3-22)	percent
γ	ratio of specific heats	-
ϕ	relative humidity	-
	or	
	latitude	degrees
λ	mean free path	feet
ν	kinematic viscosity	ft^2/sec
ρ	density of dry air = P/RT	$slug/ft^3$
ρ'	density of moist air	$slug/ft^3$
ω	earth rotation rate	rad/sec

Subscripts

n	refers to a reference altitude or to altitudes at which weather measurements are obtained
o	refers to sea level conditions

SUMMARY AND CONCLUSIONS

The atmosphere from sea level to about 400 000 feet plays an important role in the motion of reentry vehicles. In this section the general nature of the atmosphere is considered, and equations required for studies concerning vehicle motion are discussed. The variables of most concern are atmospheric density, temperature, wind, and moisture profiles (variations with altitude). The 1962 Standard Atmosphere is used in many analyses. Some of the characteristics of this atmosphere are presented, and differences from other types of standard days are noted.

The major conclusions are:

1. Most phenomena of interest in the analysis of reentry body motion occur in an altitude region called the homosphere (sea level to approximately 300 000 feet). In this region the atmosphere obeys two laws of considerable importance. The perfect gas law provides a relationship between pressure, temperature, and density; the perfect gas law in conjunction with the hydrostatic equilibrium law provides a relationship between density, temperature, and altitude. The hydrostatic law is frequently used as an interpolation equation for tabular values of density versus altitude, permitting relatively few values of the independent variable for a given accuracy. This consideration is of particular importance in trajectory simulation work.

2. Winds are obtained from direct measurements (balloon observations, or RAOB's, for the lower atmosphere and rocket observations, or ROCOB's, for the upper atmosphere), from forecasts based on observations, or from forecasts based on statistical analyses of many previous observations (climatological data). These sources are listed in the order of decreasing accuracy, and all sources

are frequently employed in some phase of analysis of body motion. A law used extensively in the forecast procedure is the geostrophic wind law, which is derived by equating the Coriolis and pressure forces. However, this law becomes invalid at low latitudes.

3. If the moisture content of the air is high, the perfect gas law must be applied using partial pressures of air and water mixtures with appropriate gas constants. Sometimes moisture is accounted for by using an effective (or virtual) temperature. The effect of water vapor is to decrease the density when it is compared with a computed density in which the moisture content is neglected. Neglect of the moisture effect results in a density error of a few percent at most, and the error decreases rapidly with decreasing altitude and decreasing temperature. For most analyses this effect may be ignored.

3.1 General Characteristics

The atmosphere is divided into three broad altitude bands called the barosphere, exosphere, and interplanetary gas (Fig. 3-1). The barosphere exists from sea level up to about 500 km (1.65×10^6 feet or 275 nmi). The exosphere exists from 500 to about 60 000 km (33 000 nmi). In the exosphere, the air density is so low that atoms hardly ever collide with one another. Molecules entering at the base of this region describe ballistic trajectories, and some travel beyond the gravitational field of the planet. In this region, temperature has no significance since there is no Maxwellian distribution of velocity. Interplanetary gas exists at altitudes above about 60 000 km.

The barosphere is subdivided into the troposphere, stratosphere, mesosphere, and thermosphere with the tropopause, stratopause, mesopause, and thermopause located between these regions, as shown in Fig. 3-1. These altitude bands are based upon the temperature variation with altitude. The region from sea level to the top of the mesophere is also called the homosphere.

The behavior of each altitude band varies somewhat with earth latitude. Many types of standard atmospheres are in common use; only three will be considered in this section. The 1962 Standard Atmosphere is typical of middle latitude locations; the Tropical Atmosphere is typical of low latitude locations (0° to 20° N. latitude), and the Polar Atmosphere is typical of high latitude locations (north of 60° N. latitude).

In the troposphere the variation of temperature with altitude is strongly influenced by the earth acting as a heat source. The temperature, in general, decreases with increasing altitude. The top of the troposphere occurs at an altitude of 36 000 feet for the Standard Atmosphere, at 55 000 feet for the Tropical Atmosphere, and at 83 000 feet for the Polar Atmosphere. Essentially all weather phenomena occur in the troposphere.

The tropopause is the top of the troposphere and is an altitude of minimum temperature. For the Standard Atmosphere the temperature is constant from 36 000 to 66 000 feet, where it begins to rise; for the tropical atmosphere the temperature begins to rise at 55 000 feet; for the polar atmosphere the temperature is constant to 96 000 feet, where it begins to rise. The temperature rise is a result of absorption of ultraviolet solar radiations by ozone. The temperature continues to rise with increasing altitude to about 156 000 feet for the Standard Atmosphere. Characteristics to sufficiently high altitudes are not available for the tropical and polar atmospheres. Above the stratosphere the temperature again decreases with increasing altitude, reaching a minimum temperature at the mesopause. For the Standard Atmosphere, this altitude is 263 000 feet. Above the mesopause the temperature again increases with increasing altitude up to the thermopause, which occurs at approximately 1 650 000 feet (275 nmi). The temperature rise is caused by the absorption of ultraviolet rays with a wavelength of 100Å.

The homosphere (sea level to 300 000 feet) is the altitude band of primary interest for analysis of reentry body motion. In this altitude region, the atmosphere is characterized by constant proportions of N_2, O_2, and argon, and the atmosphere obeys the hydrostatic equilibrium and perfect gas equations.

For analysis of reentry vehicles, the atmospheric property of most interest is air density; of secondary interest is air temperature. The ratios of density for the tropical and polar atmospheres to the density for the 1962 Standard Atmosphere are shown in Fig. 3-2. It may be expected that the tropical atmosphere would have a lower density and the polar atmosphere a higher density than those of the 1962 Standard Atmosphere. However, this is true only for altitudes below about 20 000 to 30 000 feet. Therefore, depending upon the vehicle design and trajectory, the tropical day may be equivalent to an atmosphere of greater density than that of the 1962

Standard Day, and the polar day may be equivalent to an atmosphere of lesser density than that of the 1962 Standard Day.

The temperature, in addition to the effect on density, affects the speed of sound, and thus Mach number (= V/a). The speed of sound ($=\sqrt{\gamma RT}$) is proportional to the square root of the ambient temperature and these characteristics are also shown in Fig. 3-2. Note that the speed of sound at a given altitude does not vary from one standard atmosphere to another by more than about 7.5%. This amount of variation is relatively unimportant. However, extreme variations in temperature from the 1962 Standard Atmosphere, such as those of the winter months at northern latitudes, may have a significant effect on a reentry body trajectory by affecting the Mach number history.

Some characteristics of the 1962 Standard Atmosphere are given as a function of altitude in Table 3-1. More elaborate tables are given in Ref. 3-1. Similar data for the tropical and polar days are given in Refs. 3-2 and 3-3.

3.2 Variation of Density and Temperature with Altitude

Consider an elementary volume of air (page 52) of base area dxdy and height dh. If the element of volume is in static equilibrium (the acceleration of the element of volume is zero), then the following equation applies:

$$dxdy\left(P + \frac{dP}{dh}\,dh\right) - Pdxdy + W = 0 \,.$$

The weight of the volume of air is given by:

$$W = \rho g dxdydh \,.$$

Therefore,

$$dP = -\rho g dh \,. \qquad (3\text{-}1)$$

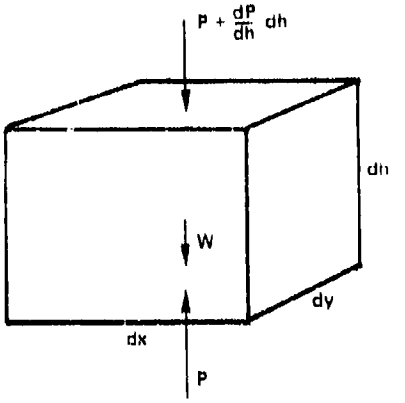

This equation is called the hydrostatic equilibrium equation, and all three standard atmospheres discussed in this section obey this equation. A second equation that is valid in the homosphere is the perfect gas law which states:

$$P = \rho RT \, , \tag{3-2}$$

Differentiating Eq. (3-2):

$$dP = R(Td\rho + \rho dT) \, . \tag{3-3}$$

Substituting Eq. (3-3) into Eq. (3-1) and expressing g in terms of g_o:

$$\frac{d\rho}{\rho} + \frac{dT}{T} = -\frac{g_o}{RT}\frac{g}{g_o}\,dh \, . \tag{3-4}$$

By definition:

$$dh_G = \frac{g}{g_o}\,dh \tag{3-5}$$

where h_G is called the geopotential altitude and h is the geometric altitude. If g is assumed to vary inversely with the square of the distance from the center of the earth:

$$\frac{g}{g_o} = \left(\frac{R_o}{R_o + h} \right)^2 , \tag{3-6}$$

Substituting Eq. (3-6) into Eq. (3-5) and integrating:

$$h_G = \frac{h}{1 + \frac{h}{R_o}} \tag{3-7}$$

or

$$h = \frac{h_G}{1 - \frac{h_G}{R_o}} . \tag{3-8}$$

In the remainder of this section, the solution to Eq. (3-4) will be given in terms of the geopotential altitude. However, the results may be obtained in terms of h by using Eq. (3-8). It should be noted that, since $R_o \approx 2.09 \times 10^7$ feet, $h \approx h_G$ for low altitudes. Even at $h = 100\,000$ feet, h_G and h differ by only 477 feet.

In terms of h_G, Eq. (3-4) becomes:

$$\frac{d\rho}{\rho} + \frac{dT}{T} = - \frac{g_o}{RT} dh_G . \tag{3-9}$$

The closed form solution to Eq. (3-9) depends upon the nature of the variation of T with h_G. For practical applications it is necessary to consider only two cases, a constant temperature (isothermal) relation and a linear relation.

Consider an altitude interval from h_{G_n} to h_G. Integrating over this altitude band, Eq. (3-9) becomes:

$$\ln \frac{\rho}{\rho_n} + \ln \frac{T}{T_n} = - \frac{g_o}{R} \int_{h_{G_n}}^{h_G} \frac{1}{T} \, dh_G \quad . \tag{3-10}$$

If T is constant, Eq. (3-10) may be integrated to give:

$$\rho = \rho_n \exp\left(\frac{h_{G_n} - h_G}{H} \right) \tag{3-11}$$

where

$$H = \frac{RT}{g_o} \quad . \tag{3-12}$$

If T varies linearly over the altitude band, then:

$$T = T_n + \frac{dT}{dh_G} (h_G - h_{G_n}) \quad , \tag{3-13}$$

In this case, Eq. (3-10) may be integrated to give:

$$\rho = \rho_n \left(\frac{T}{T_n} \right)^{- \left(1 + \frac{g_o}{R \frac{dT}{dh_G}} \right)} \quad , \tag{3-14}$$

For calculations, it is frequently desirable to define the density and temperature variations with h_G by an equation rather than to use tables. If the atmosphere obeys the hydrostatic equation, it may be divided into altitude bands for which the temperature is accurately defined by linear variations of T with h_G. Then the density and temperature within a given band are defined using Eqs. (3-11), (3-13), and (3-14) and the conditions at either the lower or upper boundary of the band.

The characteristics of the 1962 Standard Atmosphere may be defined to within 0.5% accuracy using Eqs. (3-11), (3-13), and (3-14) and the data in Table 3-2.

For simple calculations, it is frequently assumed that the entire atmosphere is at a constant temperature. Such an atmosphere is called an isothermal or exponential atmosphere. In this case, Eq. (3-11) becomes

$$\rho = \rho_o \exp\left(-\frac{h_G}{H}\right). \qquad (3\text{-}15)$$

Values of ρ_o and H are selected to provide the best accuracy for ρ in the altitude region of most interest for the particular study. The quantity H is called the scale height. From Eq. (3-11), the scale height is the change in altitude corresponding to a change in density (or pressure, since T is constant) by a factor of $1/e$.

3.3 Nonstandard Atmosphere

Frequently it is necessary to consider atmospheres other than the Standard Atmospheres. The quantities of primary interest for studies of reentry body motion (neglecting such specialized studies as the effects of wind shear and wind gust) are density, temperature, horizontal wind direction, and horizontal wind speed. These data are available from observations, forecasts, or climatological characteristics. The latter data are characteristics based on statistical analyses of many observations.

Observations are made in two altitude regions. Balloons are used to obtain temperature, pressure, dew point, and wind data at altitudes from the surface up to the highest altitude possible. Frequently, the upper limit in altitude is about 30 000 feet. Sometimes the data extend to observations at about 100 000 feet. These observations are called RAOB's. In the northern hemisphere, RAOB's are obtained daily at 00Z and 12Z hours at many observation points. Rockets are used to make observations of

temperature, density (sometimes), and winds as a function of geometric altitude for altitudes from about 60 000 to 200 000 feet. Data from these soundings are called ROCOB's and are made only at a very few locations, usually near 12Z hours Mondays, Wednesdays, and Fridays.

3.3.1 RAOB Data – Dry Air

The RAOB pressure and temperature data are converted to density data by Eq. (3-2). The geopotential altitude corresponding to the observed P and T are calculated using the hydrostatic equation. Since data are obtained at a large number of altitudes, the temperatures from one measurement to the next may be averaged and used as a constant so that Eq. (3-11) applies and may be written in the form:

$$h_{G_{n+1}} = h_{G_n} + \frac{R(T_n + T_{n+1})}{2\, g_o} \ln \frac{\rho_n}{\rho_{n+1}} \qquad (3\text{-}16)$$

where n corresponds to the measurement at one altitude and n+1 corresponds to the measurement at the succeeding altitude.

Equation (3-16) is evaluated in stepwise fashion starting at the surface conditions where h_{G_n} is the surface elevation of the observation location.

3.3.2 RAOB Data – Moist Air

The values of density computed using Eq. (3-2) are valid provided the effect of water vapor may be neglected. The effect of water vapor on density may be evaluated by writing the equation for the density of the air-water mixture as the sum of the partial densities:

$$\rho' = \frac{P_A}{RT} + \frac{P_w}{R_w T} \qquad (3\text{-}17)$$

where

$$P = P_A + P_w \quad . \tag{3-18}$$

In terms of ρ and using $R/R_w = 0.622$:

$$\rho' = \rho\left(1 - 0.378 \frac{P_w}{P}\right) . \tag{3-19}$$

If the moisture content is given in terms of relative humidity, $\phi = P_w/P_s$, rather than P_w, then:

$$\rho' = \rho\left(1 - 0.378\, \phi \frac{P_s}{P}\right) \quad . \tag{3-20}$$

The water vapor pressure, P_w, is the saturation pressure at T_D, and P_s is the saturation pressure at T. Empirical equations for the saturation vapor pressures are:

$$\left.\begin{aligned} P_w &= \exp\left(22.65 - \frac{9900}{T_D}\right) . \\ P_s &= \exp\left(22.65 - \frac{9900}{T}\right) . \end{aligned}\right\} \tag{3-21}$$

The effect of water vapor is to decrease the density compared to a computed density which ignores the effect of moisture. The percent difference in density is given by:

$$\begin{aligned} \epsilon &= 100\left(\frac{\rho - \rho'}{\rho}\right) = \frac{37.8}{P} \exp\left(22.65 - \frac{9900}{T_D}\right) \\ &= \frac{37.8}{P}\, \phi \exp\left(22.65 - \frac{9900}{T}\right) . \end{aligned} \tag{3-22}$$

A plot of the error as a function of altitude and dew point is given in Fig. 3-3. Also shown are the standard

temperatures for the 1962 Standard Day and the Standard Tropical Day. For these standard days, the effect of 100% relative humidity ($T_D = T$) on percent change in density is maximum at sea level and is about 0.7% for the 1962 Standard Day and about 1.8% for the Standard Tropical Day. Only for very hot humid days is water vapor likely to have any significant effect on density, and even this effect is significant only for very low altitudes.

3.3.3 ROCOB Data

The effect of moisture is negligible at altitudes where ROCOB data are obtained; therefore Eq. (3-2) is valid. When density and temperature both are available from an observation, the only data reduction required is the conversion from geometric altitude to geopotential altitude by Eq. (3-7). However the density data are usually not measured directly. In this case, Eq. (3-16) may be used in the following form:

$$\rho_{n+1} = \rho_n \exp\left[\frac{2 g_o}{R(T_n + T_{n+1})}\left(h_{G_n} - h_{G_{n+1}}\right)\right] \quad (3\text{-}23)$$

where ρ_{n+1} is obtained in stepwise fashion using a known initial value of density (from RAOB data, for example), measured T, and h_G computed from Eq. (3-7) using measured h.

3.3.4 Winds

A wind is defined in magnitude (speed) and direction from which it is blowing, measured clockwise from the north. In some current forecast procedures, the predicted winds are not based on measured winds but upon measured pressures and temperature, using the geostrophic wind equations.

The geostrophic wind is obtained by balancing the horizontal pressure force acting on an elementary mass

of air by the Coriolis force. The Coriolis force is perpendicular to the horizontal velocity of the elementary mass and, in the Northern Hemisphere, is directed to the right (to the left in the Southern Hemisphere). The magnitude of the force acting on an elementary mass of air, ρdxdydh, is given by the equation:

$$F_c = 2V_w \rho\omega \sin \phi \, dxdydh \, . \qquad (3-24)$$

A horizontal pressure force acts on the elementary mass whenever a horizontal pressure gradient exists. Consider the following horizontal high pressure system. Let x be the horizontal distance perpendicular to the isobars, y the horizontal distance parallel to the isobars, and h the vertical dimension.

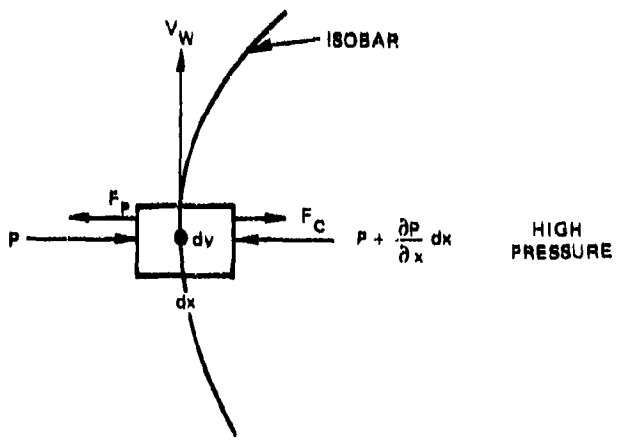

The pressure on the two surfaces of area dxdh are equal, so that the net pressure force acting on the mass in a direction parallel to the isobar is zero. The pressure on the two dxdy surfaces are unequal, but the weight of air is just balanced by the pressure force (hydrostatic

equilibrium is assumed), so that no net vertical force exists. Let the pressure acting on the dydh surface that is farthest from the high pressure center be P. Then the pressure on the dydh surface nearest the center is $P + \frac{\partial P}{\partial x} dx$. The corresponding forces are Pdydh and $(P + \frac{\partial P}{\partial x} dx)$dydh. Therefore, the net force is:

$$F_P = \frac{\partial P}{\partial x} dxdydh \ . \qquad (3\text{-}25)$$

The total horizontal pressure force is perpendicular to the isobar and directed away from the high pressure. Since the geostrophic wind is obtained by a balance of the pressure and Coriolis forces, the Coriolis force is perpendicular to the isobar and acts toward the high pressure center, as shown in the sketch. For a Coriolis force in this direction, the wind must be directed along the isobar with high pressure to the right (for the Northerm Hemisphere). Since $F_c = F_p$, from Eqs. (3-24) and (3-25):

$$V_w = \frac{\partial P/\partial x}{2\rho\omega \sin\phi} \ . \qquad (3\text{-}26)$$

Equation (3-26), the geostrophic wind equation, is accurate except for the first few thousand feet above the surface where friction effects cause the wind to be inclined away from the isobar toward low pressure and the magnitude is lower than that given by Eq. (3-26). Typically, the maximum deviation in direction is 25°, and the maximum deviation in speed is a factor of one-third to one-half the geostrophic wind, depending upon surface roughness. In addition, the equation is not valid at latitudes near the equator. The equation is valid for the Southern Hemisphere, but the direction of the velocity along the isobar is opposite to that discussed for the Northern Hemisphere.

Equation (3-26) is applied at various altitude levels to obtain the variation of wind speed with altitude. The

wind direction is obtained from the slope of the isobar at the location of interest. Therefore, accuracy in wind characteristics requires accurate estimates of density, horizontal pressure gradient, and shape of the isobars.

REFERENCES

3-1 U.S. Standard Atmosphere, 1962, prepared under sponsorship of National Aeronautics and Space Administration, United States Air Force, and United States Weather Bureau, Washington, D. C., December 1962.

3-2 Climatic Extremes for Military Equipment, Mil. Std. 210A, 2 August 1967.

3-3 L. F. Fehlner and E. V. Nice, Tabulation of Standard Atmospheres at 100-Foot Intervals of Altitude, APL/JHU TG 313-1, August 1958.

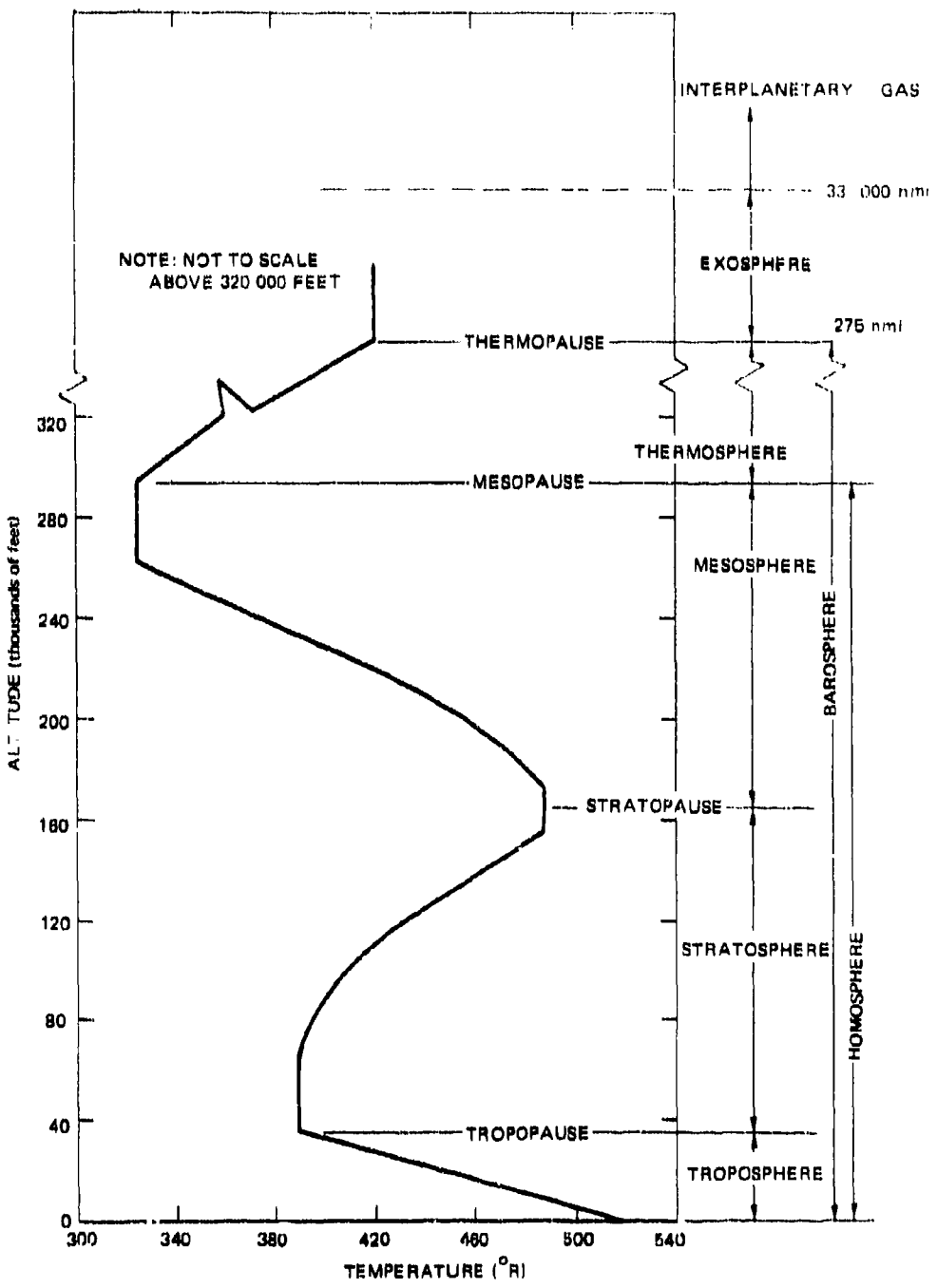

Fig. 3-1 TYPICAL ATMOSPHERIC TEMPERATURE PROFILE AND ALTITUDE REGIONS

Preceding page blank

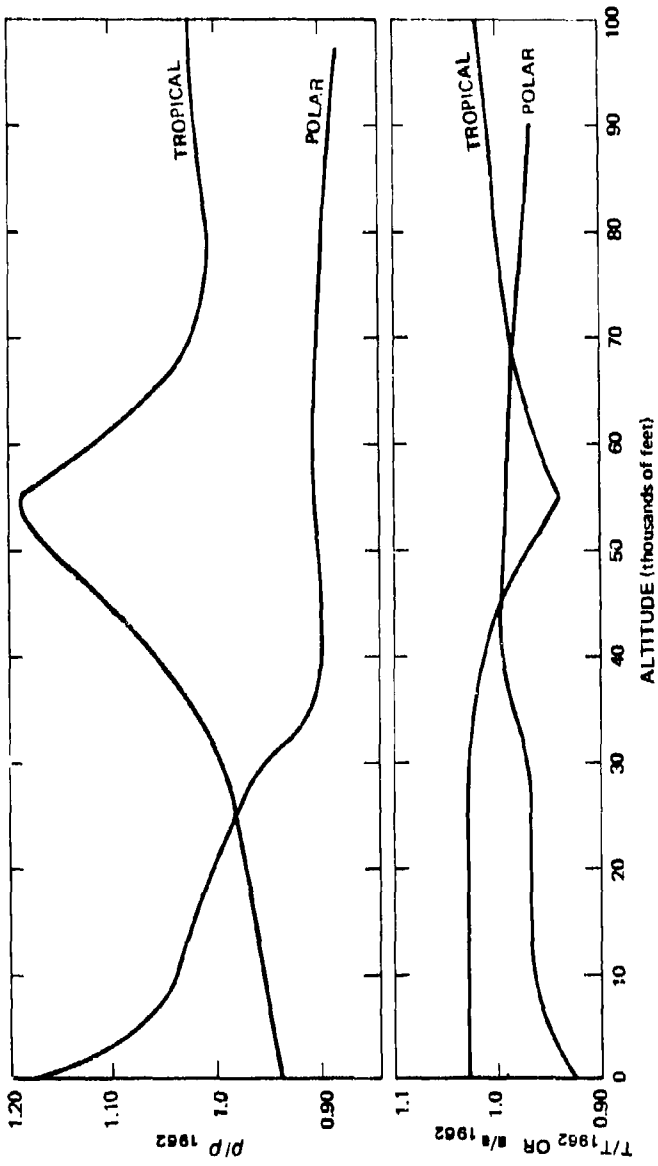

Fig. 3-2 STANDARD ATMOSPHERE CHARACTERISTICS

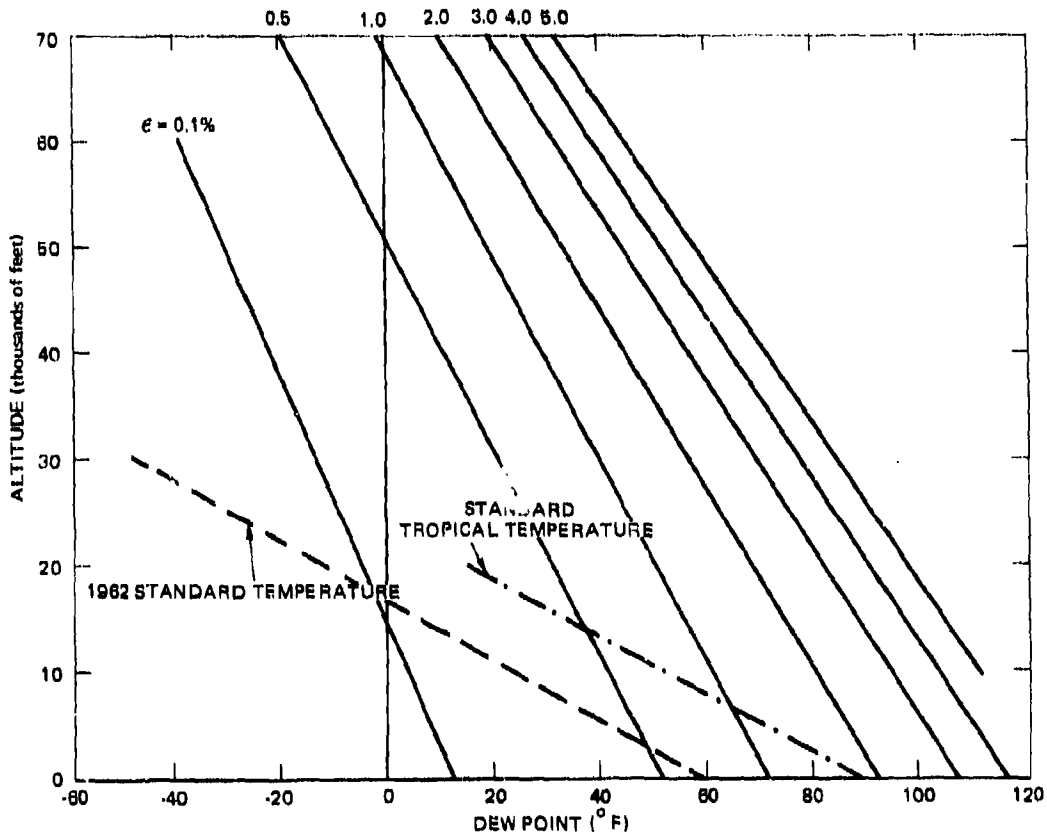

Fig. 3-3 EFFECT OF WATER VAPOR ON DENSITY

Table 3-1

1962 Standard Atmosphere

h (thousands of feet)	ρ/ρ_o	P/P_o	T (°R)	H (feet)	a (ft/sec)	g (ft/sec^2)	ν (ft^2/sec)	λ (feet)
S. L.	1.00	1.00	519	27.7E+3	1116	32.17	1.57E-4	2.18E-7
10	0.739	0.688	483	25.8E+3	1077	32.14	2.01E-4	2.95E-7
20	0.533	0.460	447	23.9E+3	1037	32.11	2.62E-4	4.08E-7
30	0.375	0.298	412	22.0E+3	995	32.08	3.49E-4	5.81E-7
40	0.247	0.186	390	20.9E+3	968	32.05	5.06E-4	8.81E-7
50	0.153	0.115	390	20.9E+3	968	32.02	8.16E-4	1.42E-6
60	0.949E-1	0.714E-1	390	20.9E+3	968	31.99	1.32E-3	2.29E-6
70	0.586E-1	0.443E-1	392	21.1E+3	971	31.96	2.14E-3	3.72E-6
80	0.361E-1	0.276E-1	398	21.4E+3	978	31.93	3.52E-3	6.03E-6
90	0.224E-1	0.174E-1	403	21.7E+3	984	31.90	5.74E-3	9.73E-6
100	0.140E-1	0.110E-1	409	22.0E+3	991	31.87	9.30E-3	1.56E-5
150	0.145E-2	0.134E-2	479	25.9E+3	1073	31.72	1.02E-1	1.50E-4
200	0.222E-3	0.195E-3	457	24.9E+3	1048	31.57	6.42E-1	9.81E-4
250	0.296E-4	0.201E-4	362	19.2E+3	920	31.42	3.87E 0	7.35E-3
300	0.195E-5	0.125E-5	333	18.3E+3	894	31.27	5.61E-1	1.12E-1
350	0.132E-6	0.112E-6	435	24.2E+3	1021	31.12	1.03E+3	1.63E 0
400	0.152E-7	0.211E-7	694	39.8E+3	1285	30.97	1.28E+4	1.38E+1

ρ_o = 0.002377 slug/ft^3

P_o = 2116 lb/ft^2

Table 3-2

Constants for the 1962 Standard Atmosphere

h_G (feet)	T (°R)	$\frac{dT}{dh_G}$ * (°R/ft)	ρ (slug/ft^3)
0.000	518.670	-3.56619991E-03	2.37680982E-03
36089.238	389.970	0.00000000E+00	7.06119929E-04
65616.750	389.970	5.48639800E-04	1.70820000E-04
104985.875	411.570	1.53619982E-03	2.56609928E-05
154199.375	487.170	0.00000000E+00	2.76979972E-06
170603.625	487.170	-1.09729986E-03	1.47349965E-06
200131.188	454.770	-2.19459995E-03	4.87189993E-07
259186.313	325.170	0.00000000E+00	3.88259984E-08
291153.188	325.170	1.69529999E-03	6.15079898E-09
323002.625	379.170	2.83429981E-03	9.65109992E-10
354753.250	469.170	5.68669662E-03	1.90709989E-10
386406.125	649.170	1.14439987E-02	4.72659967E-11
480780.813	1729.170	8.63499939E-03	3.56239951E-12
512045.938	1999.170	5.77439740E-03	2.24879924E-12
543215.188	2179.170	4.06099856E-03	1.55919982E-12
605268.375	2431.170	2.92699994E-03	8.43449984E-13
728243.750	2791.170	2.38109985E-03	3.03459948E-13
939894.688	3295.170	2.01519998E-03	6.95599719E-14
1234645.000	3889.170	1.63550000E-03	1.26079973E-14
1520799.000	4357.168	1.10109989E-03	3.05989996E-15
1798726.000	4663.168	7.32979970E-04	9.00309837E-16
2068776.000	4861.168	0.00000000E+00	3.04629894E-16

*The temperature gradient is applicable to the altitude band beginning at the altitude for which the gradient is listed and ending at the next highest altitude.

4. EQUATIONS OF MOTION

The motion of a reentry body during ballistic flight is affected primarily by five factors:

1. Gravity,
2. Earth rotation,
3. Atmosphere,
4. Body dynamics,
5. Asymmetries.

Each factor is considered in simplified form to show the general effects on the trajectory.

4.1 EFFECTS OF GRAVITY

SYMBOLS FOR SECTION 4.1

Symbol	Definition	Typical Units
g	acceleration of gravity	ft/sec^2
I	constant defined by Eq. (4.1-15)	-
K	constant defined by Eq. (4.1-5)	-
R	range	feet or nmi
r	distance from the center of the earth to a point on the trajectory	feet
$\bar{r}$	r/r_o	-
t	time	seconds
V	velocity	ft/sec
$\bar{V}$	$V/\sqrt{g_o r_o}$	-
γ	flight path angle	degrees
θ	central angle, measured from apogee	radians or degrees

Subscripts

a	refers to conditions at apogee
e	refers to conditions on the surface of the earth
o	refers to initial conditions

SUMMARY AND CONCLUSIONS

The effect of gravity only on the trajectory of a ballistic missile is considered. Equations that define the trajectory (velocity, time, flight path angle, altitude, and range) in terms of initial conditions are presented.

Plots are given which show the relationship of range and flight time as a function of initial velocity and flight path angle for minimum and nonminimum energy trajectories. Also shown are plots of range sensitivity to initial velocity and flight path angles. An example of the uses of the equations is given in Example 1, Section 4.6.

The major conclusions are:

1. A ballistic missile follows an elliptical flight path. For a given initial velocity, there is an initial flight path angle that results in maximum range, and the trajectory is called a minimum energy trajectory. For minimum energy trajectories, the flight path angle decreases from 45° for very short range to approximately 32° for a range of 3000 nmi; the velocity increases from 0 ft/sec at zero range to approximately 20 000 ft/sec at 3000-nmi range; the total flight time increases from 0 seconds at zero range to about 1300 seconds for 3000-nmi range; the trajectory apogee increases from 0 nmi at 0 nmi range to about 550 nmi at 3000-nmi range (a maximum apogee of about 700 nmi occurs for a range of 5500 nmi and a flight path angle of 22.5°).

2. Trajectories for which the initial flight path angles are greater than those for the minimum energy trajectory are called lofted trajectories; trajectories for which the initial flight path angles are less than those for the minimum energy trajectory are called delofted, or depressed, trajectories. For a given range, the total flight time increases with increasing flight path angle.

3. The range for a minimum energy trajectory is extremely sensitive to initial velocity (about 2800 ft/ft/sec at 3000-nmi range) but is very insensitive to initial flight path angle. With increasing loft at a range of 3000 nmi, the sensitivity to initial velocity decreases but the sensitivity to initial flight path angle increases. For delofted trajectories at 3000-nmi range, the sensitivity to both initial velocity and initial flight path angle is greater than that for a minimum energy trajectory.

Consider a nonrotating, spherical earth without an atmosphere. The geometry of the trajectory is shown in the sketch.

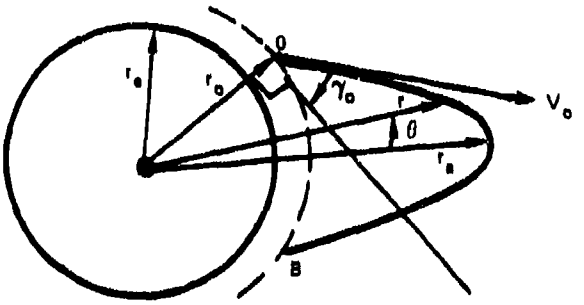

The trajectory of a body with initial velocity V_o at r_o and fired with a flight path γ_o may be obtained by applying the laws of gravity, conservation of energy, and conservation of angular momentum as defined by Eqs. (4.1-1), (4.1-2), and (4.1-3), respectively.

$$g_o r_o^2 = gr^2 \tag{4.1-1}$$

$$\frac{V_o^2}{2} - \frac{V^2}{2} = g_o r_o - gr \tag{4.1-2}$$

$$r_o V_o \cos \gamma_o = rV \cos \gamma \tag{4.1-3}$$

It may be shown that the trajectory is elliptical for $\frac{V_o^2}{2g_o r_o} < 1$, parabolic for $\frac{V_o^2}{2g_o r_o} = 1$, and hyperbolic for

$\frac{V_o^2}{2g_o r_o} > 1$. For ballistic vehicles, $\frac{V_o^2}{2g_o r_o}$ is always less than 1 so that the trajectory is elliptical. Using Eqs. (4.1-1) through (4.1-3) and the properties of an ellipse, it may be shown that the trajectory is defined by the equation:

$$\bar{r} = \frac{\bar{V}_o^{\,2} \cos^2 \gamma_o}{1 - K \cos \theta} \qquad (4.1\text{-}4)$$

where

$$\bar{r} = \frac{r}{r_o}$$

$$\bar{V}_o^{\,2} = \frac{V_o^2}{g_o r_o}$$

$$K = \left[1 - \bar{V}_o^{\,2} (2 - \bar{V}_o^{\,2}) \cos^2 \gamma_o\right]^{1/2} . \qquad (4.1\text{-}5)$$

The range is the arc length OB and is given by the equation:

$$R = 2 r_o \theta_o \qquad (4.1\text{-}6)$$

where θ_o can be obtained from Eq. (4.1-4) by setting $\bar{r} = 1$ and solving for $\cos \theta_o$. Thus:

$$\cos \theta_o = \frac{1 - \bar{V}_o^{\,2} \cos^2 \gamma_o}{K}$$

or

$$\tan \theta_o = \frac{\bar{V}_o^{\,2} \cos \gamma_o \sin \gamma_o}{1 - \bar{V}_o^{\,2} \cos^2 \gamma_o} . \qquad (4.1\text{-}7)$$

It should be noted that the equations derived above are general insofar as the reference altitude, r_o, is concerned. That is, r_o is not necessarily a surface condition. However, if r_o is not a surface condition, care must be exercised in evaluating the reference velocity, $\sqrt{r_o g_o}$, and R_e. In terms of surface conditions:

$$\sqrt{r_o g_o} = \sqrt{(r_e g_e)\,\frac{r_e}{r_o}} = 26\,000\sqrt{\frac{r_e}{r_o}} \quad . \qquad (4.1\text{-}8)$$

$$R_e = 2r_e\theta_o \quad . \qquad (4.1\text{-}9)$$

From Eqs. (4.1-6) and (4.1-7), it is observed that a given range may be obtained for various combinations of V_o and γ_o. However, there is one combination of V_o and γ_o that results in minimum V_o. This trajectory, called the minimum energy trajectory (MET), represents the minimum booster impulse for a given range or, alternatively, represents the maximum range that may be obtained from a given booster. The minimum energy trajectory is obtained by operating on Eq. (4.1-7) using standard procedures for obtaining maximum or minimum values. The results are the following:

$$\left.\begin{aligned} \gamma_o &= \frac{57.3}{4}\left(\pi - \frac{R}{r_o}\right) \\ \text{or} \qquad \gamma_o &= 45 - \frac{\theta_o}{2} \end{aligned}\right\} \qquad (4.1\text{-}10)$$

$$\overline{V}_{o_{min}}^{\,2} = 1 - \tan^2\gamma_o \qquad (4.1\text{-}11)$$

It is noted that γ_o decreases from 45° at very short range to 0° at maximum range ($R/r_o = \pi$). The velocity increases from 0 at zero range to $V_o = \sqrt{g_o r_o}$ at maximum range. The latter velocity is the velocity for a circular

orbit. For ranges that will be considered in this report (R = 1000 to 3000 nmi) the values of γ_o and V_o computed from Eqs. (4.1-6) and (4.1-7) are shown in Figs. 4-1 and 4-2. For all examples given in this section, $r_o = r_e = 2.09 \times 10^7$ feet.

The time of flight may be derived in the following manner. The rate of change in θ is given by the following expression:

$$\dot{\theta} = - \frac{V \cos \gamma}{r} \quad . \tag{4.1-12}$$

The negative sign is required since, for convenience in deriving the equation of the ellipse, θ is measured from apogee. Using Eqs. (4.1-3) and (4.1-12) the equation for time becomes:

$$t = \frac{r_o}{V_o \cos \gamma_o} \int_{\theta}^{\theta_o} \bar{r}^2 d\theta \quad . \tag{4.1-13}$$

Substituting for $\ddot{\bar{r}}$ from Eq. (4.1-4) and integrating gives the result:

$$t = \sqrt{\frac{r_o}{g_o}} (\bar{V}_o \cos \gamma_o)^3 \, I \tag{4.1-14}$$

where I is given by the equation:

$$I = \frac{1}{\bar{V}_o^2 (2 - \bar{V}_o^2) \cos^2 \gamma_o} \left[\frac{K \sin \theta}{1 - K \cos \theta} + \frac{2}{\sqrt{1 - K^2}} \tan^{-1} \left(\frac{\sqrt{1 - K^2} \tan (\theta/2)}{1 - K} \right) \right] \Bigg|_{\theta}^{\theta_o} , \tag{4.1-15}$$

and is evaluated between the limits θ and θ_o.

If one is interested in just the total trajectory time, Eqs. (4.1-14) and (4.1-15) may be simplified by noting

that the trajectory is symmetrical about $\theta = 0$, and the equation for the time becomes:

$$t = \frac{2V_o}{g_o} \frac{\cos \gamma_o}{\left(2 - \overline{V}_o^2\right)} \left[\frac{K \sin \theta_o}{1 - K \cos \theta_o} + \frac{2}{\sqrt{1 - K^2}} \tan^{-1} \left(\frac{\sqrt{1 - K^2} \tan (\theta_o/2)}{1 - K} \right) \right] . \quad (4.1\text{-}16)$$

A plot of Eq. (4.1-16) is shown for a range of 3000 nmi in Fig. 4-3. For a given range, time increases with increasing initial loft angle, γ_o. The minimum time for a range from 0 to B is that computed for a circular orbit trajectory from 0 to B; that is $\gamma_o = 0$, $V_o = \sqrt{g_o r_o}$, and $t = \frac{R}{\sqrt{g_o r_o}} = 692$ seconds for R = 3000 nmi. For a minimum energy trajectory, $K = \tan \gamma_o$ and Eq. (4.1-16) may be written as:

$$t = 2\sqrt{\frac{r_o}{g_o}} \cos^3 \gamma_o \left[\tan \gamma_o \sqrt{1 - \tan^2 \gamma_o} + 2 \tan^{-1} \left(\frac{\sqrt{1 - \tan^2 \gamma_o} \tan \frac{R}{4r_o}}{1 - \tan \gamma_o} \right) \right] . \quad (4.1\text{-}17)$$

The time for a minimum energy trajectory varies from 0 seconds at zero range to $\pi\sqrt{r_o/g_o} = 2520$ seconds for maximum range ($R = \pi r_o$). For ranges of 1000 to 3000 nmi, the flight time is shown in Fig. 4-4.

The local flight path angle may be expressed in the form:

$$\tan \gamma = - \frac{dr}{r d\theta} . \quad (4.1\text{-}18)$$

Solving for $dr/d\theta$ from Eq. (4.1-4) and substituting into Eq. (4.1-18):

$$\tan \gamma = \frac{K \sin \theta}{1 - K \cos \theta} \quad . \tag{4.1-19}$$

Differentiating Eq. (4.1-19) with respect to t and using Eq. (4.1-12), it may be shown that $\dot{\gamma}$ is given by the following equation:

$$\dot{\gamma} = \frac{K(K - \cos \theta)}{(1 - K \cos \theta)^2} \frac{V \cos^3 \gamma}{r} \quad . \tag{4.1-20}$$

Evaluating Eq. (4.1-20) for conditions near impact, it may be shown that $\dot{\gamma}$ is very small for 1000 to 3000 nmi trajectories. Therefore, in the absence of an atmosphere, the flight path during reentry is nearly a straight line. This fact will be useful later when we consider the effects of the atmosphere.

The velocity at any point along the trajectory may be obtained by solving Eqs. (4.1-1), (4.1-2), and (4.1-4) to obtain the following equation:

$$\overline{V} = \frac{\sqrt{K^2 - 2K \cos \theta + 1}}{\overline{V}_o \cos \gamma_o} \quad . \tag{4.1-21}$$

At apogee $\theta = \gamma = 0$, and from Eqs. (4.1-4) and (4.1-21):

$$\overline{r}_a = \frac{\overline{V}_o^{\,2} \cos^2 \gamma_o}{1 - K} \quad ,$$

$$\overline{V}_a = \frac{1 - K}{\overline{V}_o \cos \gamma_o} \quad .$$

orbit. For a minimum energy trajectory, $K = \tan \gamma_o$ and $\overline{V}_o^2 = 1 - \tan^2 \gamma_o$, so that the altitude $(r - r_o)$ and velocity at apogee are given by the equations:

$$h_a = r_o \left[(\sin \gamma_o + \cos \gamma_o) \cos \gamma_o - 1 \right] \qquad (4.1\text{-}22)$$

$$V_a = \frac{\sqrt{g_o r_o}}{\cos \gamma_o} \sqrt{\frac{1 - \tan \gamma_o}{1 + \tan \gamma_o}} \qquad (4.1\text{-}23)$$

or

$$V_a / V_o = \frac{1}{\cos \gamma_o + \sin \gamma_o} \quad . \qquad (4.1\text{-}24)$$

For a minimum energy trajectory, the altitude at apogee is maximum ($h_a \approx 700$ nmi for $r_o = r_e$) for $\gamma_o = 22.5°$ ($R \approx 5500$ nmi) and varies from about 250 nmi for R = 1000 nmi to about 550 nmi for R = 3000 nmi. Since the sensible atmosphere extends to about 50 nmi, most of the trajectory occurs in the exoatmosphere. The ratio of velocity at apogee to initial velocity decreases from 1 at zero range to $1/\sqrt{2}$ for maximum range. For ranges of 1000 to 3000 nmi, V_a/V_o varies from 0.71 to 0.72.

Another consideration of interest is the sensitivity of range to the initial values of V_o and γ_o. These sensitivity values may be obtained in the following manner:

$$\frac{\partial R}{\partial V_o} = \frac{\partial R}{\partial \theta_o} \frac{\partial \theta_o}{\partial V_o} \quad . \qquad (4.1\text{-}25)$$

$\partial R / \partial \theta_o$ and $\partial \theta_o / \partial V_o$ may be obtained from Eqs. (4.1-6) and (4.1-7) so that:

$$\frac{\partial R}{\partial V_o} = 2 \sqrt{\frac{r_o}{g_o}} \frac{\overline{V}_o \sin 2\gamma_o}{K^2} \quad . \qquad (4.1\text{-}26)$$

Similarly, $\partial R/\partial \gamma_o$ may be obtained from Eq. (4.1-7):

$$\frac{\partial R}{\partial \gamma_o} = \frac{2r_o}{57.3} \frac{\overline{V}_o^{\,2} (\cos 2\gamma_o - \overline{V}_o^{\,2} \cos^2 \gamma_o)}{K^2} \qquad (4.1\text{-}27)$$

Plots of Eqs. (4.1-26) and (4.1-27) are shown in Figs. 4-5 and 4-6, respectively. Note that the range of a minimum energy trajectory is sensitive to initial speed but not to initial flight path angle. With increasing loft angle, the range sensitivity to V_o decreases but range sensitivity to γ_o increases.

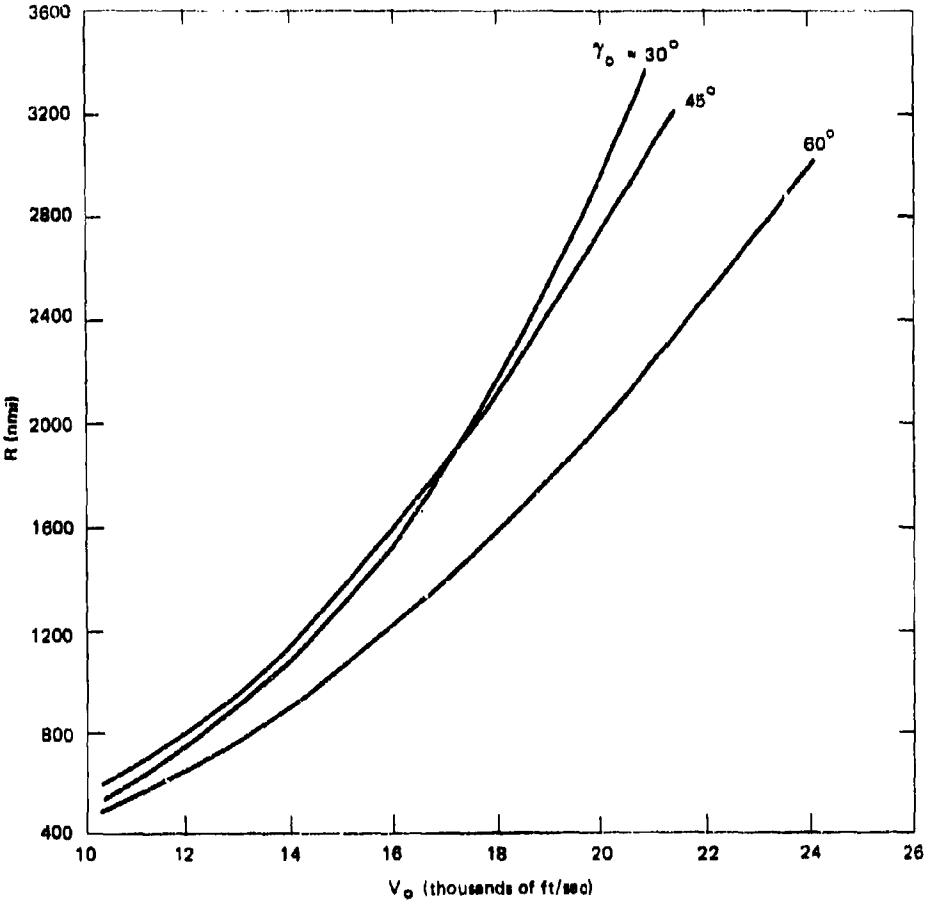

Fig. 4-1 RANGE VERSUS γ_o AND V_o

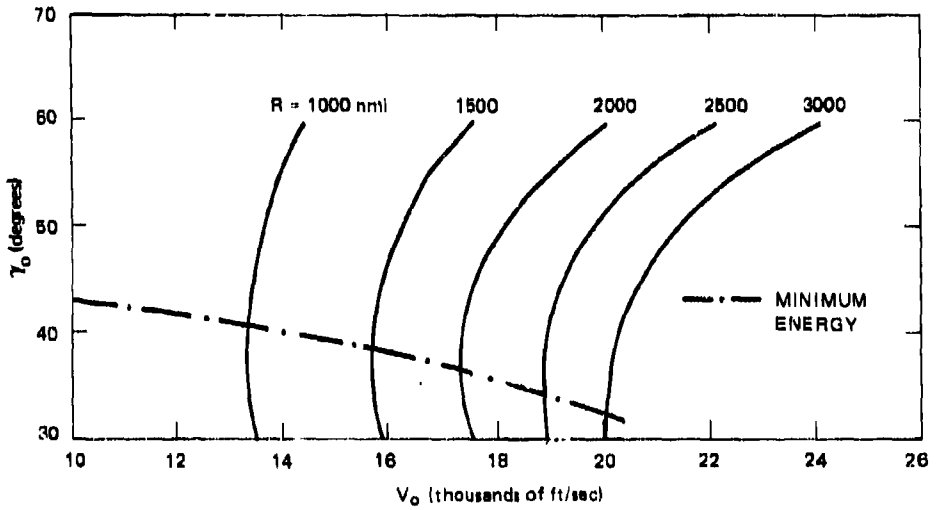

Fig. 4-2 INITIAL γ_o VERSUS V_o AND RANGE

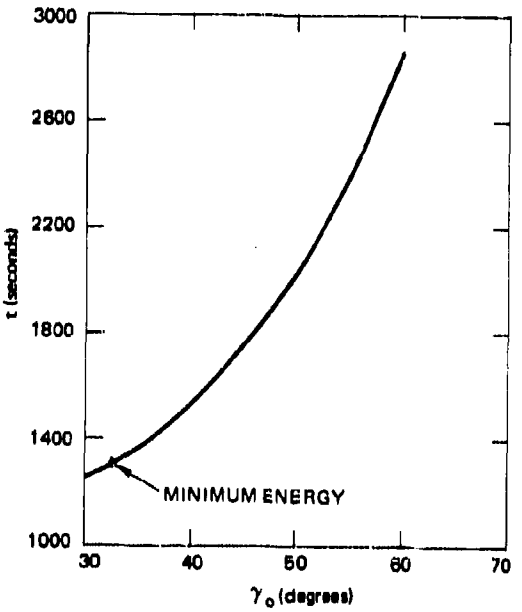

Fig. 4-3 FLIGHT TIME VERSUS γ_o, R = 3000 NMI

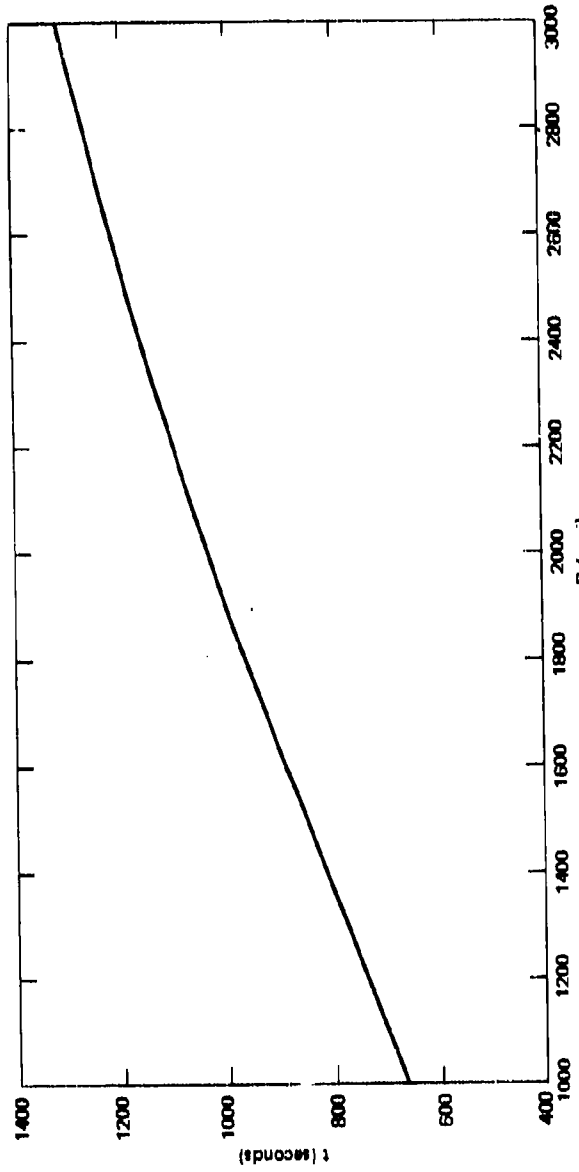

Fig. 4-4 FLIGHT TIME VERSUS RANGE, MINIMUM ENERGY TRAJECTORY

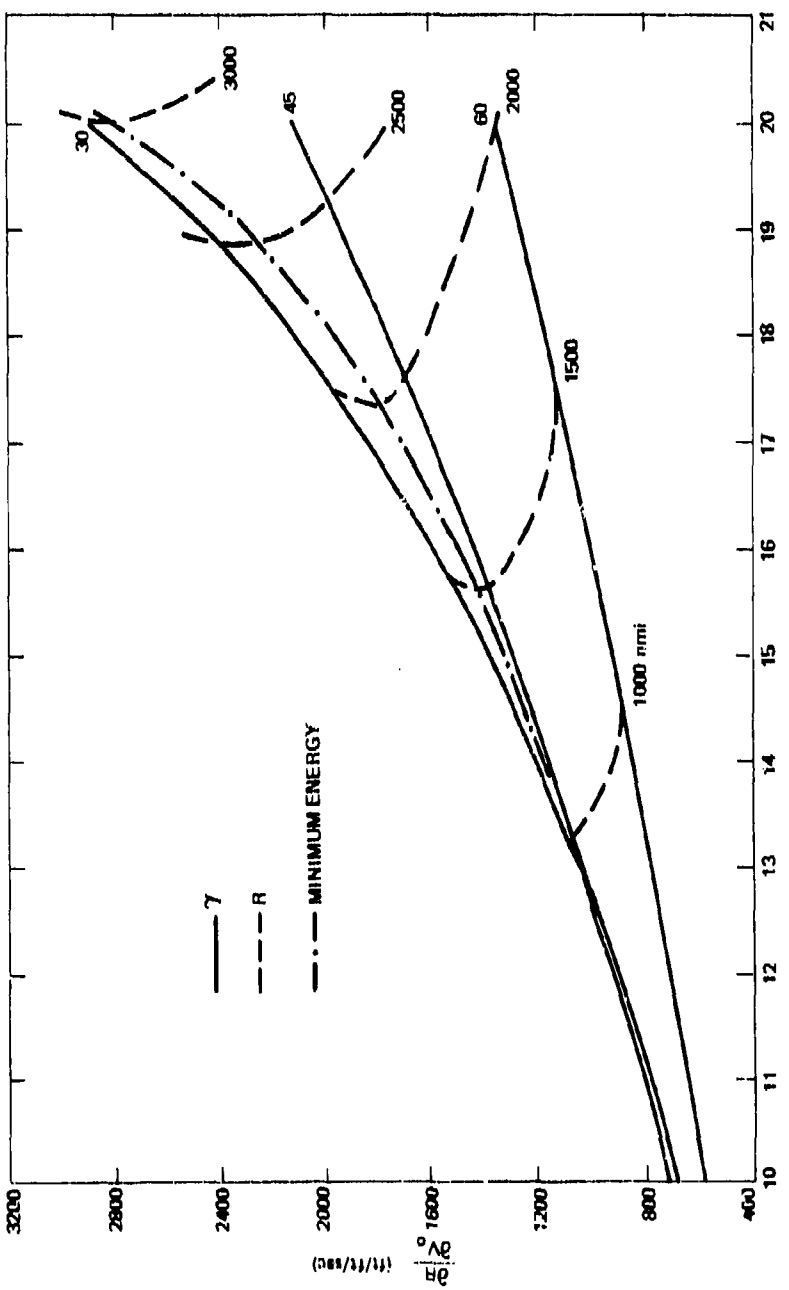

Fig. 4-5 RANGE SENSITIVITY TO V_o

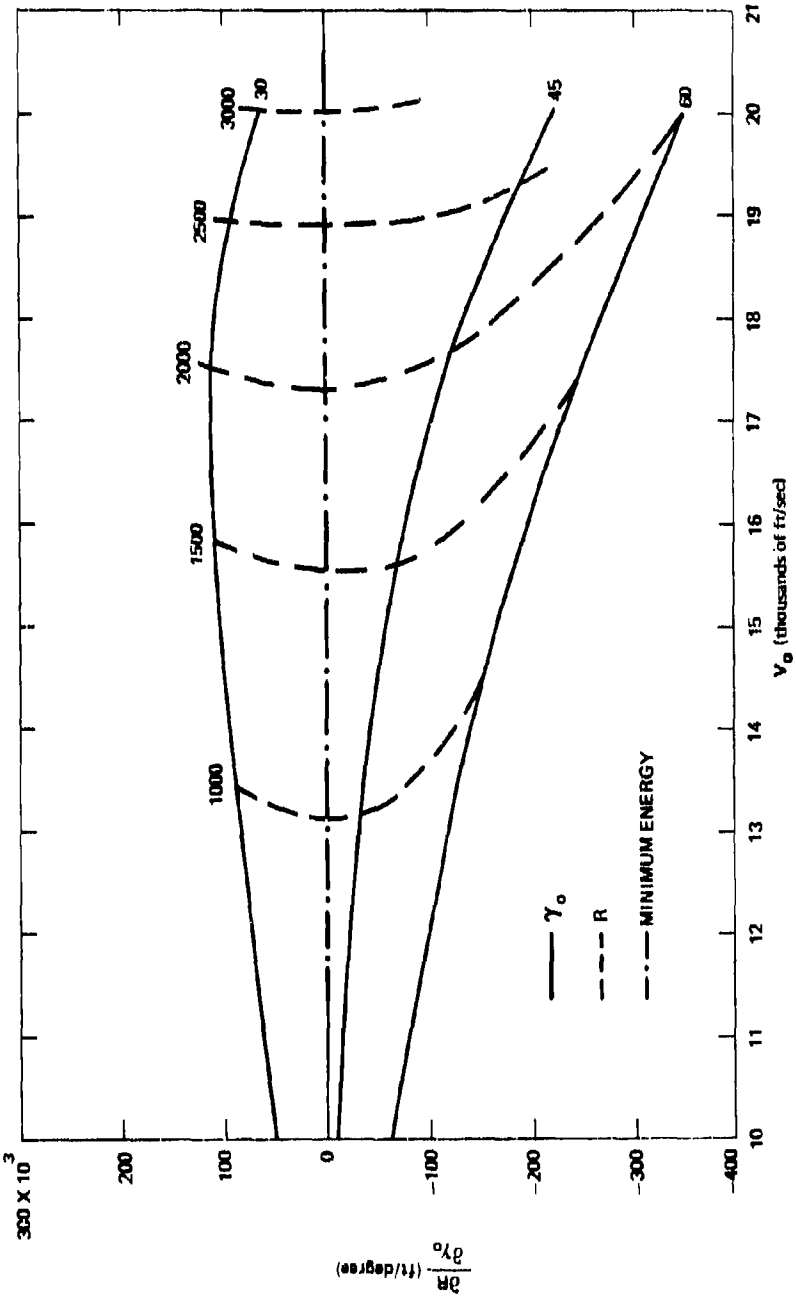

Fig. 4-6 RANGE SENSITIVITY TO γ_o

4.2 EFFECTS OF EARTH ROTATION

SYMBOLS FOR SECTION 4.2

Symbol	Definition	Typical Units
C_A	axial force coefficient	-
h	altitude	feet or nmi
I	refers to the impact location	-
L	refers to the launch location	-
R	range from L to I	nmi
r	$r_e + h$	feet
r_e	earth radius = 2.09×10^7 = 3441	feet nmi
S	reference area	ft^2
t	total flight time	seconds
Δt	increment in reentry time	seconds
V	velocity in inertial coordinates	ft/sec
W	vehicle weight	pounds
β	vehicle ballistic coefficient, $\frac{W}{C_A S}$	lb/ft^2
γ	flight path angle in inertial coordinates (positive for launch angles)	degrees
ϕ	latitude, positive for N. latitude	degrees
Λ	longitude, positive for E. longitude	degrees
$\Delta\Lambda$	earth rotation angle during time t	degrees
ψ	azimuth angle, positive direction is clockwise from north	degrees
ψ_{LI}	azimuth angle from L to I (Eq. (4.2-19))	degrees
θ_o	half the range angle for nonrotating earth (Eq. (4.1-7))	radian

Symbol	Definition	Typical Units
θ_e	half the range angle for rotating earth (Eq. (4.2-17))	radians
ω_e	earth rotation rate = 0.729×10^{-4}	rad/sec

Subscripts

e	refers to quantities measured relative to rotating earth
I	refers to impact condition
L	refers to launch condition

SUMMARY AND CONCLUSIONS

The equations of motion given in the preceding section are applicable to the rotating earth case provided the trajectory is defined in the inertial axis system. Therefore, initial conditions must be computed taking into consideration the velocity of the rotating earth. In addition, the amount of earth rotation during the time interval from launch to impact must be accounted for. In this section equations are given for evaluating the magnitude of these effects and an example is given in Section 4.6, Example 2.

The major conclusions are:

1. Compared to a nonrotating earth calculation, the effect of a rotating earth on a missile fired eastward is to increase the initial inertial velocity and to decrease the initial flight path angle. Westward firings result in a decreased velocity and an increased flight path angle. The largest change in velocity (about 1500 ft/sec) occurs for launches at the equator, for eastward or westward firings, and for very low flight path angles.

2. Compared to a nonrotating earth calculation, the effect of a rotating earth on a missile fired eastward is to increase the range and flight time. The impact latitude is the same for both calculations. For a westward firing the range and flight time are decreased.

The three basic laws used in Section 4.1 to define the equations of motion are valid for a coordinate system fixed in space (nonrotating earth). Two major effects of the earth's rotation on the flight of ballistic vehicles will be considered.

1. The launch site has a velocity caused by the earth's rotation so that launch velocity and launch direction are modified compared to the nonrotating earth solution.

2. The earth rotates while the missile is in flight, thereby affecting the location of the impact point.

Assume that a booster imparts to a vehicle a velocity V_e at an azimuth angle ψ_e and a flight path angle γ_e, where all three quantities are measured relative to a rotating earth. The earth geometry required for this study is shown in the sketch, page 102.

The vehicle will travel in an orbital (or trajectory) plane that contains the velocity vector in inertial space, V, and the center of the earth. The characteristics of the trajectory are defined by the equations derived in Section 4.1, provided inertial quantities are used. The inertial quantities may be obtained from earth reference quantities as shown below. The velocity vector is divided into three components:

$$\text{Radial component} = V \sin \gamma \qquad (4.2\text{-}1)$$

$$\text{North component} = V \cos \gamma \cos \psi \qquad (4.2\text{-}2)$$

$$\text{East component} = V \cos \gamma \sin \psi \qquad (4.2\text{-}3)$$

Preceding page blank

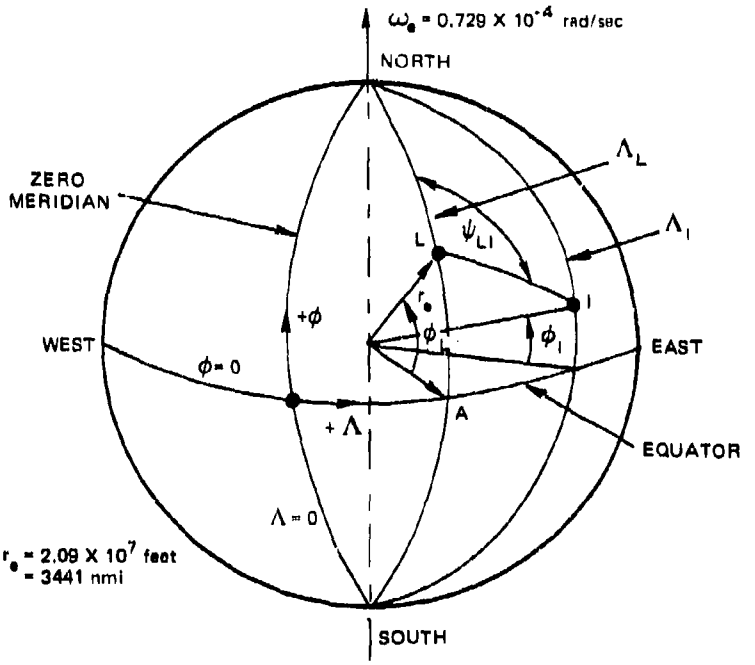

In inertial coordinates the radial component and north component of velocity are the same as those measured in the earth fixed axes, but the east component is increased by $\omega_e r \cos \phi$. Therefore, the components of the inertial velocity, V, are:

$$\text{Radial component} = V_e \sin \gamma_e \qquad (4.2\text{-}4)$$

$$\text{North component} = V_e \cos \gamma_e \cos \psi_e \qquad (4.2\text{-}5)$$

$$\text{East component} = V_e \cos \gamma_e \sin \psi_e + \omega_e r \cos \phi \qquad (4.2\text{-}6)$$

The azimuth angle, flight path angle, and velocity in inertial coordinates may be obtained from the following equations:

$$\tan \psi = \frac{\text{eastward component of velocity}}{\text{northward component of velocity}}$$

$$\frac{\tan \psi}{\tan \psi_e} = 1 + \frac{\omega_e r \cos \phi}{V_e \cos \gamma_e \sin \psi_e} \qquad (4.2\text{-}7)$$

$$\sin \gamma = \frac{\text{radial component of velocity}}{\text{total velocity}}$$

$$\frac{\sin \gamma}{\sin \gamma_e} = \frac{V_e}{V} \qquad (4.2\text{-}8)$$

$$\frac{V}{V_e} = \left[1 + 2 \cos \gamma_e \sin \psi_e \frac{\omega_e r \cos \phi}{V_e} + \left(\frac{\omega_e r \cos \phi}{V_e} \right)^2 \right]^{1/2} \qquad (4.2\text{-}9)$$

For launch velocities of interest, the velocity ratio is given by the approximation:

$$\frac{V}{V_e} = 1 + \cos \gamma_e \sin \psi_e \frac{\omega_e r \cos \phi}{V_e} \qquad (4.2\text{-}10)$$

$$\omega_e = 0.729 \times 10^{-4} \text{ rad/sec} \qquad (4.2\text{-}11)$$

$$r \approx r_e = 2.09 \times 10^7 \text{ feet} \qquad (4.2\text{-}12)$$

$$\therefore \omega_e r_e = 1520 \text{ ft/sec} . \qquad (4.2\text{-}13)$$

From Eqs. (4.2-8) and (4.2-10), it is observed that for eastward launches (ψ_e = 0° to 180°, $V/V_e > 1$ and tends to be maximum for launches from the equator (ϕ = 0) for

minimum energy trajectories (minimum V_e), for direct east firings ($\psi_e = 90$), and for low flight path angles ($\gamma_e \to 0$). For eastward trajectories the inertial velocity is increased and the flight path angle is decreased (compared to the values for a nonrotating earth); for westward firings, V is decreased and γ increased (compared to the values for a nonrotating earth). The maximum variation of V/V_e from unity is $\pm \omega_e r/V_e$. For $V_e \geq 10\,000$ ft/sec the maximum variation in V/V_e is about 15%.

Given values of V_e and γ_e, the inertial values of V and γ may be obtained from Eqs. (4.2-8) and (4.2-10). These values of V and γ may be used in equations given in Section 4.1. However, the range computed by Eq. (4.1-9) corresponds to the range measured along a sphere fixed in space. The range measured on the rotating earth (in the absence of an atmosphere) may be computed as shown below.

The orbital plane defined by V and the center of the earth remains fixed in space. During the flight time the earth rotates through an angle:

$$\Delta\Lambda = 57.3\, \omega_e\, t \,. \qquad (4.2\text{-}14)$$

For given inertial launch conditions, the impact latitude is unaffected by ω_e and, from spherical trigonometry,

$$\sin \phi_I = [\sin 2\theta_o \cos \phi_L \cos \psi_L + \cos 2\theta_o \sin \phi_L] \qquad (4.2\text{-}15)$$

where θ_o is the value computed from Eq. (4.1-7) for $\gamma_o = \gamma$ and $V_o = V$. The impact longitude is given by:

$$\Lambda_I = \Lambda_L - 57.3\omega_e t + \sin^{-1}\left(\frac{\sin \psi_L \sin 2\theta_o}{\cos \theta_I}\right) \qquad (4.2\text{-}16)$$

where t is the flight time computed from Eqs. (4.1-7) and (4.1-16) for $V_o = V$ and $\gamma_o = \gamma$.

Given ϕ_L, Λ_L, ϕ_I, and Λ_I the range may be computed from the equation:

$$R = 2r_e\theta_e \quad . \tag{4.2-17}$$

From the spherical geometry shown in the sketch, the range angle $2\theta_e$ may be obtained from;

$$\cos 2\theta_e = \cos \phi_I \cos \phi_L \cos \Delta\Lambda + \sin \phi_I \sin \phi_L \quad . \tag{4.2-18}$$

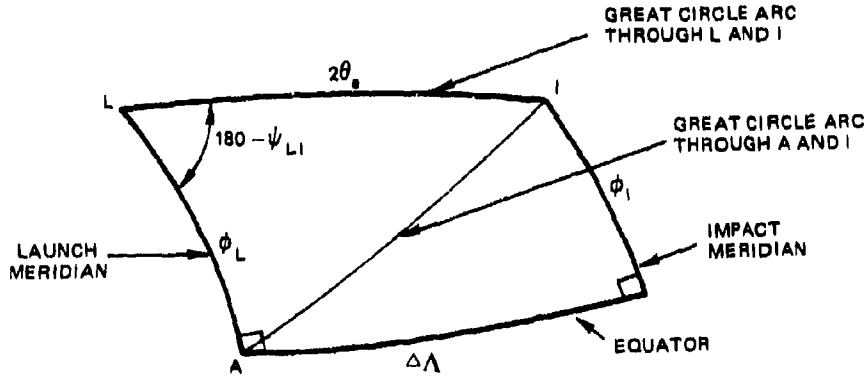

The bearing of the impact from the launch site may be obtained from

$$\cos \psi_{LI} = \frac{\cos 2\theta_e \cos \phi_L - \cos \phi_I \cos \Delta\Lambda}{\sin 2\theta_e \sin \phi_L} \quad . \tag{4.2-19}$$

For $\phi_L = 0$, Eq. (4.2-19) becomes:

$$\cos \psi_{LI} = \frac{\sin \phi_I}{\sqrt{1 - \cos^2 \phi_I \cos^2 \Delta\Lambda}} \quad . \qquad (4.2\text{-}20)$$

Sometimes V, γ, and ψ are given and it is desirable to obtain the corresponding quantities relative to a rotating earth. The required equations are:

$$\frac{V_e}{V} = \left[1 - \frac{2\,\omega_e r \cos\gamma \sin\psi \cos\phi}{V} + \left(\frac{\omega_e r}{V}\right)^2 \cos^2\phi\right]^{1/2} \qquad (4.2\text{-}21)$$

$$\frac{\sin\gamma_e}{\sin\gamma} = \frac{V}{V_e} \qquad (4.2\text{-}22)$$

$$\frac{\tan\psi_e}{\tan\psi} = 1 - \frac{\omega_e r \cos\phi}{V \cos\gamma \sin\psi} \quad . \qquad (4.2\text{-}23)$$

4.3 EFFECTS OF ATMOSPHERE

4.3 EFFECTS OF ATMOSPHERE

SYMBOLS FOR SECTION 4.3

Symbol	Definition	Typical Units
A	axial force	pounds
a	speed of sound	ft/sec
C_A	axial force coefficient	-
C_{m_q}	pitch damping coefficient	-
C_N	normal force coefficient	-
C_{N_α}	$dC_N/d\alpha$	-
D	damping factor (Eq. (4.5-20))	-
d	reference length	feet
g	acceleration of gravity	ft/sec^2
g_X	longitudinal acceleration	g
H	scale height = RT/g	feet
h	altitude above sea level	feet
h_{max}	altitude at V_{max}	feet
$I_1(K)$	$\sum_{n=1}^{\infty} \frac{(K/2)^n}{n \cdot n!}$	-
$I_2(k)$	$e^{-K} \sum_{n=0}^{\infty} \frac{(2K)^n}{1 \cdot 3 \cdot 5 \cdots (2n+1)}$	"
I_Y	pitch (or yaw) moment of inertia	$slug\text{-}ft^2$
K	parameter defined by Eq. (4.3-6)	-
k_1	constant defined by Eq. (4.3-26)	-
L	reference length	feet
M	Mach number = V/a	-
m	vehicle mass	slugs
P	atmospheric pressure	lb/ft^2

Symbol	Definition	Typical Units
$\bar{q}$	dynamic pressure = $\frac{\gamma}{2} PM^2$	lb/ft^2
q_s	stagnation heating rate per unit area	$Btu/ft^2 sec$
Q	total heat per unit area absorbed at the stagnation point	Btu/ft^2
R	gas constant = 1716	$ft^2/sec^2 - {}^\circ R$
R_e	Reynolds number, VL/ν	-
R_N	vehicle nose radius	feet
S	reference area	ft^2
T	atmospheric temperature	$^\circ R$
t	time	seconds
$\Delta t_1, \Delta t_2$	intervals of time defined by Eqs. (4.3-20) and (4.3-21)	seconds
V	vehicle velocity	ft/sec
W	vehicle weight	pounds
$X_{c.p.}$	distance from vehicle nose to the c.p.	feet
$X_{c.g.}$	distance from vehicle nose to the c.g.	feet
ΔX	$X_{c.p.} - X_{c.g.}$	feet
α	vehicle angle of attack	radians
β	ballistic coefficient = $\frac{W}{C_A S}$	lb/ft^2
γ	reentry flight path angle (always negative)	degrees
ν	kinematic viscosity	ft^2/sec
ρ	atmospheric density	$slug/ft^3$
ω_A	aerodynamic pitch frequency	rad/sec

Subscripts

ave	refers to average over the time interval
E	refers to reentry conditions (K=0)
i	refers to initial conditions
o	refers to sea level conditions
max	refers to maximum value except as noted

A dot over a symbol means the first derivative with respect to time.

SUMMARY

When a vehicle moves through an atmosphere, aerodynamic forces are generated that affect vehicle motion. The magnitude of these forces is influenced strongly by the missile velocity and atmospheric density. In this section approximate equations are derived for missile velocity, ambient density (or pressure and temperature), and related parameters.

Assuming that the axial force is the only force acting on the missile, and making other appropriate simplifications, equations are derived for velocity, time, dynamic pressure, longitudinal deceleration, Reynolds number, stagnation point heating rate, and the total heat absorbed at the stagnation point as functions of a parameter (K) which, for a given missile, atmosphere, and trajectory, is defined by altitude only. Most of these quantities increase from zero at reentry, reach a maximum value, and then decrease prior to impact. Equations are given for the maxima and the value of K at which they occur.

An example illustrating the use of these equations is given in Section 4.6, Example 4.

The boost phase of the trajectory is guided to such a high altitude that atmospheric effects during the exit phase are usually negligible. Therefore, this discussion is limited to the reentry phase.

Customarily, reentry into the sensible atmosphere is assumed to begin at an altitude of 400 000 feet. The velocity increases slightly under the effect of gravity, reaches a maximum value, and then decreases under the influence of aerodynamic drag.

The maximum velocity occurs when the axial force is just equal to the component of gravity along the flight path, or:

$$C_A \bar{q} S = - W \sin \gamma$$

Using the definitions of $\bar{q}$ and β, this equation becomes:

$$\rho = - \frac{2\beta \sin \gamma}{V_{max}^2}$$

If the reentry velocity, V_E, is given for some altitude above that corresponding to V_{max}, the maximum velocity may be estimated using the equation:

$$V_{max} = V_E + kg \frac{(h_E - h_{max})}{V_E}$$

where k is a constant having a magnitude between 0 (for $h_E \approx h_{max}$) and 1 (for $h_E \gg h_{max}$). A precise value of k is not important since the difference between V_E and V_{max} is small and, in fact, is usually neglected. However, if a little more accuracy is desired, the equations for ρ and V_{max} may be solved by successive approximation.

The remainder of this section considers the motion of the vehicle during the deceleration phase. During this

period the general behavior of the body may be obtained by simplified equations of motion based on the following assumptions:

1. The earth is flat and nonrotating.
2. The only force acting on the body is the axial force, and the axial force coefficient is constant.
3. The reentry flight path angle is constant.

The reentry phase is of relatively short duration and short range so that the assumption of a flat nonrotating earth is justified for this study. The assumption that the axial force is the only force acting on the body implies that the angle of attack is always zero and that the effect of gravity is negligible compared to the effect of axial force. More precise methods of computing trajectories may be used to show that the effect of α is usually small. Except for the very-high-altitude and, sometimes, the very-low-altitude portions of the reentry trajectory, the assumption that $\frac{W \sin \gamma}{A}$ is small is justified for approximate solutions to the equations of motion. Precise methods of computing trajectories may be used to show that assumption 3 is valid for a large portion of most trajectories and that the validity tends to be improved for high weight and low axial force bodies and for steep reentry angle trajectories. For many reentry bodies and trajectories in current use, the assumption of constant γ is valid all the way to impact.

The geometry of the trajectory in which A is the only force acting is shown in the sketch.

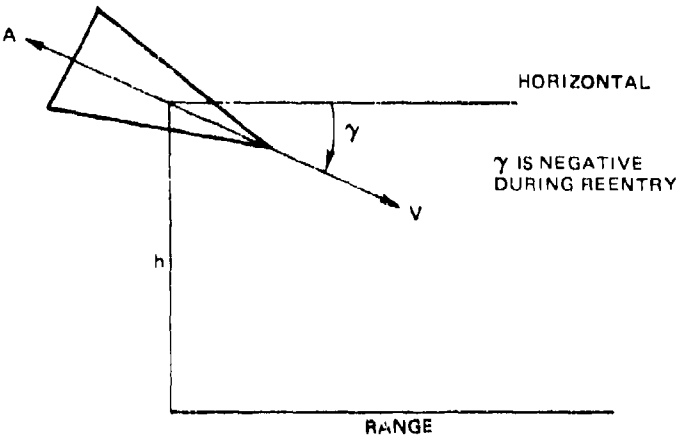

The equation of motion along the flight path is:

$$-A = \frac{W}{g} \frac{dV}{dt} \quad . \tag{4.3-1}$$

Expressing the axial force in terms of coefficients as discussed in Section 2:

$$-C_A (1/2)\rho V^2 S = \frac{W}{g} \frac{dV}{dt} \quad . \tag{4.3-2}$$

Since the flight path is a straight line, $dh/dt = V \sin\gamma$ and Eq. (4.3-2) may be written in the form:

$$\frac{dV}{V} = - \frac{C_A g \rho S}{2W} \frac{dh}{\sin\gamma} \quad . \tag{4.3-3}$$

The term $W/C_A S$ occurs frequently in reentry equations and is called the ballistic coefficient, β. For an atmosphere in static equilibrium (see Eq. (3-1)), $dP = -\rho g dh$. When these substitutions are made, Eq. (4.3-3) becomes:

$$\frac{dV}{V} = \frac{dP}{2\beta \sin\gamma} \quad . \tag{4.3-4}$$

Using initial conditions $V = V_i$ at $P = P_i$, Eq. (4.3-4) is readily integrated to give:

$$V = V_i e^{\frac{K_i - K}{2}} \tag{4.3-5}$$

where K is defined by the equation:

$$K = \frac{-P}{\beta \sin\gamma} \quad . \tag{4.3-6}$$

Equation (4.3-5) is valid provided $\frac{e^K}{K} \ll \frac{V_E^2}{2gH}$. This condition is a restatement of assumption 2 listed above. Therefore the equation tends to become invalid at low reentry velocities and at very low and very high values of K. The limitation at very low values of K is not serious and was discussed at the beginning of this section. On the other hand, the limitation at high values of K may have significant consequences (see Section 5.1.2 for example). When the initial altitude is high, $K_i \approx 0$ and the equations may be simplified. For some applications of these equations the initial condition is not a high altitude condition. Therefore for completeness the K_i term is retained in Eq. (4.3-5) and subsequent equations.

Other trajectory characteristics of interest may be derived (Ref. 4-1) and the results are given in Eqs. (4.3-7)through (4.3-29). The time from altitude h_i (defined by P_i) to any other altitude (defined by P) is given by:

$$t - t_i = \frac{-H_{ave}}{V_E \sin\gamma}\left[\ln\frac{P}{P_i} + I_1(K) - I_1(K_i)\right] \tag{4.3-7}$$

where the I_1 function is plotted in Figs. 4-7 and 4-8. The dynamic pressure is given by the equation:

$$\bar{q} = \frac{-V_i^2 m \sin\gamma}{2 C_A S H} \left| \frac{K}{e^{K - K_i}} \right| , \qquad (4.3\text{-}8)$$

The longitudinal acceleration is given by:

$$g_X = \frac{K V_i^2 \sin\gamma}{2gH e^{K-K_i}} . \qquad (4.3\text{-}9)$$

The Reynolds number based on body length is given by:

$$R_e = \frac{V_i L}{\nu_e^{(K/2-K_i/2)}} . \qquad (4.3\text{-}10)$$

The heating rate at the body stagnation point is indicative of the severity of the heating environment. This rate is given by:

$$q_s = \frac{412}{\sqrt{R_N \rho_o}} \left(\frac{V_i}{26\,000} \right)^3 \sqrt{\frac{P}{T}} e^{3(K_i - K)} . \qquad (4.3\text{-}11)$$

The total heat absorbed at the stagnation point from h_i to h is:

$$Q_s - Q_{s_i} = \frac{-1.69}{\sqrt{R_N \rho_o}} \left(\frac{V_E}{26\,000} \right)^2 \frac{\sqrt{T_{ave}}}{\sin\gamma} \left[\sqrt{P}\ I_2(K) - \sqrt{P_i}\ I_2(K_i) \right] \qquad (4.3\text{-}12)$$

where $I_2(K)$ is plotted in Fig. 4-9.

The dynamic pressure, longitudinal deceleration, Reynolds number, and stagnation heating rate all have a

trend which increases from zero at reentry to a maximum value and then (depending upon the body and trajectory characteristics) decreases.

The approximate pressure at which the maximum values of these functions are reached may be obtained by assuming T is a constant, $K_1 = 0$, setting the derivative of the function with respect to K to zero, and solving for the maximum. The error introduced by assuming T is a constant is small. At $K_1 = 0$, $V_1 = V_E$ and the equations for the maxima and their K, P, and V/V_E values are shown below.

Equation	K	P	V/V_E	
$\bar{q} = \frac{-\beta V_E^2 \sin\gamma}{9330T}$	1	$-\beta \sin\gamma$	0.606	(4.3-13)
$g_X = \frac{V_E^2 \sin\gamma}{9330T}$	1	$-\beta \sin\gamma$	0.606	(4.3-14)
$R_e/L = 0.368 \frac{V_E}{\nu}$	2	$-2\beta \sin\gamma$	0.368	(4.3-15)
$q_s = \frac{144.3}{\sqrt{\rho_o}} \left(\frac{V_e}{26\,000}\right)^3 \sqrt{\frac{-\beta \sin\gamma}{R_N T}}$	1/3	$-(\beta/3) \sin\gamma$	0.846	(4.3-16)

The longitudinal acceleration is a characteristic of considerable importance since it is a quantity that can readily be measured on a flight test vehicle. It is interesting to note that for an isothermal atmosphere $g_{X_{max}}$ is highly dependent upon V_E, moderately dependent upon γ and T, and independent of the vehicle weight and axial force (β). However the altitude at which $g_{X_{max}}$ occurs is dependent upon β. The greater the β or the steeper the reentry angle, the lower the altitude for $g_{X_{max}}$.

The g_X versus time curve has two inflection points, which may be determined in the following manner:

$$\dot{g}_X = \frac{dg_X}{dK}\frac{dK}{dt} \quad . \tag{4.3-17}$$

It may be shown that:

$$\frac{dK}{dt} = -\frac{V_E \sin\gamma}{H} Ke^{-K/2} \tag{4.3-18}$$

and

$$\dot{g}_X = -\frac{V_E^3 \sin^2\gamma}{2g(H)^2} K(1-K)e^{-3K/2} \quad , \tag{4.3-19}$$

The inflection point occurs where Eq. (4.3-19) is maximum or minimum. It may be shown that this occurs at $K = 1/3$ and $K = 2$, which correspond to $\frac{g_X}{g_{X_{max}}} = 0.650$ and 0.736, respectively, or $P = -(1/3)\beta \sin\gamma$ and $-2\beta \sin\gamma$, respectively.

Using Eq. (4.3-7), the time between the high altitude inflection point and $g_{X_{max}}$ is given by:

$$\Delta t_1 = -\frac{80T_{ave}}{V_E \sin\gamma} \tag{4.3-20}$$

and the time from $g_{X_{max}}$ to the low altitude inflection point is given by:

$$\Delta t_2 = -\frac{77T_{ave}}{V_E \sin\gamma} \quad . \tag{4.3-21}$$

From Eqs. (4.3-9) and (4.3-14):

$$\frac{g_X}{g_{X_{max}}} = 2.72 \frac{K}{e^K} \quad , \tag{4.3-22}$$

Therefore, using just the telemetry g_X trace, the ratio of $g_X/g_{X_{max}}$ is a good indication of the K history. The K history can be converted to air pressure history from known β and γ (Eq. (4.3-6)), and the pressure history can be converted to altitude history from known atmospheric characteristics. A plot of $g_X/g_{X_{max}}$ versus K is given in Fig. 4-10.

Other quantities required for succeeding sections are listed below for convenient reference.

$$\omega_A^2 = \frac{V_E^2 C_{N_\alpha} \Delta Xm \sin(-\gamma)}{2 C_A I_Y H} \frac{K}{e^K} \tag{4.3-23}$$

$$\dot{\omega}_A = V_E^2 \left[\frac{C_{N_\alpha} \Delta Xm \sin^3(-\gamma)}{8 C_A I_Y H^3} \right]^{1/2} \frac{(1-K)\sqrt{K}}{e^K} \tag{4.3-24}$$

$$D = \left[k_1 - C_{m_q} \right] \left[\frac{\sin(-\gamma)}{2C_A \frac{\Delta X}{d} k_1 \frac{H}{d}} \right]^{1/2} \sqrt{K} \tag{4.3-25}$$

$$k_1 = C_{N_\alpha} \left(1 - \frac{I_X}{I_Y} \right) \frac{I_Y}{md^2} \tag{4.3-26}$$

$$\dot{\bar{q}} = \frac{V_E^3 m \sin^2\gamma}{2C_A SH^2} \frac{(1 - K)\, K}{e^{3K/2}} \qquad (4.3\text{-}27)$$

$$\frac{d\bar{q}}{dK} = \frac{V_E^2 m \sin(-\gamma)}{2C_A SH} \frac{(1 - K)}{e^{K}} \qquad (4.3\text{-}28)$$

$$\dot{P} = \frac{V_E W \sin^2\gamma}{C_A SH} \frac{K}{e^{K/2}} \qquad (4.3\text{-}29)$$

The 1962 Standard Atmosphere characteristics required for evaluating these equations are listed in Table 3-1.

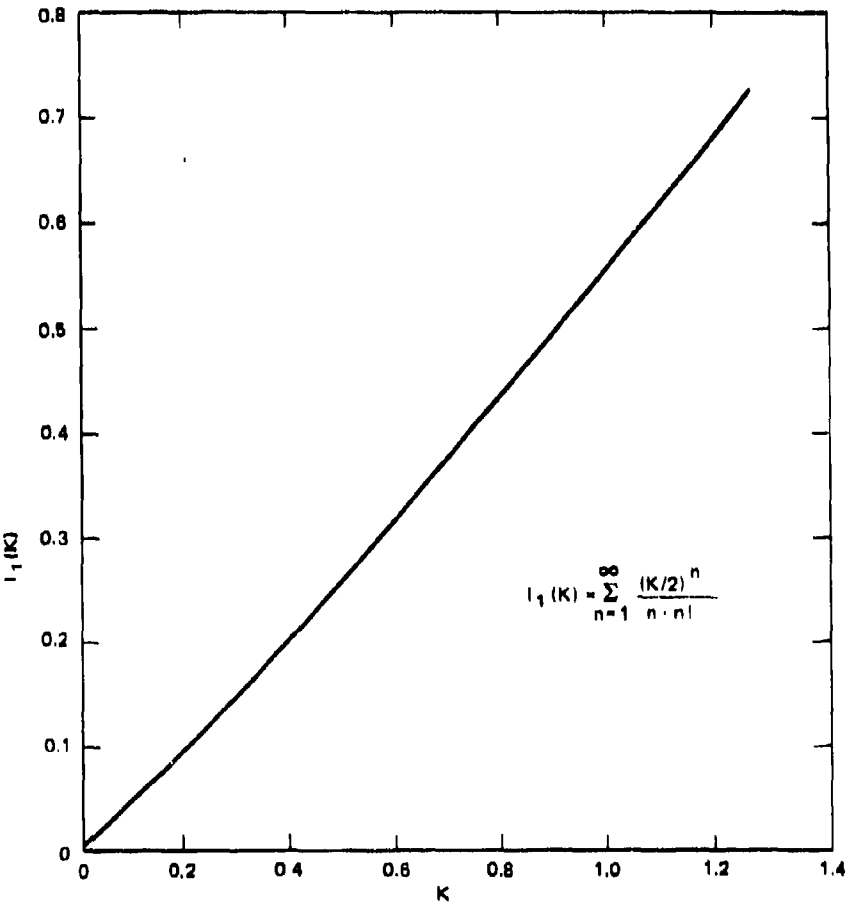

Fig. 4-7 VARIATION OF I_1 (K) WITH K

Preceding page blank

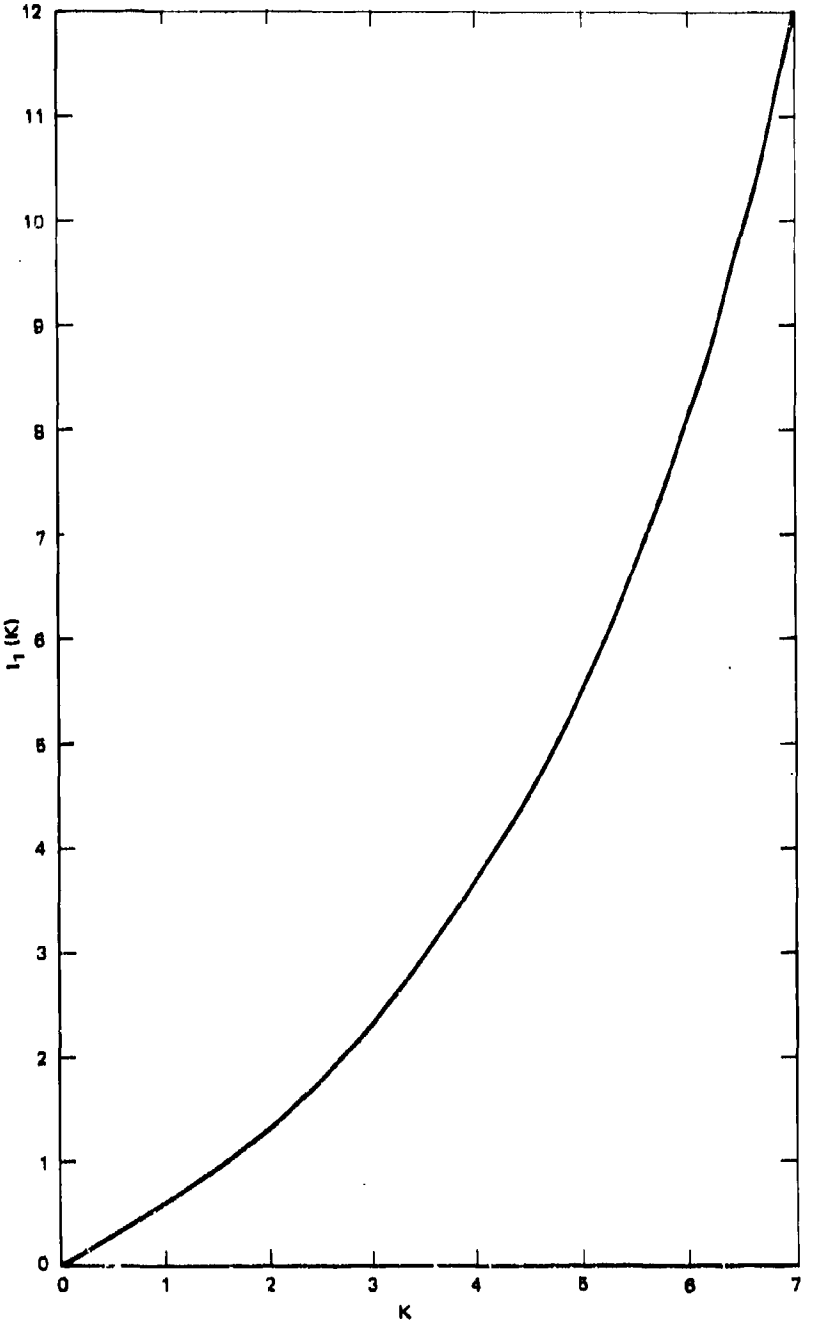

Fig. 4-8 VARIATION OF I_1 (K) WITH K

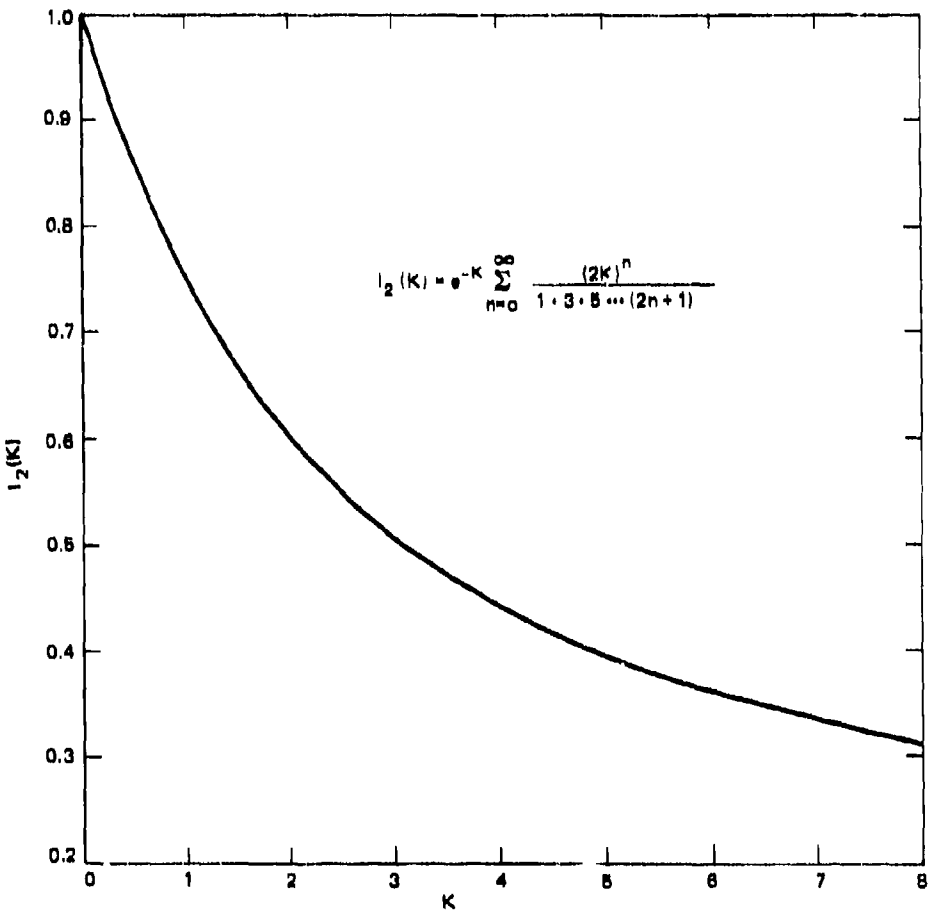

Fig. 4-9 VARIATION OF I_2 (K) WITH K

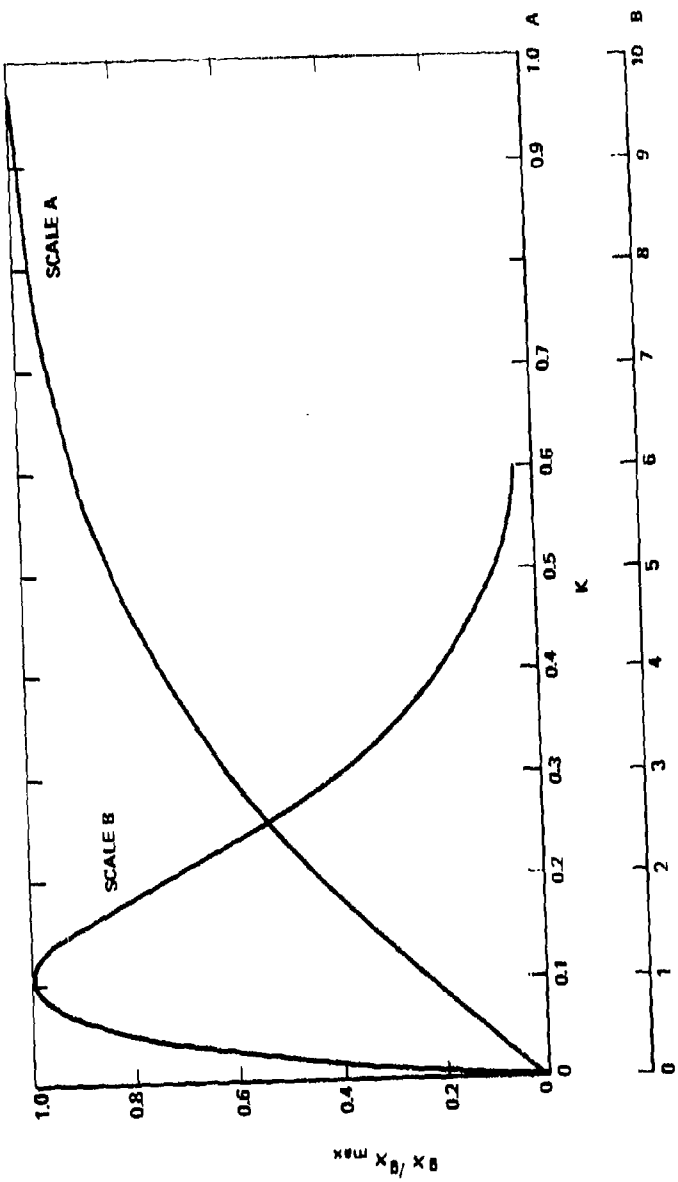

Fig. 4-10 $g_X/g_{X\,max}$ VERSUS K

4.4 EFFECTS OF BODY DYNAMICS

SYMBOLS FOR SECTION 4.4

Symbol	Definition	Typical Units
a	constant defined by Eq. (4.4-52)	-
C_1, C_2	constants in Eq. (4.4-33)	-
C_3, C_4, C_5	constants defined by Eqs. (4.4-45), (4.4-58), and (4.4-61)	-
C_A	axial force coefficient	-
C_N	normal force coefficient	-
C_{N_α}	$dC_N/d\bar{\alpha}$	-
C_{ℓ_p}	roll damping derivative	-
C_{m_q}	pitch damping derivative	-
d	reference length	feet
F_X, F_Y, F_Z	aerodynamic forces along body axes X, Y, Z	pounds
F_α	$C_{N_\alpha} \bar{q} S$	lb/rad
g	acceleration of gravity	ft/sec^2
g_L	load factor = N/W	-
H	scale height = RT/g or angular momentum	feet $slug\text{-}ft^2/sec$
I_X, I_Y, I_Z	moments of inertia about principal axes X, Y, Z	$slug\text{-}ft^2$
J_o	zero order Bessel function	-
K	$-P/(\beta \sin\gamma)$	-
k_1	constant defined by Eq. (4.4-30)	rad/sec
k_2	constant defined by Eq. (4.4-31)	rad/sec^2

Symbol	Definition	Typical Units
ℓ, m, n	aerodynamic rolling moment, pitching moment, and yawing moment, respectively	lb-ft
m	mass = W/g	slugs
M_p	roll damping factor, $C_{\ell_p} \frac{\bar{q}Sd^2}{V}$	lb-ft-sec
M_q	pitch damping factor, $C_{m_q} \frac{\bar{q}Sd^2}{V}$	lb-ft-sec
M_r	yaw damping factor, $C_{n_r} \frac{\bar{q}Sd^2}{V}$	lb-ft-sec
N	total lateral force, $\sqrt{F_Y^2 + F_Z^2}$	pounds
P	ambient air pressure	lb/ft^2
p, q, r	roll rate, pitch rate, yaw rate, respectively	rad/sec
$\bar{q}$	dynamic pressure	lb/ft^2
R	gas constant = 1716	$ft^2/sec^2 - °R$
S	reference area	ft^2
T	temperature	°R
t	time	seconds
u, v, w	missile velocity along X, Y, Z axes, respectively	ft/sec
V	missile velocity	ft/sec
W	missile weight	pounds
X	constant defined in Eq. (4.4-40)	-
ΔX	$X_{c.p.} - X_{c.g.}$	feet
$X_{c.g.}$	distance from missile nose to the c.g.	feet

Symbol	Definition	Typical Units
$X_{c.p.}$	distance from missile nose to the c.p.	feet
α	angle of attack in the XZ plane	radians
$\bar{\alpha}$	vector angle of attack $\lvert\bar{\alpha}\rvert = \sqrt{\alpha^2 + \beta^2}$	radians
β	angle of attack in the XY plane	radians
	or ballistic coefficient, $W/C_A S$	lb/ft^2
γ	flight path angle, negative for re-entry trajectories	degrees
ϵ	angle defined by Eq. (4.4-22)	degrees
$\emptyset$	angle defined by Eq. (4.4-23)	degrees
θ	angle between the missile X-axis and the local horizontal	degrees
ω_g	frequency defined by Eq. (4.4-21)	rad/sec
ω_T	transverse rate $= \sqrt{q^2 + r^2}$	rad/sec
ω	total spin vector $= \sqrt{p^2 + q^2 + r^2}$	rad/sec
ω_A	aerodynamic frequency defined by Eq. (4.4-36)	rad/sec
$\bar{\omega}$	frequency defined by Eq. (4.4-49)	rad/sec
τ_B	period defined by Eq. (4.4-24)	seconds
τ_S	period defined by Eq. (4.4-25)	seconds
ψ	phase angle	degrees

Subscripts

E	refers to conditions at entry
o	refers to conditions at t = 0

A dot over a symbol means the first derivative with respect to time. Two dots over a symbol mean the second derivative with respect to time.

SUMMARY AND CONCLUSIONS

In the preceding section, the effects of the atmosphere on vehicle velocity and related factors were considered. In the present section, attention is given to the effects of the atmosphere on the dynamic behavior of the vehicle. We are concerned here with the rotational motion of the vehicle about its center of gravity over relatively short periods of time. Six-degree-of-freedom equations of motion are presented and interpreted in terms of body motion characteristics in the absence of aerodynamic forces (for example, motion in the exoatmosphere, where gyroscopic motion is important) at low altitudes where aerodynamic forces dictate the motion and at high altitudes where aerodynamic and gyroscopic forces are both important. Dynamic motion is important in the analysis of body heating and lateral loads. Equations are given for body rotational frequencies that are observed on telemetry traces from on-board equipment or from tracking radar signal strength traces. Numerical illustrations are given in Examples 3 and 5, Section 4.6.

The major conclusions are:

1. In the absence of aerodynamic forces, a reentry-type body that is spun about its longitudinal axis will follow a motion pattern determined by conditions at the initiation of the spin. If spin is applied so that neither pitch nor yaw rate is introduced, the vehicle will maintain a fixed attitude in space. If a pitch and/or a yaw rate (sometimes the vector sum is called the transverse rate) is experienced when spin is introduced, the missile's longitudinal axis traces a cone whose apex is at the missile center of gravity. The magnitude of the cone angle and the period of motion are functions of the transverse rate, missile roll rate, and moments of inertia about the longitudinal and transverse axes.

2. If the body contains rate gyros, the body rate observed on the telemetry trace during the exoatmospheric portion of flight will show a sinusoidal trace. The half-amplitude is the transverse rate existing at the time of spin-up, and the period is a function of the roll rate and the moments of inertia about the longitudinal and transverse axes.

3. During the low altitude portion of the reentry phase, aerodynamic forces dictate the motion of the vehicle. Generally, a missile reenters the atmosphere with some initial angle of attack. To prevent excessive lateral loads and heating problems the missile is designed so that the aerodynamic forces cause the angle of attack to approach zero rapidly. It is shown that for a symmetrical missile the angle of attack follows a damped oscillatory motion provided certain static and dynamic stability criteria are met. The frequency of the oscillation is called the aerodynamic frequency. This frequency increases from zero at reentry, reaches a maximum, and then (depending upon the trajectory and reentry conditions) decreases until impact.

4. At high altitudes, both aerodynamic and gyroscopic moments are important. The gyroscopic moments tend to maintain the body at a fixed altitude; the aerodynamic moments tend to rotate the body so that zero angle of attack is maintained. Typically, gyroscopic motion predominates at altitudes above about 300 000 feet; aerodynamic moments predominate at altitudes below about 100 000 feet; both effects are important at the intermediate altitudes.

In Section 4.3 the body was constrained to motion along a straight-line flight path. Therefore the equations of motion were reduced to a one-degree-of-freedom problem. In this section, we consider the six-degree-of-freedom problem. However, the equations are simplified by making the following assumptions:

1. The effect of gravity will be neglected.
2. The body is assumed to have symmetry about the longitudinal axis.

The primary interest in this section is to consider how the body behaves over a relatively short time span. For this purpose the effect of gravity may be shown to be very small. By assuming the body to be symmetric about the longitudinal axis, the principal axes coincide with the body axes, and the equations of motion are simplified since the product-of-inertia terms are zero.

The equations of motion are presented in a body axis system (Fig. 4-11) which remains fixed with respect to the body. The body rate terms in the equations of motion are the rates sensed by rate gyros mounted in a vehicle; the body translational acceleration terms are those that would be measured by accelerometers mounted at the vehicle center of gravity. The six equations defining the six degrees of freedom are:

$$\dot{p}I_X = \ell - qr(I_Z - I_Y) \qquad (4.4\text{-}1)$$

$$\dot{q}I_Y = m - pr(I_X - I_Z) \qquad (4.4\text{-}2)$$

$$\dot{r}I_Z = n - pq(I_Y - I_X) \qquad (4.4\text{-}3)$$

$$\dot{u} = \frac{F_X g}{W} + vr - wq \qquad (4.4\text{-}4)$$

$$\dot{v} = \frac{F_Y g}{W} + wp - ur \qquad (4.4\text{-}5)$$

$$\dot{w} = \frac{F_Z g}{W} + uq - vp \ , \qquad (4.4\text{-}6)$$

The auxiliary equations required are:

$$\ell = M_p p \qquad (4.4\text{-}7)$$

$$m = F_Z \Delta X + M_q q \qquad (4.4\text{-}8)$$

$$n = -F_Y \Delta X + M_r r \qquad (4.4\text{-}9)$$

$$V = \sqrt{u^2 + v^2 + w^2} \qquad (4.4\text{-}10)$$

$$\tan \bar{\alpha} = \frac{\sqrt{v^2 + w^2}}{u} \qquad (4.4\text{-}11)$$

$$F_X = -C_A \bar{q} S \qquad (4.4\text{-}12)$$

$$F_Y = -F_\alpha \bar{\alpha} \frac{v}{\sqrt{v^2 + w^2}} = -F_\alpha \beta \qquad (4.4\text{-}13)$$

$$F_Z = -F_\alpha \bar{\alpha} \frac{w}{\sqrt{v^2 + w^2}} = -F_\alpha \alpha \qquad (4.4\text{-}14)$$

$$F_\alpha = \left(\frac{C_N \bar{q} S}{\bar{\alpha}} \right) = C_{N_\alpha} \bar{q} S \ . \qquad (4.4\text{-}15)$$

4.4.1 Zero Aerodynamic Forces

Consider first the case of flight in the exoatmosphere where all aerodynamic terms are zero. In this region only gyroscopic effects exist.

Since the body is assumed to be symmetrical, $I_Z = I_Y$ and Eq. (4.4-1) reduces to the condition where p equals a constant. Differentiation of Eq. (4.4-2) gives:

$$\ddot{q} + p\dot{r}\,\frac{(I_X - I_Z)}{I_Y} = 0 \ , \qquad (4.4\text{-}16)$$

Substituting for $\dot{r}$ from Eq. (4.4-3) and noting that $I_Z = I_Y$:

$$\ddot{q} + p^2 \left(\frac{I_Y - I_X}{I_Y}\right)^2 q = 0 \qquad (4.4\text{-}17)$$

The solution to this differential equation is:

$$q = \omega_T \cos\left[p\left(1 - \frac{I_X}{I_Y}\right) t + \psi\right] \ .$$

If time is measured from the time when $q = q_{max}$, then $\psi = 0$ and

$$q = \omega_T \cos p\left(1 - \frac{I_X}{I_Y}\right) t \qquad (4.4\text{-}18)$$

$$\dot{q} = -\omega_T p\left(1 - \frac{I_X}{I_Y}\right) \sin p\left(1 - \frac{I_X}{I_Y}\right) t \ .$$

Substituting into Eq. (4.4-2):

$$r = -\omega_T \sin p(1 - \frac{I_X}{I_Y})\, t \qquad (4.4\text{-}19)$$

$$\therefore\ q^2 + r^2 = \omega_T{}^2 \ . \qquad (4.4\text{-}20)$$

Therefore, the pitch or yaw rate measured by a rate gyro mounted on a vehicle is a sinusoidal oscillation of half-amplitude ω_T having a frequency:

$$\omega_g = p(1 - \frac{I_X}{I_Y}) \ . \qquad (4.4\text{-}21)$$

This equation is convenient for checking the calibration constant for the roll rate gyro in flight test work. The term ω_T is sometimes called the body transverse rate.

The solution to the equations of motion in body axes provides information regarding the time history of quantities that may be sensed by "on-board" instrumentation, but no information is provided on the motion of the vehicle in space.

The motion in space is obtained by solving the equations of motion written in the inertial axis system. It is shown (Ref. 4-2) that, in the absence of aerodynamic forces, the motion of the body may be described physically as a "body cone" rolling along a "space cone" (or "cone of precession"), as shown in the sketch, page 141.

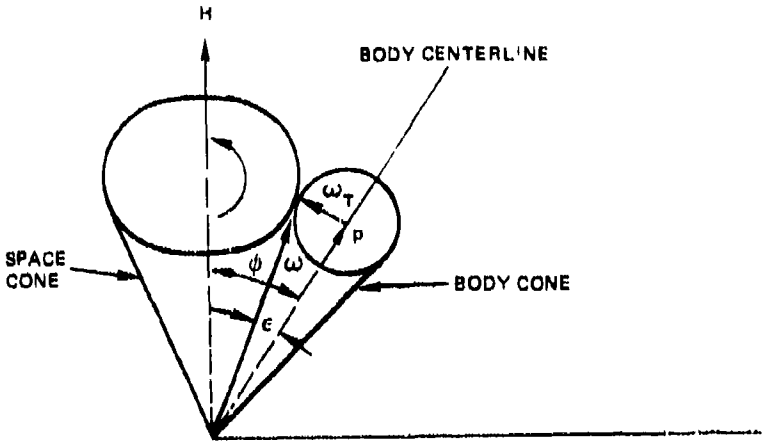

The centerline of the space cone is the angular momentum vector which remains fixed in space. The centerline of the body cone is the vehicle's longitudinal axis of symmetry (roll rate axis). The semicone angle of the body cone is defined by the equation:

$$\tan \epsilon = \frac{\omega_T}{p} \qquad (4.4\text{-}22)$$

The angle between the body centerline and the centerline of the space cone is constant and is given by:

$$\tan \phi = \frac{\omega_T}{p} \frac{I_Y}{I_X} \qquad (4.4\text{-}23)$$

where ω_T is defined by Eq. (4.4-20). It should be noted that the magnitude of the total spin vector, $\omega = \sqrt{p^2 + q^2 + r^2}$,

is constant and lies along the space cone surface. Assuming a positive roll rate and $I_X < I_Y$, the body centerline rotates about H in a clockwise direction (as shown above) when viewed by an observer looking toward +H. The transverse rate vector rotates about the body centerline so that the period is given by:

$$\tau_B = \frac{2\pi}{(1 - \frac{I_X}{I_Y})p} \qquad (4.4\text{-}24)$$

and corresponds to the frequency given previously in Eq. (4.4-21). The body centerline processes about the space cone with a period:

$$\tau_S = \frac{2\pi}{\frac{I_X}{I_Y} p \sqrt{1 + \tan^2 \phi}} \quad . \qquad (4.4\text{-}25)$$

For reentry bodies of current design, τ_S is an order of magnitude greater than τ_B.

The utility of the physical picture described above may be illustrated by the following example. Suppose we wish to determine the coning motion for a specified set of conditions at reentry. In particular, select a condition at $t = 0$ where $\bar{\alpha} = \bar{\alpha}_o$ and lies in the body XZ plane, which is the plane of the trajectory. Consider first the case of $q_o = 0$ and $r = r_o$, where r_o is positive and may be represented by a vector along the +Z body axis. Since ω lies on the surface on the space cone and the body cone is external to the space cone, the angular momentum vector lies in the trajectory plane and $\bar{\alpha}$ varies from $\bar{\alpha}_o$ (a maximum value) to $\bar{\alpha}_o - 2\phi$ (a minimum value). Similarly, if r_o is negative, $\bar{\alpha}$ varies from $\bar{\alpha}_o$ (a minimum value) to a maximum value of $\bar{\alpha}_o + 2\phi$. The body-fixed Y-axis at $t = 0$ is directed toward the right of the trajectory as viewed by an observer looking toward the impact point. Therefore for an initial condition of pitch rate only, if q_o is positive,

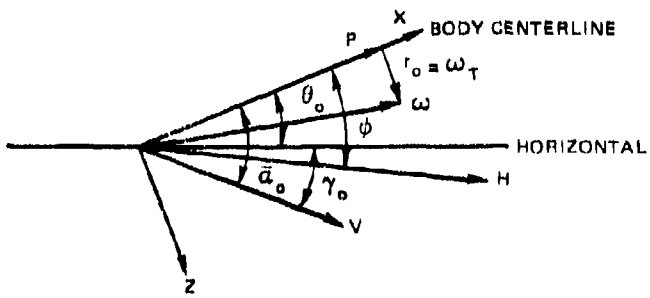

the angular momentum vector is directed to the right of the trajectory so that the nose of the vehicle remains in or to the right of the trajectory plane. Similarly, if q_o is negative, the vehicle nose is always in or to the left of the trajectory plane.

4.4.2 Zero Gyroscopic Forces

Consider next the case where the aerodynamic terms are much greater than the gyroscopic terms (body rate terms). In addition we will make the following assumptions:

1. The trajectory region of interest is over a very short time period so that the dynamic pressure is constant.
2. The roll rate is zero.
3. The pitching motion is planar (i.e., only pitch or only yaw motion).
4. $\bar{\alpha}$ is small so that the use of linearized derivatives is valid, and $\cos \bar{\alpha} \approx 1$; $\sin \bar{\alpha} \approx \bar{\alpha}$.

Suppose that at some point along the trajectory the vehicle is perturbed to some $\bar{\alpha} = \bar{\alpha}_o$. We wish to study the

resulting motion of the vehicle under the influence of just aerodynamic forces. The geometry of the trajectory is shown in the diagram.

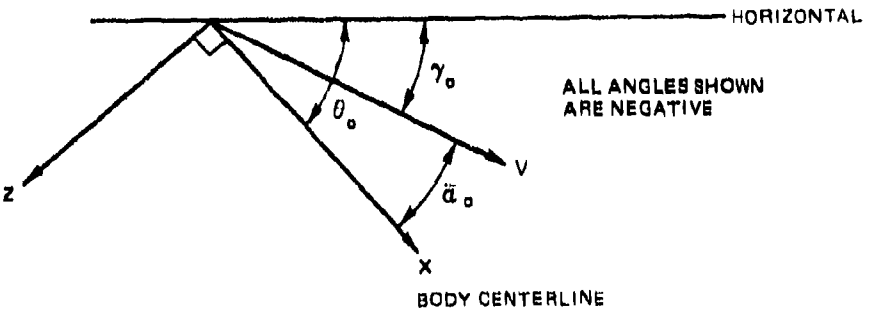

From Eqs. (4.4-2) and (4.4-8):

$$\dot{q}I_Y = F_Z \Delta X + M_q q \ .$$

From the geometry of the trajectory:

$$\left.\begin{aligned} \theta &= \gamma + \bar{\alpha} \\ \dot{\theta} = q &= \dot{\gamma} + \dot{\bar{\alpha}} \\ \ddot{\theta} = \dot{q} &= \ddot{\gamma} + \ddot{\bar{\alpha}} \end{aligned}\right\} \ . \qquad (4.4\text{-}26)$$

From Eqs. (4.4-6) and (4.4-26), using a small $\bar{\alpha}$ approximation, and noting that $u = V \cos \bar{\alpha}$ and $w = V \sin \bar{\alpha}$, it may be shown that:

$$\dot{\gamma} = - \frac{F_Z g}{WV} \ . \qquad (4.4\text{-}27)$$

Using the linear relationship between C_N and $\bar{\alpha}$:

$$\left.\begin{aligned} F_Z &= - C_{N_\alpha} \bar{\alpha} \bar{q} S \\ \dot{F}_Z &= - C_{N_\alpha} \dot{\bar{\alpha}} \bar{q} S \\ \ddot{F}_Z &= - C_{N_\alpha} \ddot{\bar{\alpha}} \bar{q} S \end{aligned}\right\} \quad . \tag{4.4-28}$$

Using Eqs. (4.4-25) through (4.4-28), it may be shown that the body motion is defined by the differential equation:

$$\ddot{\bar{\alpha}} + k_1 \dot{\bar{\alpha}} + k_2 \bar{\alpha} = 0 \tag{4.4-29}$$

where

$$k_1 = \frac{C_{N_\alpha} \bar{q} S}{\frac{W}{g} V} - \frac{C_{m_q} \bar{q} S d^2}{I_Y V} \tag{4.4-30}$$

$$k_2 = \frac{C_{N_\alpha} \Delta X \bar{q} S}{I_Y} - \frac{C_{m_q} C_{N_\alpha} (\bar{q} S d)^2}{\frac{W}{g} V^2 I_Y} \quad . \tag{4.4-31}$$

For bodies of interest, the C_{m_q} term of Eq. (4.4-31) is very small compared to the C_{N_α} term, and the equation for k_2 becomes:

$$k_2 = \frac{C_{N_\alpha} \Delta X \bar{q} S}{I_Y} \quad . \tag{4.4-32}$$

For statically stable vehicles, k_2 is positive, and the solution to Eq. (4.4-29) is:

$$\bar{\alpha} = e^{-\frac{k_1}{2}t}\left[C_1 \sin t\sqrt{k_2 - \frac{k_1^2}{4}} + C_2 \cos t\sqrt{k_2 - \frac{k_1^2}{4}}\right] \qquad (4.4\text{-}33)$$

where C_1 and C_2 are arbitrary constants defined by the initial conditions. Let $\bar{\alpha} = \bar{\alpha}_o$ and $\dot{\bar{\alpha}} = 0$ at $t = 0$ so that $C_2 = \bar{\alpha}_o$ and $C_1 = 0$ and Eq. (4.4-33) becomes:

$$\bar{\alpha} = \bar{\alpha}_o e^{-\frac{k_1}{2}} \cos t\sqrt{k_2 - \frac{k_1^2}{4}} \quad . \qquad (4.4\text{-}34)$$

Therefore, for a statically stable vehicle, the $\bar{\alpha}$ history is oscillatory and is damped (converges to zero) provided $k_1 > 0$. If $k_1 < 0$, $\bar{\alpha}$ diverges even though the vehicle is statically stable. Some flight tests of reentry vehicles have been observed to exhibit this type of $\bar{\alpha}$ divergence. To assure $\bar{\alpha}$ convergence, then:

$$\left.\begin{array}{ll} k_2 > 0 \text{ or } \Delta X > 0 & \text{static stability} \\ k_1 > 0 \text{ or } C_{N_\alpha} - C_{m_q}\dfrac{md^2}{I_Y} > 0 & \text{dynamic stability} \end{array}\right\} \qquad (4.4\text{-}35)$$

The frequency of the oscillation is given by the equation:

$$\omega_A = \sqrt{k_2 - \frac{k_1^2}{4}} \quad .$$

For most bodies $k_2 \gg \frac{k_1^2}{4}$ and the frequency becomes:

$$\omega_A = \sqrt{\frac{C_{N_\alpha} \Delta X \bar{q} S}{I_Y}} \quad . \tag{4.4-36}$$

This frequency, called the aerodynamic pitch frequency, is of great importance in the motion of reentry bodies as will be shown later. It should be noted that ω_A is zero at reentry ($\bar{q} = 0$) and, for constant C_{N_α} and ΔX, ω_A is proportional to $\sqrt{\bar{q}}$.

A solution to the equations of motion (Ref. 4-3), in which the dynamic pressure was allowed to vary, shows only small differences from the results given above except for very blunt bodies and nearly zero values of ΔX.

The aerodynamic frequency may be evaluated as a function of altitude (T, K) using equations derived in Section 4.3. From Eqs. (4.3.8) and (4.4.36):

$$\omega_A^2 = \frac{V_E^2 C_{N_\alpha} \Delta X m \sin(-\gamma)}{2 C_A I_Y H} \frac{K}{e^K} \tag{4.4-37}$$

4.4.3 Nonzero Gyroscopic and Aerodynamic Forces

At very high altitudes the dynamic motion of the body is governed by the gyroscopic terms in the equations of motion; at low altitudes where the dynamic pressure is high, the aerodynamic forces predominate. We look next at the transition from one region to the other.

Using the equations of Ref. 4-3 and the reentry characteristics given in Section 4.3, it may be shown that for $p = q = r = 0$ at reentry the $\bar{\alpha}$ history is defined by the equation:

$$\frac{\bar{\alpha}}{\bar{\alpha}_E} = \frac{J_o\left[-\frac{2\omega_A H}{V_E \sin\gamma} e^{\frac{K}{2}}\right]}{\exp\left|\frac{K}{4C_A}\left(C_{N_\alpha} - C_{m_q}\frac{md^2}{I_Y} - 2C_A\right)\right|} \quad (4.4\text{-}38)$$

where $J_o(X)$ is the zero order Bessel function of the first kind plotted in Fig. 4-12. Writing ω_A in terms of K using Eq. (4.4-37):

$$\frac{\bar{\alpha}}{\bar{\alpha}_E} = \frac{J_o\left(\sqrt{-\frac{2Hm}{\sin\gamma}\frac{C_{N_\alpha}\Delta X}{C_A I_Y}}\,K\right)}{\exp\left[\frac{K}{4C_A}\left(C_{N_\alpha} - C_{m_q}\frac{md^2}{I_Y} - 2C_A\right)\right]} \quad (4.4\text{-}39)$$

Therefore, for a given vehicle and trajectory, the $\bar{\alpha}$ history is a function of P and T only and P is the predominant factor. Even without the exponential damping function in the denominator of Eq. (4.4-39), the $\bar{\alpha}$ history is a damped oscillation about $\bar{\alpha} = 0$, and the frequency is the aerodynamic frequency, ω_A. For conditions near entry ($\frac{\bar{\alpha}}{\bar{\alpha}_E} \approx 1$), $K \approx 0$ so that the exponential term in Eq. (4.4-39) ≈ 1, and writing K in terms of P:

$$\frac{\bar{\alpha}}{\bar{\alpha}_E} \approx J_o\left(\sqrt{\frac{2SH}{g\sin^2\gamma}\frac{C_{N_\alpha}\Delta X}{I_Y}}\,P\right) = J_o(X) \quad (4.4\text{-}40)$$

Equation (4.4-40) may be used to determine the altitude (P) at which the atmosphere begins to affect the body motion. Arbitrarily selecting $\bar{\alpha}/\bar{\alpha}_E = 0.99$ as the condition when the atmosphere begins to affect the body motion, from the Bessel function tables, the argument, X, corresponding to $\bar{\alpha}/\bar{\alpha}_E = 0.99$ is 0.2.

$$\therefore \quad P = \frac{0.02\, I_Y g \sin^2 \gamma}{SHC_{N_\alpha} \Delta X} \quad . \tag{4.4-41}$$

The altitude for the first peak in $\bar{\alpha}$ corresponding to $X = 3.83$ shown in Fig. 4-12 may be obtained from:

$$P = \frac{7.34\, I_Y g \sin^2 \gamma}{SHC_{N_\alpha} \Delta X} \quad . \tag{4.4-42}$$

The $\bar{\alpha}$ envelope could be obtained directly from $J_o(X)$ tables; however, for $\bar{\alpha}/\bar{\alpha}_E$ less than about 0.8, $J_o(X)$ is approximated quite closely by the equation:

$$J_o(X) = \frac{\cos\left(\frac{\pi}{4} - X\right)}{\sqrt{\frac{\pi}{2} X}} \quad . \tag{4.4-43}$$

Therefore, the envelope corresponding to Eq. (4.4-38) is:

$$\frac{\bar{\alpha}}{\bar{\alpha}_E} = \frac{\sqrt{\frac{-V_E \sin \gamma}{\pi \omega_A H}}}{e^{C_3 K}} \tag{4.4-44}$$

where

$$C_3 = \frac{1}{4} \left(\frac{C_{N_\alpha}}{C_A} - \frac{C_{m_q}}{C_A} \frac{md^2}{I_Y} - 1 \right) \tag{4.4-45}$$

and is primarily the aerodynamic damping term. At high altitudes where e^K and $e^{C_3 K} \approx 1$:

$$\frac{\bar{\alpha}}{\bar{\alpha}_E} = \left[\frac{2gI_Y \sin^2\gamma}{\pi^2 SHC_{N_\alpha} \Delta XP}\right]^{1/4} , \qquad (4.4\text{-}46)$$

The α convergence at high altitudes is a function of body mass characteristics (I_Y, S, $X_{c.g.}$), aerodynamic characteristics (C_{N_α}, $X_{c.p.}$), type of trajectory (γ), and atmospheric properties (T, P). For a given trajectory, mass, and aerodynamic characteristics, $\bar{\alpha}$ is inversely proportional to $\sqrt[4]{TP}$ or approximately to $\sqrt[4]{P}$. For a given mass, aerodynamic characteristics, and altitude, the $\bar{\alpha}$ convergence is proportional to $\sqrt{\sin\gamma}$. That is, at a given altitude, the $\bar{\alpha}$ for a shallow trajectory will have converged more than that for a steep trajectory. Increasing C_{N_α} and ΔX tends to increase the convergence at a given altitude; increasing I_Y/S tends to decrease the convergence.

If $p \neq 0$ at reentry, the early $\bar{\alpha}$ history is changed. The gyroscopic terms tend to maintain the body motion about the angular momentum vector, which is fixed in space and usually is not directed along the velocity vector. The aerodynamic terms tend to cause oscillation about the velocity vector. As a result, in the initial phase of reentry, $\bar{\alpha}$ oscillates about an angle of attack which, itself, is gradually reduced as the aerodynamic forces increase. The equations defining α and β for the case of $\omega_T = 0$ are (Ref. 4-4):

$$\left.\begin{aligned} \alpha &= A\cos\bar{\omega}t \\ \beta &= -A\sin\bar{\omega}t \end{aligned}\right\} \qquad (4.4\text{-}47)$$

$$A = \frac{\bar{\alpha}_E \left[\sqrt{\omega_A{}^2 + \left(\frac{1}{2} \frac{I_X}{I_Y} p \right)^2} + \frac{1}{2} \frac{I_X}{I_Y} p \right]}{2 \sqrt{\omega_A{}^2 + \left(\frac{1}{2} \frac{I_X}{I_Y} p \right)^2}} \qquad (4.4\text{-}48)$$

$$\bar{\omega} = \sqrt{\omega_A{}^2 + \left(\frac{1}{2} \frac{I_X}{I_Y} p \right)^2} - \frac{1}{2} \frac{I_X}{I_Y} p \quad . \qquad (4.4\text{-}49)$$

In the initial phase of reentry where $\omega_A \ll \frac{1}{2} \frac{I_X}{I_Y} p$, the $\bar{\alpha}$ envelope is given by:

$$\frac{\bar{\alpha}}{\bar{\alpha}_E} \approx \left[1 - \left(\frac{\omega_A}{\frac{I_X}{I_Y} p} \right)^2 \right] \quad , \qquad (4.4\text{-}50)$$

Where ω_A is not small compared to $\frac{1}{2} \frac{I_X}{I_Y} p$, it may be shown (Ref. 4-5) that the ratio $\bar{\alpha}$ with roll to $\bar{\alpha}$ without roll is given by the equation:

$$\frac{\bar{\alpha}_p}{\bar{\alpha}_{p=0}} = \sqrt{\frac{a}{\tanh a}} \qquad (4.4\text{-}51)$$

$$a = \frac{-\pi}{2} \frac{HpI_X}{V_E I_Y \sin \gamma} \quad . \qquad (4.4\text{-}52)$$

For values of a greater than about 3, tanh a = 1, and the $\bar{\alpha}$ history corresponding to Eq. (4.4-44) is:

$$\frac{\bar{\alpha}}{\bar{\alpha}_E} = \frac{\sqrt{\frac{1}{2}\frac{I_X}{I_Y}\frac{p}{\omega_A}}}{e^{C_3 K}} \quad . \tag{4.4-53}$$

Therefore, at high altitudes where $e^{C_3 K} \approx 1$, the $\bar{\alpha}$ envelope converges to $\bar{\alpha} = 0$ in proportion to $\sqrt{p/\omega_A}$.

For a nonrolling vehicle at reentry, $\bar{\alpha}$ begins to decrease when the aerodynamic moment is sufficiently high, and this altitude can be estimated using Eq. (4.4-41). For a rolling vehicle, $\bar{\alpha}$ begins to decrease when the aerodynamic moment is significant relative to the gyroscopic moment. This altitude may be estimated using Eq. (4.4-50) and solving for ω_A at $\frac{\bar{\alpha}}{\bar{\alpha}_E} = 0.99$, so that:

$$\frac{\omega_A}{p} = 0.1\,\frac{I_X}{I_Y} \quad . \tag{4.4-54}$$

Substituting for $\omega_A{}^2$ using Eq. (4.4-37) and assuming $e^K = 1$:

$$\rho = \frac{P}{RT} = \frac{0.02 I_X{}^2}{I_Y C_{N_\alpha} \Delta X S V_E{}^2}\, p^2 \quad . \tag{4.4-55}$$

A rapid convergence in $\bar{\alpha}$ is desirable in order to prevent excessive lateral loads resulting from the $\bar{\alpha}_E$. The lateral load factor is given by:

$$g_L = \frac{N}{W} = C_{N_\alpha} \bar{\alpha}_E \frac{S}{W} \bar{q} \frac{\bar{\alpha}}{\bar{\alpha}_E} \quad . \tag{4.4-56}$$

For a nonrolling vehicle, using $\bar{\alpha}/\bar{\alpha}_E$ from Eq. (4.4-44) and $\bar{q}$ from Eq. (4.3-8), it may be shown that the maximum envelope of g_L is given by:

$$\frac{g_L}{\bar{\alpha}_E} = -\frac{V_E^2 \sin\gamma}{gH}\left[\frac{-\sin\gamma}{8\pi}\left(\frac{C_{N_\alpha}}{C_A}\right)^3\left(\frac{I_Y}{md^2}\right)\left(\frac{d^2}{\Delta X\, H}\right)\right]^{1/4}\frac{K^{3/4}}{C_4 K_e} \quad (4.4\text{-}57)$$

$$C_4 = \frac{1}{2}\left[1+\frac{1}{2}\left(\frac{C_{N_\alpha}}{C_A}-\frac{C_{m_q}}{C_A}\frac{md^2}{I_Y}\right)\right] = C_3 + 0.75 \quad (4.4\text{-}58)$$

Neglecting the small variation in H with K, the maximum occurs at:

$$K = \frac{3}{4}\frac{1}{C_4} \quad . \quad (4.4\text{-}59)$$

Using Eq. (4.4-59) and substituting for the constants in Eq. (4.4-57), the magnitude of $(g_L/\bar{\alpha}_E)_{max}$ is given by:

$$\left(\frac{g_L}{\bar{\alpha}_E}\right)_{max} = 0.128\frac{V_E^2}{gH}(-\sin\gamma)^{5/4}\left(\frac{C_{N_\alpha}}{C_5}\right)^{3/4}\left(\frac{I_Y}{m\,\Delta X H}\right)^{1/4} \quad (4.4\text{-}60)$$

where

$$C_5 = \frac{1}{2}C_A + \frac{1}{4}C_{N_\alpha} - \frac{1}{4}C_{m_q}\frac{md^2}{I_Y} = C_A C_4 \quad . \quad (4.4\text{-}61)$$

In evaluating Eq. (4.4-60), $\bar{\alpha}_E$ must be in radians.

The corresponding equations for a rolling vehicle at reentry are:

$$\frac{g_L}{\bar{\alpha}_E} = 0.42 \left[\left(\frac{C_{N_\alpha}}{C_A} \right)^3 \left(\frac{I_X}{I_Y} \right)^2 \left(\frac{dp^2}{g} \right) \left(\frac{-V_E^2 \sin\gamma}{gH} \right)^3 \left(\frac{L_Y}{md^2} \right) \left(\frac{d}{\Delta X} \right) \right]^{1/4} \frac{K^{3/4}}{C_4 R} \qquad (4.4\text{-}62)$$

and

$$\left(\frac{g_L}{\bar{\alpha}_E} \right)_{max} = 0.16 \left(\frac{V_E^2}{gH} \right)^{3/4} (-\sin\gamma)^{3/4} \left(\frac{C_{N_\alpha}}{C_5} \right)^{3/4} \left(\frac{I_X}{I_Y} \right)^{1/2} \left(\frac{L_Y p^2}{W \Delta X} \right)^{1/4} . \qquad (4.4\text{-}63)$$

The maximum value of g_L for a rolling vehicle also occurs at $K = \frac{3}{4} \frac{1}{C_4}$.

The ratio of maximum g_L for a rolling vehicle to maximum g_L for a nonrolling vehicle, obtained from Eqs. (4.4-60) and (4.4-63), is:

$$\frac{g_{L_p}}{g_{L_{p=0}}} = 1.25 \left[\frac{-Hp}{V_E \sin\gamma} \frac{I_X}{I_Y} \right]^{1/2} . \qquad (4.4\text{-}64)$$

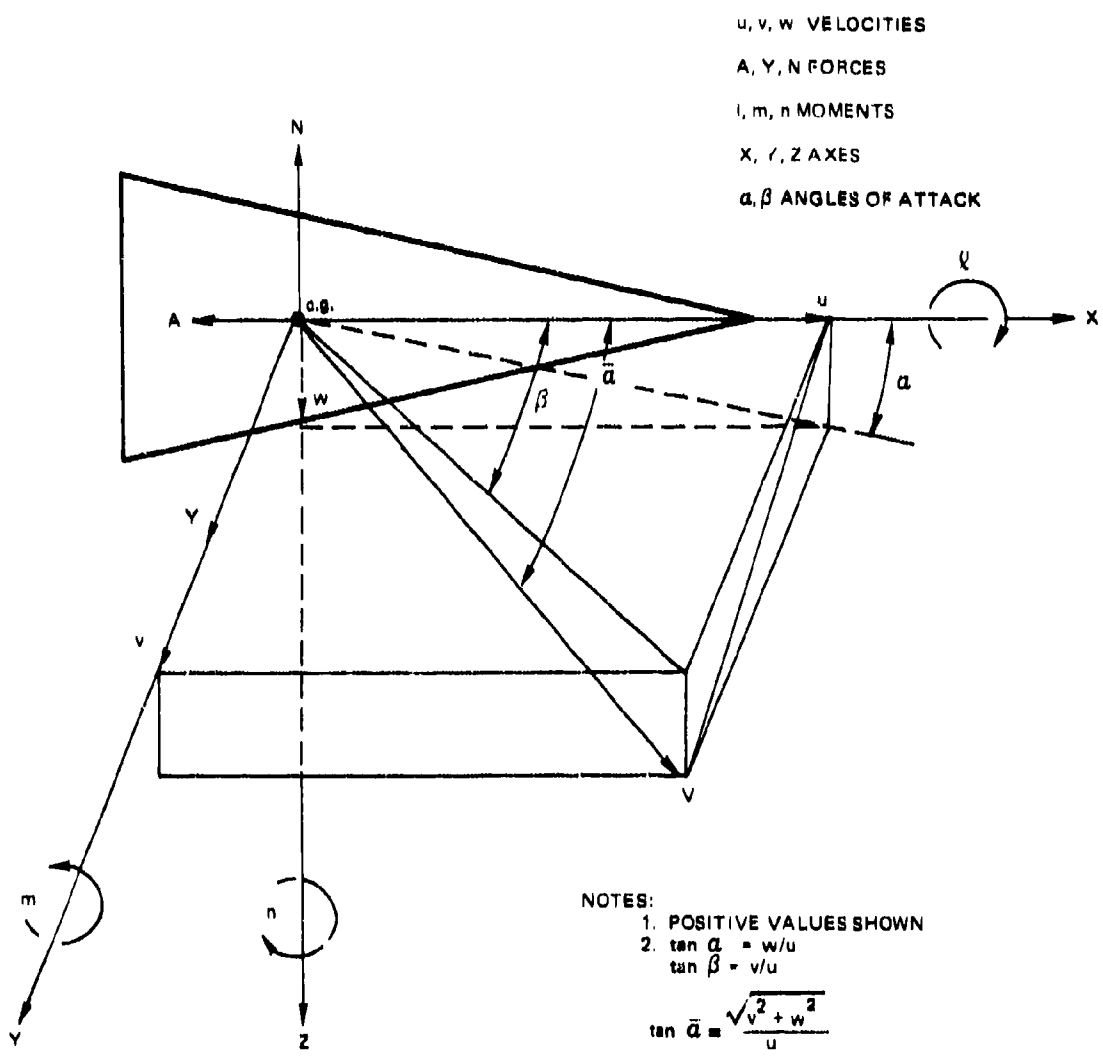

Fig. 4-11 BODY AXIS SYSTEM

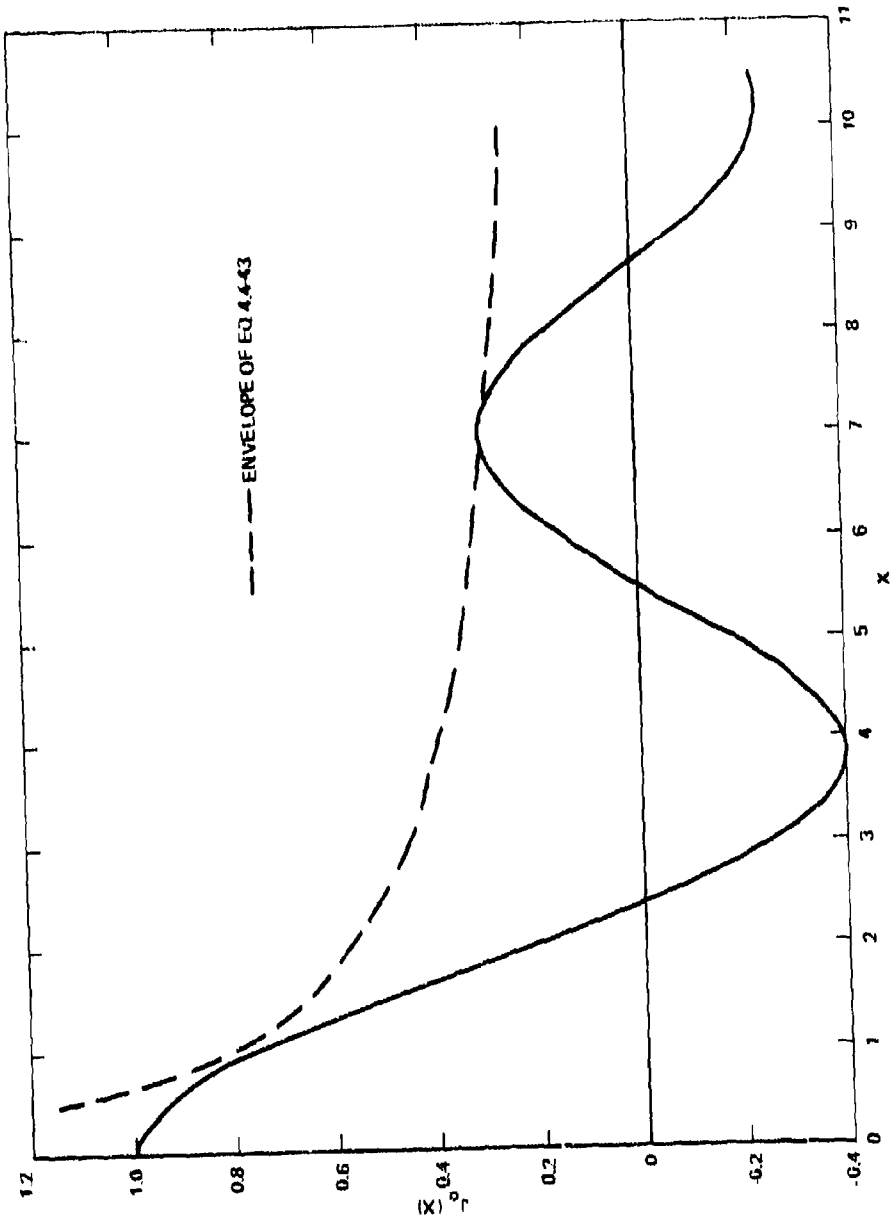

Fig. 4-12 VARIATION OF $J_o(X)$ WITH X

4.5 EFFECTS OF ASYMMETRIES

SYMBOLS FOR SECTION 4.5

Symbol	Definition	Typical Units
A	amplification factor in angle of attack	-
a, a_1, a_2	constants defined by Eqs. (4.5-82), (4.5-87), and (4.5-88)	-
C_A	axial force coefficient	-
C_ℓ	roll moment coefficient, $\ell/\bar{q}Sd$	-
C_{ℓ_p}	roll damping coefficient, $\partial C_\ell/\partial(pd/V)$	-
C_m	pitching moment coefficient, $m/\bar{q}Sd$	-
C_{m_o}	pitching moment coefficient at $\alpha = 0$	-
$\bar{C}_{m_o}$	$\sqrt{C_{m_o}^2 + C_{n_o}^2}$	-
C_{m_q}	pitch damping coefficient, $\partial C_m/\partial(qd/V)$	-
C_N	normal force coefficient	-
C_{n_o}	yawing moment coefficient at $\beta = 0$	-
C_{N_α}	$dC_N/d\alpha$	-
C_1, C_2	constants in Eq. (4.5-110)	rad/sec
c.g.	center of gravity	-
c.p.	center of pressure	-
D	damping function defined by Eq. (4.5-20)	-
d	reference diameter	feet
F	$\sqrt{F_Y^2 + F_Z^2}$	pounds
F_A	asymmetry factor defined by Eq. (4.5-72)	-

Preceding page blank

Symbol	Definition	Typical Units
F_X, F_Y, F_Z	forces along the X, Y, Z body axes	pounds
F_α	$C_{N_\alpha} \bar{q}S$	lb/rad
$F(\lambda, D)$	function defined by Eq. (4.5-47)	-
F_1, F_2	factors defined by Eqs. (4.5-62) and (4.5-73)	-
F_3, F_4	factors defined by Eq. (4.5-125)	-
G	roll amplification factor defined by Eq. (4.5-37)	-
G_R	G required for roll "lock-in"	-
G'	roll amplification factor defined by Eq. (4.5-80)	-
g	acceleration of gravity	ft/sec^2
g_X	longitudinal acceleration	g
G_1, G_2	roll amplification factors defined by Eqs. (4.5-81) and (4.5-84)	-
H	scale height, RT/g	feet
h	altitude	feet
I_X, I_Y, I_Z	moments of inertia about X, Y, Z axes	$slug\text{-}ft^2$
I_{XY}, I_{XZ}, I_{YZ}	products of inertia about X, Y, Z axes (Eqs. (4.5-99) to (4.5-101))	$slug\text{-}ft^2$
K	$-P/(\beta \sin\gamma)$	-
k, k_1	constants defined by Eqs. (4.5-59) and (4.5-60)	-
ℓ, m, n	aerodynamic moments about X, Y, Z	lb-ft
ℓ_o, m_o, n_o	asymmetric moments about X, Y, Z	lb-ft
M	Mach number	-
M_p	roll damping moment/p	lb-ft-sec

Symbol	Definition	Typical Units
M_q	pitch damping moment/q	lb-ft-sec
M_r	yaw damping moment/r	lb-ft-sec
m	vehicle mass	slugs
P	ambient air pressure	lb/ft^2
$\overline{P}$	probability	-
p, q, r	body rates about the X, Y, Z axes	rad/sec
p_r	reduced roll rate = $p\sqrt{1 - I_X/I_Y}$	rad/sec
$\dot{p}_{0_{max}}$	roll acceleration term defined by Eq. (4.5-38)	rad/sec^2
Δp	$p - p_E$	rad/sec
$\overline{q}$	dynamic pressure $(\gamma/2)PM^2$	lb/ft^2
R	gas constant = 1716	$ft^2/sec^2 - °R$
r	radial c.g. offset, always positive	feet
S	reference area	ft^2
T	ambient air temperature	°R
t	time	seconds
V	vehicle velocity	ft/sec
W	vehicle weight	pounds
$X_{c.g.}$	distance from vehicle nose to the c.g.	feet
$X_{c.p.}$	distance from vehicle nose to the c.p.	feet
ΔX	$X_{c.p.} - X_{c.g.}$	feet
$Y_{c.g.}$, $Z_{c.g.}$	center of gravity offset along Y and Z axis	feet
α	angle of attack in the XZ plane	radians
α_δ	angle of attack resulting from δ in the XZ plane at $\lambda \to \infty$	radians

Symbol	Definition	Typical Units
$\bar{\alpha}$	total vector angle of attack = $\sqrt{\alpha^2 + \beta^2}$	radians
$\bar{\alpha}_\delta$	$\sqrt{\alpha_\delta^{\ 2} + \beta_\delta^{\ 2}}$	radians
β	angle of attack in the XY plane or ballistic coefficient, $W/C_A S$	radians lb/ft^2
β_δ	angle of attack resulting from δ in the XY plane at $\lambda \to \infty$	radians
δ_α	inclination of principal axis in the XZ plane	radians
δ_β	inclination of principal axis in the XY plane	radians
δ	$\sqrt{\delta_\alpha^{\ 2} + \delta_\beta^{\ 2}}$	radians
ϵ	angle defined by Eq. (4.5-83)	degrees
γ	reentry flight path angle, always negative or ratio of specific heat, 1.4	degrees -
ϕ	space cone half-angle or angle defined by Eq. (4.5-31)	degrees degrees
θ	$\sin^{-1} \dfrac{\bar{\alpha}_{o_{c.g.}}}{\bar{\alpha}_{o_M}}$	degrees
λ	p_r/ω_A	-
Λ	$\cos^{-1}\left[\dfrac{(\bar{\alpha}_o\ r/d)_{min}}{\bar{\alpha}_o\ r/d}\right]$	degrees

Symbol	Definition	Typical Units
ψ	angle defined in Section 4.5.1	degrees
$\Delta\psi$	angle defined in Section 4.5.1	degrees
τ_s	period of oscillation	seconds
ω_A	aerodynamic pitch frequency	rad/sec
ω_g	$p(1 - I_X/I_Y)$	rad/sec
$\vec{\omega}_T$	transverse rate vector, $\vec{q} + \vec{r}$	rad/sec

Subscripts

c.g.	refers to c.g. or is caused by c.g. offset
E	refers to reentry condition
e	refers to equilibrium condition
i	refers to conditions at $t = 0$ or to an elementary quantity
M	caused by asymmetric moments
max	refers to maximum value
min	refers to minimum value
o	refers to conditions at $p = 0$
R	refers to resonance conditions
S.L.	refers to sea level conditions

A dot over a symbol means the first derivative with respect to time.
Two dots over a symbol means the second derivative with respect to time.
An arrow over a symbol means a vector quantity.

SUMMARY AND CONCLUSIONS

A reentry body is normally spun about its longitudinal axis to provide stability during the exoatmospheric phase of flight and to reduce dispersion resulting from phenomena that occur during reentry. Ideally, the roll rate remains nearly constant during reentry. However, under the influence of mass and aerodynamic asymmetries, the roll rate may change radically. Under certain conditions the roll rate may change so that the roll rate and the aerodynamic pitch frequency are nearly the same for long intervals of time. When this occurs the roll rate is said to "lock-in" with the aerodynamic frequency. This situation is sometimes disastrous since the angles of attack and thus the lateral loads become very large. The loading situation may be aggravated further by aerothermoelastic interaction. On the other hand, the asymmetries may cause the magnitude of the roll rate to decrease and change sign. In this case the missile will be driven off course in proportion to and in the direction of the lateral loads existing at the time the roll rate is nearly zero. Even if the roll rate passes rapidly through zero roll rate, the impact dispersion may be excessive for high performance vehicles.

The six-degree-of-freedom equations are modified to include various types of asymmetry, and the conditions under which excessive loads and/or dispersion may exist are discussed.

The major conclusions are:

1. The effects on body motion of aerodynamic asymmetries (abnormal pitching, yawing, and rolling moments, and center of pressure offset from the longitudinal axis of the missile) and mass asymmetries (center of gravity offset from the longitudinal axis of the missile, products of inertia, and unequal pitch and yaw moments of inertia) are considered. All asymmetries considered

have some effect on body motion. However, for reasonable magnitudes of asymmetry, the effects of unequal pitch and yaw moments of inertia are negligible, the effects of any one of the other asymmetries are small, but the effects on vehicle performance of some combinations of the asymmetries may be catastrophic.

2. Unacceptable vehicle performance is likely if either resonance (resulting in large lateral loads) or zero roll rate (resulting in large impact dispersion) occurs during reentry. In either case the asymmetries must cause both a trim angle of attack and a roll torque. Therefore, a center of gravity offset combined with either an asymmetric pitching (or yawing) moment or with nonzero products of inertia or a pure rolling moment asymmetry combined with either of these asymmetries is apt to result in unacceptable performance.

3. The conditions under which adverse performance is likely to occur are dependent upon many variables so that each vehicle must be analyzed separately. Nevertheless, the following trends may be stated. The probability of encountering difficulties resulting from combined asymmetries is increased for missiles:

- o Having low stability margin
- o Having resonance at an altitude near maximum dynamic pressure
- o Having low normal force per degree angle of attack and/or a low pitch damping moment
- o Flying shallow trajectories
- o Having slender shapes
- o Having small dimensions.

4. Detailed equations are presented for evaluating the probability of encountering "lock-in" or spin through zero roll rate for a missile of any arbitrary design. Comments are made regarding the accuracy of these equations. Illustrations of the use of these equations are given in Examples 5, 6, and 7, Section 4.6.

In the derivation of the equations given in Section 4.4, it was assumed that the body was symmetrical. We consider next the effects on vehicle motion of asymmetry in mass and external shape.

Asymmetries in mass and external shape result from design and manufacturing tolerances or from in-flight phenomena and may cause one or more of the following anomalies:

Aerodynamics

1. A change in normal force characteristics
2. A change in pitching moment characteristics
3. A lateral shift in center of pressure
4. A pure roll torque.

Mass

5. A lateral shift in center of gravity
6. Nonzero products of inertia
7. Unequal pitch and yaw moments of inertia.

The effect of asymmetries on normal force is usually negligible but the effect on the pitching moment is very significant. A lateral shift in the center of pressure has the same effect as a lateral shift in the center of gravity, and these two effects will be combined in the following discussion. For convenience, the effect will be referred to as a center of gravity offset effect, but it is important to remember that the same effect results from a center of pressure offset. This section will be limited to the following asymmetries:

1. Asymmetric moment, m_o and n_o
2. Center of gravity offset, $Z_{c.g.}$ and $Y_{c.g.}$
3. Nonzero products of inertia, I_{XY} and I_{XZ}

4. Unequal pitch and yaw moments of inertia

5. Pure roll torque, ℓ_o.

The asymmetries have negligible effect on all portions of the trajectory except for the reentry phase.

To account for the asymmetries, the equations given in Section 4.4 must be modified to the following (see the sketch on page 170):

$$\dot{p} I_X = \ell - qr(I_Z - I_Y) + I_{XY}(\dot{q} - pr) + I_{XZ}(\dot{r} + pq) + I_{YZ}(q^2 - r^2) \qquad (4.5\text{-}1)$$

$$\dot{q} I_Y = m - pr(I_X - I_Z) + I_{XY}(\dot{p} + rq) + I_{XZ}(r^2 - p^2) + I_{YZ}(\dot{r} - pq) \qquad (4.5\text{-}2)$$

$$\dot{r} I_Z = n - pq(I_Y - I_X) + I_{XY}(p^2 - q^2) + I_{XZ}(\dot{p} - rq) + I_{YZ}(\dot{q} + pr) \qquad (4.5\text{-}3)$$

$$\ell = M_p p + F_Y Z_{c.g.} - F_Z Y_{c.g.} + \ell_o \qquad (4.5\text{-}4)$$

$$m = F_Z \Delta X + M_q q - F_X Z_{c.g.} + m_o \qquad (4.5\text{-}5)$$

$$n = - F_Y \Delta X + M_r r + F_X Y_{c.g.} + n_o \qquad (4.5\text{-}6)$$

4.5.1 Effect of Asymmetric Moment

Assuming that only an asymmetric moment (m_o and n_o) exists, Eq. (4.5-1) reduces to:

$$\dot{p} I_X = M_p p \,, \qquad (4.5\text{-}7)$$

Therefore the roll rate decreases slightly under the influence of viscous damping, M_p. The trim equations ($\dot{q} = \dot{r} = 0$) become:

$$F_Z \Delta X + M_q q + m_o = pr(I_X - I_Z) \,, \qquad (4.5\text{-}8)$$

$$-F_Y \Delta X + M_r r + n_o = pq(I_Y - I_X) \,. \qquad (4.5\text{-}9)$$

Consider first the trim conditions for p = 0. The pitch damping terms are negligible for this case, and the trim equations become:

$$F_{Z_o} = -\frac{m_o}{\Delta X} \quad . \tag{4.5-10}$$

$$F_{Y_o} = \frac{n_o}{\Delta X} \quad . \tag{4.5-11}$$

Writing F_Y and F_Z in terms of α and β (Eqs. (4.4-13) to (4.4-15)) and expressing m_o and n_o in coefficient form ($m_o = C_{m_o} \bar{q} S d$ and $n_o = C_{n_o} \bar{q} S d$):

$$\alpha_o = \frac{C_{m_o}}{C_{N_\alpha} \frac{\Delta X}{d}} \quad . \tag{4.5-12}$$

$$\beta_o = -\frac{C_{n_o}}{C_{N_\alpha} \frac{\Delta X}{d}} \quad . \tag{4.5-13}$$

The total angle of attack is:

$$\bar{\alpha}_o = \frac{\left[\left(C_{m_o}\right)^2 + \left(C_{n_o}\right)^2\right]^{1/2}}{C_{N_\alpha} \frac{\Delta X}{d}} = \frac{\bar{C}_{m_o}}{C_{N_\alpha} \frac{\Delta X}{d}} \tag{4.5-14}$$

and the plane of $\bar{\alpha}_o$ defined by the direction of F_o is given by the equation:

$$\cot \psi_o = \frac{F_{Y_o}}{F_{Z_o}} = \frac{C_{n_o}}{-C_{m_o}} = \frac{-\beta_o}{-\alpha_o} \quad . \tag{4.5-15}$$

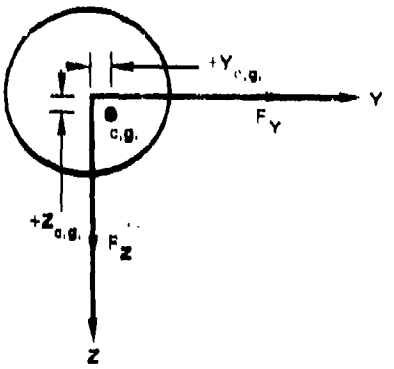

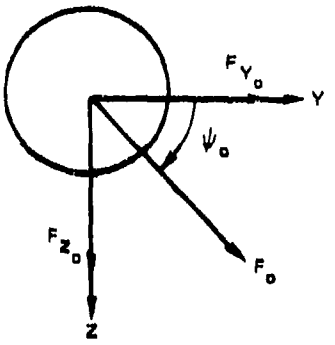

Note that for ψ_o = 0° to 90° β is - and α is -
= 90° to 180° β is + and α is -
= 180° to 270° β is + and α is +
= 270° to 360° β is - and α is +

The angle ψ_o also defines the plane of the asymmetry. That is, for zero roll rate the total angle of attack, $\bar{\alpha}_o$, is in a plane containing the asymmetry. For example, if the asymmetry results from a flat spot on the body, the flat is located at a circumferential location $\psi = \psi_o$ or $\psi = \psi_o + 180°$ (depending upon the fore and aft location of the asymmetry).

The effect of roll rate is to modify the magnitude of $\bar{\alpha}$ and to cause the total lateral force to be rotated out of the plane of the asymmetry. These effects are given by the following equations (Ref. 4-6) based on theory given in Refs. 4-7 and 4-8.

$$A = \left|\frac{\bar{\alpha}}{\bar{\alpha}_o}\right| = \left[(1 - \lambda^2)^2 + D^2\lambda^2 \right]^{-1/2} \qquad (4.5\text{-}16)$$

$$\tan \Delta\psi = \frac{-D\lambda}{1 - \lambda^2} \qquad (4.5\text{-}17)$$

$$A \cos \Delta\psi = \frac{1 - \lambda^2}{(1 - \lambda^2)^2 + D^2\lambda^2} \qquad (4.5\text{-}18)$$

$$A \sin \Delta\psi = \frac{-D\lambda}{(1 - \lambda^2)^2 + D^2\lambda^2} \qquad (4.5\text{-}19)$$

$$D = \frac{\frac{F_\alpha}{mV}\left(1 - \frac{I_X}{I_Y}\right) - \frac{M_q}{I_Y}}{\omega_A\sqrt{1 - \frac{I_X}{I_Y}}} \qquad (4.5\text{-}20)$$

$$\lambda = \frac{p\sqrt{1 - \frac{I_X}{I_Y}}}{\omega_A} = \frac{p_r}{\omega_A} \qquad (4.5\text{-}21)$$

From Eq. (4.5-16) it is apparent that the amplification factor increases from 1 at $\lambda = 0$ to a maximum value $\left[D^2(1 - \frac{D^2}{4})\right]^{-1/2}$ at $\lambda = \sqrt{1 - \frac{D^2}{2}}$ and then decreases to 0 at $\lambda \to \infty$. Thus, at λ greater than about $\sqrt{2}$ (depending upon the value of D), the trim angle of attack is attenuated by the effects of roll rate. Typical values of D are of the order of 0 to 0.2 so that A_{max} occurs near $\lambda = 1$ and $A_{max} \approx 1/D$. The condition of $\lambda = 1$ is called the pitch-yaw-roll, or simply the roll resonance condition. Since

$I_X/I_Y \approx 0.1$, the resonance condition is very close to the condition $p/\omega_A = 1$. Note that near resonance the pitch damping term, D, plays a very important roll in limiting α.

The value of D is always positive for conditions (static and dynamic stability) for which Eqs. (4.5-16) and (4.5-17) are valid. Therefore, from Eq. (4.5-17) for positive roll rates the plane of $\bar{\alpha}$ for a rolling vehicle is rotated counterclockwise ($\Delta\psi$ is negative) from ψ_o. At resonance, the plane is rotated 90° from ψ_o; at very high values of λ, the plane is rotated 180° from ψ_o.

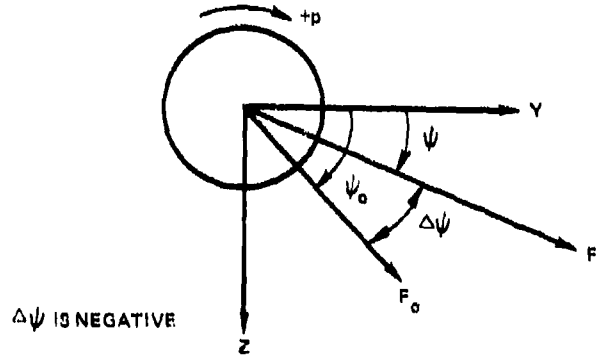

For example, assume that an angle of attack is produced by a flap at the aft end of the body as shown in the sketch on page 173.

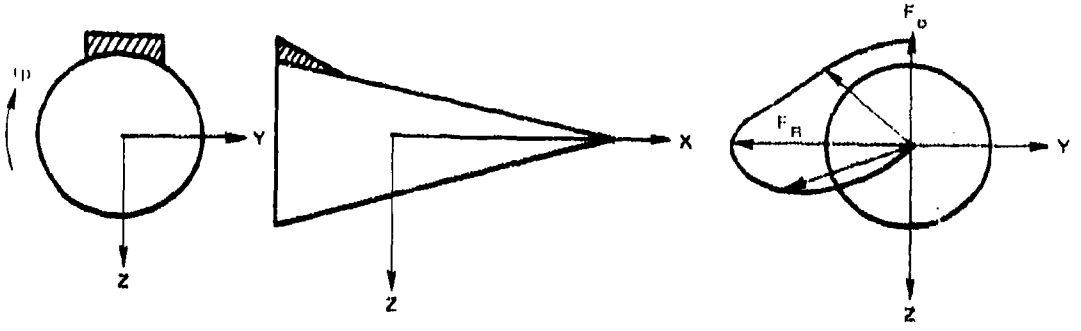

At zero roll rate, this flap produces a $+\alpha$ or a force $F = F_o$ along the -Z axis. As the roll rate increases in a positive direction, F rotates counterclockwise. At resonance $F = F_R = F_o/D$ and is directed along the -Y axis. As the roll rate increases further, F continues to rotate counterclockwise and decreases in magnitude. In the limit (very high roll rates) $F \rightarrow 0$ and is directed along the +Z axis.

To further illustrate the behavior of Eqs. (4.5-16) and (4.5-17), Fig. 4-13 shows plots of A and $\Delta\psi$ as functions of λ for D = 0 and 0.2. Note that neither A nor $\Delta\psi$ changes very rapidly for λ from 0 to about 0.5. Practically all the change in $\Delta\psi$ occurs from $\lambda = 0.8$ to 1.4. For λ greater than about 1.4, $\bar{\alpha}_o$ is attenuated.

The effect of damping is small except near $\lambda = 1$ where the effect on both A and $\Delta\psi$ is large. As the reentry body descends through the atmosphere, ω_A increases, and unless the body is given a very high spin rate the resonance condition will occur at least once during reentry. If $\bar{\alpha}_o$ were zero, the resonance condition

would have no effect on the trajectory. If the only asymmetry were the asymmetric moments (n_o and m_o), the effect of resonance would normally be minor since p is essentially constant (changes by viscous damping only) and ω_A would pass through the resonance condition too rapidly to produce significant changes in the trajectory. The $\bar{\alpha}$ would increase somewhat over the $\bar{\alpha}_o$ value, resulting in corresponding increases in body lift and drag, but the time duration would be short. Therefore, the effect of an asymmetric moment, by itself, has negligible effect on the trajectory for reasonable values of m_o and n_o.

4.5.2 Offset Center of Gravity

The effect on trim conditions of the center of gravity offset (again neglecting M_q) for p = 0 is given by:

$$F_Z = F_X \frac{Z_{c.g.}}{\Delta X} \tag{4.5-22}$$

$$F_Y = F_X \frac{Y_{c.g.}}{\Delta X} \tag{4.5-23}$$

Substituting for F_X, F_Y, and F_Z from Eqs. (4.4-12) through (4.4-15):

$$\alpha_o = \frac{C_A}{C_{N_\alpha}} \frac{Z_{c.g.}}{\Delta X} \tag{4.5-24}$$

$$\beta_o = \frac{C_A}{C_{N_\alpha}} \frac{Y_{c.g.}}{\Delta X} \tag{4.5-25}$$

$$\bar{\alpha}_o = \frac{C_A}{C_{N_\alpha}} \left[\left(\frac{Z_{c.g.}}{\Delta X} \right)^2 + \left(\frac{Y_{c.g.}}{\Delta X} \right)^2 \right]^{1/2} = \frac{r}{\Delta X} \frac{C_A}{C_{N_\alpha}} \tag{4.5-26}$$

The effect of roll rate is to modify the magnitude of $\bar{\alpha}_0$ and to change the plane in which it acts in accordance with Eqs. (4.5-16) and (4.5-17). However, unlike the aerodynamic asymmetry, the center of gravity offset affects the roll rate equation (see Eq. (4.5-4)). The effect on roll rate is illustrated by the sketch.

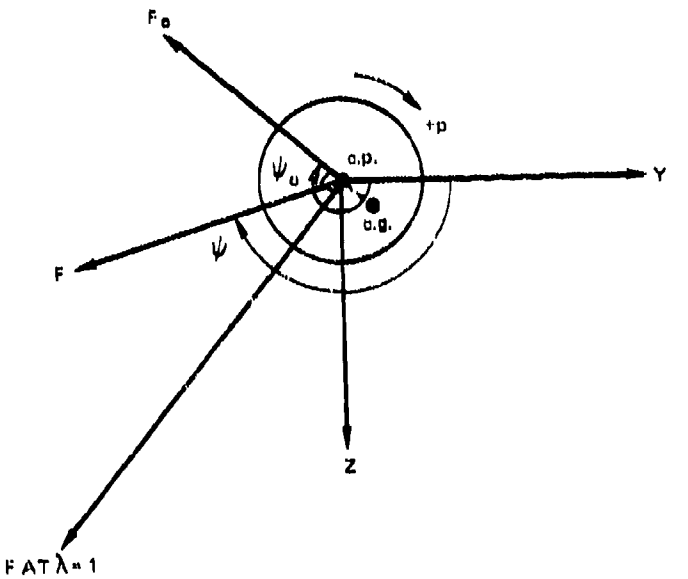

For zero roll rate, $\bar{\alpha}_0$ is in a plane containing the center of gravity, and F_0 acts through the center of pressure directed away from the center of gravity as shown by ψ_0. However, for a positive roll rate the force vector F is rotated counterclockwise from F_0 as explained previously. Therefore, F results in a negative roll torque that tends to decrease the roll rate. A similar argument for a negative roll rate shows that the center of gravity offset results in a positive roll torque, again tending to drive the roll rate toward zero. Therefore, the effect of the center of gravity offset alone behaves as a roll damping effect and, in fact, must be accounted for when attempting to extract C_{ℓ_p} from experimental roll rate decay data. For

reasonable values of the center of gravity offset, the effect on roll rate is small except near resonance where the roll moment arm is maximum (see sketch above).

4.5.3 Combined Asymmetry ($\bar{C}_{m_o}$ and r)

Both the center of gravity offset and asymmetric moment result in minor effects on the trajectory when considered separately. However, this is not the case when the two types of asymmetry are combined. Using the described procedures, the trim angles of attack at zero roll rate for this case are given by the equations:

$$\alpha_o = \frac{C_{m_o} + C_A \frac{Z_{c.g.}}{d}}{C_{N_\alpha} \frac{\Delta X}{d}} \qquad (4.5\text{-}27)$$

$$\beta_o = \frac{C_A \frac{Y_{c.g.}}{d} - C_{n_o}}{C_{N_\alpha} \frac{\Delta X}{d}} \qquad (4.5\text{-}28)$$

$$\bar{\alpha}_o = \left[\alpha_o^2 + \beta_o^2\right]^{1/2} \qquad (4.5\text{-}29)$$

The direction of F_o is given by the equation:

$$\cot \psi_o = \frac{-\beta_o}{-\alpha_o} = \frac{C_{n_o} - C_A \frac{Y_{c.g.}}{d}}{-C_{m_o} - C_A \frac{Z_{c.g.}}{d}} \quad . \qquad (4.5\text{-}30)$$

The proper quadrant for ψ_o is again determined as indicated in Section 4.5.1. An important variable for this combined asymmetry is the angle, ϕ, between the plane of the center of gravity and the plane of $\bar{\alpha}$.

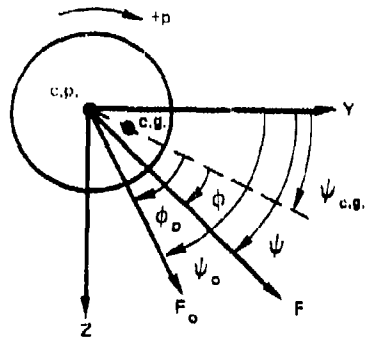

$$\emptyset = \psi - \psi_{c.g.} \qquad (4.5\text{-}31)$$

where

$$\cot \psi_{c.g.} = \frac{Y_{c.g.}}{Z_{c.g.}} \quad . \qquad (4.5\text{-}32)$$

$\psi_{c.g.}$ = 0° to 90° if $Y_{c.g.}$ is + and $Z_{c.g.}$ is +
= 90° to 180° if $Y_{c.g.}$ is - and $Z_{c.g.}$ is +
= 180° to 270° if $Y_{c.g.}$ is - and $Z_{c.g.}$ is -
= 270° to 360° if $Y_{c.g.}$ is + and $Z_{c.g.}$ is -

It must be assumed that the center of gravity offset and moment asymmetries are completely independent variables so that $\emptyset_o$ may have any value. For purposes of illustrating the significance of $\emptyset_o$ it is convenient to consider "in plane" asymmetries ($\emptyset_o$ = 0° or 180°) and "out of plane" asymmetries ($\emptyset_o$ = 90° or 270°). For the in plane asymmetry, if $\emptyset_o$ = 180°, the effect is the same as that

described previously for the center of gravity offset. If $\phi_o = 0°$, the magnitude of the roll rate will increase indefinitely ($\dot{p}$ is always positive) if the initial roll rate is positive and will always increase negatively if the initial roll rate is negative. This case is shown in the sketch.

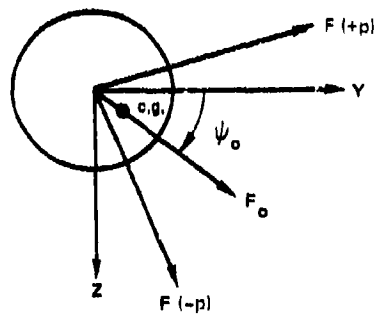

At p = 0, F_o passes through the center of gravity. If the roll rate is initially positive F must be counterclockwise from F_o as shown, so that a positive roll torque develops driving p to a larger positive value. Since F must lie between ψ_o and ψ_o - 180°, the roll torque is always positive. Similarly, if the initial roll rate is negative, the roll torque produced by the asymmetries is always negative.

For out of plane asymmetries, the case of $\phi_o = 90°$ is sketched for an initial positive roll rate. Let the asymmetric force be located initially at F (counterclockwise from F_o since p is positive). The roll torque is negative and p decreases. For decreasing p, λ decreases (assuming ω_A is constant) and F rotates clockwise. The roll rate becomes zero when $F = F_o$ and then the vehicle begins to spin up in the negative direction. This process continues

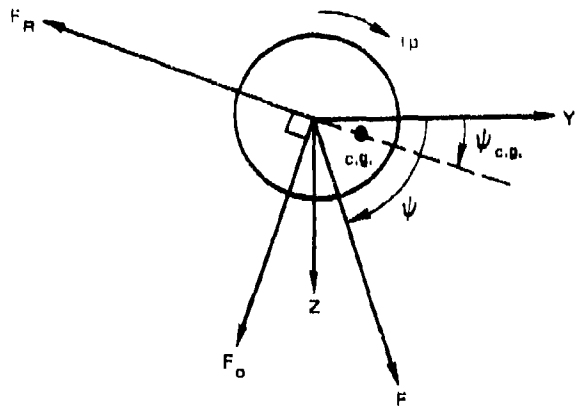

until F rotates 90° from F_o. This point is an equilibrium roll rate position, since at higher negative roll rates the roll torque becomes positive, driving F to a less negative roll rate. This equilibrium roll position also corresponds to the resonance condition. For ϕ_o = 270° the same phenomenon occurs except that the roll torque causes spin-up to resonance at positive roll rates and therefore does not spin through zero roll rate.

The potential problems resulting from these combined asymmetries are:

1. Excessive spin rates resulting in structural or payload failures
2. Prolonged periods of roll resonance resulting in high lateral loads and high drag (structural failure and excessive impact dispersion)
3. Spin through zero roll rate resulting in large impact errors (see Section 5.4.2).

Both in plane and out of plane components of the asymmetry can have disastrous results on vehicle performance. However, the in plane asymmetries are less likely to cause difficulty because significant roll torques are developed only at conditions near resonance. Also, this type of asymmetry cannot produce the problem of spin through zero.

4.5.4 Effect of Combined Asymmetries on Roll Rate

All the potential problems resulting from a combination of asymmetric moment and center of gravity offset listed in Section 4.5.3 exist because of changes in roll rate during reentry. In this section we will consider the roll behavior in more detail.

If $I_Y = I_Z$ and if the products of inertia are zero, the roll acceleration (Eq. (4.5.1)) becomes:

$$\dot{p} = \frac{M_p p + F_Y Z_{c.g.} - F_Z Y_{c.g.} + \ell_o}{I_X} \quad . \qquad (4.5\text{-}33)$$

Neglecting the roll damping and pure roll torque terms and expressing the numerator in terms of F, r, and ϕ:

$$\dot{p} = \frac{- Fr \sin \phi}{I_X} \quad . \qquad (4.5\text{-}34)$$

Since $F = C_{N_\alpha} \bar{q} S \bar{\alpha}$, Eq. (4.5-34) may be written:

$$\dot{p} = \frac{-C_{N_\alpha} \bar{q} S \bar{\alpha} r \sin \phi}{I_X} \quad . \qquad (4.5\text{-}35)$$

The roll acceleration may be written as a product of two terms:

$$\dot{p} = G \dot{p}_{o_{max}} \qquad (4.5\text{-}36)$$

where

$$G = -\frac{\bar{\alpha}}{\bar{\alpha}_o} \sin \phi = -A \sin \phi \qquad (4.5\text{-}37)$$

$$\dot{p}_{o_{max}} = \frac{C_{N_\alpha} \bar{q} S \bar{\alpha}_o r}{I_X} \quad . \qquad (4.5\text{-}38)$$

The G term contains the effects of roll rate and ϕ_o; the $\dot{p}_{o_{max}}$ term contains the body geometry, environmental, and basic asymmetry terms. Note that $\dot{p}_{o_{max}}$ is the positive roll acceleration that would exist for zero roll rate if the plane of $\bar{\alpha}_o$ were normal to the center of gravity plane (that is, $\phi_o = 270°$). Since $\phi = \phi_o + \Delta\psi$, Eq. (4.5-37) may be written:

$$G = -A \cos \Delta\psi \, (\sin \phi_o + \cos \phi_o \tan \Delta\psi) \, , \qquad (4.5\text{-}39)$$

Substituting for $\tan \Delta\psi$ and $A \cos \Delta\psi$ from Eqs. (4.5-17) and (4.5-18), Eq. (4.5-39) becomes:

$$G = \frac{D\lambda \cos \phi_o - (1 - \lambda^2) \sin \phi_o}{(1 - \lambda^2)^2 + D^2\lambda^2} \quad . \qquad (4.5\text{-}40)$$

We will define $\dot{p} = 0$ as the roll equilibrium condition. For this condition either $\dot{p}_{o_{max}}$ or G must be zero. For a reentry body in the sensible atmosphere ($\bar{q} \neq 0$), $\dot{p}_{o_{max}}$ is zero only if $\bar{\alpha}_o$ or r is zero. Generally, neither $\bar{\alpha}_o$ nor r is zero and the roll rate of a reentry body having combined asymmetries will vary until G = 0. Defining λ_e as the value of λ at G = 0, from Eq. (4.5-40), $\lambda_e = \pm\infty$, or λ_e must satisfy the equation:

$$\tan \phi_o = \frac{D\lambda_e}{1 - \lambda_e^2} \qquad (4.5\text{-}41)$$

Equation (4.5-41) may be solved for λ_e:

$$\lambda_e = \frac{-D \cot \phi_o \pm \sqrt{(D \cot \phi_o)^2 + 4}}{2} \ . \qquad (4.5\text{-}42)$$

For very large values of D cot ϕ_o ($\phi_o \approx 0°$ or 180°):

$$\lambda_e = 0 \ . \qquad (4.5\text{-}43)$$

For very small values of D cot ϕ_o ($\phi_o \approx 90°$ or 270°):

$$\lambda_e = 1 - \frac{D}{2} \cot \phi_o \quad \text{or} \quad -(1 + \frac{D}{2} \cot \phi_o) \ . \qquad (4.5\text{-}44)$$

Equation (4.5-42) is plotted as a function of D cot ϕ_o in Fig. 4-14.

The roll equilibrium condition, λ_e, may be stable or unstable; that is, if the roll rate is changed slightly, λ changes slightly from λ_e. If the roll torque developed at λ tends to drive λ back to λ_e, the equilibrium condition is stable; if the roll torque developed tends to drive λ away from λ_e, the condition is unstable. The λ_e condition is stable if $(dG/d\lambda)_{\lambda_e}$ is negative and unstable if $(dG/d\lambda)_{\lambda_e}$ is positive. It may be shown that $dG/d\lambda$ is given by:

$$\frac{dG}{d\lambda} = \frac{D \cos \phi_o \left[1 + (2 - D^2)\lambda^2 - 3\lambda^4\right] + 2\lambda \sin \phi_o \left[(D^2 - 1) + 2\lambda^2 - \lambda^4\right]}{\left[(1 - \lambda^2)^2 + D^2\lambda^2\right]^2} \ . \qquad (4.5\text{-}45)$$

Therefore, the condition for λ_e stability is that:

$$F(\lambda_e, D) > \tan \phi_o \qquad (4.5\text{-}46)$$

where

$$F(\lambda, D) = \frac{D\left[3\lambda^4 - (2 - D^2)\lambda^2 - 1\right]}{2\lambda\left[(D^2 - 1) + 2\lambda^2 - \lambda^4\right]} \quad . \qquad (4.5\text{-}47)$$

For in plane asymmetries the condition for stability reduces to:

$$\cos \phi_o \left| 1 + (2 - D^2)\lambda^2 - 3\lambda^4 \right| < 0 \quad . \qquad (4.5\text{-}48)$$

Since $\lambda_e = 0$, the condition is stable for $\phi_o = 180°$ and unstable for $\phi_o = 0°$.

For out of plane asymmetries, the condition for stability reduces to:

$$\sin \phi_o \, \lambda \left| (D^2 - 1) + 2\lambda^2 - \lambda^4 \right| < 0 \quad . \qquad (4.5\text{-}49)$$

Since $\lambda_e = \pm 1$, the condition is unstable for $\lambda_e = +1$ and $\phi_o = 90°$ or $\lambda_e = -1$ and $\phi_o = 270°$; the condition is stable for $\lambda_e = +1$ and $\phi_o = 270°$ or $\lambda_e = -1$ and $\phi_o = 90°$.

Another characteristic of interest is the maximum values of G. The term maximum is used to mean either a positive or negative maximum. Maximum values occur at values of λ obtained by setting the numerator of Eq. (4.5-45) to zero giving the expression:

$$\tan \phi_o = F(\lambda, D) \quad . \qquad (4.5\text{-}50)$$

For $\phi_o = 0°$ or $180°$, neglecting terms smaller than D^2, Eq. (4.5-50) may be solved for values of λ and G_{max} giving the result:

$$\lambda = \pm\left(1 - \frac{D^2}{8}\right) . \qquad (4.5\text{-}51)$$

From Eq. (4.5-40):

$$G_{max} = \pm \frac{\left(1 + \frac{D^2}{16}\right) \cos \phi_o}{D} . \qquad (4.5\text{-}52)$$

Therefore, at $\lambda \approx +1$ $\quad G_{max} \approx \frac{1}{D}$ for $\phi_o = 0°$

$\lambda \approx -1$ $\quad G_{max} \approx -\frac{1}{D}$ for $\phi_o = 0°$

$\lambda \approx +1$ $\quad G_{max} \approx -\frac{1}{D}$ for $\phi_o = 180°$

$\lambda \approx -1$ $\quad G_{max} \approx \frac{1}{D}$ for $\phi_o = 180°$

For $\phi_o = 90°$ or $270°$, Eq. (4.5-50) may be solved for λ, giving the following equation:

$$\lambda = \pm\sqrt{1 \pm D} , \qquad (4.5\text{-}53)$$

From Eq. (4.5-40):

$$G_{max} = \pm \frac{\sin \phi_o}{D(2 \pm D)} . \qquad (4.5\text{-}54)$$

The value of G is the same for $\pm\lambda$. The $\pm$ sign in Eq. (4.5-54) corresponds to the $\pm D$ term in Eq. (4.5-53). Therefore for $\phi_o = 90°$, $G_{max} \approx 1/2D$ at $\lambda = \pm\sqrt{1 + D}$, and $G_{max} \approx -1/2D$ at $\lambda = \pm\sqrt{1 - D}$. For $\phi_o = 270°$, $G_{max} \approx -1/2D$ at $\lambda = \pm\sqrt{1 + D}$ and $G_{max} \approx 1/2D$ at $\lambda = \pm\sqrt{1 - D}$. Note that, for a given α_o and r (i.e., $\dot{p}_{o_{max}}$), the potential roll torque for an in plane asymmetry is approximately twice that of the out of plane asymmetry.

For the general value of ϕ_o, the maximum values of G may be obtained from a plot of $F(\lambda, D)$. Since $F(-\lambda, D) = -F(\lambda, D)$, it is necessary to plot only the $+\lambda$ values of the function. The maximum values of G for $+\lambda$ are obtained at $F(\lambda, D) = \tan \phi_o$; the values of $-\lambda$ are obtained at $F(\lambda, D) = -\tan \phi_o$.

A summary of the characteristics of G is given in the table for in plane and out of plane asymmetries.

ϕ_o	0°		90°		180°		270°	
	G_{max}	λ	G_{max}	λ	G_{max}	λ	G_{max}	λ
Positive G_{max}	$1/D$	$1-\frac{D^2}{4}$	$1/2D$	$\pm\sqrt{1+D}$	$1/D$	$-1+\frac{D^2}{4}$	$1/2D$	$\pm\sqrt{1-D}$
Negative G_{max}	$-1/D$	$-1+\frac{D^2}{4}$	$-1/2D$	$\pm\sqrt{1+D}$	$-1/D$	$1-\frac{D^2}{4}$	$-1/2D$	$\pm\sqrt{1+D}$
λ_e	0		±1		0		±1	
λ_e Stability	Unstable		Unstable at +1 Stable at -1		Stable		Stable at +1 Unstable at -1	

Typical plots of G versus λ for $D = 0.2$ are shown for $\phi_o = 0°$, 45°, and 90° in Fig. 4-15. The values of G at a given λ for $\phi_o = 180°$ and 270° are the negatives of the values for $\phi_o = 0°$ and 90°, respectively. Note that for in plane asymmetries the roll torque from combined asymmetries is small except for a narrow band of λ in the vicinity of ±1 (i.e., near resonance conditions). However, for out of plane asymmetries the roll torque may be appreciable for all values of λ between about -1.5 to 1.5 except at $\lambda = \pm 1$.

The function $F(\lambda, D)$ is shown for $D = 0.2$ in Fig. 4-16. Using Eq. (4.5-50) as the condition for G_{max}, note that, except for small values of ϕ_o (less than $\phi_o = 45°$), all values of G_{max} tend to be near $\lambda = 0$ or $\lambda = \pm 1$. Furthermore the magnitude of G_{max} tends to be small when it occurs at values of λ other than ≈ 1. For example, the maxima for $\phi_o = 45°$ or $F(\lambda, D) = 1$ are shown in Fig.

4-16 to occur at $\lambda = 0.12$, 0.74, and 1.06. From Fig. 4-15 the corresponding values of G_{max} are -0.7, -0.9, and 4.1, respectively.

4.5.5 Roll Resonance

One of the potential problems resulting from asymmetries is prolonged periods of roll resonance. During this period the angle of attack increases, resulting in large lateral acceleration and high drag. If the resonance occurs during the heating portion of the trajectory, the problem may be amplified by distortion resulting from asymmetric heating since at $\bar{\alpha}$ one ray along the body remains on the windward side of the body and is heated more than a corresponding ray on the leeward side.

In this section we will consider conditions under which prolonged periods of resonance may occur. The term "lock-in" will be used to describe a roll history in which p_r tends to follow ω_A so that $\lambda \approx$ constant. That is, $\dot{p}_r/\dot{\omega}_A = 1$. It should be noted that this does not necessarily imply that resonance ($\lambda = \pm 1$) exists. However, asymmetries are usually small enough that roll amplification is required to cause significant changes in roll rate and the necessary amplification can occur only for conditions at or near resonance.

Typical values of roll rate at reentry are 1 to 2 Hz, and the static margin typically is 3% to 4% of body length. For these conditions, the peak value of ω_A is much greater than p_E so that $\lambda = 1$ will occur at least once during reentry. If the range is short enough or the reentry angle shallow enough, the resonance condition may occur a second time, as shown in the sketch on page 187.

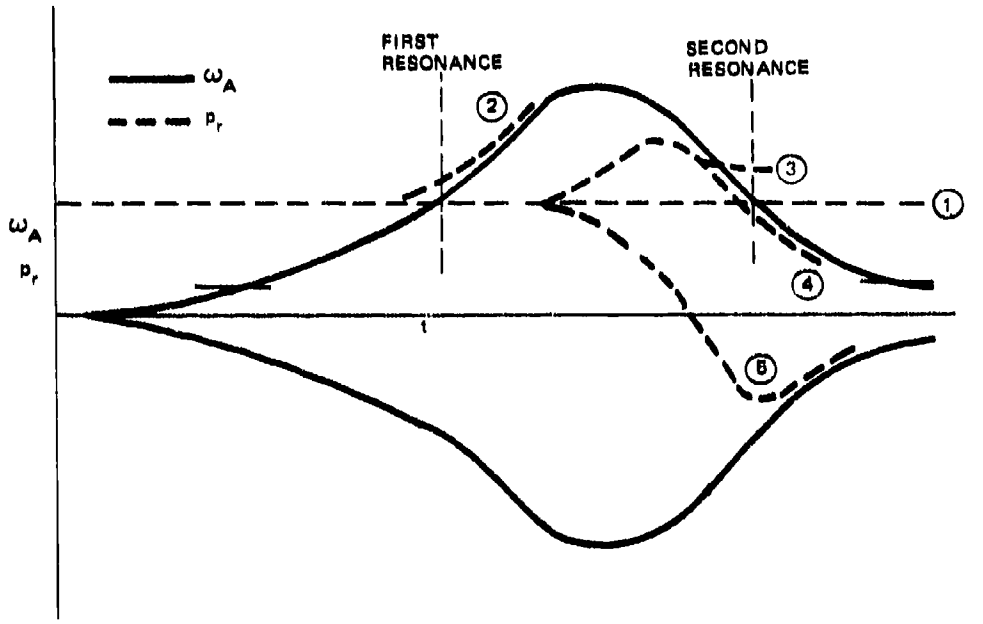

A vehicle having no roll torque would exhibit a reduced roll rate (p_r) trace shown by 1. The roll rate would pass through "first" and "second" resonance without incident. However, if asymmetries exist, the roll rate may lock-in on ω_A as shown by 2 through 5. Curve 2 is typical of the case of large asymmetries that exist early in the reentry phase. In this case lock-in may occur at "first" resonance. In the more usual case, asymmetries develop as a result of the heating environment so that "spin-up" (cases 3 and 4) or "spin-down" (case 5) occurs after "first" resonance. For cases 3 and 4 the angle ϕ_o is between 180° and 360° so that "spin up" occurs; for case 5, ϕ_o is between 0° and 180° so that "spin down" occurs. Cases 3 and 4 indicate that p may lock-in to ω_A (case 4) or may cut through the ω_A curve (case 3).

The roll lock-in conditions are the same whether the vehicle has positive or negative roll rate at reentry.

To simplify the presentation, only positive roll rate will be considered in the remainder of this discussion.

If the reduced roll acceleration ($\dot{p}_r$), produced by asymmetries, is equal to or greater than $\dot{\omega}_A$, lock-in may occur. In equation form, lock-in may occur when:

$$\frac{\dot{p}}{\dot{\omega}_A} \geq \frac{1}{\sqrt{1 - \frac{I_X}{I_Y}}} \quad . \tag{4.5-55}$$

Using Eqs. (4.4-37) and (4.3-18), it may be shown that $\dot{\omega}_A$ is given by the equation (neglecting variations in temperature with altitude):

$$\dot{\omega}_A = V_E^2 \left[- \frac{C_{N_\alpha} \Delta X m \sin^3 \gamma}{8 C_A I_Y H^3} \right]^{1/2} \frac{(1 - K)\sqrt{K}}{e^K} \quad . \tag{4.5-56}$$

Using Eqs. (4.3-8), (4.5-36), and (4.5-38), $\dot{p}$ is given by the equation:

$$\dot{p} = \frac{- G V_E^2 m \sin \gamma \, C_{N_\alpha}}{2 I_X H C_A} \bar{\alpha}_o r \frac{K}{e^K} \quad . \tag{4.5-57}$$

Therefore, lock-in may occur if the following inequality is satisfied:

$$\bar{\alpha}_o \frac{r}{d} G \geq \left[\frac{- C_A \Delta X}{2 C_{N_\alpha} H} \frac{I_X}{m d^2} \frac{I_X \sin \gamma}{I_Y \left(1 - \frac{I_X}{I_Y}\right)} \right]^{1/2} \frac{1 - K_R}{\sqrt{K_R}} \quad . \tag{4.5-58}$$

Equation (4.5-58) may be simplified further by noting that, for a given altitude (or given value of K), the minimum

asymmetry that may result in lock-in is given by Eq. (4.5-58) for $G = G_{max}$. If trim conditions are realized (see Section 4.5.10), then G_{max} is given approximately by (see Eqs. (4.5-52) and (4.5-54)):

$$G_{max} = k/D \tag{4.5-59}$$

where k has the following values:

ϕ_o	λ	k
0°	1	1
90°	$1 + \frac{D}{2}$	0.5
90°	$1 - \frac{D}{2}$	-0.5
180°	1	-1
270°	$1 + \frac{D}{2}$	-0.5
270°	$1 - \frac{D}{2}$	0.5

Using Eq. (4.5-20) and the definitions of F_α and M_q, an expression for D is:

$$D = \left[k_1 - C_{m_q}\right]\left[\frac{-\sin\gamma}{2C_A \frac{\Delta X}{d} k_1 \frac{H}{d}}\right]^{1/2} \sqrt{K} \tag{4.5-60}$$

where

$$k_1 = C_{N_\alpha}\left(1 - \frac{I_X}{I_Y}\right)\frac{I_Y}{md^2} .$$

Substituting Eqs. (4.5-59) and (4.5-60) into (4.5-58), and noting from previous discussions that G_{max} occurs near the resonance condition for in plane or out of plane asymmetries:

$$\bar{\alpha}_o \frac{r}{d} \geq F_1 \frac{(1 - K_R)}{k} \tag{4.5-61}$$

where

$$F_1 = \frac{-(I_X/I_Y)\sin\gamma}{2C_{N_\alpha}\frac{H}{d}\left(1 - \frac{I_X}{I_Y}\right)}\left[k_1 - C_{m_q}\right] \qquad (4.5\text{-}62)$$

and K_R is the value of K at the resonance condition.

The general behavior of Eq. (4.5-61) is shown in the sketch.

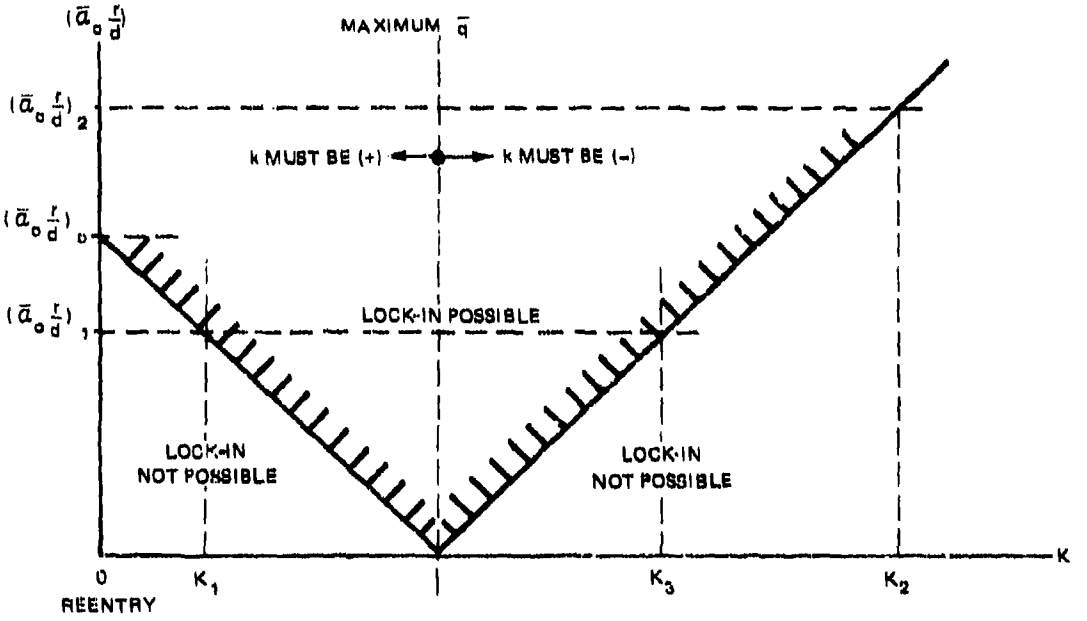

Following reentry ($K = 0$), assume that resonance ($G \approx G_{max}$) occurs at an altitude where $K_R = K_1$. If $\bar{\alpha}_o\, r/d \geq (\bar{\alpha}_o\, r/d)_1$, lock-in is likely to occur at first resonance provided $k > 0$ and lock-in will continue at least to $K = 1$ unless dynamic effects (roll rate and $\bar{\alpha}$ oscillations) or roll damping effects (see Section 4.5.6) cause "break out." Break out will occur at $K_R = 1$ unless ϕ_o is such that $\dot{p}$ and therefore G change sign near $\lambda = 1$. Therefore, from Fig. 4-15, break out will occur at $K_R = 1$ for in plane asymmetry ($\phi_o = 0°$ or $180°$) but may not occur for out of plane asymmetries ($\phi_o = 90°$ or $270°$). Break out would occur, however, even for the out of plane asymmetry at K_3. To be assured of freedom from lock in at all conditions:

$$\left(\bar{\alpha}_o \frac{r}{d}\right) \leq \left(\bar{\alpha}_o \frac{r}{d}\right)_1 \quad \text{or} \quad \left(\bar{\alpha}_o \frac{r}{d}\right)_2 ,$$

whichever is the more restrictive. The subscript 2 refers to the second resonance condition.

Neglecting a change in roll rate during reentry, it may be shown that $|1 - K_2| \geq |1 - K_1|$. Since the slope of the $\bar{\alpha}_o\, r/d$ curve for $K = 0$ to 1 is the negative of the slope for $K > 1$, the $(\bar{\alpha}_o\, r/d)_1$ limit is always the more restrictive condition. Therefore, from the resonance standpoint, it is desirable to select a low value of p_E so that first resonance occurs at as high an altitude as possible. The maximum asymmetry allowable is obtained by evaluating Eq. (4.5-61) at $K = 0$ so that to avoid lock in:

$$\bar{\alpha}_o \frac{r}{d} < \frac{F_1}{k} \quad . \tag{4.5-63}$$

In Eq. (4.5-61), the asymmetries are given in terms of $\bar{\alpha}$ and r. The asymmetric moment coefficient is a better parameter for some purposes since the moment coefficient is a direct function of the asymmetry whereas $\bar{\alpha}_o$ depends also upon C_{N_α} and vehicle stability (ΔX). The components of $\bar{\alpha}$ are shown in the sketch on page 192.

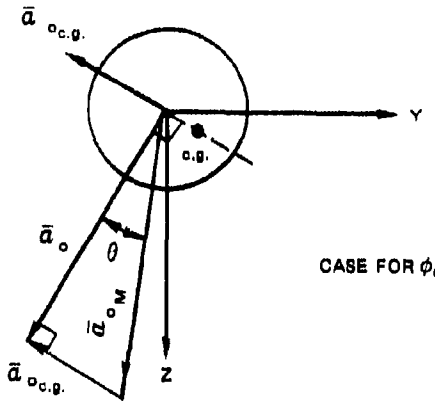

CASE FOR $\phi_o = 90^\circ$ IS SHOWN

The component of $\bar{\alpha}_o$ resulting from the center of gravity offset is always directed away from the center of gravity, whereas the component resulting from asymmetric moments may be in any plane. The components of $\bar{\alpha}_o$ are (see Eqs. (4.5-27), (4.5-28), and (4.5-29)):

$$\bar{\alpha}_{o_{c.g.}} = \frac{C_A \frac{r}{d}}{C_{N_\alpha} \frac{\Delta X}{d}} \qquad (4.5\text{-}64)$$

$$\bar{\alpha}_{o_M} = \frac{\bar{C}_{m_o}}{C_{N_\alpha} \frac{\Delta X}{d}} \qquad (4.5\text{-}65)$$

where

$$\bar{C}_{m_o} = \sqrt{C_{m_o}^2 + C_{n_o}^2} \quad . \qquad (4.5\text{-}66)$$

For $\phi_o = 0°$, $\bar{\alpha}_{o_M}$ must be directed toward the center of gravity and $\bar{\alpha}_{o_M} > \bar{\alpha}_{o_{c.g.}}$. Then:

$$\bar{\alpha}_o = \frac{\bar{C}_{m_o} - C_A \frac{r}{d}}{C_{N_\alpha} \frac{\Delta X}{d}} \quad . \tag{4.5-67}$$

For $\phi_o = 180°$:

$$\bar{\alpha}_o = \frac{\bar{C}_{m_o} + C_A \frac{r}{d}}{C_{N_\alpha} \frac{\Delta X}{d}} \quad . \tag{4.5-68}$$

For $\phi_o = 90°$ or $270°$:

$$\bar{\alpha}_o = \left[\left(\frac{\bar{C}_{m_o}}{C_{N_\alpha} \frac{\Delta X}{d}} \right)^2 - \left(\frac{C_A \frac{r}{d}}{C_{N_\alpha} \frac{\Delta X}{d}} \right)^2 \right]^{1/2} \quad . \tag{4.5-69}$$

Usually, $\bar{\alpha}_{o_{c.g.}} << \bar{\alpha}_{o_M}$, so that Eq. (4.5-69) is given approximately by the expression:

$$\bar{\alpha}_o = \frac{\bar{C}_{m_o}}{C_{N_\alpha} \frac{\Delta X}{d}} \left[1 - \frac{1}{2} \left(\frac{C_A}{\bar{C}_{m_o}} \frac{r}{d} \right)^2 \right] \quad . \tag{4.5-70}$$

Substituting for $\bar{\alpha}_o$, Eq. (4.5-61) becomes:

$$F_A < F_2 \frac{\Delta X}{d} \frac{(1 - K_R)}{k} \tag{4.5-71}$$

where

$$\left.\begin{aligned} F_A &= \overline{C}_{m_o} \frac{r}{d}\left[1 - \frac{C_A}{\overline{C}_{m_o}} \frac{r}{d}\right] \quad \text{for } \phi_o = 0° \\ &= \overline{C}_{m_o} \frac{r}{d}\left[1 + \frac{C_A}{\overline{C}_{m_o}} \frac{r}{d}\right] \quad \text{for } \phi_o = 180° \\ &= \overline{C}_{m_o} \frac{r}{d}\left[1 - \frac{1}{2}\left(\frac{C_A}{\overline{C}_{m_o}} \frac{r}{d}\right)^2\right] \quad \text{for } \phi_o = 90° \text{ or } 270°. \end{aligned}\right\} \quad (4.5\text{-}72)$$

$$F_2 = C_{N_\alpha} F_1 \,. \quad (4.5\text{-}73)$$

The limiting asymmetry values may be obtained for any in plane or out of plane asymmetry using Eq. (4.5-71) with the appropriate value of k given in the table in Section 4.5.5. Note however that $(1 - K_R)/k$ must be positive.

The possibilities for lock-in are shown using the roll amplification diagrams shown on page 195.

At reentry, for a positive roll, $\lambda \to +\infty$ so that $G \to 0$ and the roll rate remains constant. As the altitude decreases, ω_A increases and therefore λ decreases. As $\lambda \to 1$, G is no longer negligible and, if the $\dot{p}_r$ produced at points a ($\phi_o = 0°$, 90°, or 270°) is equal to or greater than $\dot{\omega}_A$, lock-in may occur at some value of λ between a and b where G is just large enough to satisfy Eq. (4.5-55). As the maximum dynamic pressure ($K \to 1$) is approached, $\dot{\omega}_A$ decreases, becoming zero at K = 1, and then it becomes negative. As a result p must reverse sign if lock-in continues. Neither the $\phi_o = 0°$ nor $\phi_o = 90°$ asymmetry case can produce the $\dot{p}$ characteristics required

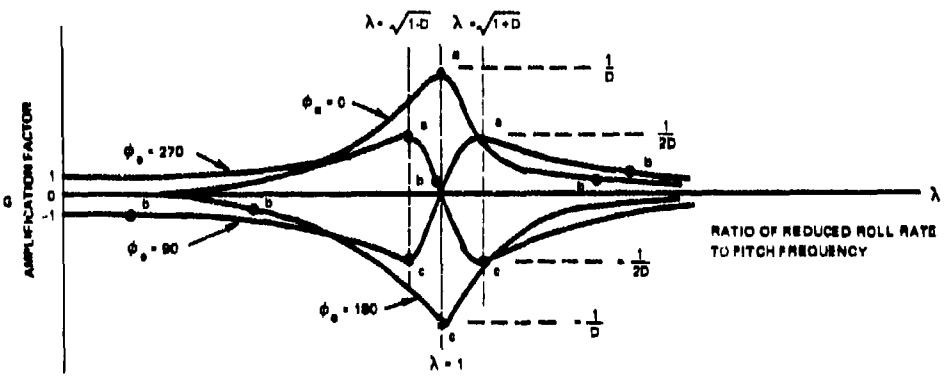

to satisfy the $\dot{\omega}_A$ variation, and lock-in cannot be maintained at $K > 1$. However, lock-in may continue to exist for $\phi_o = 270°$ until the negative $\dot{p}$ required for lock-in is greater than that given by point c. For the $\phi_o = 180°$ case, lock-in cannot occur since k (or G_{max}) is < 0. The vehicle would pass through first resonance with a slight reduction in roll rate. Both $\dot{p}$ and $\dot{\omega}_A$ tend to cause a rapid transit (both effects tend to reduce λ) through the resonance condition. As ω_A increases, λ decreases to some low value and p remains nearly constant. However as ω_A decreases at $K > 1$, λ increases. Lock-in at this time (second resonance) requires a negative $\dot{p}$ and may occur between points b and c if $\dot{p}$ at c is large enough. For $\phi_o = 90°$, the shape of the G curve is such that lock-in

could occur at second resonance between b and c. However, if the torque at c is large enough to cause lock-in and if the asymmetry existed at reentry, then lock-in would have occurred between a and b at first resonance, and λ would never be less than 1 + D. Therefore lock-in at second resonance would not occur. If, on the other hand, the asymmetry developed during reentry and after first resonance, then second resonance lock-in for ϕ_o = 90° is possible.

Note that lock-in may occur only when $dG/d\lambda$ is negative since, for positive slopes, λ is unstable for reasons discussed for λ_e stability in Section 4.5.4.

The most restrictive limitation occurs for first resonance lock-in with the in plane asymmetry with ϕ_o = 0°. For this case, with first resonance near K = 0, if lock-in is to be avoided:

$$F_A = \overline{C}_{m_o} \frac{r}{d} \left[1 - \frac{C_A}{\overline{C}_{m_o}} \frac{r}{d} \right] < F_2 \frac{\Delta X}{d} \quad . \qquad (4.5\text{-}74)$$

For $\dfrac{C_A}{\overline{C}_{m_o}} \dfrac{r}{d} \ll 1$:

$$\overline{C}_{m_o} r < dF_2 \frac{\Delta X}{d} \quad . \qquad (4.5\text{-}75)$$

From Eqs. (4.5-62), (4.5-73), and (4.5-75), note that the allowable asymmetry is governed by the following parameters:

Parameter	Related Factor	$C_{m_o}r$ to avoid lock-in tends to be low for:
Vehicle stability margin	$\Delta X/d$	Small $\Delta X/d$
Resonance altitude	$1 - K_R$	$K_R \neq 1$
Plane of asymmetries	k	0° or 180° (compared to 90° or 270°)
Aerodynamic coefficients	C_{N_α} and C_{m_q}	Low C_{N_α} and C_{m_q}
Type of trajectory	$\sin\gamma$	Low γ (shallow reentry angles)
Atmosphere	H	High H
Vehicle slenderness	I_X/I_Y and C_{m_q}	Low I_X/I_Y and C_{m_q}
Mass distribution factor	I_Y/md^2	Low I_Y/md^2
Vehicle size	d	Low d

Since there are so many variables, it is not possible to present generalized curves of allowable asymmetry. However several observations are noteworthy. Consider a family of bodies differing only by a scale factor. Values of C_{N_α}, C_{m_q}, I_X/I_Y, and I_Y/md^2 will be approximately the same for all bodies. If it is further specified that all bodies have the same stability margin (same $\Delta X/d$), then for a given atmosphere and trajectory, Eqs. (4.5-62), (4.5-73), and (4.5-75) show that the allowable $C_{m_o}r$ is proportional to d^2. Therefore, small bodies may be particularly sensitive to mass and aerodynamic asymmetries.

Note also that for a given allowable F_A the allowable $\overline{C}_{m_o}$ (Eq. (4.5-72)) has a minimum value for ϕ_o = 0°, 90°, or 270°. For ϕ_o = 0°, the minimum occurs at:

$$\frac{r}{d} = \frac{1}{2}\,\frac{\overline{C}_{m_o}}{C_A}$$

and the minimum $\overline{C}_{m_o}$ is given by:

$$\overline{C}_{m_o} < 2 \left[C_A \frac{\Delta X}{d} F_2 (1 - K_R) \right]^{1/2} . \qquad (4.5\text{-}76)$$

For $\phi_o = 90°$ or $270°$, the minimum occurs at:

$$\frac{r}{d} = \sqrt{2/3} \frac{\overline{C}_{m_o}}{C_A} \qquad (4.5\text{-}77)$$

and the minimum value is given by:

$$\overline{C}_{m_o} < 2.29 \left[C_A \frac{\Delta X}{d} F_2 (1 - K_R) \right]^{1/2} . \qquad (4.5\text{-}78)$$

Therefore for a fixed value of F_A the minimum value for $\overline{C}_{m_o}$ for an out of plane asymmetry is about 15% greater than that for an in plane asymmetry.

4.5.6 Effect on Lock-in of Roll Damping and Pure Roll Torque

The roll damping, M_p, and pure asymmetric roll torque, ℓ_o, terms in Eq. (4.5-33) are usually negligible. However, under some conditions these terms could be significant. For example, at usual roll rates M_p is small, but if lock-in occurs and drives the roll rate to high values, M_p may become a significant torque and may, in fact, break the lock-in condition.

Rewriting Eq. (4.5-36) to include the M_p and ℓ_o terms:

$$\dot{p} = G' \dot{p}_{o_{max}} \qquad (4.5\text{-}79)$$

where

$$G' = G + G_1 + G_2 \,. \tag{4.5-80}$$

The amplification factor G is defined by Eq. (4.5-37). The factor G_1 is defined by the equation:

$$G_1 = \frac{M_p p}{I_X \dot{p}_{o_{max}}} \tag{4.5-81}$$

$$= \frac{C_{\ell_p} \frac{pd}{V}}{C_{N_\alpha} \bar{\alpha}_o \frac{r}{d}} \,.$$

Using Eq. (4.5-21) to eliminate p:

$$G_1 = \frac{C_{\ell_p} \frac{\omega_A d\lambda}{V\sqrt{1 - \frac{I_X}{I_Y}}}}{C_{N_\alpha} \bar{\alpha}_o \frac{r}{d}}$$

and using Eq. (4.3-23) for ω_A:

$$G_1 = \left[\frac{-\Delta XK \sin\gamma}{2HC_A k_1}\right]^{1/2} \frac{C_{\ell_p}}{\bar{\alpha}_o \frac{r}{d}} \lambda = a\lambda \,. \tag{4.5-82}$$

The value of a is always negative. Therefore if the G curve is drawn, the $G' = G + G_1$ (assuming $G_2 = 0$) values are the ordinates measured from a λ axis which is rotated counterclockwise through an angle, ϵ, where:

$$\tan\epsilon = a \,. \tag{4.5-83}$$

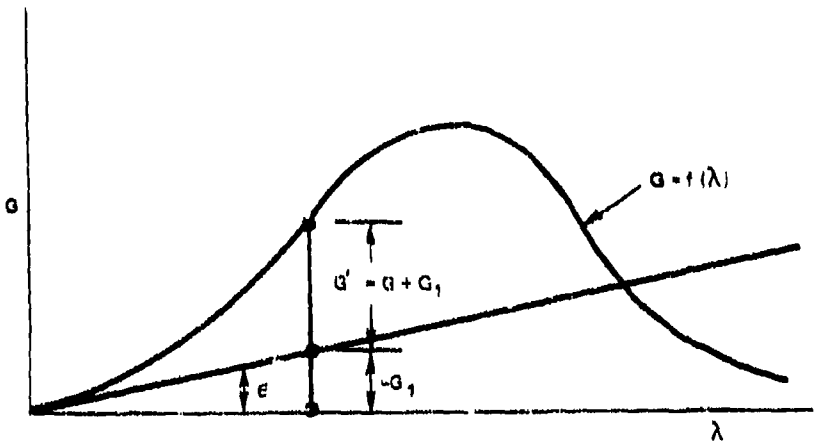

Similarly:

$$G_2 = \frac{\ell_o}{I_X \dot{p}_{o_{max}}} = \frac{C_{\ell_o}}{C_{N_\alpha} \bar{\alpha}_o \frac{r}{d}} \quad . \qquad (4.5\text{-}84)$$

If $G_1 = 0$, the values of $G' = G + G_2$ are the ordinates of the G curve measured from a λ axis that is shifted by an amount $\frac{-C_{\ell_o}}{C_{N_\alpha} \bar{\alpha}_o \frac{r}{d}}$ as sketched (for a negative value of C_{ℓ_o}).

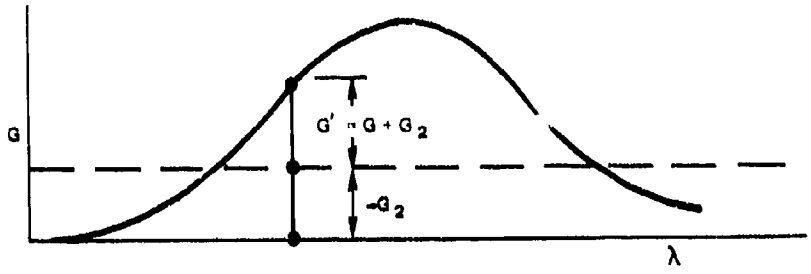

Suppose an in plane asymmetry exists and $\bar{\alpha}_o$ and r/d are such that an amplification factor, $G = G_R$ (see Eq. (4.5-58)), could result in a lock-in condition at first resonance if $C_{\ell_p} = 0$. Lock-in may then occur at point A in the sketch.

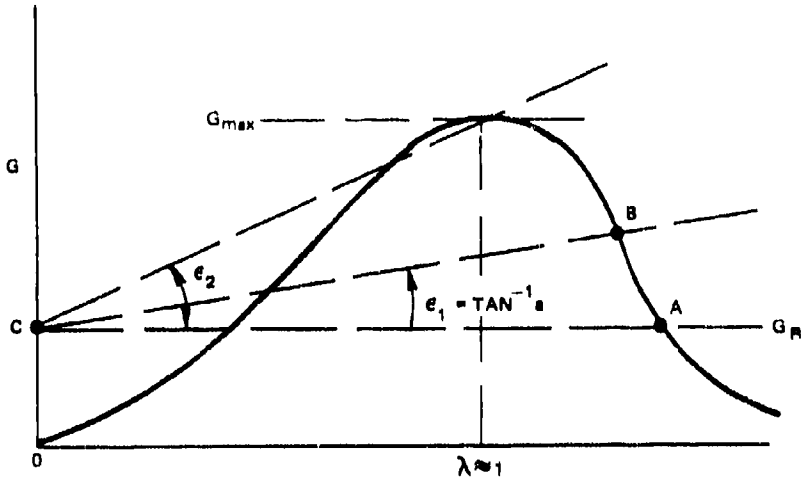

However, suppose $C_{\ell_p} \neq 0$ so that ϵ for resonance at the initial roll rate is given by ϵ_1. The resonance condition then is obtained by drawing the line BC as shown, giving a lock-in condition at B. As resonance continues, K increases and therefore ϵ increases. If ϵ exceeds the value shown by ϵ_2, the torque required to sustain resonance is unavailable and break out occurs.

Using Eqs. (4.5-58) and (4.5-60), and noting that $\tan \epsilon = \dfrac{G_{max} - G_R}{\lambda_{G_{max}}} \approx G_{max} - G_R$, it may be shown that roll damping will cause break out when the following inequality is satisfied:

$$C_{\ell_p} \geq \frac{2(H/d)C_A k_1 \bar{\alpha}_o \frac{r}{d}}{\left[k_1 - C_{m_q}\right] \sin(-\gamma)} \frac{k}{K_R} - C_A \frac{I_X}{md^2}\left(\frac{1 - K_R}{K_R}\right), \quad (4.5\text{-}85)$$

Roll damping tends to decrease the possibility of lock-in at first resonance and, if lock-in occurs, tends to increase the possibility of break out. The opposite effects occur at second resonance.

When C_{ℓ_o} exists (but not C_{ℓ_p}), lock-in cannot exist unless

$$G_{max} - G_R - \frac{C_{\ell_o}}{C_{N_\alpha} \bar{\alpha}_o \frac{r}{d}} > 0 .$$

Using Eqs. (4.5-58) and (4.5-60), lock-in cannot occur at first resonance if C_{ℓ_o} has a sign opposite to that of the initial roll rate and a magnitude given by the following inequality:

$$C_{\ell_o} > \frac{a_1 \bar{\sigma}_o \frac{r}{d}}{\sqrt{K_R}} - \frac{a_2(1 - K_R)}{\sqrt{K_R}} \qquad (4.5\text{-}86)$$

where $1 \geq K_R > 0$

$$a_1 = \frac{C_{N_\alpha} k}{k_1 - C_{m_q}} \sqrt{\frac{2C_A \frac{\Delta X}{d} k_1 \frac{H}{d}}{\sin(-\gamma)}} \qquad (4.5\text{-}87)$$

$$a_2 = \frac{l_X}{I_Y} \sqrt{\frac{C_A \frac{\Delta X}{d} k_1 \sin(-\gamma)}{2\left(1 - \frac{I_X}{I_Y}\right)^2 \frac{H}{d}}} \,, \qquad (4.5\text{-}88)$$

If the sign of C_{ℓ_o} is the same as that of the initial roll rate, the effect of C_{ℓ_o} is to increase the probability of lock-in; if C_{ℓ_o} and p_E have opposite signs, the effect is to decrease the probability of lock-in.

4.5.7 Spin Through Zero Roll Rate

In the previous sections, the problem of roll resonance was considered. A second problem resulting from variations of roll rate during reentry occurs when the roll rate becomes equal to or passes through zero. When $p = 0$ and an asymmetry, $\bar{\alpha}_o$, exists, the lateral acceleration resulting from $\bar{\alpha}_o$ is fixed in space and the missile moves off course in the direction of F_o. The impact dispersion produced may be much larger than that required for satisfactory performance. In this section we will consider the conditions for which spin through zero may occur.

Referring to curve 5 in the first sketch in Section 4.5.5, spin down through zero roll rate may occur when

an out of plane component of asymmetry exists and is in a direction to reduce the magnitude of the roll rate. Therefore, one condition for $p = 0$ is that $180° > \phi_o > 0°$. The second condition is that the magnitude of $\dot{p}$ is large enough to result in $p = 0$ prior to impact.

For the asymmetries of interest in this problem, the vehicle usually passes through first resonance with little change in roll rate so that most of the change in roll rate occurs at λ near zero so that roll amplification is negligible. The roll acceleration, then, is given by Eq. (4.5-35):

$$\dot{p} = \frac{-C_{N_\alpha} \bar{q}S \bar{\alpha}_o r \sin \phi_o}{I_X} \quad . \tag{4.5-89}$$

For very small angles of attack ($\bar{\alpha}_o$):

$$g_X = \frac{1}{g} \frac{dV}{dt} = - \frac{C_A \bar{q}S}{W} \quad .$$

Therefore:

$$\bar{q}S = - \frac{m}{C_A} \frac{dV}{dt} \quad . \tag{4.5-90}$$

Substituting Eq. (4.5-90) into (4.5-89):

$$\frac{dp}{dt} = \frac{C_{N_\alpha} \bar{\alpha}_o r \sin \phi_o}{I_X} \frac{m}{C_A} \frac{dV}{dt} \quad . \tag{4.5-91}$$

If p and V are assumed to be the only dependent variables, Eq. (4.5-91) may be integrated to give:

$$p - p_E - \Delta p = \frac{C_{N_\alpha} \bar{\alpha}_o r \sin \phi_o}{C_A I_X} mV_E \left(\frac{V}{V_E} - 1 \right) , \tag{4.5-92}$$

Substituting for V/V_E using Eq. (4.3-5):

$$\Delta p = - \frac{C_{N_\alpha} \bar{\alpha}_o \frac{r}{d} \sin \phi_o}{C_A \left(I_X/md^2\right)} \frac{V_E}{d} \left(1 - e^{-K/2}\right) . \qquad (4.5\text{-}93)$$

If $|\Delta p| > p_E$ at $K = K_{SL}$, spin through zero will occur prior to impact. The altitude (or K) at which zero roll rate occurs may be obtained from Eq. (4.5-93):

$$e^{-K/2} = 1 - \frac{p_E C_A \frac{I_X}{md^2}}{C_{N_\alpha} \bar{\alpha}_o \frac{r}{d} \frac{V_E}{d} \sin \phi_o} \qquad (4.5\text{-}94)$$

or

$$K = -2 \ln \left[1 - \frac{p_E C_A \frac{I_X}{md^2}}{C_{N_\alpha} \bar{\alpha}_o \frac{r}{d} \frac{V_E}{d} \sin \phi_o} \right] . \qquad (4.5\text{-}95)$$

The minimum asymmetries which may cause zero roll rate occur for $\phi_o = 90°$. For this case, Eq. (4.5-95) may be written in terms of the moment coefficient using Eq. (4.5-70):

$$K = -2 \ln \left\{ 1 - \frac{p_E C_A \frac{I_X}{md^2} \frac{\Delta X}{d}}{\bar{C}_{m_o} \frac{r}{d} \frac{V_E}{d} \left[1 - \frac{1}{2} \left(\frac{C_A}{\bar{C}_{m_o}} \frac{r}{d} \right)^2 \right]} \right\} \qquad (4.5\text{-}96)$$

If spin through zero is to be avoided for the entire trajectory, Eqs. (4.5-95) and (4.5-96) indicate that the following inequalities must be satisfied:

$$\bar{\alpha}_o \frac{r}{d} \leq \frac{\frac{p_E d}{V_E} \frac{I_X}{md^2} \frac{C_A}{C_{N_\alpha}}}{1 - \exp\left(\frac{\bar{P}_{S.L.}}{2\beta \sin\gamma}\right)} \qquad (4.5\text{-}97)$$

or in terms of $\bar{C}_{m_o}$:

$$F_A = \bar{C}_{m_o} \frac{r}{d}\left[1 - \frac{1}{2}\left(\frac{C_A}{\bar{C}_{m_o}} \frac{r}{d}\right)^2\right] \leq \frac{\frac{p_E d}{V_E} C_A \frac{I_X}{md^2} \frac{\Delta X}{d}}{1 - \exp\left(\frac{\bar{P}_{S.L.}}{2\beta \sin\gamma}\right)} \quad . \qquad (4.5\text{-}98)$$

Using the assumptions listed in Section 4.5.5, page 197, note that the allowable $\bar{C}_{m_o} r$ is proportional to d^2. Therefore, as in the case of the roll resonance problem, small vehicles are particularly susceptible to the spin through zero problem.

The probability of encountering the spin through zero problem on a given vehicle is highly dependent upon the missile-to-missile variation in ϕ_o. If the asymmetries are such that ϕ_o is always 90°, and if $\bar{\alpha}_o$ r/d always exceeds the value given by Eq. (4.5-97), then all the missiles will spin through zero. On the other hand, if ϕ_o always lies between 180° and 360°, the probability of encountering spin through zero is zero regardless of the value of $\bar{\alpha}_o$ r/d. If the missile-to-missile variation in ϕ_o is random, the probability of encountering spin through zero is given by:

$$\bar{P} = \frac{\Lambda}{\pi}$$

where Λ is an angle between 0 and $\pi/2$ radians defined by:

$$\Lambda = \cos^{-1}\left[\frac{\left(\bar{\alpha}_o\ r/d\right)_{min}}{\bar{\alpha}_o\ r/d}\right]$$

and $(\bar{\alpha}_o\ r/d)_{min}$ is the value of $\bar{\alpha}_o\ r/d$ given by Eq. (4.5-97). For this assumption, the probability of encountering spin through zero varies from 0 at $\bar{\alpha}_o\ r/d = (\bar{\alpha}_o\ r/d)_{min}$ to 50% at $\bar{\alpha}_o\ r/d \gg (\bar{\alpha}_o\ r/d)_{min}$.

4.5.8 Effect on Products of Inertia

The products of inertia are defined by the following equations:

$$I_{XY} = \Sigma m_i X_i Y_i \qquad (4.5\text{-}99)$$

$$I_{XZ} = \Sigma m_i X_i Z_i \qquad (4.5\text{-}100)$$

$$I_{YZ} = \Sigma m_i Y_i Z_i \qquad (4.5\text{-}101)$$

The I_{YZ} term is negligible for most reentry bodies and is omitted from this analysis. If I_{XY} and I_{XZ} are not zero, the principal axes pass through the center of gravity but are rotated through an angle δ measured clockwise from the body centerline. For small asymmetries, the rotation angles are (for $I_Y = I_Z$):

$$\delta_\beta = \frac{I_{XY}}{I_Y - I_X} \qquad (4.5\text{-}102)$$

$$\delta_\alpha = \frac{-I_{XZ}}{I_Y - I_X} \qquad (4.5\text{-}103)$$

$$\delta = \sqrt{\delta_\beta^{\,2} + \delta_\alpha^{\,2}} \qquad (4.5\text{-}104)$$

where δ_β is a rotation about the Z axis and δ_α is a rotation about the Y axis.

Consider a mass asymmetry in which $I_{XZ} = 0$ but $I_{XY} \neq 0$, as illustrated by the sketch.

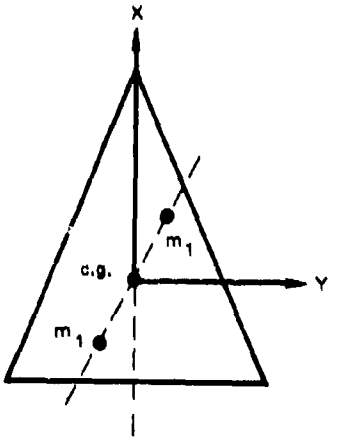

Assume the vehicle is symmetrical except for two small masses, m_1, located at (X_1, Y_1) and $(-X_1, -Y_1)$ so that $I_{XY} = 2m_1X_1Y_1$. If the missile is now rotated about the X axis, the centrifugal force acting on each m_1 produces a yawing moment about the Z axis.

Returning to the case where $I_{XY} \neq 0$, $I_{XZ} \neq 0$, and the mass asymmetry forces are much greater than the aerodynamic forces ($\lambda \to \infty$), and retaining only the larger asymmetry terms (p is moderately large but I_{XY}, I_{XZ}, q, r, $\dot{p}$, $\dot{q}$, and $\dot{r}$ are assumed to be sufficiently small that the square or product of two small terms may be neglected) of Eqs. (4.5-1), (4.5-2), and (4.5-3), the equations of motion become:

$$\dot{p} = 0 \tag{4.5-105}$$

$$\dot{q} = r\omega_g - p^2 \frac{I_{XZ}}{I_Y} \tag{4.5-106}$$

$$\dot{r} = -q\omega_g + p^2 \frac{I_{XY}}{I_Y} \tag{4.5-107}$$

where $\omega_g = p\left(1 - \frac{I_X}{I_Y}\right)$.

Differentiating Eq. (4.5-106):

$$\ddot{q} = \omega_g \dot{r} \, . \tag{4.5-108}$$

Using Eqs. (4.5-107) and (4.5-108):

$$\ddot{q} + \omega_g{}^2 q = \omega_g p^2 \frac{I_{XY}}{I_Y} \, . \tag{4.5-109}$$

The solution to this differential equation is:

$$q = C_1 \sin \omega_g t + C_2 \cos \omega_g t + p \frac{I_{XY}}{I_Y - I_X} \tag{4.5-110}$$

$$\dot{q} = C_1 \omega_g \cos \omega_g t - C_2 \omega_g \sin \omega_g t \, . \tag{4.5-111}$$

From Eqs. (4.5-106) and (4.5-111):

$$r = C_1 \cos \omega_g t - C_2 \sin \omega_g t + p \frac{I_{XZ}}{I_Y - I_X} \, . \tag{4.5-112}$$

From Eqs. (4.5-110) and (4.5-112):

$$\left(q - p\frac{I_{XY}}{I_Y - I_X}\right)^2 + \left(r - p\frac{I_{XZ}}{I_Y - I_X}\right)^2 = C_1^2 + C_2^2 \quad .$$

Therefore, the q - r plot is a circle of radius $\sqrt{C_1^2 + C_2^2}$ with center at $q = p\frac{I_{XY}}{I_Y - I_X}$, $r = p\frac{I_{XZ}}{I_Y - I_X}$. In other words, the telemetry traces for a body having nonzero I_{XY} and I_{XZ} show a q which oscillates about the value $q = p\frac{I_{XY}}{I_Y - I_X}$ and an r which oscillates about $r = p\frac{I_{XZ}}{I_Y - I_X}$. The constants C_1 and C_2 may be evaluated from given conditions at t = 0.

$$C_1 = r_i - p\frac{I_{XZ}}{I_Y - I_X} \quad . \qquad (4.5\text{-}113)$$

$$C_2 = q_i - p\frac{I_{XY}}{I_Y - I_X} \quad . \qquad (4.5\text{-}114)$$

Equations (4.5-113) and (4.5-114) may be used to evaluate I_{XY} and I_{XZ} from flight test data if p, q, and r are known accurately.

In space, where the aerodynamic forces are zero, the principal X axis moves along a cone. The cone half-angle is given by the equation (see Eq. 4.4-23):

$$\tan \phi = \frac{\sqrt{C_1^2 + C_2^2}}{p}\frac{I_Y}{I_X} \quad . \qquad (4.5\text{-}115)$$

The period of the rotation about the space cone is given by Eq. (4.4-25). Since the body centerline rolls around the principal axis, the angle of attack oscillates with a relatively long period (τ_s) and a peak-to-peak amplitude of 2ϕ with a superimposed short period ($1/p$) oscillation with peak-to-peak amplitude of 2δ.

The constant shift in q and/or r resulting from nonzero products of inertia may be interpreted in terms of angle of attack using the following equations (see Ref. 4-9).

$$\beta_\delta = \frac{q}{p} = \frac{I_{XY}}{I_Y - I_X} \tag{4.5-116}$$

$$\alpha_\delta = \frac{r}{p} = \frac{I_{XZ}}{I_Y - I_X} \tag{4.5-117}$$

When the missile descends to altitudes where the aerodynamic forces are no longer negligible, assuming that α_o and β_o may exist as well as α_δ and β_δ, the total angle of attack is given by the equation (see Ref. 4-9):

$$|\bar{\alpha}| = A\left[(\beta_o + \lambda^2\beta_\delta)^2 + (\alpha_o + \lambda^2\alpha_\delta)^2\right]^{1/2} \tag{4.5-118}$$

where A is defined by Eq. (4.5-16). The direction of the trim force is defined by the equation:

$$\psi = \psi_o + \Delta\psi \tag{4.5-119}$$

where

$$\tan\psi_o = \frac{-\alpha_o}{-\beta_o} \tag{4.5-120}$$

if α_o and $\beta_o \neq 0$.

$$\tan\psi_o = \frac{I_{XZ}}{I_{XY}} \tag{4.5-121}$$

if $\alpha_o = \beta_o = 0$, and

$$\left.\begin{aligned} \Delta\psi &= \tan^{-1}\left(\frac{\alpha_o + \lambda^2 \alpha_\delta}{\beta_o + \lambda^2 \beta_\delta}\right) - \tan^{-1}\left(\frac{D\lambda}{1-\lambda^2}\right) - \tan^{-1}\frac{\alpha_o}{\beta_o} \\ \text{or} \\ \Delta\psi &= -\tan^{-1}\left(\frac{D\lambda}{1-\lambda^2}\right) \end{aligned}\right\} \quad (4.5\text{-}122)$$

if either α_o and β_o or α_δ and $\beta_\delta = 0$.

The proper quadrant for ψ_o may be obtained from the signs of the numerator and denominator in Eq. (4.5-120). For $\alpha_o = \beta_o = 0$, the trim angle of attack is just that resulting from products of inertia.

Let

$$\bar{\alpha}_\delta = \sqrt{\alpha_\delta^2 + \beta_\delta^2} \qquad (4.5\text{-}123)$$

Then, the amplification factor in terms of $\bar{\alpha}_\delta$ is given by:

$$\text{Amplification factor} = \left|\frac{\bar{\alpha}}{\bar{\alpha}_\delta}\right| = \lambda^2 A \qquad (4.5\text{-}124)$$

The amplification factor is zero at $\lambda = 0$, has the same amplification as that for aerodynamic trim at $\lambda = 1$ (namely, A), and approaches unity as $\lambda \to \infty$. Therefore the products of inertia may be important at λ near or greater than unity and, in combination with the center of gravity offset, could result in resonance lock-in. The effect may either augment or diminish the effect of other asymmetries, depending upon the signs and magnitudes (see discussion below) of I_{XY} and I_{XZ}. However the product of inertia asymmetry in combination with the center of gravity offset cannot result in spin through zero since the roll torque at $p = 0$ is zero.

Consider a vehicle having a positive roll rate at reentry and a combined in-plane asymmetry consisting of a center of gravity offset along the +Y axis and a positive product of inertia I_{XY}. At reentry ($\lambda \to \infty$) a positive I_{XY} results in a positive β (Eq. (4.5-116)) or a force F_∞, along the -Y axis. Since F rotates clockwise as λ decreases, F_Z is always negative and the roll acceleration resulting from F is always positive, and therefore lock-in at first resonance is a possibility.

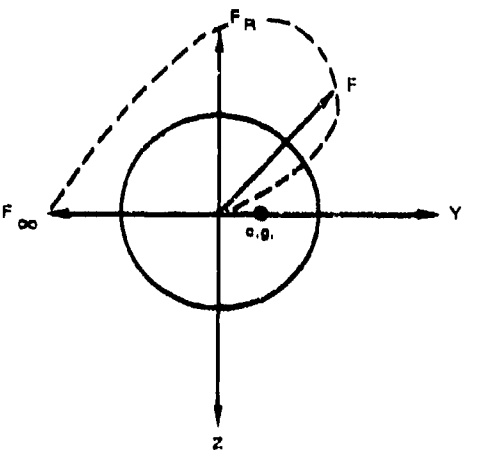

Solving Eqs. (4.5-1) and (4.5-2) simultaneously and retaining just the $\dot{p}$ contributions resulting from aerodynamic forces:

$$\dot{p} = \frac{\ell}{I_X} + \frac{I_{XY}}{I_X}\frac{m}{I_Y}$$

Substituting for ℓ and m using Eqs. (4.5-4) and (4.5-5):

$$\dot{p} = -\frac{F_Z Y_{c.g.}}{I_X} + \frac{I_{XY}}{I_X}\frac{F_Z \Delta X}{I_Y}$$

Note that $\dot{p}$ resulting from the second term on the right side of the equation is negative since F_Z is always negative. Similarly, if a negative I_{XY} had been selected F_Z would always be positive. Therefore this term results in a negative $\dot{p}$ regardless of the sign of I_{XY} and, for positive roll rates at reentry, tends to prohibit first resonance lock-in but tends to cause second resonance lock-in.

In a manner similar to that used in deriving the criterion for lock-in for an aerodynamic asymmetry and a center of gravity offset (Eq. (4.5-61)), the criterion for lock-in with a product of inertia and a center of gravity offset is:

$$\bar{\alpha}_\delta \frac{r}{d} - \bar{\alpha}_\delta^2 \left(1 - \frac{I_X}{I_Y}\right)\frac{\Delta X}{d} - F_1 \left|1 - K_R\right| \geq 0$$

This inequality is identical to the inequality for an aerodynamic asymmetry and a center of gravity offset (Eq. (4.5-61)) only for the particular case of a neutrally stable vehicle ($\Delta X/d = 0$), which is not of practical interest. For any statically stable vehicle (positive $\Delta X/d$), $\bar{\alpha}_\delta$ r/d is always greater than $\bar{\alpha}_o$ r/d for a given F_1 and K_R. Solving for $\bar{\alpha}_\delta$ at the boundary (the above equation set to zero) using the binomial theorem:

$$\bar{\alpha}_\delta = \left(F_3 \frac{r}{d}\right)\left[1 \pm \sqrt{1 - \frac{F_4|1 - K_R|}{\left(F_3 \frac{r}{d}\right)^2}}\right] \qquad (4.5\text{-}125)$$

where

$$F_3 = \frac{1}{2\left(1 - \frac{I_X}{I_Y}\right)\frac{\Delta X}{d}}$$

$$F_4 = 2F_1F_3 .$$

Note that lock-in cannot occur unless:

$$F_3 \frac{r}{d} \geq \sqrt{F_4|1 - K_R|} .$$

For the minimum value of $F_3\, r/d$,

$$\bar{\alpha}_\delta = F_3 \frac{r}{d} = \sqrt{F_4|1 - K_R|} .$$

Another lock-in requirement is that:

$$\bar{\alpha}_{\delta_{min}} \leq \bar{\alpha}_\delta \leq \bar{\alpha}_{\delta_{max}}$$

where $\bar{\alpha}_{\delta_{min}}$ and $\bar{\alpha}_{\delta_{max}}$ are given by Eq. (4.5-125) using the negative and positive signs of the radical term, respectively. The general requirements for lock-in for this type of combined asymmetry are as shown in the sketch for a particular value of K_R.

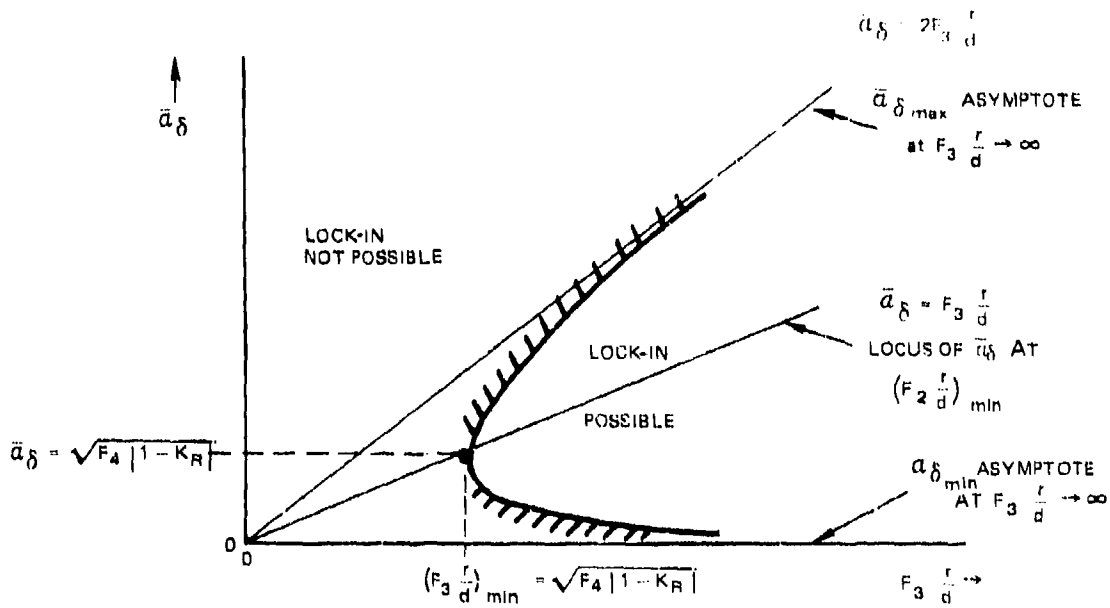

Note that $(F_3\ r/d)_{min}$ decreases from $\sqrt{F_4}$ at reentry ($K_R = 0$) to 0 at maximum dynamic pressure ($K_R = 1$) and then increases to $\sqrt{F_4 |1 - K_{S.L.}|}$ at impact. Current reentry vehicles are designed such that first resonance occurs at $K_R \approx 0$, so that $|1 - K_R| \approx 1$. Assuming p does not change during reentry, it may be shown that $|1 - K_R| > 1$ at second resonance. Therefore lock-in is not possible at first or second resonance for any value of $\bar{\alpha}_\delta$ if the vehicle can be constructed so that:

$$\frac{r}{d} \leq \frac{\sqrt{F_4}}{F_3} = \sqrt{2F_1/F_3} \quad .$$

Substituting for F_1 and F_3, this inequality becomes:

$$\frac{r}{d} \leq \left\{ 2 \frac{I_X}{I_Y} \frac{\Delta X}{H} \left[\left(1 - \frac{I_X}{I_Y} \right) \frac{I_Y}{md^2} - \frac{C_{m_q}}{C_{N_\alpha}} \right] \sin(-\gamma) \right\}^{1/2} \quad .$$

For a given shape, I_X/I_Y, I_Y/md^2, and C_{m_q}/C_{N_α} tend to be independent of size. Then, for a given shape and $\Delta X/d$, the allowable center of gravity offset varies as $d^{3/2}$ and $[\sin(-\gamma)]^{1/2}$. Therefore, small bodies flying shallow-angle trajectories are more susceptible to lock-in than are large bodies flying steep-angle trajectories.

4.5.9 Unequal Pitch and Yaw Moment of Inertia

For a body whose only asymmetry is unequal pitch and yaw moment of inertia, the equations of motion (neglecting small terms) become:

$$\dot{p}I_X = (I_Y - I_Z)qr \qquad (4.5\text{-}126)$$

$$\dot{q}I_Y = m - pr(I_X - I_Z) \qquad (4.5\text{-}127)$$

$$\dot{r}I_Z = n - pq(I_Y - I_X) \quad . \qquad (4.5\text{-}128)$$

The significance of the $(I_Y - I_Z)qr$ term in Eq. (4.5-126) is shown (for $I_Z > I_Y$) in the sketch. The body has mass symmetry except for two small equal masses located on the Y axis equally distant (ΔY) from the center of gravity. At some instant, the body has a transverse rate of rotation shown by the vector $\vec{\omega}_T$. At this time the

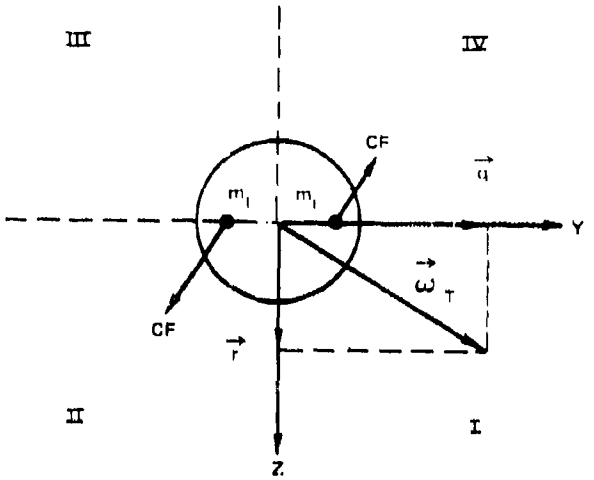

CF = CENTRIFUGAL FORCE

body rotates about an axis coincident with $\vec{\omega}_T$, and the centrifugal force acting on m_1 produces a couple $-2m_1 \Delta Y^2 qr = (I_Y - I_Z)qr$ about the X axis. The roll torque is negative when $\vec{\omega}_T$ lies in quadrants I and III and positive when $\vec{\omega}_T$ lies in quadrants II and IV. At very high altitudes ($\lambda \rightarrow \infty$), the terms m and n in Eqs. (4.5-127) and (4.5-128) are negligible and the equations for q and r are those given by Eqs. (4.4-18) and (4.4-19):

$$q = \omega_T \cos \omega_g t \qquad (4.5\text{-}129)$$

$$r = -\omega_T \sin \omega_g t \ . \qquad (4.5\text{-}130)$$

At $t = 0$, $\vec{\omega}_T$ lies along the positive Y axis and, for positive p, rotates counterclockwise with constant amplitude and frequency as t increases. Therefore, the asymmetric mass and the rotation of $\vec{\omega}_T$ result in a roll rate oscillation. Two cycles of oscillation in roll rate occur for each revolution of $\vec{\omega}_T$ about the Z axis. The equation for the roll rate history is obtained by substituting Eqs. (4.5-129) and (4.5-130) into (4.5-126) and integrating to give:

$$p - p_i = \frac{\omega_T^2}{2p_i}\left(\frac{I_Y - I_Z}{I_Y - I_X}\right)\frac{I_Y}{I_X}\sin^2 \omega_{g_i} t \qquad (4.5\text{-}131)$$

where

$$\omega_{g_i} = p_i\left(1 - \frac{I_X}{I_Y}\right) .$$

Therefore, the roll rate trace in the exoatmosphere oscillates as a squared sine function with a peak-to-peak amplitude of:

$$\left|\frac{\omega_T^2}{2p_i}\left(\frac{I_Y - I_Z}{I_Y - I_X}\right)\frac{I_Y}{I_X}\right| .$$

The frequency of the oscillation is $2\omega_{g_i}$.

When the vehicle descends to altitudes where aerodynamic forces are no longer negligible, the $\vec{\omega}_T$ develops a pattern of motion that depends upon the initial conditions and the vehicle's aerodynamic characteristics.

Unless the rotation of $\vec{\omega}_T$ about the Z axis becomes very slow, a net change in the magnitude of p is unlikely and the effect on the reentry trajectory is negligible. Under some conditions it has been found (Ref. 4-10) that the direction of rotation $\vec{\omega}_T$ about the Z axis actually changed directions during reentry. During the period when the rotation changed sign, a significant reduction in roll rate occurred.

The possibility of encountering difficulty as a result of unequal I_Y and I_Z appears to be remote, and this type of asymmetry is not considered further in this report.

4.5.10 Applicability of Trim Characteristics at Resonance

In preceding subsections, it was assumed that trim conditions are attained at first resonance. However the resonance condition is approached very rapidly and large changes in trim occur. Unless the missile can respond very quickly to the changing trim conditions, the missile will pass through resonance without attaining large amplifications in the angle of attack. The weathercock frequency, ω_A, is an indication of the ability of the missile to respond to a change in trim. If ω_A is high the missile response time is short; if ω_A is low the missile response time is long. Since

$$\omega_A^2 = \frac{C_{N_\alpha} \Delta X \bar{q} S}{I_Y} ,$$

ω_A is proportional to $\sqrt{\bar{q}}$. Therefore, no matter how much static stability (ΔX) the missile has, the response time is always long at very high altitudes. If resonance occurs at a sufficiently high altitude, trim conditions are not attained and the loads and lock-in criteria based on trim equations are not valid.

The conditions for which trim theory is valid have not been examined in the literature. In order to provide some insight into this problem, a brief study was made of the lock-in criteria using a six-degree-of-freedom trajectory simulation.

Trajectories were computed for three bodies having the following mass and aerodynamic characteristics:

Characteristic	Body A	Body B	Body C
C_A	0.104	0.104	0.104
C_{N_α}	2	0.88	2
C_{m_q}	-1	-1	-2.28
$\Delta X/d$	0.114	0.261	0.114
I_X	30	3	3
m	31.1	31.1	31.1
d	3.5	3.5	3.5
I_Y	300	30	30

Body A is the body used for all examples in this report, and additional characteristics for this body are given in Table 2-1. Bodies B and C have the same value of F_1 (see Eq. (4.5-62)) as has A. Therefore, the lock-in criterion (based on trim conditions) for a combined asymmetry consisting of a center of gravity offset and an aerodynamic trim (see Eq. (4.5-61)) is the same for all three bodies. However, for a given altitude, ω_A is higher for B and C than that for A by a factor of about 3, and therefore, for resonance at high altitudes, B and C are more likely to attain trim conditions than A.

The trajectory initial conditions used in this study are V_E = 20 000 ft/sec, γ_E = -30°, and h_E = 400 000 feet. An in plane combined asymmetry was used for the first set of calculations. The asymmetry consisted of a center of gravity offset (r/d = 0.001) along the +Y axis and a positive yaw moment coefficient (C_{n_o}). The altitude for first resonance was varied from about 40 000 to 140 000 feet by changing the initial roll rate. For each initial roll rate, C_{n_o} was increased until lock-in occurred. Out of plane asymmetries were considered using the same

center of gravity offset with positive and negative values of pitch moment coefficient (C_{m_o}). Values of $\bar{\alpha}_o$ are correctly related to C_{n_o} and C_{m_o} (see Eqs. (4.5-67), (4.5-68), and (4.5-69)).

Three aspects of trim theory are important in the establishment of lock-in criteria.

1. Maximum angle of attack occurs at $\lambda = 1$ $\left(\text{or } \omega_A = p_E \sqrt{1 - \frac{I_X}{I_Y}} \right)$.

2. At $\lambda = 1$ the amplification in angle of attack ($\bar{\alpha}/\bar{\alpha}_o$ or $\bar{\alpha}/\bar{\alpha}_\delta$) is 1/D.

3. At $\lambda = 1$ the plane of the angle of attack (defined by $\Delta\psi$) has rotated 90° from its value at reentry (K = 0).

The results from the six-degree-of-freedom trajectories for body A with $p_E = 1000°/sec$ (corresponding to first resonance at 89 000 feet)show that none of the three assumptions was valid for this resonance altitude. The magnitude and plane of $\bar{\alpha}$ lagged the trim values and the peak amplification was much less than 1/D. The sketch shows a comparison of the $\bar{\alpha}$ and $\Delta\psi$ time histories as given by trim and simulation results.

The trim $\bar{\alpha}$ history reached a peak value at $\lambda = 1$ where lock-in was assumed to occur and then decreased with increasing time, since D increased with time. The trim value of $|\Delta\psi|$ decreased from 180° to 90° at $\lambda = 1$ and remained at 90° as time increased. The simulation results show that $\bar{\alpha}$ built up to a maximum value but lock-in did not occur. Following $\bar{\alpha}_{max}$, the missile began a coning motion with no large excursions in roll rate. The peak $\bar{\alpha}$ was about one-third of the trim value at the initial first resonance altitude; the peak $\bar{\alpha}$ occurred about 1.5 seconds

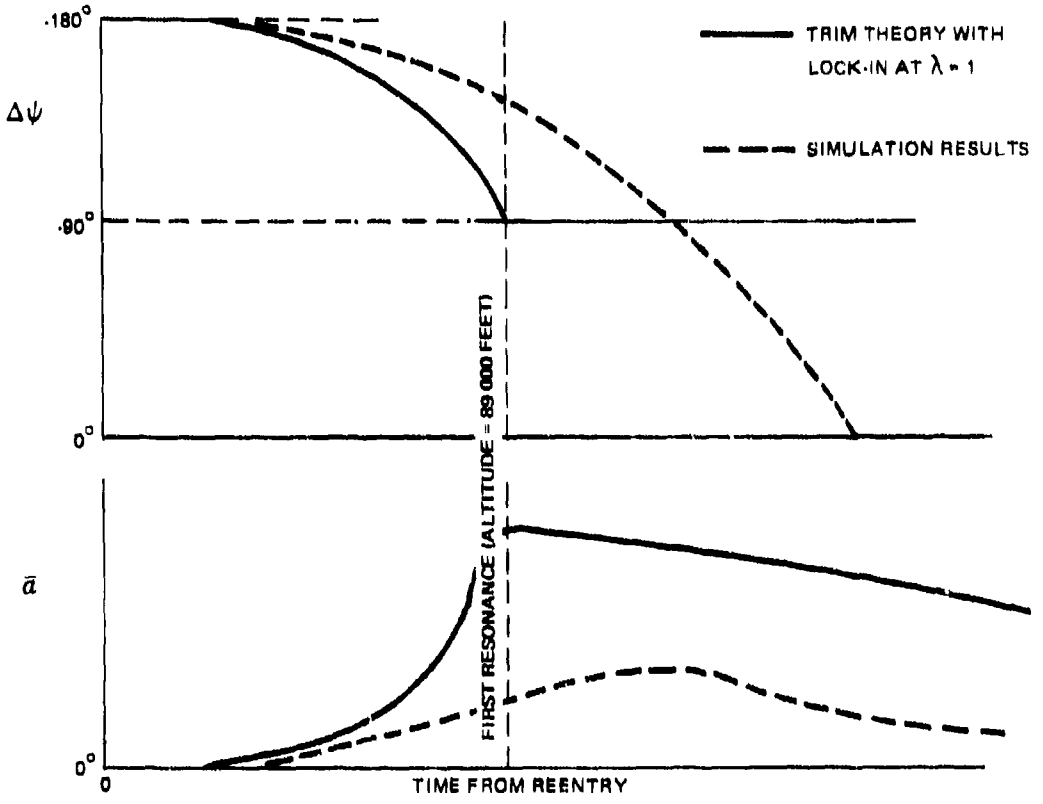

later, or about 15 000 feet lower in altitude than that corresponding to first resonance altitude; the plane of $\bar{\alpha}$ rotated through an angle of 90° about 0.7 second later, or about 7000 feet lower in altitude than that corresponding to first resonance altitude. The angle of attack amplification effect results in larger values of the asymmetries required for lock-in than those given by trim theory. Under some conditions the lag effects would be similar to lowering the first resonance altitude and, thus, asymmetries required for lock-in based on trim theory would be too high. However, for altitudes where first resonance usually occurs, the amplification effect is predominant and the required asymmetries for lock-in based on trim theory are too low.

The condition required for lock-in is given by Eq. (4.5-58). If trim conditions are attained, then Eq. (4.5-58) may be simplified to Eq. (4.5-61). Both equations are plotted in Fig. 4-17 for body A for an in plane (k = 1) and an out of plane (k = 1/2) asymmetry. Note that the assumption that trim conditions exist implies very large values of the roll amplification factor G at the higher altitudes. Also shown are the $\bar{\alpha}_o$ r/d values required for lock-in obtained from simulation results. At the lower altitudes trim theory provided the correct criterion for lock-in for in-plane asymmetry; at the higher altitudes the values of $\bar{\alpha}_o$ r/d required for lock-in obtained from simulation results were somewhat higher than those given by trim theory. In fact, the lock-in boundary is very nearly a constant G contour. The results also indicate that the $\bar{\alpha}_o$ r/d value required for lock-in for the out of plane asymmetry is about twice that required for the in plane asymmetry as predicted by trim theory.

Similar trajectories for bodies having in plane asymmetries were calculated for bodies B and C for an altitude of 136 000 feet only. These results (Figs. 4-18 and 4-19) show that bodies B and C achieve an effective roll amplification of about 18 compared to a value of about 12 for body A. Although B and C have the same response, C was much closer to a trim condition than was B. Note that for an altitude of 136 000 feet the trim condition for C corresponds to $G \approx 27$, whereas trim for B corresponds to $G \approx 60$.

These results indicate that ω_A is one factor which affects the attainment of trim but it is not the only factor, and much work is required in order to define conditions for which trim theory is applicable.

Trajectories were also computed for body A for a combined in-plane asymmetry consisting of a product of inertia and a center of gravity offset. In this case $\bar{\alpha}_\delta$ was held constant at 0.636° and r was varied until lock-in occurred. The altitude for first resonance was 89 000 feet. The results show that lock-in occurred at a value of

$\bar{\alpha}_\delta$ r/d $\approx 2.6 \times 10^{-5}$. If the asymmetry had been an aerodynamic asymmetry and a center of gravity offset, the simulation value of $\bar{\alpha}_o$ r/d would have been 1.2×10^{-5} (see Fig. 4-17). This ratio of about 2 to 1 between the two types of combined asymmetries is nearly the ratio obtained using trim Eqs. (4.5-81) and (4.5-125). Therefore, although trim was not attained for either set of asymmetries, the relative behavior in terms of lock-in criteria was properly predicted using trim equations.

Until additional data become available regarding the applicability of the trim equations, the following comments appear to be valid:

1. Trim equations provide a valid criterion for the lock-in condition provided the roll amplification factor implied by trim is not too high.

2. At resonance altitudes where trim conditions imply very high values of G, trim is not attained, and trim theory predicts asymmetry boundaries that are too low.

3. Values of $\bar{\alpha}_o$ r/d required for lock-in at very high altitudes tend to follow a constant G contour rather than that defined by the trim equation.

4. The limits of G for which trim conditions are attained are probably a function of many variables. For the bodies, trajectory, and initial reentry conditions used in this study, values of G greater than 10 to 20 were not attained. Until more work is done on this problem, trim theory may be used to estimate the asymmetries required for lock-in. However, the results for conditions corresponding to values of G greater than about 20 should be considered as questionable.

5. For an out of plane asymmetry, the required $\bar{\alpha}_o$ r/d for lock-in is larger than that for the in plane asymmetry as predicted by trim theory. Also the relative magnitude of combined asymmetry, α_δ and r, and combined asymmetry, $\bar{\alpha}_o$ and r, are properly defined by trim equations.

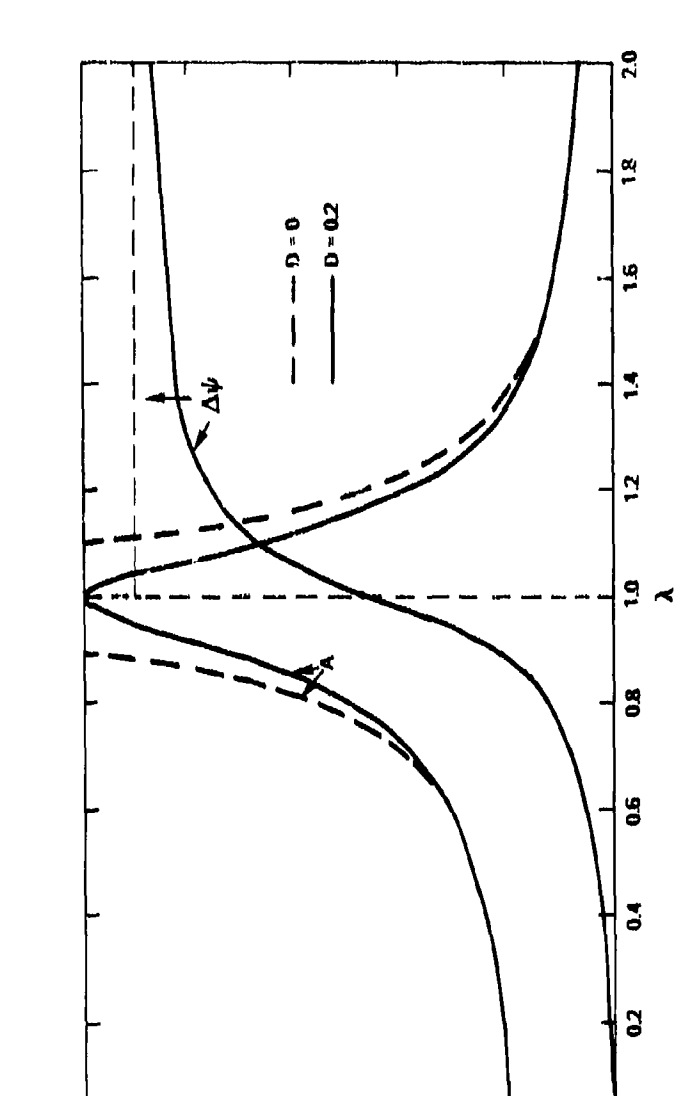

Fig. 4-13 VARIATION OF A AND Δψ WITH λ

Preceding page blank

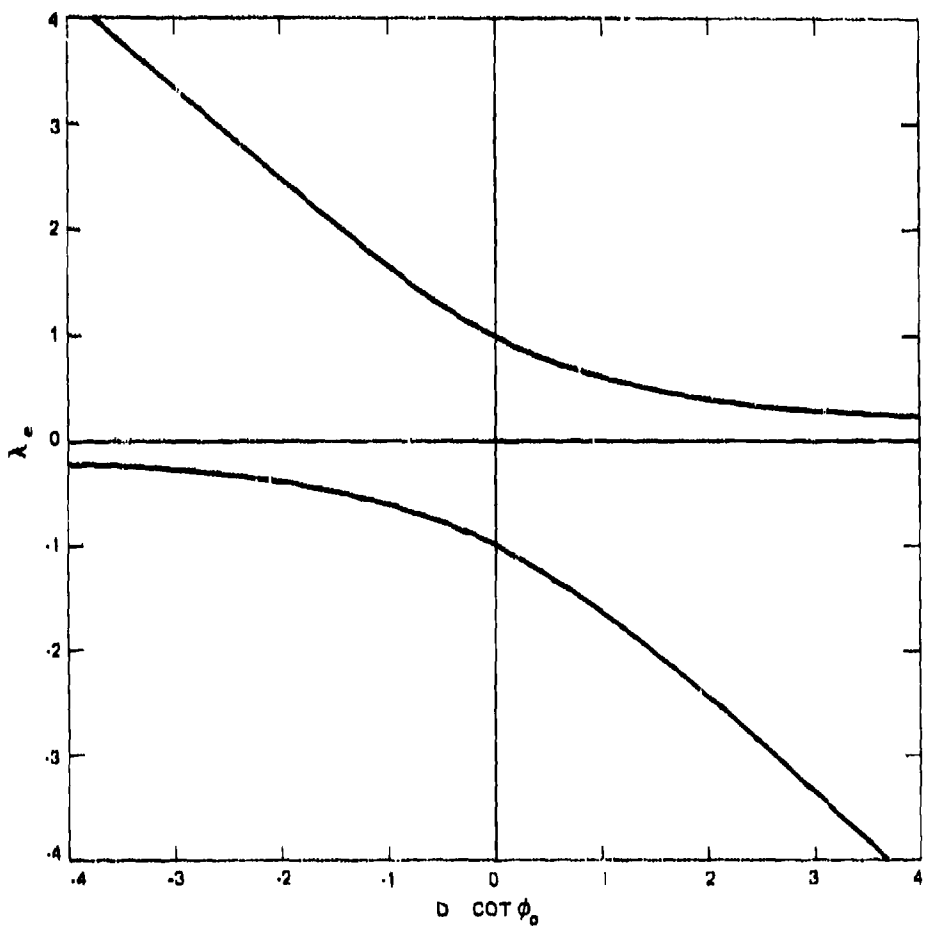

Fig. 4-14 VARIATION OF λ_e WITH D COT ϕ_o

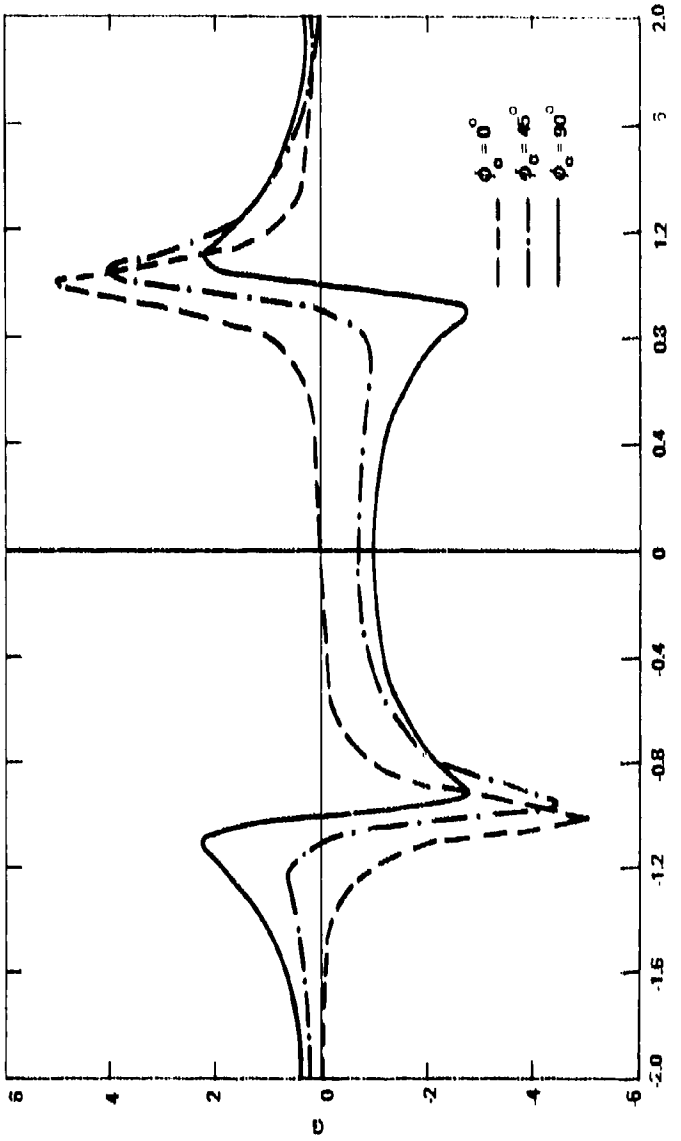

Fig. 4-15 VARIATION OF G WITH λ AND ϕ_o. D = 0.2

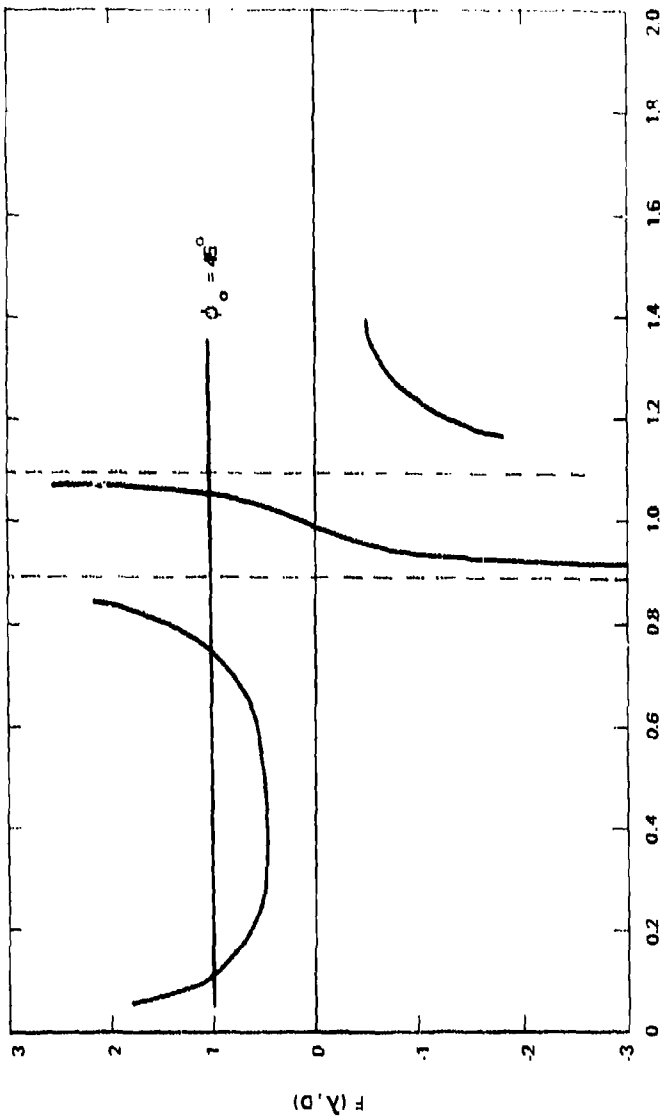

Fig. 4-16 VARIATION OF F (λ, D) WITH λ, D = 0.2

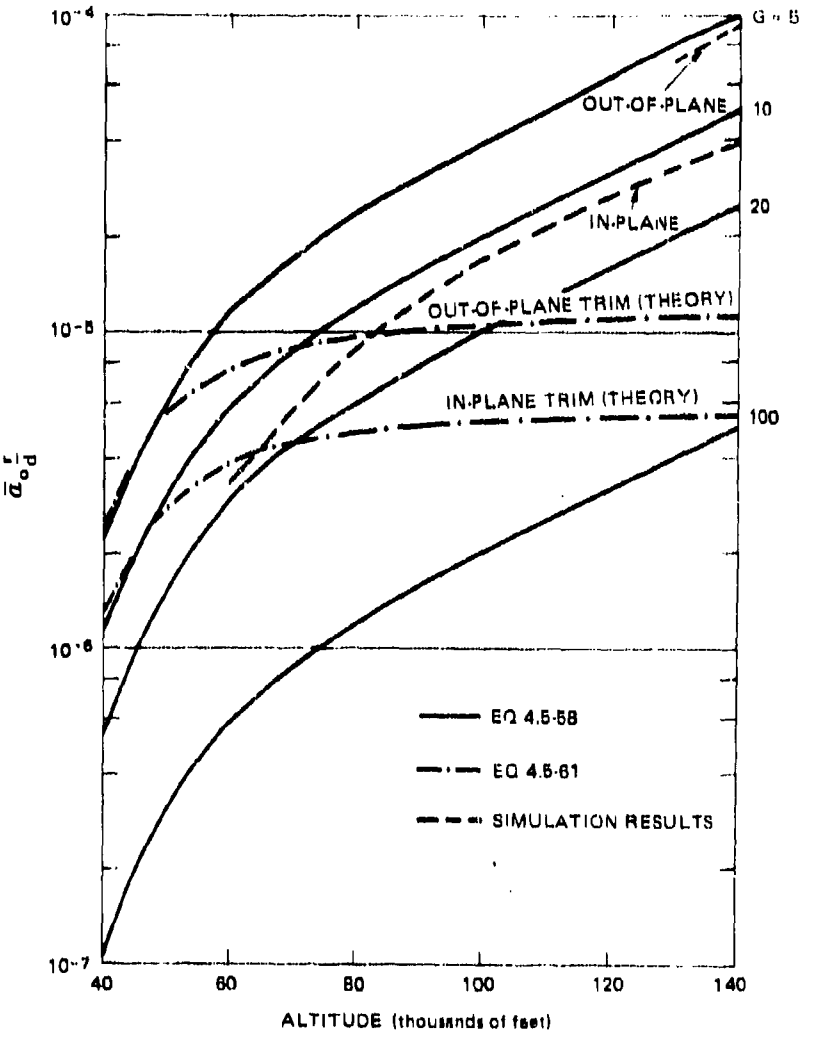

Fig. 4-17 ROLL LOCK-IN CRITERIA, BODY A

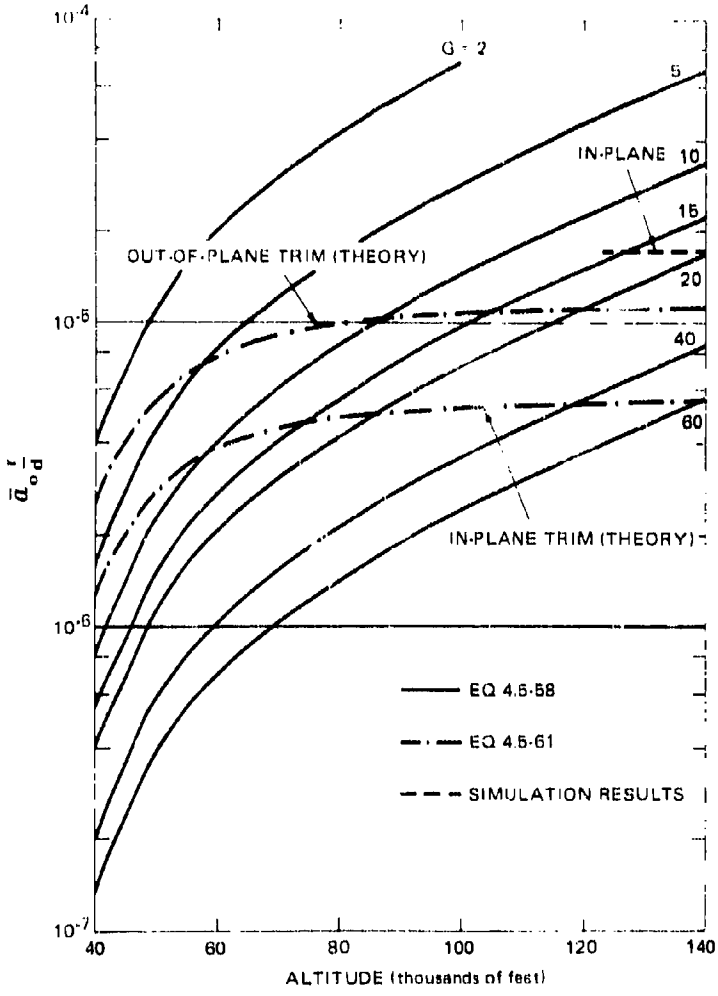

Fig. 4-18 ROLL LOCK-IN CRITERIA, BODY B

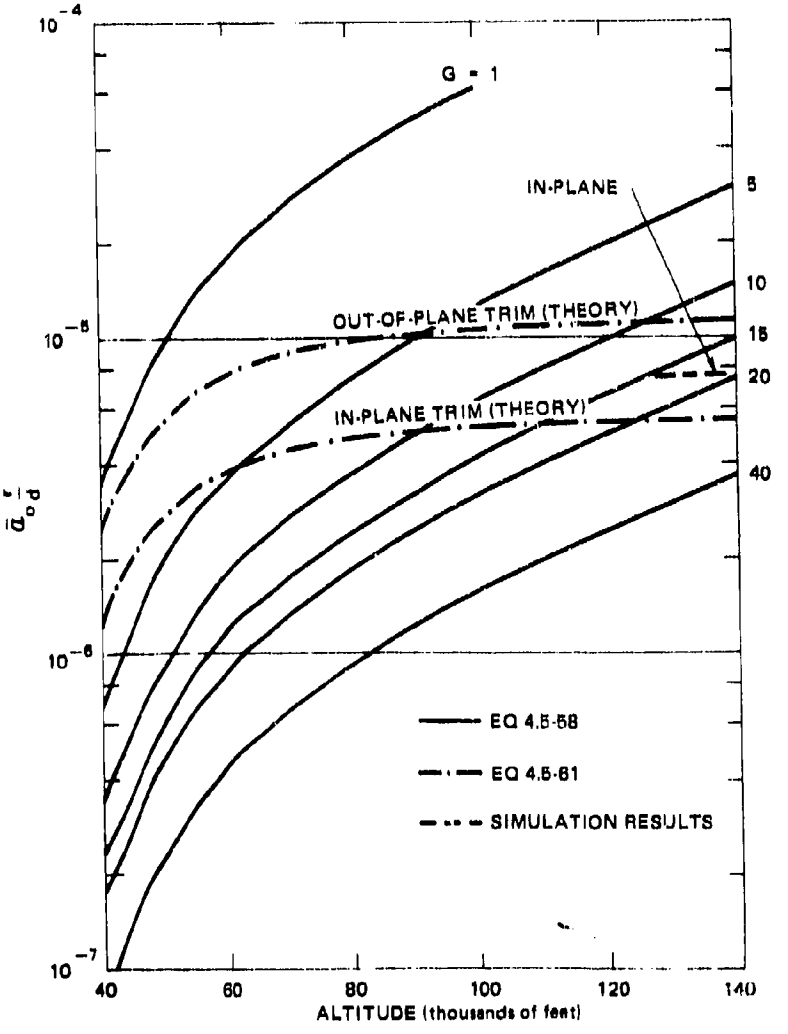

Fig. 4-19 ROLL LOCK-IN CRITERIA, BODY C

4.6 EXAMPLES

SUMMARY

Examples illustrating the material presented in Section 4 are presented in this subsection. The following specific problems are considered:

Example 1 - Minimum energy trajectory for non-rotating earth

Example 2 - Ballistic trajectory for rotating earth

Example 3 - Body motion (oscillation) characteristics in the exoatmosphere

Example 4 - Histories of reentry velocity and related factors

Example 5 - Body loads as affected by a combined asymmetry (center of gravity offset and a distorted body)

Example 6 - Roll lock-in as affected by the combined asymmetry of Example 5

Example 7 - Roll lock-in as affected by a combined asymmetry – center of gravity offset and nonzero product of inertia

4.6.1 Example 1

Compute the characteristics of a minimum energy trajectory (MET) for a nonrotating earth for a launch from $\phi_L = 0°$, $\Lambda_L = 0°$ to a target at $\phi_I = 45°$, $\Lambda_I = 45°$.

The range is(Eqs. (4.2-17) and (4.2-18))
R = 3610 nmi.

The range angle is (Eq. (4.2-18)) $2\theta_o = 2\theta_e = 60°$.

The azimuth angle at launch is (Eq. (4.2-20))
$\psi_{LI} = 35.4°$.

For an MET, the initial flight path angle is (Eq. (4.1-10))

$$\gamma_o = 45° - 15° = 30°.$$

From Eq. (4.1-11) $\overline{V}_o = 0.815$ and, assuming the initial altitude to be sea level, the initial velocity is

$$V_o = 0.815\ (26\ 000) = 21\ 200 \text{ ft/sec}.$$

The peak altitude of the trajectory is (Eq. (4.1-22))
$h_a = 635$ nmi.

The velocity at peak altitude is (Eq. (4.1-24))
$V_a = 15\ 500$ ft/sec, or about 73% of the initial velocity.

The time to impact is (Eq. (4.1-17)) t = 1480 seconds.

4.6.2 Example 2

For a rotating earth, determine the characteristics of a trajectory fired with initial conditions V_o, γ_o, and ψ_{LI} (relative to earth) computed in Example 1.

The inertial quantities V, γ, and ψ at launch are (Eqs. (4.2-7), (4.2-8), and (4.2-10)):

Preceding page blank

$$\frac{\tan \psi_L}{\tan \psi_e} = 1 + \frac{1520(1)}{21\ 200 \cos 30 \sin 35.4} = 1.142$$

$$\tan \psi_L = 1.142 \tan 35.4$$

$$\psi_L = 39.1°$$

$$\frac{V_L}{V_e} = 1 + \cos 30 \sin 35.4 \left| \frac{1520(1)}{21\ 000} \right| = 1.036$$

$$V_L = 1.036\ (21\ 200) = 22\ 000 \text{ ft/sec}$$

$$\overline{V}_L = \frac{22\ 000}{26\ 000} = 0.845$$

$$\frac{\sin \gamma_L}{\sin \gamma_e} = \frac{21\ 200}{22\ 000} = 0.963$$

$$\sin \gamma_L = 0.963\ (0.50) = 0.482$$

$$\gamma_L = 28.9°$$

Therefore the effect of earth rotation is to increase the initial inertial velocity by about 3.6%, to lower the flight path angle by 1.1°, and to increase the azimuth angle by 3.7°. These changes would have opposite signs if the vehicle had been fired in a westerly direction.

Using $\overline{V}_L$ and γ_L for $\overline{V}_o$ and γ_o, the equations given in Section 4.1 apply. However, note that the trajectory is not an MET since Eq. (4.1-11) is not satisfied. For the given V_L a minimum energy trajectory would have $\gamma_L = 28.1$ so that the trajectory being considered is slightly high compared to an MET.

The nonrotating earth range angle is (Eq. (4.1-7)):

$2\theta_o = 67.4°$.

The corresponding range, $r_o(2\theta_o) = 4020$ nmi, is the arc length traveled in inertial space (or the range on a nonrotating spherical earth for initial conditions V_L, γ_L, and ψ_L).

The impact time is (Eqs. (4.1-5) and (4.1-16))
$t = 1660$ seconds.

The impact latitude is unaffected by earth rotation and is $\phi_I = 45°$.

The impact longitude is (Eq. (4.2-16)) $\Lambda_I = 49.4°$.

The impact range is (Eqs.(4.2-17) and (4.2-18))
$R = 3780$ nmi.

A summary of the results is given below:

Quantity	Nonrotating Earth	Rotating Earth
Flight time (seconds)	1480	1660
Impact latitude (degrees)	45.0	45.0
Impact longitude (degrees)	45.0	49.4
Impact range (nmi)	3610	3780

For the initial conditions used, the effect of earth rotation is to increase the range by 170 nmi and to increase the flight time by 180 seconds.

4.6.3 Example 3

The typical reentry body, having mass characteristics defined in Table 2-1, is separated from its booster in the exoatmosphere. At separation, the body is spun about its longitudinal axis at a rate of 360°/sec and,

unintentionally, is given a transverse rate of 60°/sec. Determine the characteristics of the body motion during its travel in the exoatmosphere.

The only forces acting on the missile are weight and the forces resulting from the body rates. Under the influence of these forces, the body is gyroscopically stabilized, and the transverse rate imparted at separation results in the conical motion described in Section 4.4.1. The period of the motion is (Eq. (4.4-25)):

$$\tau_s = 5.12 \text{ seconds.}$$

The signal strength of a tracking radar varies with the attitude of the reentry vehicle. Therefore, the radar signal strength would oscillate with a period $\tau_s = 5.12$ seconds.

The semicone angle of the space cone is (Eq. (4.4-23)) $\phi = 59°$. The body rates measured by on-board rate gyros have the following characteristics (assuming a symmetrical vehicle):

1. The roll rate is constant and equal to 360°/sec.

2. The pitch and yaw rates very sinusoidally about zero with peak values of ±60°/sec. The pitch and yaw rates are 90° out of phase. The period shown on the traces is (Eq. (4.4-24)):

$$\tau_B = 1.11 \text{ seconds.}$$

If the body were spin stabilized so that the total angular momentum vector $\vec{H}$ were along the flight path direction at reentry, during the early phase of reentry $\bar{\alpha}$ would be constant and equal to 59°. However, the pitch and yaw (inertial) components of $\bar{\alpha}$ would oscillate with a half-amplitude of 59° and a period of 5.12 seconds.

4.6.4 Example 4

Determine the effect of the atmosphere on the motion of the reentry body using the following reentry conditions:

h_E = 400 000 feet
V_E = 20 000 ft/sec
γ_E = -30°
p_E = 0°/sec and 360°/sec (6.28 rad/sec)
$\bar{\alpha}_E$ = 10°
ω_T = 0

Use the 1962 Standard Atmosphere given in Table 3-1 and the mass and aerodynamic characteristics given in Table 2-1.

Since ω_T = 0, the vehicle is not in a conical motion as was described in the previous problem. The angle of attack $\bar{\alpha}$ remains constant and in the original plane (inertial pitch and yaw angles of attack remain constant) until aerodynamic forces begin to affect the motion by causing a decay in $\bar{\alpha}$. Using $\bar{\alpha}/\bar{\alpha}_E$ = 0.99 as the beginning of the $\bar{\alpha}$ decay, for p_E = 360°/sec:

$$\frac{\rho}{\rho_o}(\text{Eq. (4.4-55)}) = 3.21 \times 10^{-7} .$$

From Table 3-1, this density ratio corresponds to an altitude between 300 000 and 350 000 feet. A more complete table shows the altitude to be h = 332 000 feet. If the initial roll rate were zero, Eq. (4.4-41) could be used to obtain the altitude at which the $\bar{\alpha}$ decay begins

$$\frac{P}{P_o} H = \frac{0.02\,(300)\,(32.2)\,(0.25)}{0.65\,(2)\,(0.4)\,(2116)} = 2.96 \times 10^{-3} \text{ feet.}$$

Using the characteristics of the 1962 Standard Atmosphere, this value of $\frac{P}{P_0}$ II corresponds to an altitude of about 350 000 feet. Therefore, the effect of the 360°/sec spin rate was to delay the $\bar{\alpha}$ decay by about 18 000 feet.

The $\bar{\alpha}$ decay histories may be computed using Eqs. (4.4-44) and (4.4-53). In order to evaluate these equations, the variations of ω_A and K with altitude are required. These characteristics, obtained using Eqs. (4.3-6) and (4.3-23) and the atmosphere defined in Table 3-1, are listed in Table 4-1. From Eq. (4.4-45) and Table 2-1, the damping constant is:

$$C_3 = 7.6.$$

About 60% of C_3 comes from the $C_{N_{\dot{\alpha}}}$ term and 40% from the C_{m_q} term. The $\bar{\alpha}$ decay history for the rolling body was computed using Eq. (4.4-53), and the results are shown in Fig. 4-20. Also shown is the case of the nonrolling missile and the case of a rolling missile with $C_3 = 0$. For the rolling vehicle, the effect of the C_3 damping term is negligible for altitudes above about 150 000 feet. For altitudes below about 60 000 feet, the $\bar{\alpha}$ history for the rolling case (with damping) is nearly the same as that for the nonrolling case. However, at altitudes above 60 000 feet, the angle of attack at a given altitude for the rolling body is significantly higher than that for the nonrolling body. This fact could be important for some missiles in which the peak lateral load occurs at these altitudes. For the body studied, the peak lateral load resulting from $\bar{\alpha}_E$ occurs at an altitude (Eq. (4.4-59)) for which:

$$K = \frac{3}{4}\frac{1}{(7.6 + 0.75)} = 0.090$$

From Table 4-1, this value of K corresponds to an altitude of about 85 000 feet. The altitude for maximum g_L is the same whether or not the missile is rolling. However, as a result of the $\bar{\alpha}$ histories, $g_{L_{max}}$ for the

rolling missile is about 45% greater than that for a nonrolling vehicle (Eqs. (4.4-60) and (4.4-63)). For $\bar{\alpha}_E = 10°$, $g_{L_{max}}$ for a rolling vehicle is 2.75g compared to 1.9g for a nonrolling vehicle.

The reentry velocity, Mach number, and Reynolds number are important environmental factors that affect body loads and temperature. The time history of these characteristics estimated using Eqs. (4.3-5), (4.3-7), and (4.3-10) and the atmospheric characteristics given in Table 3-1 are listed in Table 4-1.

The Mach number history shows that the vehicle is in the hypersonic regime ($M \geq 6$) down to an altitude of about 15 000 feet and is supersonic from 15 000 feet to impact. The Reynolds number history shows that transition on the body would be expected at an altitude of about 110 000 feet ($R_e \approx 10^7$) with laminar flow at higher altitudes and turbulent flow at lower altitudes. The heating rate to the conical surface of the body would increase by a factor of 2 to 3 when the flow becomes turbulent, and therefore asymmetries that result from heating would be expected to increase rapidly at the transition altitude. The aerodynamic frequency data show that roll resonance ($\lambda = p\sqrt{1 - \frac{I_X}{I_Y}}\Big/\omega_A = 1$) occurs at an altitude of about 135 000 feet. It should be noted that the vehicle is approaching a second resonance condition at impact, and any asymmetries that exist near altitudes of 135 000 feet and sea level are likely to be amplified. The computed values of M/R_e show that free molecular flow regime begins at altitudes well above 400 000 feet ($M/R_e \approx 10$), transition flow exists down to an altitude of about 250 000 feet ($M/\sqrt{R_e} \approx 0.1$), slip flow exists at altitudes from 250 000 to 140 000 feet ($M/\sqrt{R_e} \approx 0.01$), and continuum flow exists at altitudes from 140 000 feet to sea level. The time from 400 000 feet to impact is about 49 seconds compared with about 39 seconds if the atmosphere were absent. Therefore, the atmosphere increased the flight time by about 10 seconds.

Although not shown in the table, several other important considerations may be obtained from the equations given in Section 4.3. Using the ratio $q_s/q_{s_{max}} = 0.1$ as an indication of conditions where heating is significant, the altitudes are computed (Eqs. (4.3-11) and (4.3-16)) to be about 190 000 feet for the beginning of the heating period and about 13 000 feet for the end of heating with the maximum heating rate at an altitude of about 58 000 feet. The longitudinal deceleration(Eqs. (4.3-9) and (4.3-14)) is maximum at an altitude of about 35 000 feet where $g_{X_{max}} \approx -54g$. The inflection points in the g_X versus time curve (Eq. (4.3-19)) occur at altitudes of 58 000 and 19 000 feet.

The results obtained in this problem are summarized in Fig. 4-21. Although the altitude bands shown vary slightly depending upon vehicle geometry and trajectory characteristics, the results are typical of high β reentry bodies. Note that practically all of the quantities of interest occur at altitudes below about 150 000 feet and therefore are in the continuum flow regime. Both laminar and turbulent flow conditions exist in this altitude region, all three Mach number regimes occur (although only two occurred for this trajectory), and both oscillatory and trim types of body motion may be important.

4.6.5 Example 5

Suppose the reentry vehicle has a center of gravity offset from the body centerline of 0.042 inch. Furthermore, assume that as a result of exoatmospheric blast effects the body is distorted so that the body centerline is an arc of a circle and that the tangent to the centerline changes by 0.25° from base to nose tip. Use the same initial conditions as were used for Example 4 except use $p_E = 1000°/sec$. Assess the probability that the missile will encounter excessive lateral loads. For this problem we will define $g_L \geq 20g$ as excessive.

From Eq. (2-35) the $\overline{C}_{m_o}$ resulting from the bent body is 0.002. We will assume that the lateral location of the center of pressure and center of gravity are unaffected by the bent body.

From Eq. (4.5-65) the trim angle of attack resulting from $\overline{C}_{m_o}$ is:

$$\overline{\alpha}_{o_M} = \frac{0.002}{2 \times 0.114} \times 57.3 = 0.5°.$$

The trim angle resulting from the center of gravity offset is (Eq. (4.5-64)):

$$\overline{\alpha}_{o_{c.g.}} = \frac{0.104 \frac{0.042}{42}}{2 \times 0.114} \times 57.3 = 0.0261° .$$

Therefore, the total trim angle $\overline{\alpha}_o$ is very nearly the angle resulting from the bent body and we will use $\overline{\alpha}_o = 0.5°$. The equation for g_L is:

$$g_L = \frac{C_{N_\alpha} S}{W} \overline{q} A \overline{\alpha}_o .$$

For the moment assume that no amplification in $\overline{\alpha}_o$ occurs, so that A = 1. For this case, the largest possible value of g_L occurs at $\overline{q}_{max}$. From Eq. (4.3-13) $\overline{q}_{max}$ occurs at $P/P_o = \frac{1000}{2116}(\frac{1}{2}) = 0.237$, corresponding to an altitude of 35 000 feet and a temperature of 394°R. The magnitude of $\overline{q}_{max}$ is:

$$\overline{q}_{max} = \frac{1000\,(20\,000)^2 (0.5)}{9330\,(394)} = 54\,400 \text{ lb/ft}^2$$

and

$$g_{L_{max}} = 9.2g$$

Excessive values of g_L will not be obtained unless values of A in excess of 2 are obtained. Amplifications of this magnitude will be encountered if large excursions in roll rate occur. The possibilities that must be considered are:

1. Roll lock-in at first resonance,
2. Roll lock-in at second resonance,
3. Spin up with lock-in at some intermediate altitude,
4. Spin down with lock-in at a negative roll rate.

Assuming that lock-in is attained, from Eq. (4.5-16) A = 1/D and D may be evaluated using Eq. (4.5-60). Substituting these equations and the equation for $\bar{q}$ (Eq. (4.3-8)) into the equation for g_L, excessive loads will occur when the following inequality is satisfied.

$$\bar{\alpha}_o \geq \frac{57.3 \times 20 \,(k_1 - C_{m_q})\, gd}{C_{N_\alpha} V_E^2} \left[\frac{2C_A \frac{H}{d}}{\frac{\Delta X}{d} k_1 \sin\gamma} \right]^{1/2} \frac{\rho^K}{\sqrt{K}}$$

where $\bar{\alpha}_o$ is expressed in degrees.

Substituting for the mass, aerodynamic, and trajectory parameters, and assuming H constant = 22 000 feet:

$$\bar{\alpha}_o \geq 0.043 \frac{\rho^K}{\sqrt{K}} .$$

This inequality is plotted in Fig. 4-22. It is observed that $\bar{\alpha}_o = 0.5°$ is large enough to result in excessive loads at some altitudes. The first and second resonance altitudes are the altitudes for which $\omega_A = p_{r_E} = p_E \sqrt{1 - \frac{I_x}{I_Y}}$ rad/sec

Values of ω_A were computed using Eq. (4.3-23) and the results are shown in Fig. 4-23. First resonance occurs at an altitude of about 89 000 feet, and second resonance occurs at an altitude of about 4000 feet. Therefore roll lock-in at first resonance would result in excessive loads, but lock-in at second resonance would not.

Depending upon the value of ϕ_o, the roll rate may not lock-in at first resonance but may either spin up or spin down. The magnitude of the decrease in roll rate is given by Eq. (4.5-93). This equation may also be used to obtain an approximate value of the spin up characteristics. However, the magnitude of Δp in this case will be underestimated slightly since the amplification in $\bar{\alpha}_o$ and the change in the angle ϕ are neglected. Using Eq. (4.5-93) and assuming values of ϕ_c = 90° and 270° (which give the largest values of Δp) values of p_r were computed and are shown in Fig. 4-23. From this consideration it is found that the asymmetries are not large enough to result in roll reversal. Therefore, resonance at negative roll rates may be eliminated as a possible condition that would result in excessive loads. However, if the vehicle does not lock in at first resonance but spins up, resonance may occur at an altitude of about 13 000 feet. From Fig. 4-22, resonance at this altitude would result in excessive loads. Therefore, the problem is reduced to an evaluation of whether or not lock-in will occur at altitudes of 89 000 and 13 000 feet.

The criterion for lock-in is (Eq. (4.5-61)):

$$\bar{\alpha}_o \frac{r}{d} \geq F_1 \frac{(1-K_R)}{k} \quad .$$

Using the data given in Tables 2-1 and 3-1 and the trajectory characteristics, the value of F_1 (Eq. (4.5-62)) is 5.4×10^{-6} for h = 89 000 feet (H = 21 700 feet) and is 4.7×10^{-6} for h = 13 000 feet (H = 25 000 feet). Using $r/d = 0.042/12(3.5) = 0.001$ and expressing $\bar{\alpha}_o$ in degrees:

$$\bar{\alpha}_o \geq 0.31 \frac{(1 - K_R)}{k} \quad \text{for } h = 89\,000 \text{ feet}$$

$$\geq 0.27 \frac{(1 - K_R)}{k} \quad \text{for } h = 13\,000 \text{ feet.}$$

Using the data of Table 4-1 a plot of K versus altitude shows that $K_R = 0.077$ at 89 000 feet and $K_R = 2.58$ at 13 000 feet. Therefore, the criteria for lock-in are:

$$\bar{\alpha}_o \geq \frac{0.286}{k} \quad \text{for } h = 89\,000 \text{ feet}$$

$$\geq \frac{-0.427}{k} \quad \text{for } h = 13\,000 \text{ feet.}$$

The value of k depends upon the value of ϕ_o and, for lock-in to occur, k must be positive for $K_R < 1$ and negative for $K_R > 1$. For this problem we must assume that ϕ_o may have any value. Therefore, we must consider the following possibilities:

Resonant Altitude	ϕ_o	k	$\bar{\alpha}_o \geq$
89 000 feet	0°	1	0.286
	90°	0.5	0.572
	270°	0.5	0.572
13 000 feet	270°	-0.5	0.854

The other two values of ϕ_o having negative values for k for the 13 000 foot case are ruled out since the $\phi_o = 270°$ value is required to provide spin up during reentry (see Eq. (4.5-33)). Of the four possibilities only the $\phi_o = 0°$ case with resonance at 89 000 feet satisfies the $\bar{\alpha}_o$ criterion.

In the preceding discussion we considered only in-plane and out-of-plane conditions. For intermediate values

of ϕ_o, $\bar{\alpha}_o$ may be divided into in-plane and out-of-plane components. Any value of ϕ_o for which the component of $\bar{\alpha}_o$ in the $\phi_o = 0°$ direction is ≥ 0.286 will result in excessive values of g_L. The possibilities are shown in Fig. 4-24. Any value of ϕ_o defined by points from A to B (shorter arc length) will result in excessive values of g_L. Since any value of ϕ_o is equally likely to occur, the probability of encountering excessive g_L is:

$$\bar{P} = \frac{2 \cos^{-1} \frac{0.286}{0.500}}{360} = 0.31 .$$

4.6.6 Example 6

For the trajectory used in Example 4, estimate as a function of p_E the maximum allowable $\bar{\alpha}_o$ combined with $r = 0.042$ inch so that neither lock-in at first resonance nor spin through zero occurs. In view of the discussion given in Section 4.5.10, assume that the criterion for lock-in is the trim equation (Eq. (4.6-61)) or $G = 20$, whichever gives the larger value of $\bar{\alpha}_o$.

The critical conditions to be investigated are the $\phi_o = 0°$ case for lock-in and the $\phi_o = 90°$ case for spin through zero.

For the lock-in case, assume that H = constant = 21 700 feet. Substituting the mass, aerodynamic, and trajectory terms into Eq. (4.5-58), the criterion for lock-in becomes:

$$\bar{\alpha}_o \geq \frac{2.65}{G} \frac{(1 - K_R)}{\sqrt{K_R}} .$$

If trim conditions are attained, the criterion for lock-in is (see Example 5):

$$\bar{\alpha}_o \geq 0.31 (1 - K_R) ,$$

Setting G = 20 in the first equation, the two equations give the same solution to $\bar{\alpha}_o$ at:

$$\frac{2.65}{20} \frac{1}{\sqrt{K_R}} = 0.31$$

or

$$K_R = 0.183 ,$$

corresponding to an altitude of about 70 000 feet (see Table 4-1). At altitudes lower than 70 000 feet (or $K_R >$ 0.183) the trim equation is used; at altitudes higher than 70 000 feet the nontrim equation is used with G = 20.

For each resonant altitude the corresponding initial roll rate may be computed from the equation:

$$p_E = \frac{\omega_A}{\sqrt{1 - \frac{I_X}{I_Y}}}$$

where ω_A is given in Table 4-1. The values of $\bar{\alpha}_o$ required for lock-in are shown as a function of p_E in Fig. 4-25.

The change in roll rate resulting from asymmetries $\bar{\alpha}_o$ and r/d is given by Eq. (4.5-93). Spin through zero roll rate will occur during reentry if Δp is negative and $|\Delta p| \geq p_E$. Using the most restrictive condition ($\phi_o = 90°$ and $K = K_{SL}$) and expressing $\bar{\alpha}_o$ and p_E in units of degrees and deg/sec, respectively, the criterion for spin through zero roll rate is:

$$\bar{\alpha}_o \geq 8.17 \times 10^{-4} \, p_E .$$

The values of $\bar{\alpha}_o$ required for spin through zero roll rate are shown in Fig. 4-25.

This problem illustrates some of the trade-offs which must be considered by the designer in selecting a roll rate for the reentry body. If the roll rate is very low, first resonance occurs at a very high altitude, where large values of $\bar{\alpha}_o$ may be tolerated without encountering lock-in. However, vehicles with low values of p_E are susceptible to spin through zero roll rate. On the other hand, for moderately high values of p_E, large values of $\bar{\alpha}_o$ may be tolerated without spinning through zero roll rate, but $\bar{\alpha}_o$ must be very low if lock-in is to be avoided. For this particular problem the best roll rate is p_E = 760°/sec where the missile could tolerate up to 0.6° in $\bar{\alpha}_o$ without encountering either adverse condition. A second possibility would be to select a value of p_E much greater than 2240°/sec. In this case spin through zero roll rate would be unlikely, and lock-in is avoided by using a roll rate that is much greater than the maximum aerodynamic frequency. This technique is sometimes referred to as "overspin."

4.6.7 Example 7

Using the trajectory of Example 4 with p_E = 1000°/sec, first resonance occurs at an altitude of 89 000 feet (K_R = 0.077). Determine the values of $\bar{\alpha}_\delta$ and r for which lock-in at first resonance may occur. Assume that the trim equation (Eq. (4.5-125)) is valid. Compare the results with $\bar{\alpha}_o$ and r given by Eq. (4.5-61).

From Eq. (4.5-62) $F_1 = 5.4 \times 10^{-6}$ (H = 21 700 feet). Using the mass and aerodynamic characteristics given in Table 2-1, F_3 = 4.87 and $F_4 = 5.26 \times 10^{-5}$. For α_δ in degree units, Eq. (4.5-125) becomes:

$$\bar{\alpha}_\delta = 279 \frac{r}{d} \left[1 \pm \sqrt{1 - \frac{2.05 \times 10^{-6}}{(r/d)^2}} \right] .$$

The $\bar{\alpha}_\delta$ boundary is shown in Fig. 4-26. At a given value of r, $\bar{\alpha}_\delta$ must be greater than $\bar{\alpha}_{\delta_{min}}$ but less than $\bar{\alpha}_{\delta_{max}}$. Lock-in cannot occur for any value of $\bar{\alpha}_\delta$ if r < 0.06 inch.

By comparison the trim equation for $\bar{\alpha}_o$ and r becomes:

$$\bar{\alpha}_o = \frac{0.286 \times 10^{-3}}{r/d} .$$

The $\bar{\alpha}_o$ boundary is also shown. It is noted that $\bar{\alpha}_o$ has no $\bar{\alpha}_{o_{max}}$ boundary, and the $\bar{\alpha}_o$ boundary is less than $\bar{\alpha}_{\delta_{min}}$.

Single points on each boundary obtained from six-degree-of-freedom simulation results (see Section 4.5.10) are also shown. The $(\bar{\alpha}_o, r)$ point was obtained by holding r constant and increasing $\bar{\alpha}_o$ until lock-in occurred. The $(\bar{\alpha}_\delta, r)$ point was obtained by holding $\bar{\alpha}_\delta$ constant and varying r until lock-in occurred. Note that the real boundaries are somewhat higher than the boundaries based on the trim equations as discussed in Section 4.5.10.

For other values of p_E, the $\bar{\alpha}_\delta$ boundary must remain within the $\bar{\alpha}_{\delta_{max}}$ and $\bar{\alpha}_{\delta_{min}}$ asymptotes shown in Fig. 4-26, and r_{min} is shifted right or left depending upon the value of K_R. Using data given in Table 4-1 and the relationship between p_E and ω_A at resonance, $p_E = \frac{\omega_A}{\sqrt{1 - \frac{I_X}{I_Y}}}$, r_{min} is shown in Fig. 4-27 as a function of p_E. For r = 0.042 inch used in the previous problem, lock-in could exist only for values of p_E that result in resonance very near to the altitude of maximum dynamic pressure (35 000 feet).

For current reentry vehicles, values of p_E are selected such that first resonance occurs at altitudes above 100 000 feet. In this altitude range r_{min} is insensitive to p_E, and the $\bar{\alpha}_\delta$ boundary shown in Fig. 4-26 is applicable to first resonance lock-in for all values of p_E

less than about 1000°/sec. For p_E = 1000°/sec considered in this problem, second resonance occurs at an altitude of about 4000 feet (neglecting a change in roll rate during reentry) where r_{min} is nearly a factor of 2 greater than r_{min} at first resonance.

REFERENCES

4-1 L. S. Glover, "Approximate Re-Entry Velocity and Heating Equations," J. Spacecraft and Rockets, January 1966.

4-2 D. T. Greenwood, "Flight Mechanics of Space and Re-Entry Vehicles," Michigan University Engineering Summer Conferences, 1964.

4-3 H. J. Allen, Motion of a Ballistic Missile Angularly Misaligned with the Flight Path upon Entering the Atmosphere and Its Effect upon Aerodynamic Heating, Aerodynamic Loads, and Miss Distance, NACA TN-4048, 1965.

4-4 R. B. Powell and R. L. Smith, "Dynamics of Spinning Re-Entry Bodies," AIAA Preprint No. 64-470, 1964.

4-5 H. I. Leon, "Angle of Attack Convergence of a Spinning Missile Descending Through the Atmosphere," J. Aerospace Sci., August 1958.

4-6 L. S. Glover, Analytical Expressions for the Effect on Roll Rate of Mass and Aerodynamic Asymmetries for Ballistic-Type Bodies, APL/JHU TG 560, March 1964.

4-7 J. D. Nicolaides, On the Free Flight Motion of Missiles Having Slight Configurational Asymmetries, Ballistic Research Laboratories, Aberdeen Proving Ground, Report 868, June 1953.

4-8 R. L. Nelson, Measurement of Aerodynamic Characteristics of Re-Entry Configurations in Free Flight at Hypersonic and Near Orbital Speeds, Lockheed Missiles and Space Division, TR 6-90-61-37, July 1961.

REFERENCES (cont'd)

4-9 A. E. Hodapp, Jr. and E. L. Clark, Jr., "The Effects of Products of Inertia on the Roll Behavior of Ballistic Re-Entry Vehicles," AIAA Paper No. 70-204, January 1970.

4-10 L. S. Glover, "Effects on Roll Rate of Mass and Aerodynamic Asymmetries for Ballistic Re-Entry Bodies," J. Spacecraft and Rockets, April 1965.

4-11 K. A. Ehricke, Principles of Guided Missile Design, Space Flight, Vol. II, "Dynamics," D. Van Nostrand Company, Inc., 1962.

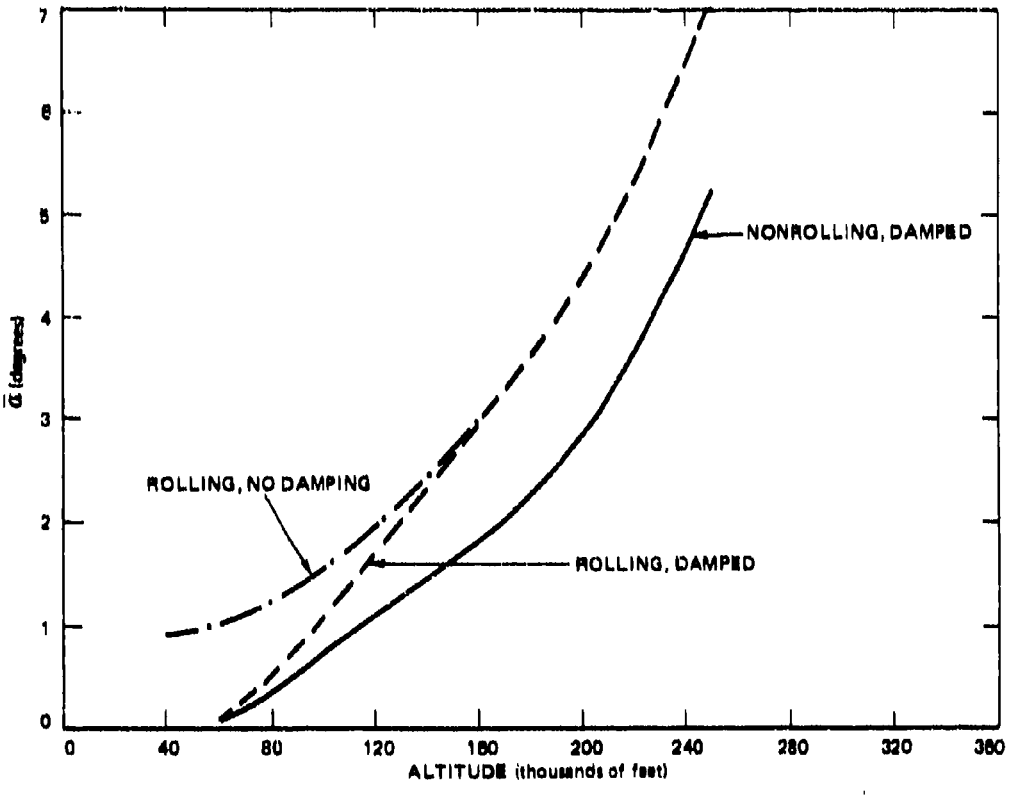

Fig. 4-20 ᾱ DECAY CHARACTERISTICS

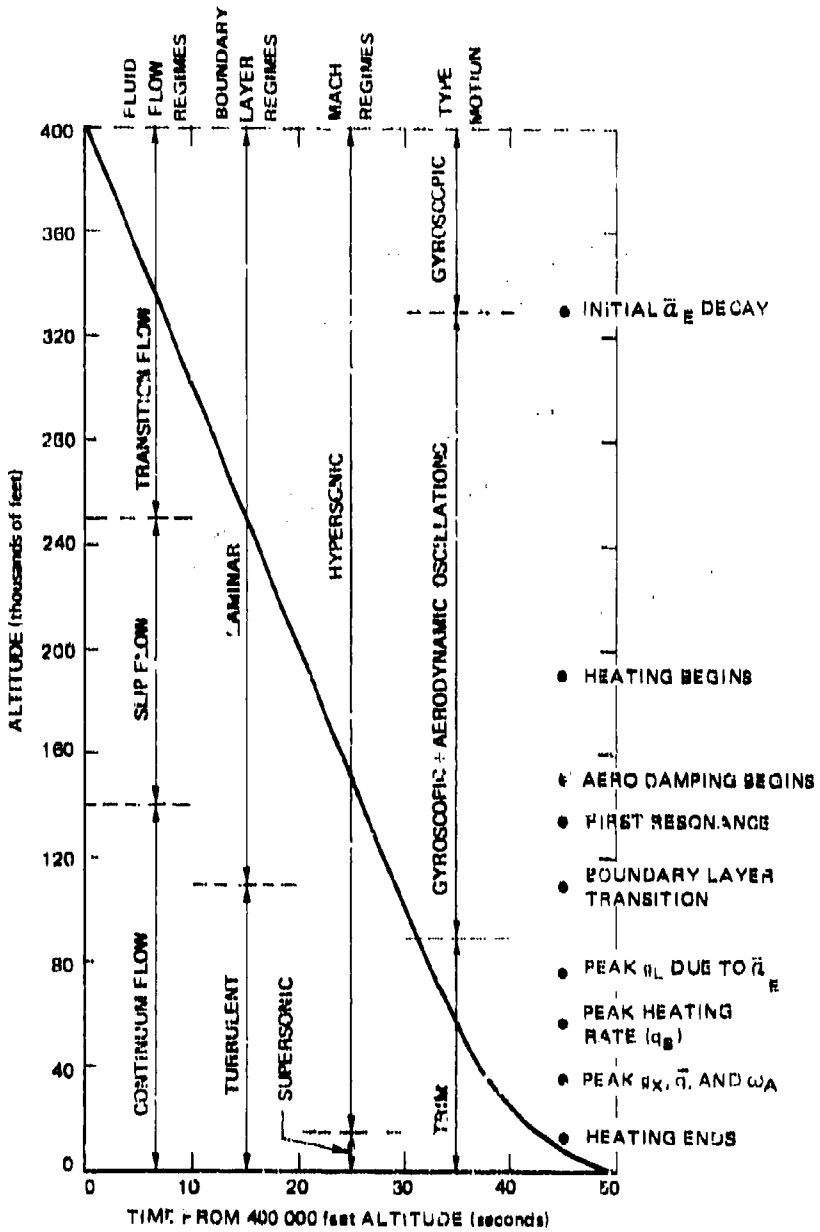

Fig. 4-21 SIGNIFICANT EVENTS

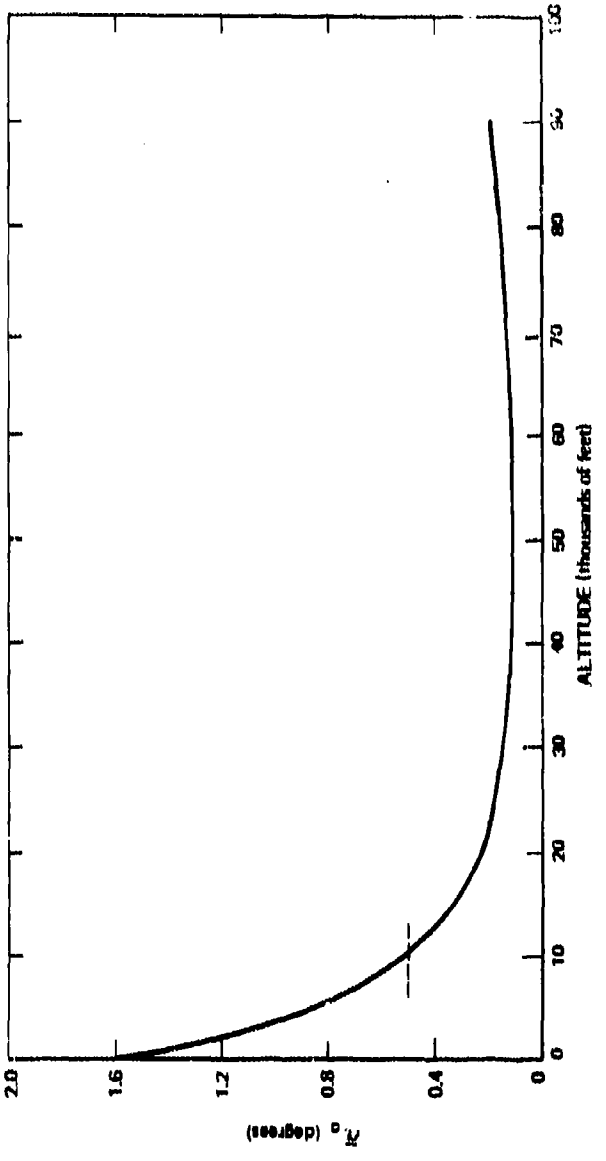

Fig. 4-22 $\bar{\alpha}_\alpha$ REQUIRED FOR $g_L = 2g$

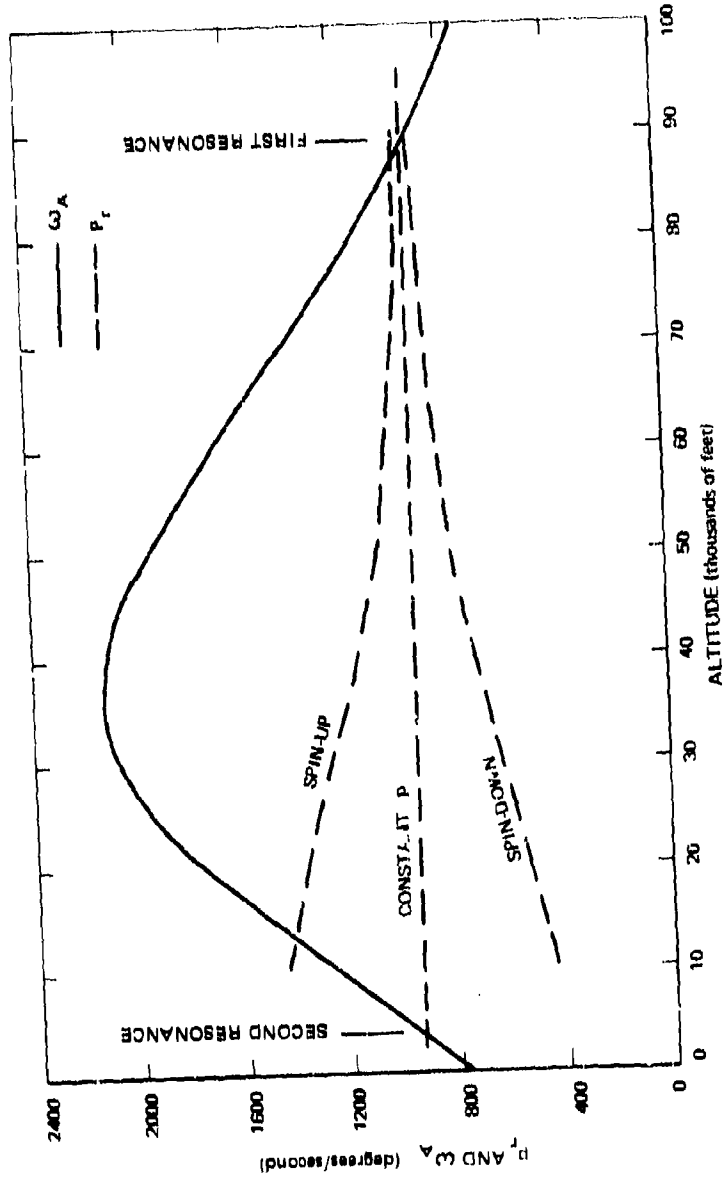

Fig. 4-23 P_r AND ω_A VERSUS ALTITUDE

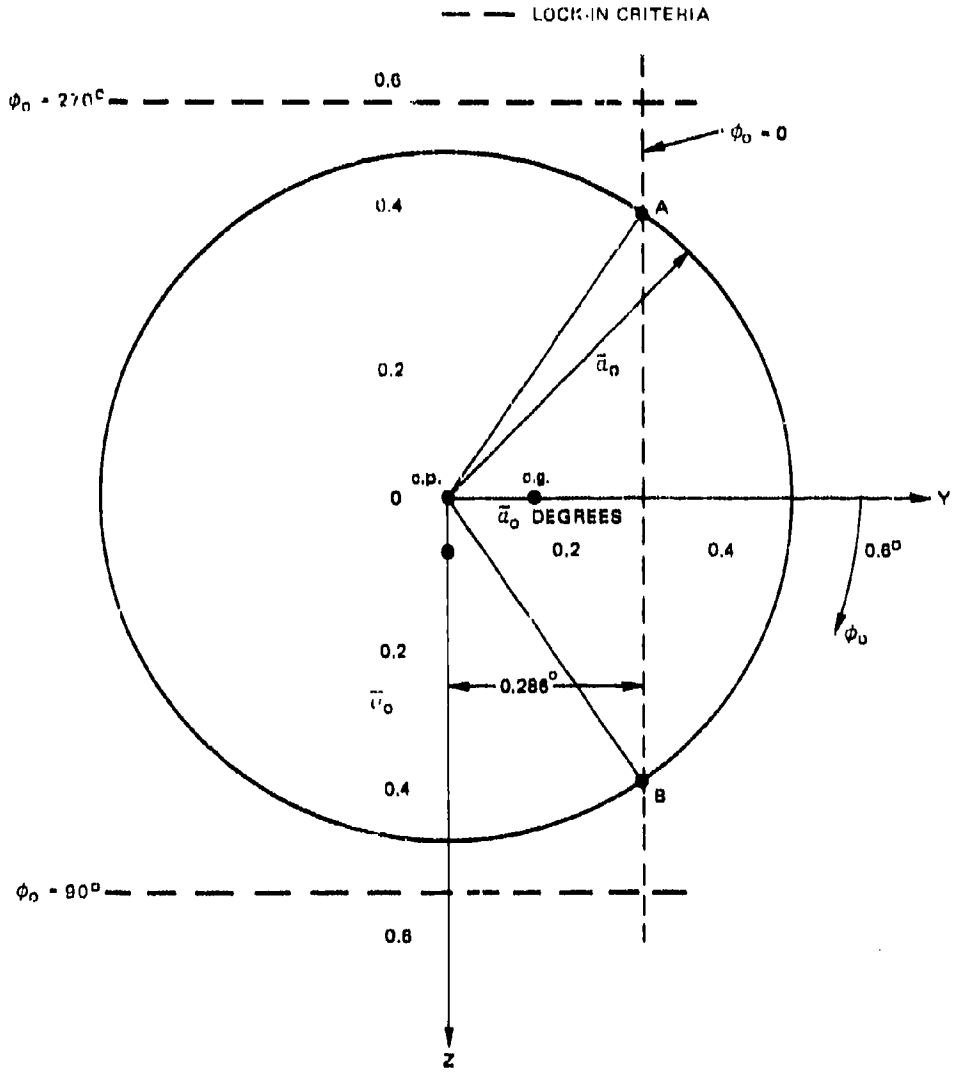

Fig. 4-24 CONDITIONS FOR ROLL RESONANCE AT h = 89 000 FEET

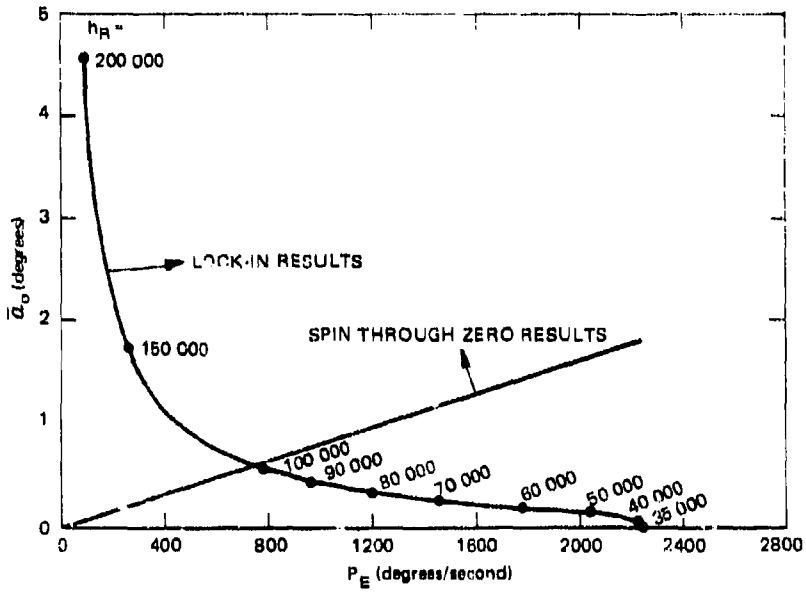

Fig. 4-25 $\bar{a}_c$ REQUIRED FOR LOCK-IN AND SPIN THROUGH ZERO ROLL RATE

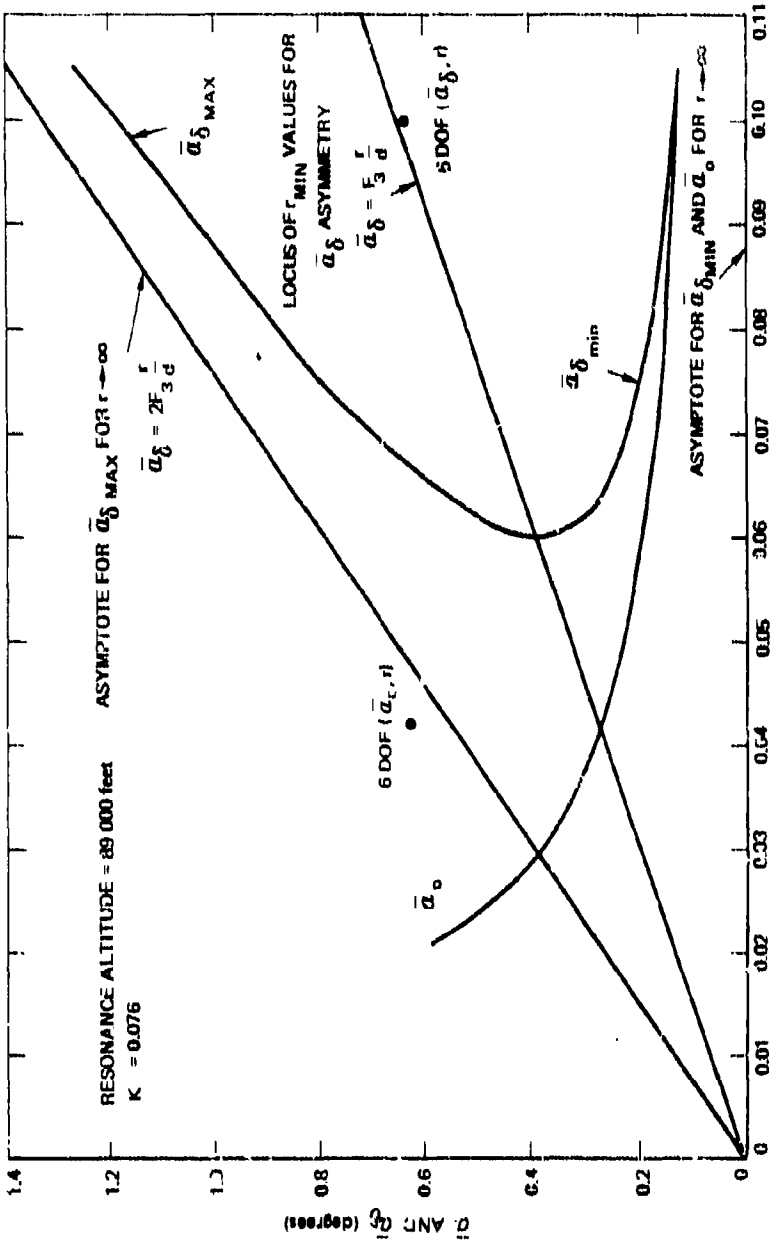

Fig. 4-26 BOUNDARIES OF $\bar{a}_o$ AND $\bar{a}_\delta$ FOR LOCK-IN AT FIRST RESONANCE

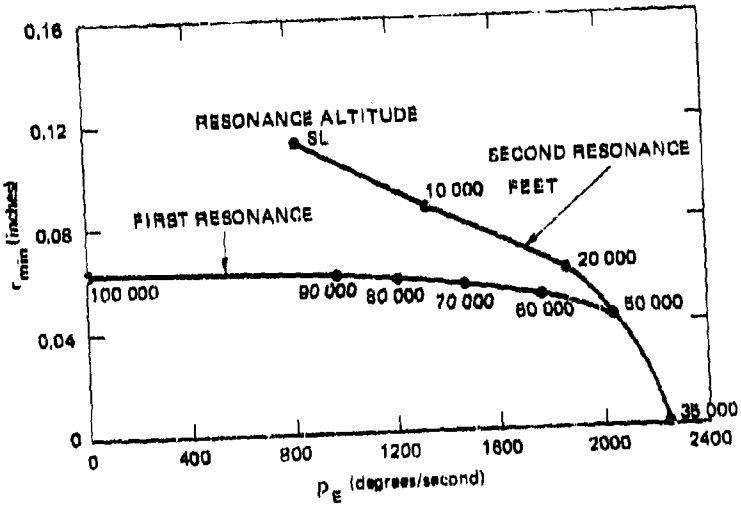

Fig. 4-27 VARIATION OF r_{min} WITH INITIAL ROLL RATE

Table 4-1

Reentry Characteristics

Altitude (thousands of feet)	K	ω_A (rad/sec)	V (ft/sec)	M	$R_e \times 10^{-6}$	$M/\sqrt{R_e}$	t (sec)
400			20 000	15.6	0.0000156	3.9	0
350			20 000	19.7	0.000195	1.4	
300		0.155	20 000	22 6	0.0036	0.38	
250		0.597	20 000	22.0	0.0525	0.097	
200	0.00083	1.65	20 000	19.4	0.315	0.034	
150	0.0057	4.23	20 000	18.9	2.0	0.013	25.0
100	0.047	12.9	20 000	20.3	22	0.0044	29.9
90	0.074	16.0	19 500	19.9	34		31.0
80	0.116	19.8	19 200	19.7	55		32.1
70	0.182	24.2	18 600	19.2	87		33.2
60	0.301	29.4	17 500	18.0	130		34.6
50	0.486	33.8	16 000	16.6	200		35.8
40	0.785	37.0	13 900	14.5	270		37.3
35	1.00	37.2	--	--	--		--
30	1.26	36.1	10 800	10.9	310		39.2
20	1.94	30.8	7 770	7.5	360		41.2
10	2.90	22.1	4 760	4.4	240		44.3
S. L.	4.23	13.4	2 470	2.2	160		49.1

5. DISPERSION

SYMBOLS FOR SECTION 5

Symbol	Definition	Typical Units
A	axial force	pounds
A_R	component of A in downrange direction	pounds
C_A	axial force coefficient = A/qS	-
C_D	drag coefficient = D/qS	-
c. g.	center-of-gravity location	inches
C_L	lift coefficient = L/qS	-
C_{L_α}	$dC_L/d\alpha$	per radian
C_{ℓ_o}	asymmetric rolling moment coefficient ℓ_o/qSd	-
C_{m_o}	moment coefficient about body Y axis at $\bar{\alpha} = 0$ (see Section 2.4)	-
$\bar{C}_{m_o}$	$\sqrt{C_{m_o}^2 + C_{n_o}^2}$	-
C_N	normal force coefficient = N/qS	-
C_{N_α}	$dC_N/d\alpha$	per radian
C_{n_o}	moment coefficient about body Z axis at $\bar{\alpha} = 0$ (see Section 2.4)	-
c. p.	center-of-pressure location	inches
D	drag, aerodynamic force parallel to V	pounds
d	vehicle reference length	feet
E	factor defined by Eq. (5-21)	feet
e	Napierian base	-
F_w	weighting factor for wind	-
F_ρ	Weighting factor for density variation	-

Symbol	Definition	Typical Units
g	acceleration of gravity	ft/sec^2
$\bar{g}$	$\left[g_Y^2 + g_Z^2\right]^{1/2}$	g
g_X, g_Y, g_Z	acceleration along body axes X, Y, and Z	g
H	scale height RT/g	feet
h	altitude	feet
I_3, I_5	functions of $K_{S.L.}$	-
I_X	moment of inertia about body axis X	$slug\text{-}ft^2$
j	index number	-
K	$-\frac{P}{\beta \sin \gamma_E}$	-
L	lift, aerodynamic force normal to V	pounds
ℓ	asymmetric rolling moment	ft-lb
N	normal force, component of aerodynamic force normal to the body centerline	pounds
	or	
	number of altitude bands	-
P	ambient pressure	lb/ft^2
p	vehicle roll rate	rad/sec
q	dynamic pressure, $\rho V^2/2$	lb/ft^2
R	range	nmi
	or	
	gas constant = 1716	$ft^2/sec^2 - °R$
R_o	radius of the earth	feet

Symbol	Definition	Typical Units
r	radial c. g. offset	inches
S	reference area	ft^2
S. L.	sea level	-
T	ambient temperature	°R
t	time	seconds
V	vehicle velocity	ft/sec
V_R	drift velocity resulting from winds	ft/sec
V_w	windspeed	ft/sec
$V_{A/M}$	velocity of the air relative to the missile	ft/sec
W	vehicle weight	pounds
$X_{c.g.}$	distance parallel to the body centerline from the nose to the c. g.	inches
$X_{c.p.}$	distance parallel to the body centerline from the nose to the c. p.	inches
ΔX	$X_{c.p.} - X_{c.g.}$	inches
$\bar{\alpha}$	angle between the body centerline and $\vec{V}_{A/M}$	radians
α_w	angle between the body centerline and the reentry flight path direction	radians
β	ballistic coefficient, $W/C_A S$	lb/ft^2
γ	flight path angle, negative for a reentry body	degrees
$\Delta\gamma$	change in flight path angle	degrees
δ	dispersion measured along the earths surface	feet
Δ	refers to an increment except as noted	-
ϕ_o	angle defined in Section 5. 4. 2	degrees

Symbol	Definition	Typical Units
$\psi_{c.g.}$	angle defined in Section 5.4.2	degrees
ρ	ambient density	$slug/ft^3$

Subscripts

c	refers to cross-track component
E	refers to conditions at reentry
o	refers to conditions at zero roll rate except as noted
R	refers to along-track component
S.L.	sea level
w	refers to quantity resulting from wind effects
ρ	refers to quantity resulting from density effect

A dot over a symbol refers to a first derivative with respect to time.
An arrow over a symbol means a vector quantity.

SUMMARY AND CONCLUSIONS

The factors most likely to cause impact dispersion are identified, and simple equations are given for estimating the magnitude of each dispersion. These factors include atmospheric wind, deviations from a standard atmospheric density profile, errors in mass, and aerodynamic asymmetries. The following examples are given to illustrate this discussion.

Example 1 - Dispersion resulting from wind and deviation in density at low and moderate altitudes.

Example 2 - Dispersion resulting from wind and deviation in density at high altitude.

Example 3 - Dispersion resulting from a trim angle of attack for a missile rolling at a constant roll rate.

Example 4 - Dispersion resulting from roll lock-in at low altitude.

Example 5 - Dispersion resulting from a combined asymmetry for which spin through zero roll rate occurs.

The major conclusions are:

1. Winds and departures from the assumed density are the chief sources of impact dispersion resulting from meteorological characteristics at the impact site. This dispersion increases rapidly as the flight path becomes shallow, as the missile velocity is decreased, and as the ballistic coefficient of the missile is decreased. The density effect is more sensitive to these missile and trajectory parameters than is the wind effect. Equations are presented for evaluating the dispersion for any wind and density profile.

2. The equations derived for evaluating the dispersion resulting from deviations in density may also be used to evaluate the dispersion resulting from perturbations in missile weight and drag.

3. The dispersion resulting from a vehicle that encounters roll resonance (but remains intact) is likely to be small. On the other hand, the dispersion resulting from a vehicle having a combined asymmetry that results in roll rate reversal is likely to be extremely large.

Aiming instructions are required in order to deliver accurately a ballistic vehicle to a predetermined impact point. To obtain launch orders, a mathematical model containing all factors that influence the trajectory is constructed. However, even with the most elaborate trajectory simulation that can be devised, the model is not perfect and the vehicle departs from the intended trajectory. The magnitude of the miss distance from the intended impact point will be referred to as the impact dispersion. In Section 4.1 some of the important factors which affect dispersion and which occur at the end of the powered phase were discussed (error in terminal velocity and flight path angle). In this section we will discuss only those perturbations that occur during reentry.

Accurate evaluation of dispersion requires use of a three- or a six-degree-of-freedom simulation. Simpler solutions, although lacking in accuracy, make it possible to isolate the important factors and provide insight into the general behavior of the various types of disturbances. These simpler solutions will be discussed here.

5.1 Meteorological Characteristics

The meteorological characteristics that may produce dispersion are:

1. Errors in wind speed and direction,
2. Errors in atmospheric density,
3. Errors in atmospheric temperature.

Temperature is included since, in addition to its effect on density, it affects also the speed of sound and, thus, the aerodynamic coefficients that depend upon Mach number. However, the effect of the speed of sound is usually small (see Section 3.1) and only the wind and density effects will be considered further.

5.1.1 Effect of Wind

Atmospheric winds are a major contributor to the dispersion of uncontrolled reentry vehicles. A simplified analysis is given in Ref. 5-1. The important portions of this theory are summarized below.

We make the following assumptions:

1. The effect of gravity is negligible.
2. The earth is nonrotating and flat.
3. The flight path angle is a constant = γ_E.
4. The angle of attack is zero.
5. The wind is a horizontal head or tail wind (except as indicated).
6. The reentry vehicle is aerodynamically stable (the center of pressure is aft of the center of gravity).
7. The weight and C_A are constant.

With these assumptions the flight geometry in the absence of wind is shown in sketch (a).

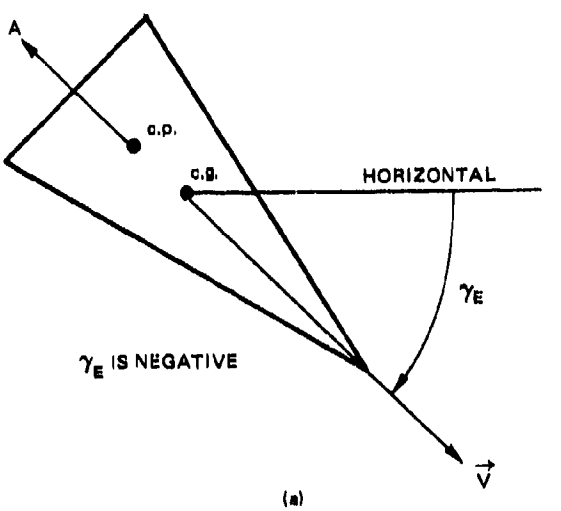

(a)

The velocity vector is along the body centerline. The only force acting is the axial force, A, and it also acts along the body centerline (by definition). Suppose now the body encounters a tail wind. The body forces that act immediately are shown in sketch (b). The missile velocity

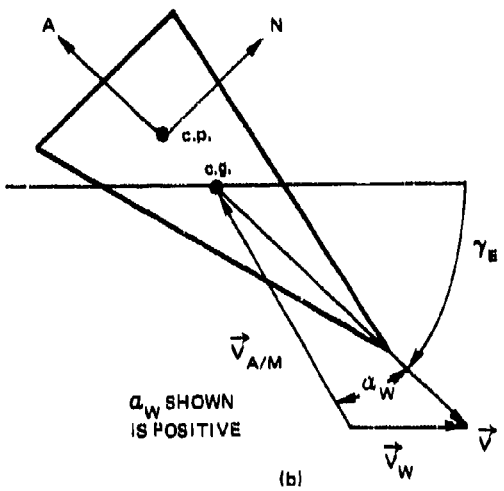

(b)

vector and A are still along the missile centerline. However the velocity vector that produces aerodynamic forces on the missile is $\vec{V}_{A/M} = \vec{V}_W - \vec{V}$. This velocity vector acts at an angle, α_W, to the body centerline and causes a normal force, N, which acts at the vehicle center of pressure. This force causes the body to pitch (weathercock) until the body centerline and $\vec{V}_{A/M}$ are aligned. The conditions that exist when the weathercock motion has damped to negligible magnitude are shown in sketch (c).

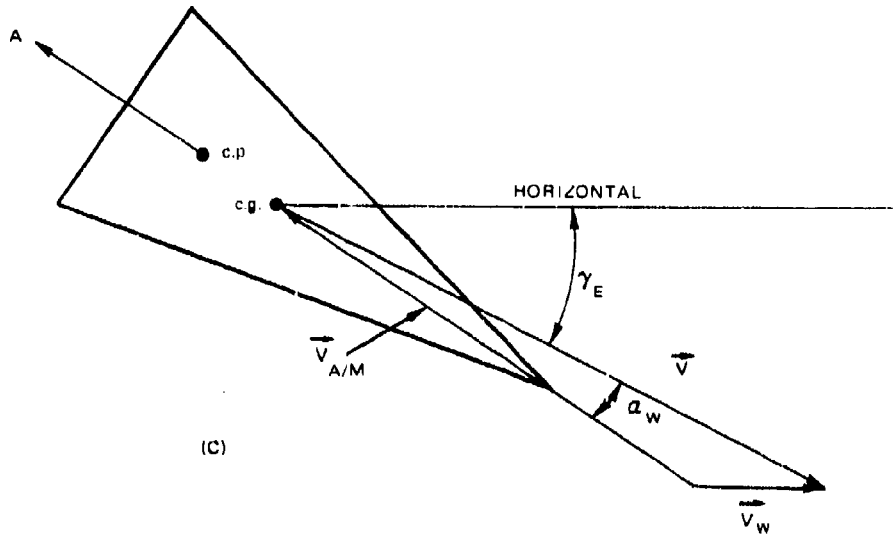

The normal force is now zero and $\vec{V}_{A/M}$ is along the body centerline. At all later times the body centerline remains aligned with $\vec{V}_{A/M}$; however, since A acts at a slight angle to $\vec{V}$ the missile acquires a drift velocity relative to the no-wind trajectory. The force and velocity diagram including the drift velocity is shown in sketch (d). We will assume that the geometry shown in sketch (d) is representative of the reentry trajectory. At any given time (or altitude) the missile velocity is assumed to be the vector sum of the no-wind velocity for that time plus the drift velocity $\vec{V}_R$. Furthermore, it is assumed that $V_R \ll V$. Using these assumptions it is shown in Ref. 5-1 that the dispersion resulting from winds is given by the equation:

$$\delta_w = - \frac{H}{V_E \sin \gamma_E} I_3 \sum_{j=1}^{N} V_{w_j} F_w \qquad (5\text{-}1)$$

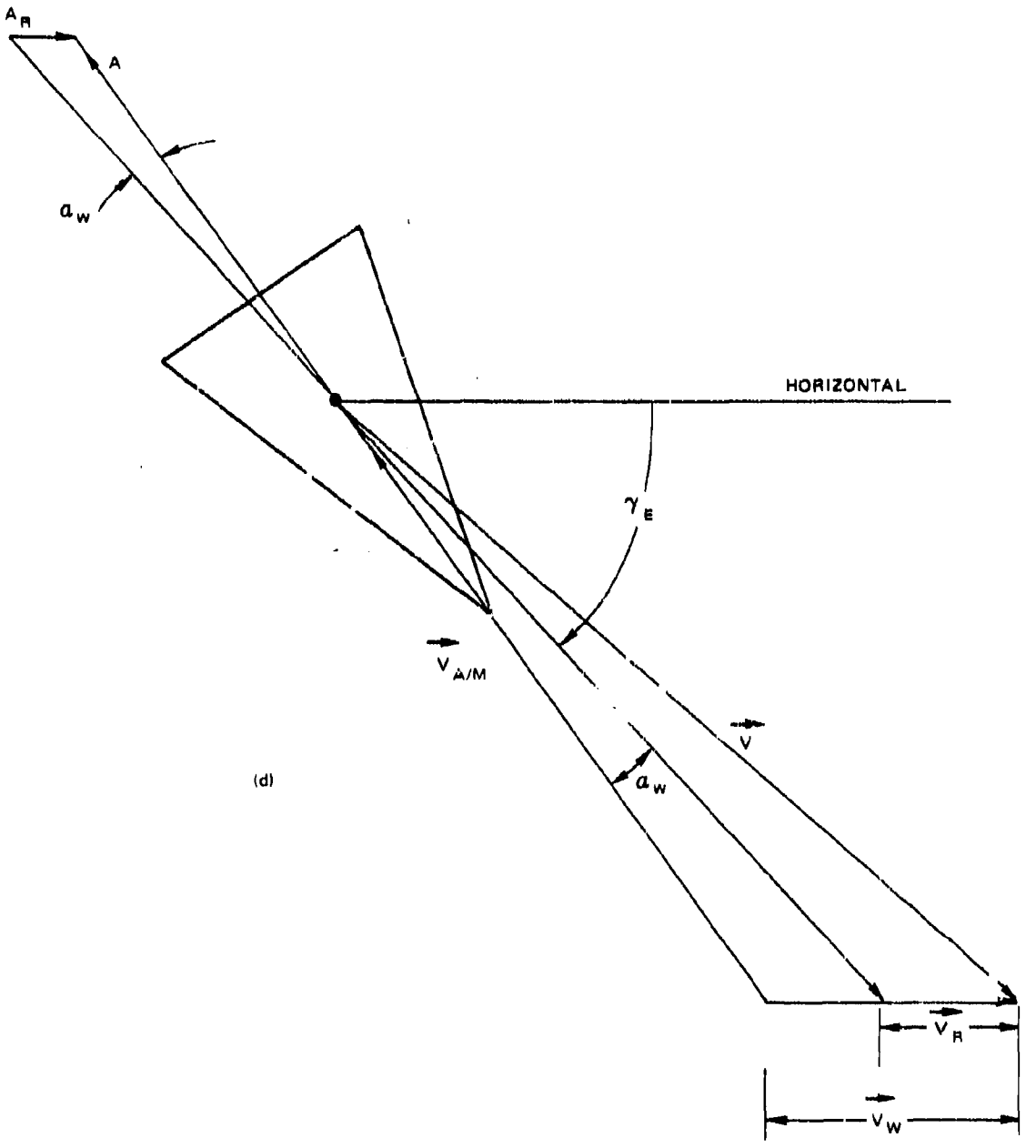

(d)

where

$$H = RT/g$$

I_3 is given in Table 5-1

F_W is given in Table 5-2,

The index number j refers to a particular altitude band. To account for a variable wind with altitude, the reentry altitude is divided into N bands where the bandwidth is small enough that V_W may be considered constant in each band.

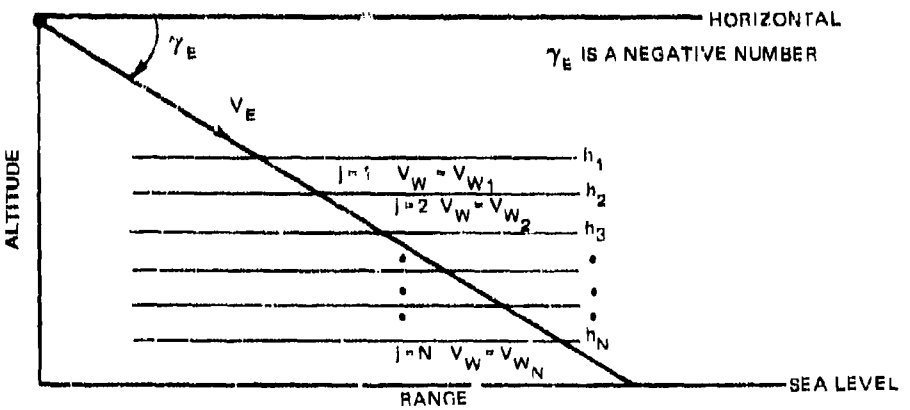

The F_W term is a weighting factor that depends upon the altitude, altitude bandwidth, and $K_{S.L.}$. Since $K_{S.L.} = -\frac{P_{S.L.}}{\beta \sin \gamma_E}$, F_W is a function of the atmosphere considered ($P_{S.L.}$ - a minor variation), the body characteristic (β), and trajectory characteristic (γ_E). For a given body

design and type of atmosphere, F_W for a given altitude and altitude bandwidth is a function of γ_E only. For most applications this variation may be neglected. When this is done the values of F_W should be evaluated at the lowest value of $|\gamma_E|$ used in the missile design. The dispersion decreases rapidly with increasing $|\gamma_E|$. Therefore, although the percentage error in δ may be large when this procedure is followed, the magnitude of the error in δ will be small.

If the altitude bandwidth is constant, the magnitude of F_W is indicative of the sensitivity of δ_W to winds in a given altitude band. From Table 5-2 it is observed that the most sensitive band corresponds to the 20 000 to 25 000 foot band for $K_{S.L.} = 1.5$, and the most sensitive altitude band decreases with increasing $K_{S.L.}$ to the 10 000 to 15 000 foot band for $K_{S.L.} = 6.0$. The calculation of the most sensitive band is treated mathematically in Ref. 5-1.

The ballistic coefficient β varies with altitude and Mach number. The value of β at hypersonic speeds should be used for this calculation (also for δ_ρ discussed in the next subsection).

The summation term in Eq. (5-1) is called the ballistic wind. By definition, a ballistic wind is a constant wind (with altitude) such that the dispersion is the same as that resulting from a variable wind. If V_W is constant at all altitudes, then Eq. (5-1) becomes:

$$\delta_W = -\frac{V_W H}{V_E \sin\gamma_E} I_3 . \qquad (5\text{-}2)$$

The quantity preceding the summation sign in Eq. (5-1) is called the range partial for winds.

In Ref. 5-1, it is shown that Eq. (5-1) is valid for either head (or tail) winds or cross winds. If the wind

is neither a head (or tail) wind nor a cross wind, the total dispersion may be obtained by computing the head wind and cross wind components of δ_W and adding the results vectorially.

Equation (5-1) has been found to be in excellent agreement with results obtained using three- or six-degree-of-freedom trajectory simulations provided $K_{S.L.}$ is not greater than about 6. For higher values of $K_{S.L.}$ the equation overestimates δ_W.

For applications where the body characteristics have been fully defined, the accuracy of Eq. (5-1) may be improved by the following procedure:

1. Using a three-degree-of-freedom trajectory program, evaluate δ_W for various values of V_E and γ_E and a constant wind.
2. Using these results and Eq. (5-1), compute I_3 and plot it as a function of γ_E.
3. Using the trajectory program, evaluate δ_W resulting from a constant wind in each altitude band. These computations are made for one value of V_E and the lowest $|\gamma_E|$ to be used for the missile.
4. Using the results of step 3 and Eq. (5-1), compute F_W.

These new values of I_3 and F_W will differ slightly from those given in Tables 5-1 and 5-2. Using these new data, the accuracy of δ_W given by Eq. (5-1) may be improved, particularly for high values of $K_{S.L.}$.

5.1.2 Effect of a Deviation in Density

The impact point of a reentry body is computed using some standard density profile (variation with altitude). If the actual profile is different from the standard

profile, the missile velocity history is affected. Therefore, deviations in density from the standard profile are a source of impact dispersion.

Using an analysis similar to that used for δ_w, it is shown (Ref. 5-1) that:

$$\delta_\rho = \left(\frac{H}{V_E \sin\gamma_E}\right)^2 \frac{g}{\tan\gamma_E} I_5 \sum_{j=1}^{N} \frac{\Delta\rho}{\rho} F_\rho \qquad (5\text{-}3)$$

where

I_5 is given in Table 5-3

F_ρ is given in Table 5-4

$\Delta\rho$ is the deviation in density from the standard value (ρ) at a given altitude.

All other terms are as defined in the previous subsection on the effect of wind.

Again, F_ρ is a weighting factor that depends upon the altitude, altitude bandwidth, and $K_{S,L,}$. The most sensitive altitude band is the 25 000 to 30 000 foot band (see Ref. 5-1 for fuller discussion) and is nearly independent of $K_{S,L,}$.

The summation term is called the ballistic density. By definition ballistic density is the constant value of $\Delta\rho/\rho$ that results in the same dispersion as the variable $\Delta\rho/\rho$.

The quantity preceding the summation sign is called the range partial for density deviation. Equation (5-3) has been found to be in excellent agreement with results obtained using three- and six-degree-of-freedom simulations, provided $K_{S,L,}$ is not too high. In Ref. 5-1 it was shown that the conditions required for the accuracy of Eq. (5-3) are those given in Figs. 5-1 and 5-2. When these conditions are exceeded, the dispersion given by Eq. (5-3) is too high.

For applications where the body characteristics have been fully defined, the accuracy of Eq. (5-3) may be improved following the same procedures given for winds in the preceding subsection.

Since values of F_ρ and F_W become very low at high altitude, one is tempted to conclude that the dispersion resulting from winds and deviations in density at altitudes above, say, 100 000 feet is negligible. For a high precision vehicle this conclusion is not necessarily valid, since the magnitudes of V_W and $\Delta\rho/\rho$ at these altitudes are usually very large.

It should be noted that, except for the direct effects ($\Delta\rho/\rho$ and V_W), the variables contributing to dispersion resulting from winds and deviations in density are the same. However δ_ρ is more sensitive to changes in the variables.

5.2 Errors in Aerodynamic Coefficients

Errors or variation in aerodynamic coefficients resulting from reentry environmental effects (such as heating) may contribute to dispersion. The most sensitive coefficient from the dispersion standpoint is the axial force coefficient, C_A.

Dispersion results when a perturbation affects the γ history during reentry. This change in γ was shown (Ref. 5-1) to result primarily from changes in the K history. In Section 5.1.2 we interpreted changes in K in terms of deviations in density. We could just as well have interpreted a variation in K as a variation in β or $\sin\gamma_E$. Since $\beta = \frac{W}{C_A S}$, then $K = -\frac{PC_A S}{W \sin\gamma_E}$, and the dispersion characteristics computed in Section 5.1.2 are equally valid for $\Delta C_A/C_A$, $-\Delta W/W$, or $-\Delta\beta/\beta$. The minus sign means that a given percent <u>increase</u> in W or β results in the same dispersion as the same percentage <u>decrease</u> in pressure, density, or axial force coefficient.

Errors in the normal force coefficient have a small effect on δ. Since in general the angle of attack is not zero, a lateral force results, and the magnitude of this force for a given trajectory depends upon $\bar{\alpha}$ and C_{N_α}. The dispersion resulting from this source arises from erroneous evaluation of lift and drag forces (see Sections 5.4.1, 5.4.2, and 5.5). This increment in dispersion is very small unless the error in C_{N_α} or the angle of attack is large.

Errors in the damping derivative may result in dispersion since this characteristic determines to some degree the $\bar{\alpha}$ history and thus the lateral force history early in the reentry phase and during periods of roll resonance (see Sections 4.4 and 4.5.5). Again the dispersion resulting from these errors is usually small.

Errors in the center of pressure location may result in dispersion since this factor also determines to some degree the $\bar{\alpha}$ history early in the trajectory and the $\bar{\alpha}$ resulting from asymmetries. The dispersion contribution is usually small.

5.3 Errors in Mass Characteristics

Errors in mass characteristics that contribute to dispersion are errors in W, $X_{c.g.}$, and the moment of inertia terms. Of these, the most significant is the error in W, which results from uncertainty in the reentry weight and uncertainty in weight loss caused by heating effects during reentry. The dispersion resulting from an error $\Delta W/W$ is the same as that from an error, $-\Delta\rho/\rho$, as discussed in Section 5.2.

The effects of $Y_{c.g.}$ and moment of inertia may cause small dispersions since these factors affect the $\bar{\alpha}$ history during reentry.

5.4 Asymmetries

The problems associated with asymmetries were discussed in detail in Section 4.5. Asymmetries produce angles of attack; angles of attack result in lift and a change in drag. For cases where angles of attack develop and the missile is rolling, the major effect on δ is the change in drag since the direction of the lift vector (in an inertial axis system) is constantly changing so that, over a period of time, the net effect of lift is "averaged out." The effect of $\bar{\alpha}$ for a rolling vehicle is usually small unless resonance conditions occur. In this case $\bar{\alpha}$ may become large and the vehicle drag will increase significantly, causing the missile to fall short of the intended target. This case can be treated as a change in C_A so that the procedures given in Section 5.1.2 may be used. A more serious contributor to dispersion is the case where $\bar{\alpha} \neq 0$ and the roll rate becomes zero. Even for a very short period of zero roll rate, large dispersions may result from small angles of attack. Since, for this case, the lift vector remains fixed in space, the vehicle moves off course in the direction of the lift. We will consider these two cases separately.

5.4.1 Rolling Vehicle with Angle of Attack

If asymmetries result in a trim angle of attack and the missile roll rate is not zero, the major contributor to dispersion is the effect of the increased drag resulting from $\bar{\alpha}$. The equation for the drag is:

$$D = C_D qS \tag{5-4}$$

where, from Eq. (2-9):

$$C_D = C_A \cos\bar{\alpha} + C_N \sin\bar{\alpha} . \tag{5-5}$$

Therefore the change in C_D resulting from $\bar{\alpha}$ is:

$$\Delta C_D = C_A \cos\bar{\alpha} + C_N \sin\bar{\alpha} - C_A \approx C_N \sin\bar{\alpha} . \tag{5-6}$$

If the aerodynamic characteristics are linear so that $C_N = C_{N_\alpha}\bar{\alpha}$ and if $\bar{\alpha}$ is small:

$$\Delta C_D = C_{N_\alpha}\bar{\alpha}^2 . \qquad (5\text{-}7)$$

Therefore the effect of $\bar{\alpha}$ may be estimated using the procedures given in Section 5.1.2 where:

$$\frac{\Delta\rho}{\rho} = \frac{\Delta C_D}{C_A} = \frac{C_{N_\alpha}}{C_A}\bar{\alpha}^2 . \qquad (5\text{-}8)$$

When working with telemetry data, it is convenient to express $\Delta C_D/C_A$ in terms of body accelerations. Substituting for $\bar{\alpha}$ using Eq. (7-11):

$$\frac{\Delta C_D}{C_A} = \frac{C_A}{C_{N_\alpha}}\left(\frac{\bar{g}}{g_X}\right)^2 . \qquad (5\text{-}9)$$

Note that $\Delta C_D/C_A$ varies as the square of $\bar{\alpha}$, and therefore the effect tends to be small at low values of $\bar{\alpha}$ but tends to increase rapidly with increasing $\bar{\alpha}$.

5.4.2 Nonrolling Vehicle with Angle of Attack

The dispersion resulting from angle of attack for a nonrolling vehicle was considered in detail in Ref. 5-2 and the results are summarized below. Consider a vehicle with a fixed angle of attack that results in a lift force L. Consider an inertial axis system YZ as shown in the sketch. If the roll rate is low compared to the aerodynamic frequency, the lift (or normal) force is in the plane containing the asymmetric force (see Section 4.5.1). Therefore L rolls with the body. As long as the roll rate is not close to zero, the effect of L on dispersion is small since the direction of L (in the inertial axis system) is constantly changing. However if the roll rate becomes

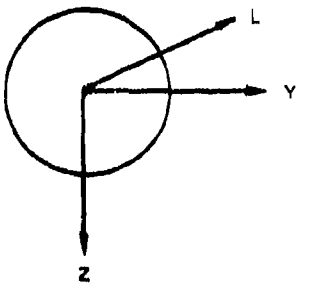

zero, even for an instant, the body will move off course in the direction of L. We will consider in this subsection the case of a vehicle that is spinning at reentry but, under the influence of body asymmetries, the direction of roll rate is reversed during entry. The duration of "near zero" roll rate is very short.

Assume that at h_o the roll rate passes through zero and that at this instant the lift is in the vertical plane. A change in flight path angle, $\Delta\gamma$, results.

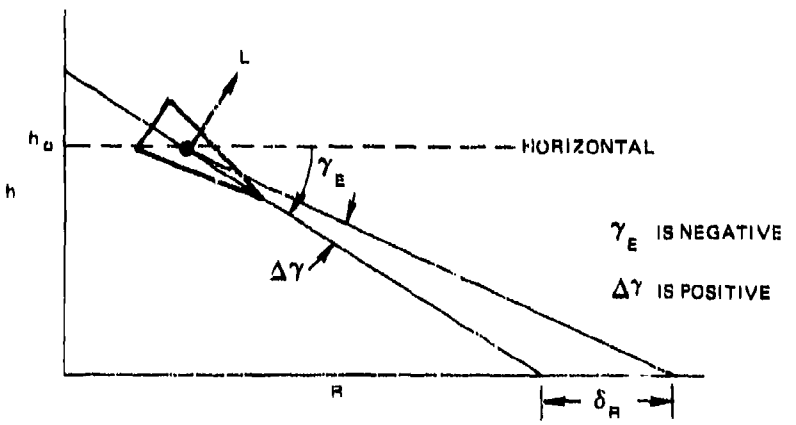

Assuming a straight line flight path and a small value for $\Delta\gamma$:

$$\delta_R = \frac{h_o \Delta\gamma}{\sin^2 \gamma_E} \quad . \tag{5-10}$$

If L is in a plane perpendicular to the vertical plane and if $\Delta\gamma$ is interpreted as the resultant change in the direction of the velocity vector:

$$|\delta_c| = \left| \frac{h_o \Delta\gamma}{\sin \gamma_E} \right| = |\delta_R \sin \gamma_E| \quad . \tag{5-11}$$

The impact pattern is elliptical with the major axis along the trajectory track and the minor axis across track. The ratio of the minor to major axis is $|\sin \gamma_E|$. The change in γ is given by the equation:

$$\Delta\gamma = \int \dot{\gamma}\, dt \tag{5-12}$$

where (see Ref. 5-3):

$$\dot{\gamma} = \frac{Lg}{WV} - \frac{g \cos \gamma}{V} + \frac{V \cos \gamma}{R_o} \quad .$$

The change in γ of interest is just that resulting from L. Therefore:

$$\Delta\gamma = \frac{g}{WV_o} \int L dt \, . \tag{5-13}$$

Equation (5-13) is valid provided the direction of L is fixed. However, since the direction of L changes over the time interval of interest, an effective value of $\int L dt$ must be used. Based on six-degree-of-freedom simulation results, it may be shown that:

$$\int L dt \approx \frac{2.116L}{\sqrt{|\dot{p}_o|}} \qquad (5\text{-}14)$$

where the constant is dimensionless. Writing $L = C_{L_\alpha} \bar{\alpha}_o q_o S$ where C_{L_α} is given by Eq. (2-10):

$$\int L dt = \frac{2.116}{\sqrt{|\dot{p}_o|}} (C_{N_\alpha} - C_A) \bar{\alpha}_o q_o S . \qquad (5\text{-}15)$$

Substituting Eqs. (5-15) and (5-13) into (5-10):

$$\delta_R = \frac{2.116\, h_o g}{W V_o \sin^2 \gamma_E} \frac{(C_{N_\alpha} - C_A)}{\sqrt{|\dot{p}_o|}} \bar{\alpha}_o q_o S . \qquad (5\text{-}16)$$

In terms of normal force $N_o = C_{N_\alpha} \bar{\alpha}_o q_o S$:

$$\delta_R = \frac{2.116\, h_o g}{W V_o \sin^2 \gamma_E \sqrt{|\dot{p}_o|}} \left(1 - \frac{C_A}{C_{N_\alpha}}\right) N_o . \qquad (5\text{-}17)$$

In terms of lateral acceleration $\bar{g}_o = \sqrt{g_{Y_o}^2 + g_{Z_o}^2} = \frac{N_o}{W}$:

$$\delta_R = \frac{2.116\, h_o g \left(1 - \frac{C_A}{C_{N_\alpha}}\right) \bar{g}_o}{V_o \sin^2 \gamma_E \sqrt{|\dot{p}_o|}} . \qquad (5\text{-}18)$$

Equation (5-18) is convenient for analysis of telemetry data since $\dot{p}_o$ and $\bar{g}_o$ are obtained directly from the data and V_o and h_o may be estimated using Eqs. (4.3-22) and

(4.3-5). Equations (5-16), (5-17), and (5-18) are valid for any combination of asymmetries.

We consider next the dispersion that results from the particular types of mass and aerodynamic asymmetries (N_o and r) shown in the sketch.

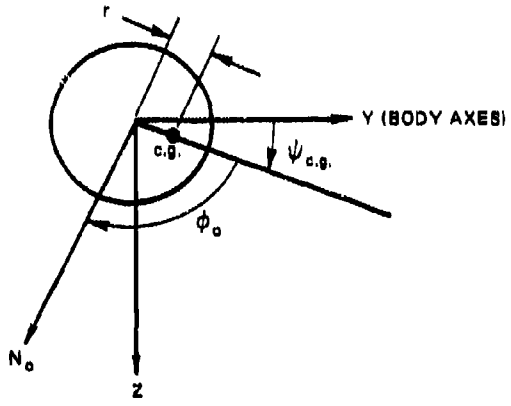

We will assume that the normal force resulting from r is very small so that the N_o results from an asymmetric moment defined by:

$$\overline{C}_{m_o} = \sqrt{C_{m_o}^2 + C_{n_o}^2} \ .$$

The trim angle of attack, $\overline{\alpha}_o$, is given by Eq. (2-27) where, in the notation of the present section, $\alpha_{TR} = \overline{\alpha}_o$ and $C_{m_o} = \overline{C}_{m_o}$. The roll acceleration, $\dot{p}_o$, is given by Eq. (4.5-35) where $\overline{q} = q_o$, $\overline{\alpha} = \overline{\alpha}_o$, and $\phi = \phi_o$. Substituting these values into Eq. (5-16), writing ρ_o in terms of H_o and P_o, and noting that $q_o = \frac{1}{2}\rho_o V_o^2$:

$$\delta_R = \frac{1.49\left(1 - \frac{C_A}{C_{N_\alpha}}\right)}{\sqrt{H_o/g}\, W \sin^2 \gamma_E}\left[\frac{\bar{C}_{m_o} S I_X}{r \frac{\Delta X}{d} \sin \phi_o}\right]^{1/2} h_o \sqrt{P_o}, \quad (5\text{-}19)$$

The constant is $2.116/\sqrt{2}$ and is dimensionless.

Equation (4.5-94) may be used to evaluate K_o and thus $h_o\sqrt{P_o}$. Using Eq. (4.5-94) and Eq. (2-27), δ_R may be expressed in terms of $\bar{\alpha}_o$ rather than $\bar{C}_{m_o}$ and $r \sin \phi_o$, giving the result:

$$\delta_R = 1.49\, \bar{\alpha}_o \sqrt{\frac{V_E P_{S.L.}}{\beta H_o p_E}} \frac{\left(\frac{C_{N_\alpha}}{C_A} - 1\right)}{\sin^2 \gamma_E} h_o \sqrt{\frac{P_o}{P_{S.L.}}\left(1 - e^{-\frac{P_o}{P_{S.L.}} \frac{K_{S.L.}}{2}}\right)} \quad (5\text{-}20)$$

Equation (5-20) shows that for a given $\bar{\alpha}_o$ (given $\bar{C}_{m_o}$ and $\Delta X/d$ primarily), the dispersion varies with h_o (variations in $r \sin \phi_o$ if other variables are held constant) in accordance with the factor:

$$E = h_o \sqrt{\frac{P_o}{P_{S.L.}}\left(1 - e^{-\frac{P_o}{P_{S.L.}} \frac{K_{S.L.}}{2}}\right)} = f(h_o, K_{S.L.}), \quad (5\text{-}21)$$

At sea level, this factor is zero since $h_o = 0$. The factor increases with increasing h_o to a maximum and then decreases, becoming zero at very high altitudes. The critical altitude (altitude for maximum E) depends upon the type of atmosphere ($P_{S.L.}$) and upon $K_{S.L.}$ (or upon β and/or γ_E). For the exponential atmosphere (Eq. (3-15))

it may be shown that E is a maximum at $h_o = H_o$ for very small values of $K_{S.L.}$ and increases to $h_o = 2H_o$ for very large values of $K_{S.L.}$. For the 1962 Standard Atmosphere, using H = constant = 23 000 feet, the critical altitude varies from about 23 000 feet at low $K_{S.L.}$ to about 46 000 feet at high $K_{S.L.}$. A plot of E versus h_o is shown for several values of $K_{S.L.}$ in Fig. 5-3.

In summary, the following conclusions were reached regarding the dispersion resulting from reversal of roll rate:

1. The dispersion may be in any direction. The locus of possible impact points is an ellipse centered at the nominal impact point. The major axis of the ellipse is along the flight path. The ratio of minor to major axis is $|\sin \gamma_E|$.

2. The magnitude of the dispersion is a function of the many factors listed below, making it impossible to draw generalized conclusions regarding the effect of specific variables.

C_A, C_{N_α}, $X_{c.p.}$	Aerodynamic	$\overline{C}_{m_o}$, r, ϕ_o	Asymmetry
W, $X_{c.g.}$, I_X	Mass	γ_E, p_E, V_E	Initial Conditions
d, S	Geometry	Type Atmosphere	

Only one type of combined asymmetries capable of resulting in $\bar{\alpha}_o$ and zero roll rate is listed above. However, other combined asymmetries such as C_{ℓ_o} and $\overline{C}_{m_o}$ could also result in roll rate reversal and large dispersion.

3. For given aerodynamic characteristics, mass, geometry, initial conditions, type of atmosphere, and $\overline{C}_{m_o}$, the $\bar{\alpha}_o$ is fixed. However, h_o (and $\bar{\alpha}_o$ to a very small extent) varies with the values of r and ϕ_o. The dispersion that results as r and/or ϕ_o is changed is maximum when h_o has some specific value. For the 1962 Standard Atmosphere, the value of h_o corresponding to δ_{max} is between 23 000 and 46 000 feet, depending upon the value of $K_{S.L.}$.

5.5 Errors in Initial Reentry Angle of Attack and Body Rates

In some cases the initial reentry angle of attack, $\bar{\alpha}$, and body rates, p, q, and r, are not known accurately. During the high altitude portion of the trajectory, these initial conditions affect the $\bar{\alpha}$ history as discussed in Section 4.4. If $\bar{\alpha}$, p, q, and r are not zero in the altitude region where the aerodynamic restoring force is small, the missile experiences coning motion such that, in general, the body centerline does not rotate about the velocity vector. Therefore, in inertial axes, the lift force does not rotate about the velocity vector as it does for a rolling vehicle at altitudes where aerodynamic forces are predominant. During the early phase of reentry, initial values of $\bar{\alpha}$, p, q, and r cause dispersion resulting from both lift and drag effects. The drag effect always tends to cause the vehicle to fall short of the intended impact point. However, the lift effect may cause dispersion in any direction depending upon the direction of the lift vector (determined by the location of the coning motion relative to the velocity vector). In general the locus of impact points resulting from these initial conditions is an ellipse whose major axis is approximately along the flight path. The ratio of the minor to major axis is approximately $|\sin \gamma_E|$. The drag effect shifts the center of the ellipse toward the launch site from the nominal point (impact for nominal $\bar{\alpha}$, p, q, and r).

The vehicle motion is rather complex, and a six-degree-of-freedom simulation is required to evaluate the magnitude of this source of dispersion. A typical order of magnitude of the semimajor axis for $\bar{\delta}$ resulting from $\bar{\alpha}$ is 5 to 10 feet per degree error in $\bar{\alpha}$. Therefore, the error is not negligible unless $\bar{\alpha}$ is known fairly accurately.

5.6 Examples

5.6.1 Example 1

Estimate as a function of γ_E the dispersion resulting from a constant 100 ft/sec headwind ($V_W = -100$) and a constant 10% increase in density ($\Delta\rho/\rho = 0.1$) from the 1962 Standard Density for the following conditions:

$$V_E = 20\,000 \text{ ft/sec}$$
$$\beta = 1000, 2000, \text{ and } 3000 \text{ lb/ft}^2 .$$

Since dispersion is most sensitive to the altitude region from 20 000 to 30 000 feet, a value of H = 23 000 feet (see Table 3-1) is used.

From Eq. (5-2):

$$\delta_w = -\frac{(-100) \times 23\,000}{20\,000} \frac{I_3}{\sin\gamma_E} = 115 \frac{I_3}{\sin\gamma_E} .$$

From Eq. (5-3):

$$\delta_\rho = \left(\frac{23\,000}{20\,000}\right)^2 \frac{32.2 \times 0.1 \times I_5}{\sin^2\gamma_E \tan\gamma_E} = 4.26 \frac{I_5}{\sin^2\gamma_E \tan\gamma_E} .$$

From Table 3-1, $P_{S.L.} = 2116 \text{ lb/ft}^2$. Then $K_{S.L.} = -\frac{2116}{\beta \sin\gamma_E}$. For a given value of β and γ_E, δ_w and δ_ρ may be computed using I_3 and I_5 obtained from Tables 5-1 and 5-3. The results are shown in Fig. 5-4. This

figure illustrates the high sensitivity of dispersion to winds and density for shallow reentry angles and low values of β. It also illustrates the fact that δ_ρ becomes insignificant at large values of γ_E whereas δ_W may be significant even for $\gamma_E = -90°$.

5.6.2 Example 2

Assume that in targeting a missile no corrections were made for winds and deviations in density from the 1962 Standard Density profile for altitudes greater than 100 000 feet. If the average wind at altitudes from 100 000 to 160 000 feet were a 300 ft/sec headwind and if the density were 30% greater than the 1962 Standard profile, estimate as a function of β the impact error resulting from these high altitude meteorological characteristics for $V_E = 20\,000$ ft/sec and $\gamma_E = -25°$. Use $H = 23\,000$ feet.

From Eq. (5-1):

$$\delta_W = \frac{23\,000(-300)}{20\,000(-0.422)} I_3 \sum_{j=2}^{4} F_W$$

$$= -817\, I_3 \sum_{j=2}^{4} F_W .$$

From Eq. (5-3):

$$\delta_\rho = \left(\frac{23\,000}{20\,000 \times 0.422} \right)^2 \frac{32.2 \times 0.3}{(-0.465)} I_5 \sum_{j=2}^{4} F_\rho$$

$$= -155\, I_5 \sum_{j=2}^{4} F_W .$$

Using values of I_3, F_W, I_5, and F_ρ given in Tables 5-1 through 5-4, δ_W and δ_ρ were computed as a

function of $K_{S.L.}$. The values of β corresponding to $K_{S.L.}$ were computed using the equation:

$$\beta = -\frac{2116}{K_{S.L.}(-0.422)} = \frac{5000}{K_{S.L.}} \quad .$$

Values of δ_w and δ_ρ are plotted in Fig. 5-5. The accuracy limit as given in Fig. 5-1 is also shown. Values of $\beta \geq 1230$ lb/ft^2 fall within the limits of accuracy; values of δ shown for β less than 1230 lb/ft^2 will be slightly high.

This problem illustrates that bodies having low values of β tend to be sensitive to meteorological characteristics even at very high altitudes.

5.6.3 Example 3

For the reentry body having the characteristics given in Table 2-1, estimate the dispersion resulting from a constant trim angle of attack $\bar{\alpha}_o$ if the missile has a constant roll rate during reentry. The trajectory characteristics are $V_E = 20\,000$ ft/sec and $\gamma_E = -30°$. Use H = 23 000 feet.

For this case the dispersion results from the increase in drag, and the effect on dispersion is equivalent to a change in density.

$$\frac{\Delta\rho}{\rho} \text{ (Eq. (5-8))} = \frac{C_{N_\alpha}}{C_A} \bar{\alpha}_o^{\,2}$$

$$= \frac{2}{0.104} \bar{\alpha}_o^{\,2}$$

$$= 19.2 \, \bar{\alpha}_o^{\,2} \text{ for } \bar{\alpha}_o \text{ in radians}$$

$$= 0.00585 \, \bar{\alpha}_o^{\,2} \text{ for } \bar{\alpha}_o \text{ in degrees.}$$

The dispersion is computed using Eq. (5-3).

$$K_{S.L.} = \frac{-2116}{1000\,(-0.50)} = 4.23$$

$$I_5 = 21 .$$

Since $\Delta\rho/\rho$ is constant for all altitudes:

$$\sum_{j=1}^{N} \frac{\Delta\rho}{\rho} F_\rho = \frac{\Delta\rho}{\rho} = 0.00585\ \bar{\alpha}_o^{\,2} .$$

Therefore:

$$\delta_\rho = \left(\frac{23\,000}{20\,000\,(-0.50)}\right)^2 \frac{32.2 \times 21}{(-0.577)} (0.00585)\,\bar{\alpha}_o^{\,2}$$

$$= -36.2\,\bar{\alpha}_o^{\,2} .$$

The missile will fall short by 9 feet for $\bar{\alpha}_o = 1/2°$, 36 feet for $\bar{\alpha}_o = 1°$, and 145 feet for $\bar{\alpha}_o = 2°$.

5.6.4 Example 4

Suppose in Example 3 the reentry body has an $\bar{\alpha}_o = 1/2°$ at reentry, the body passes through first resonance without lock-in, but the asymmetries are such that lock-in occurs at an altitude of 10 000 feet and remains until impact. Determine the dispersion.

Again, for this problem, dispersion results from the drag effect. However the angle of attack is amplified by the resonance phenomena. From Eq. (4.5-16), $\bar{\alpha} = A\bar{\alpha}_o$ and, since $\lambda = 1$ at resonance, $A = 1/D$. Using Eq. (4.5-60):

$$D = 0.115\sqrt{K} .$$

Therefore:

$$\bar{\alpha} = \frac{8.7(1/2)}{\sqrt{K}} = \frac{4.35}{\sqrt{K}} \ .$$

Substituting for $K = -\frac{P}{\beta \sin \gamma_E} = \frac{P}{P_{S.L.}} K_{S.L.} = 4.23 \frac{P}{P_{S.L.}}$,

$$\bar{\alpha} = \frac{2.11}{\sqrt{P/P_{S.L.}}} \ .$$

At h = 2500 feet $\quad P/P_{S.L.} = 0.913 \quad \bar{\alpha} = 2.21°$

h = 7500 feet $\quad P/P_{S.L.} = 0.757 \quad \bar{\alpha} = 2.42°$

From Example 3, the equivalent value of $\Delta\rho/\rho$ is $0.00585\,\bar{\alpha}_o^2$. Therefore, for h = 2500 feet, $\Delta\rho/\rho = 0.0286$; for h = 7500 feet, $\Delta\rho/\rho = 0.0343$. Assuming that the value of $\Delta\rho/\rho$ at h = 2500 feet is representative of the altitude band from sea level to 5000 feet and that the value of $\Delta\rho/\rho$ at h = 7500 feet is representative of the 5000 to 10 000 foot band:

$$\sum_{j=16}^{17} \frac{\Delta\rho}{\rho} F_\rho = 0.0286(0.049) + 0.0343(0.055) = 0.00329.$$

Using Eq. (5-3):

$$\delta_\rho = \left[\frac{23\,000}{20\,000 \times 0.5}\right]^2 \frac{32.2}{(-0.577)} \times 21 \times 0.00329 = -20 \text{ feet} \ .$$

5.6.5 Example 5

The body having characteristics given in Table 2-1 has the following asymmetries:

1. A center of gravity offset of 0.042 inch.

2. A body centerline distorted into an arc of a circle. The slope of the centerline at the body nose and base differ by the angle $\Delta\theta$.

As a function of $\Delta\theta$, assess the probability of encountering spin through zero roll rate, and estimate the dispersion that results if spin through zero roll rate occurs. Neglect the possibility of encountering roll lock-in at negative roll rate. Use the 1962 Standard Atmosphere with initial conditions, $p_E = 1000°/sec$, $V_E = 20\,000$ ft/sec, and $\gamma_E = -30°$.

From Eq. (2-35), $C_{m_o} = 0.008\,\Delta\theta$. From Eq. (2-27):

$$\bar{\alpha}_o = 57.3\,\frac{(0.008\Delta\theta)}{2(0.114)} = 2\Delta\theta$$

where $\Delta\theta$ and $\bar{\alpha}_o$ are in degrees. The altitude (in terms of K) at which the roll rate becomes zero is given by Eq. (4.5-94). Substituting for the given terms:

$$e^{-K/2} = 1 - \frac{\frac{1000}{57.3}\,(0.104)(0.079)}{2(0.001)\left(\frac{20\,000}{3.5}\right)\frac{2\Delta\theta}{57.3}\sin\phi_o}$$

$$= 1 - \frac{0.36}{\Delta\theta \sin\phi_o} \quad .$$

At sea level $K = K_{S.L.} = 2116/1000\,(0.5) = 4.23$. For zero roll rate at sea level:

$$\Delta\theta \sin\phi_o = \frac{0.36}{1 - e^{-2.115}} = 0.41° \quad .$$

Since ϕ_o may have any value from 0° to 360° and assuming no correlation between the two types of asymmetries, the probability of encountering zero roll rate during reentry is:

$$\overline{P} = \frac{\Delta\phi_o}{360}$$

where $\Delta\phi_o$ is the range in values of ϕ_o for a given $\Delta\theta$ such that

$$\Delta\theta \sin\phi_o \geq 0.41 .$$

$\Delta\theta$	$\sin\phi_o$	$\Delta\phi_o$	$\overline{P}$
0.41	1	0	0
0.50	0.82 to 1	70	0.195
0.60	0.683 to 1	94	0.261
0.70	0.585 to 1	108	0.300
0.80	0.512 to 1	118	0.328
1.0	0.41 to 1	132	0.367
2.0	0.205 to 1	156	0.434
3.0	0.137 to 1	164	0.456

The probability of encountering zero roll rate is shown as a function of $\Delta\theta$ in Fig. 5-6. The altitude, h_o, at which zero roll rate occurs is an important factor in the calculation of dispersion. For $\Delta\theta \geq 0.41$, h_o may be any value from sea level to some upper limit obtained when $\sin\phi_o = 1$ or

$$e^{-K/2} = 1 - \frac{0.36}{\Delta\theta} .$$

The upper limit to h_o is shown as a function of $\Delta\theta$ in Fig. 5-7.

The dispersion that results when spin through zero roll rate occurs may be computed using Eq. (5-20). For a given $\Delta\theta$ (or $\bar{\alpha}_o$), the dispersion may be any value from 0 to some maximum value depending upon h_o which, in

turn, depends upon ϕ_o. For low values of $\Delta\theta$, the maximum value of E (Eq. (5-21) and Fig. 5-3) correspond to the highest value of h_o ($\phi_o = 90°$). However for the larger values of $\Delta\theta$, the maximum value of E for this problem ($K_{S.L.} = 4.23$) occurs at $h_o \approx 27\,000$ feet. Using h_o data given in Fig. 5-7 and the E values given in Fig. 5-3, E_{max} for various values of $\Delta\theta$ are tabulated below.

$\Delta\theta$	h_o at E_{max}	E_{max}	$\Delta\theta\, E_{max}$
0.41	0	0	0
0.5	13 000	8 600	4 300
0.6	21 000	10 800	6 480
0.7	27 000	11 300	7 920
0.8	27 000	11 300	9 050
1.0	27 000	11 300	11 300
2.0	27 000	11 300	22 600
3.0	27 000	11 300	33 900

Using Eq. (5-20) with $\bar{\alpha}_o = 2\,\Delta\theta$:

$$\delta_{R_{max}} = 1.49\,\frac{(2\Delta\theta)}{57.3}\sqrt{\frac{20\,000 \times 2116}{1000 \times 23\,000 \times \frac{1000}{57.3}}\,\frac{\left(\frac{2}{0.104} - 1\right)}{(1/2)^2}}\;E_{max}$$

$$\delta_{R_{max}} = 1.22\Delta\theta\; E_{max}\,.$$

The values of $\delta_{R_{max}}$ may be computed using the listed values of E_{max}, and the results are shown in Fig. 5-8.

The impact may be anywhere on an ellipse having a semimajor axis of any value from zero up to the values shown in Fig. 5-8. The major axis is along the trajectory. The semiminor axis is $\delta_R/2$ (see Eq. (5-11)).

The magnitude of the dispersion is highly dependent upon ϕ_o. In the previous discussion we considered only the maximum effect. The probability of encountering a given magnitude for the major axis of the dispersion ellipse may be obtained by plotting δ_R versus ϕ_o for various values of $\Delta\theta$ as shown in Fig. 5-9. The dispersions for values of $\phi_o > 90°$ are not shown since δ_R is symmetrical about $\phi_o = 90°$. The probability of encountering or exceeding a given value of δ_R for a given $\Delta\theta$ is obtained from the ratio $\Delta\phi_o/360$ where $\Delta\phi_o$ is the range in values of ϕ_o for which δ_R equals or exceeds the specified value. The probability plot is shown in Fig. 5-10. The values of $\overline{P}$ shown for $\delta_R = 0$ are the probabilities of encountering zero roll rate shown in Fig. 5-6. As an example of the interpretation of this figure, for $\Delta\theta = 0.5°$ there is a 19% probability that zero roll rate will be encountered; there is a 16% probability that $\delta_R \geq 2500$ feet; the maximum possible dispersion is 5300 feet (the values of δ_R at $\overline{P} = 0$ are the values shown in Fig. 5-8).

Note that the dispersion that may be encountered if the missile spins through zero roll rate may be at least an order of magnitude greater than the dispersions considered in the previous problems. For example, the $\Delta\theta = 0.5°$ asymmetry corresponds to a 1° trim angle of attack. It was shown in Example 3 that if the missile does not encounter zero roll rate the resulting dispersion is about 36 feet for $\overline{\alpha}_o = 1°$. The spin through zero roll rate phenomenon is a serious problem to the designer of reentry vehicles that require good impact accuracy.

REFERENCES

5-1 L. S. Glover, Approximate Equations for Evaluating the Impact Dispersion Resulting from Reentry Winds and Deviations in Density, APL/JHU TG 1132, September 1970.

5-2 B. F. Fuess, "Impact Dispersion Due to Mass and Aerodynamic Asymmetries," J. Spacecraft and Rockets, Vol. 4, No. 10, October 1967, pp. 1402-1403.

5-3 W. H. T. Loh, Dynamics and Thermodynamics of Planetary Entry, Prentice-Hall Space Technology Series, 1963.

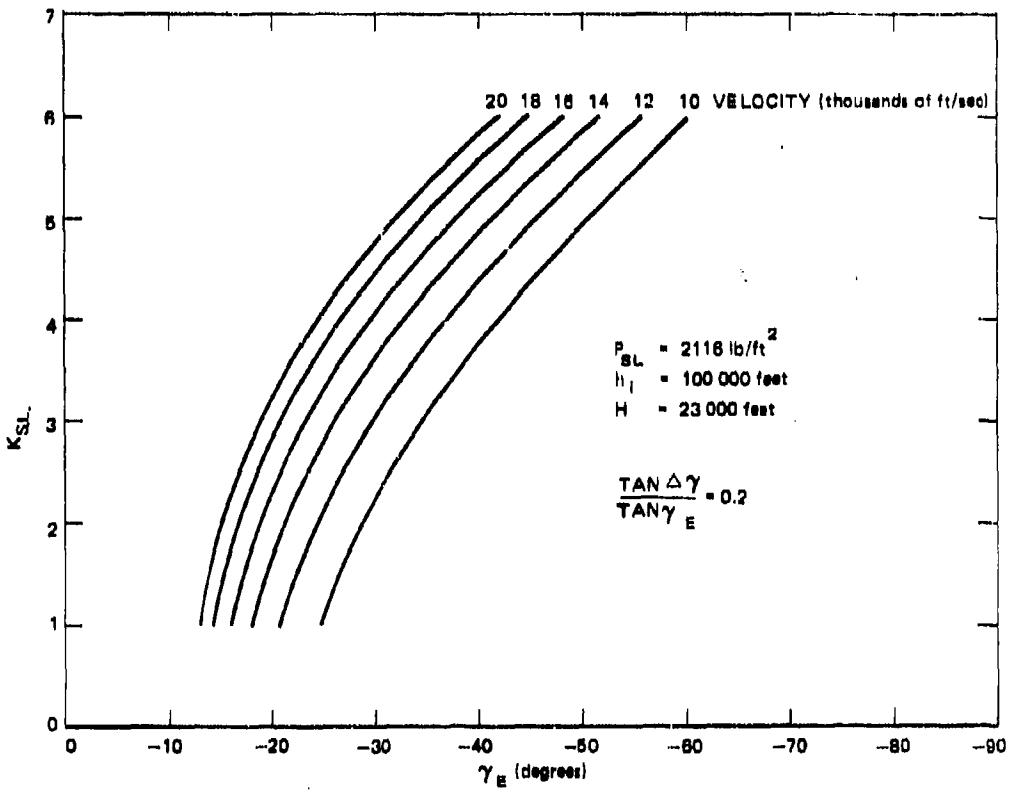

Fig. 5-1 LIMITING VALUES OF K_{SL}

Preceding page blank

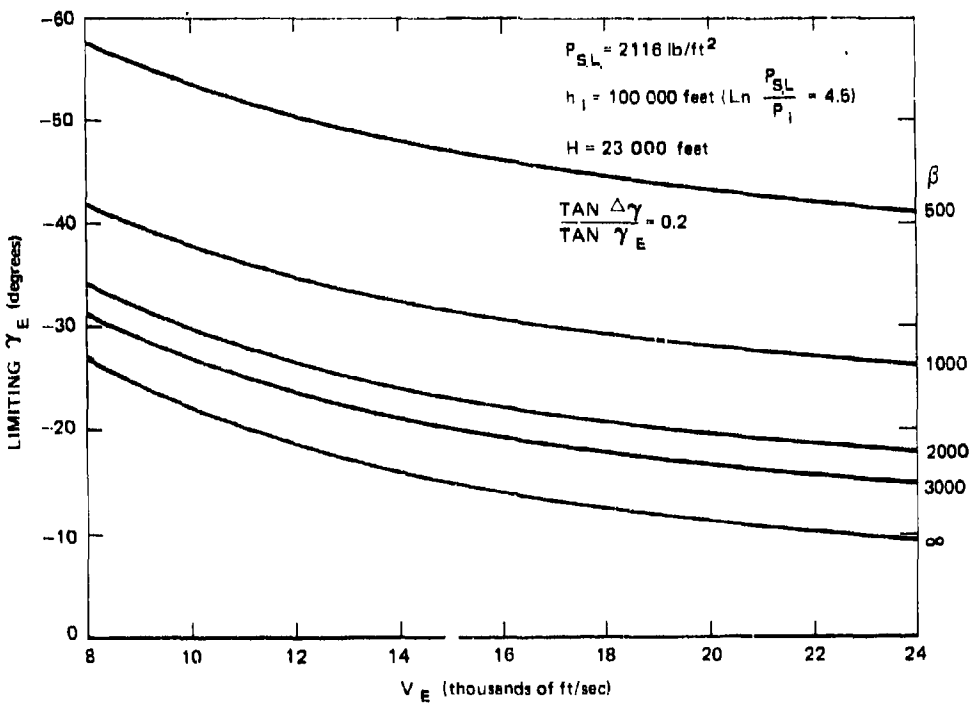

Fig. 5-2 LIMITING VALUES OF γ_E

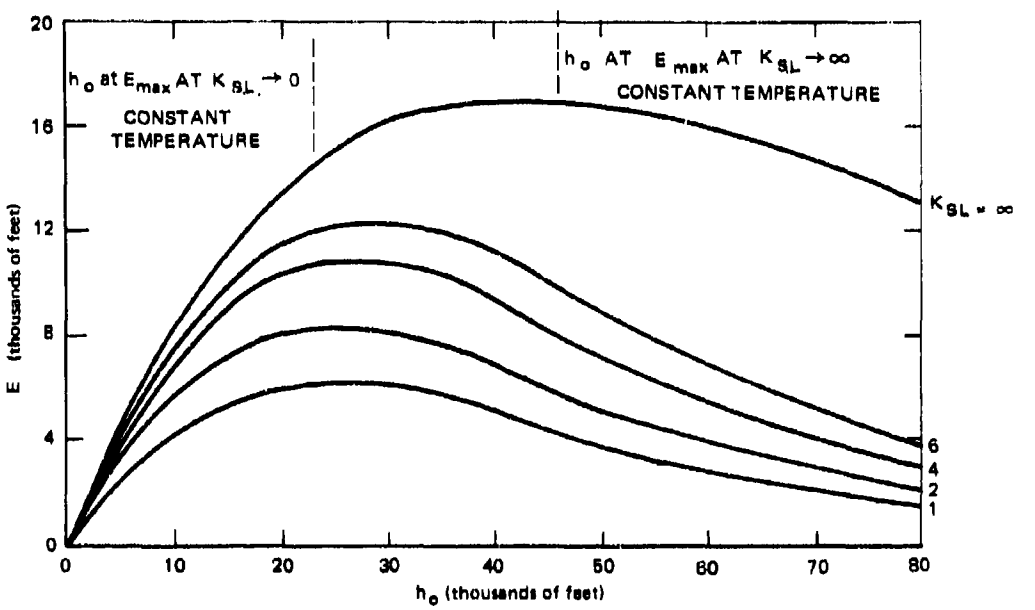

Fig. 5-3 VARIATION OF E WITH h_o, 1962 STANDARD ATMOSPHERE

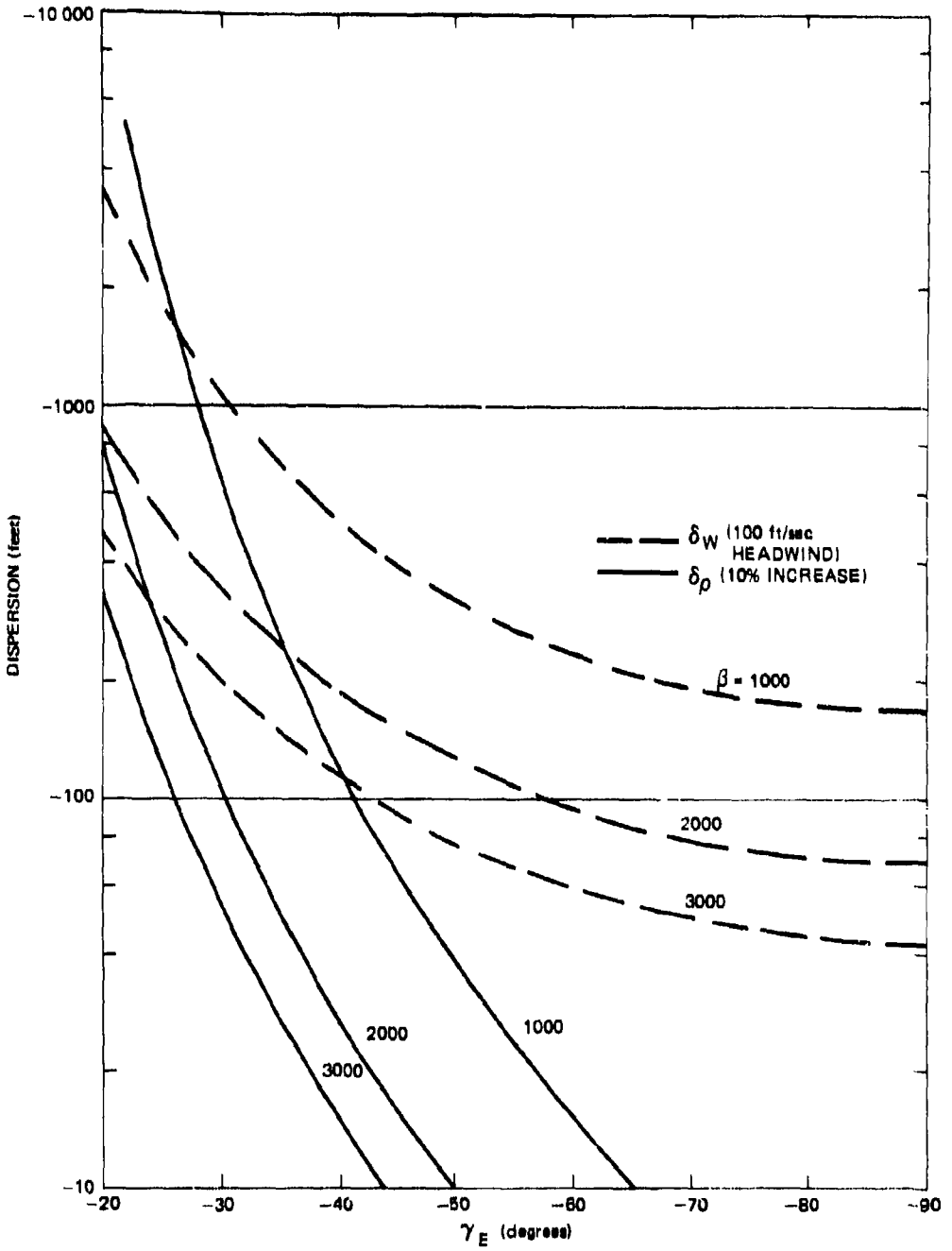

Fig. 5-4 DISPERSION RESULTING FROM WIND AND DEVIATION IN DENSITY

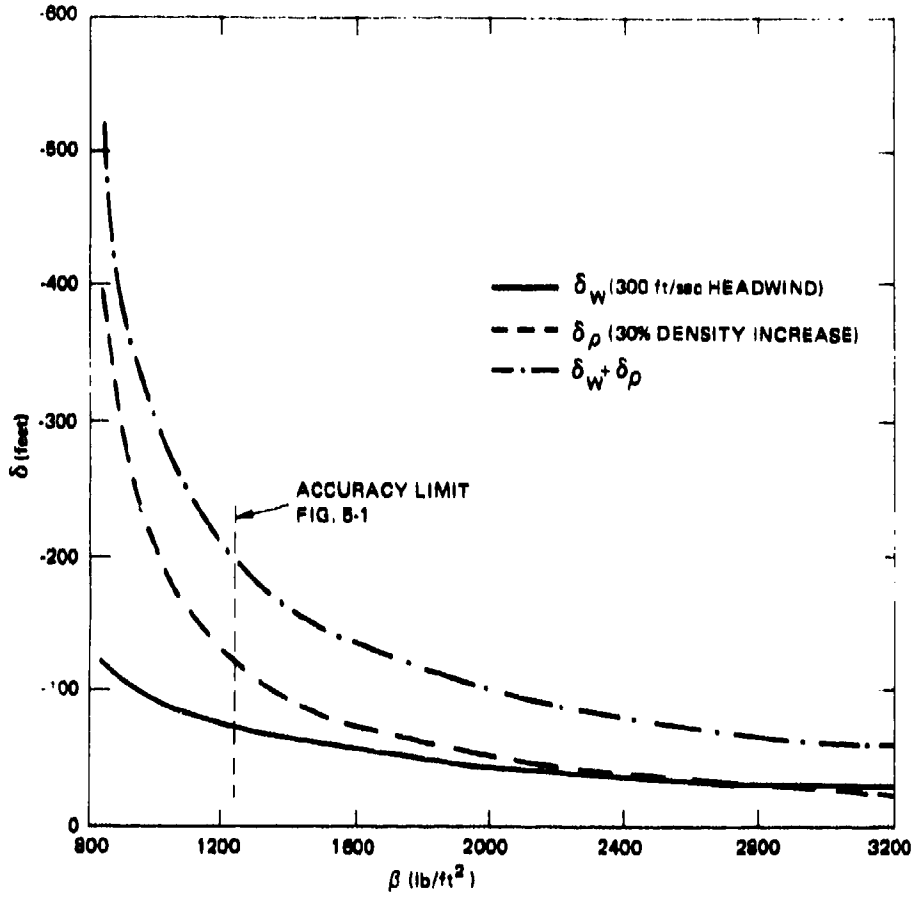

Fig. 5-5 DISPERSION RESULTING FROM METEOROLOGICAL CHARACTERISTICS AT HIGH ALTITUDE

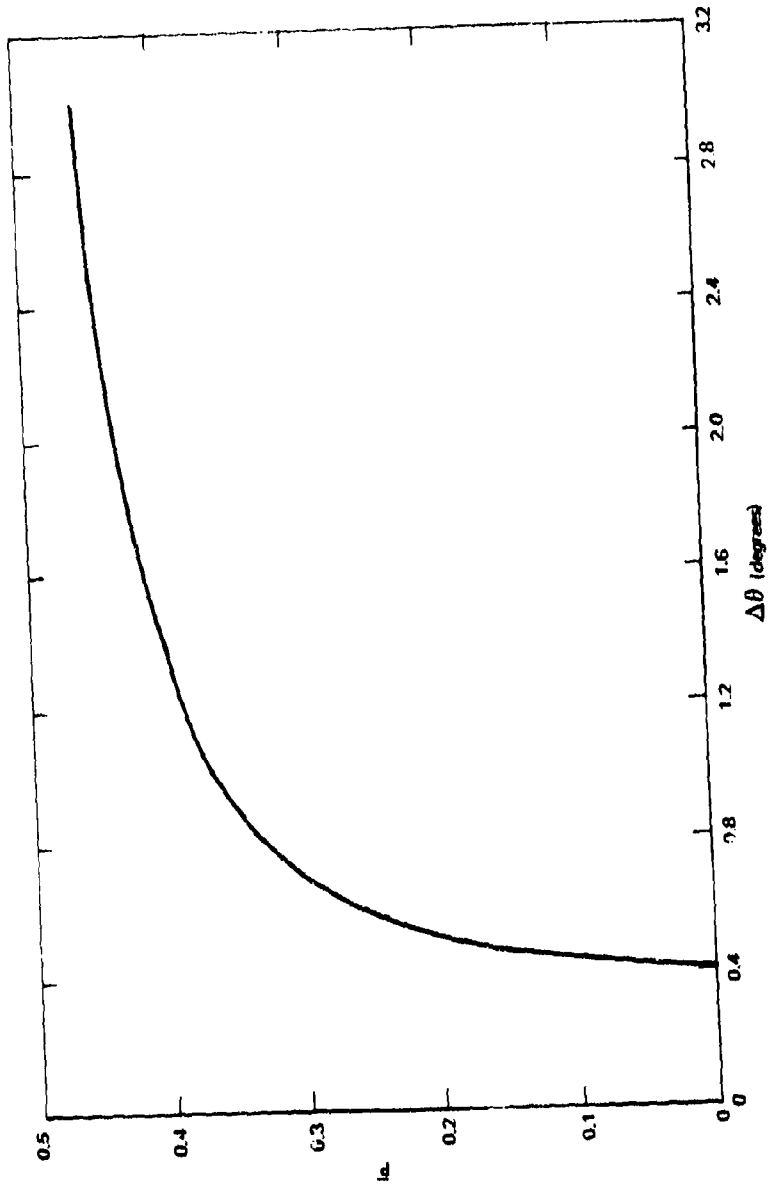

Fig. 5-6 PROBABILITY OF ENCOUNTERING ZERO ROLL RATE

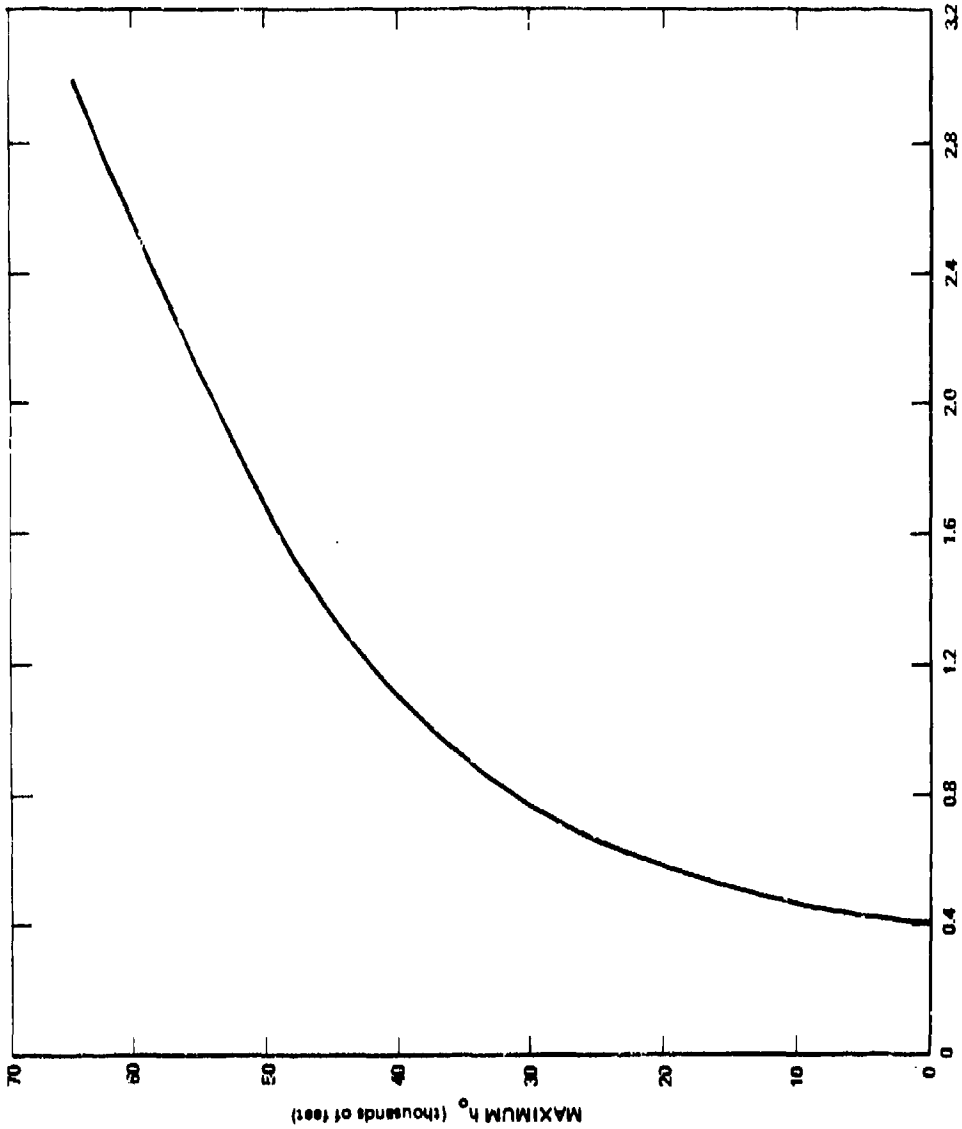

Fig. 5-7 MAXIMUM ALTITUDE FOR ZERO ROLL RATE

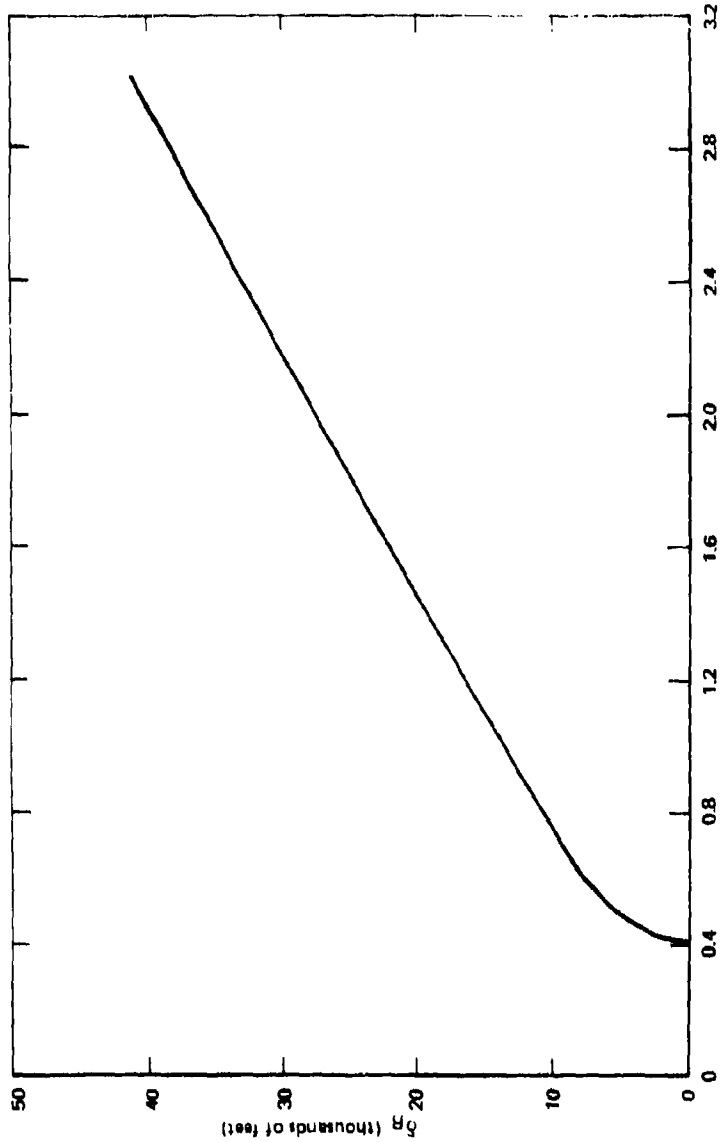

Fig. 5-8 MAXIMUM DISPERSION RESULTING FROM $\Delta\theta$ AND $\frac{f}{d}$

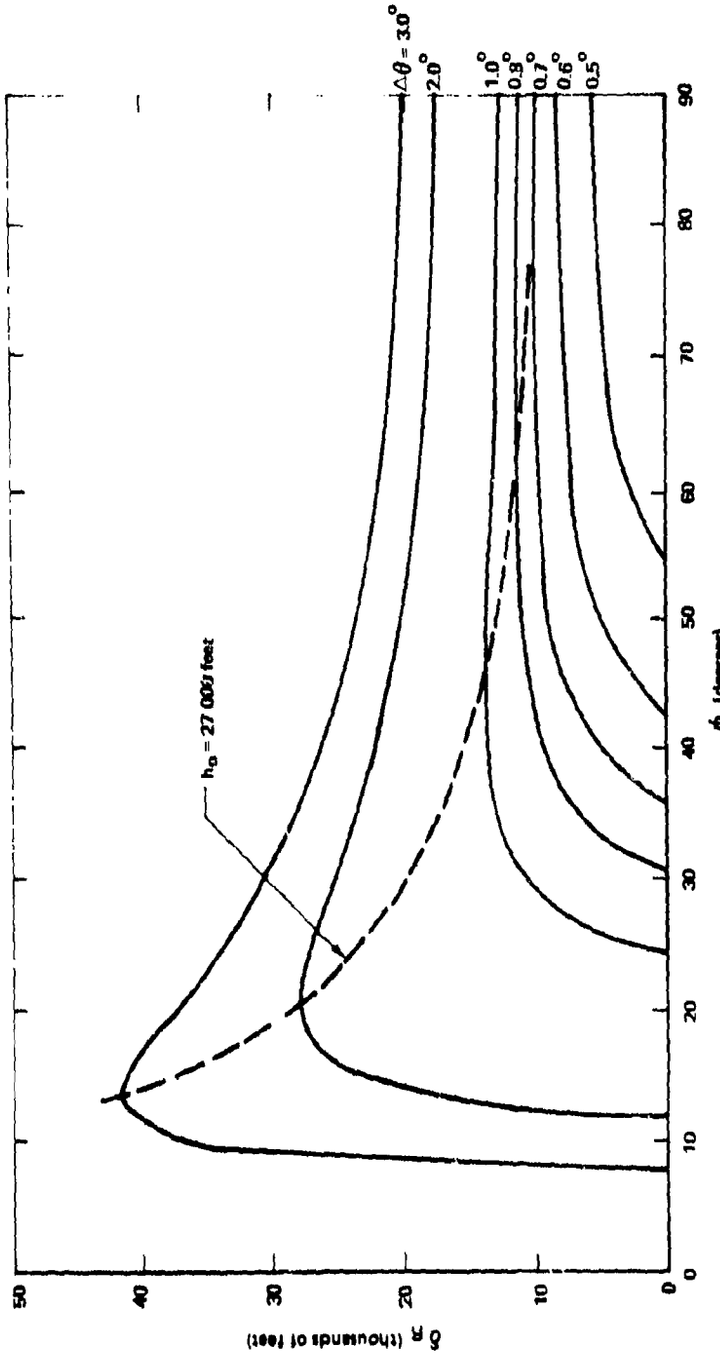

Fig. 5-9 DISPERSION VERSUS ϕ_o

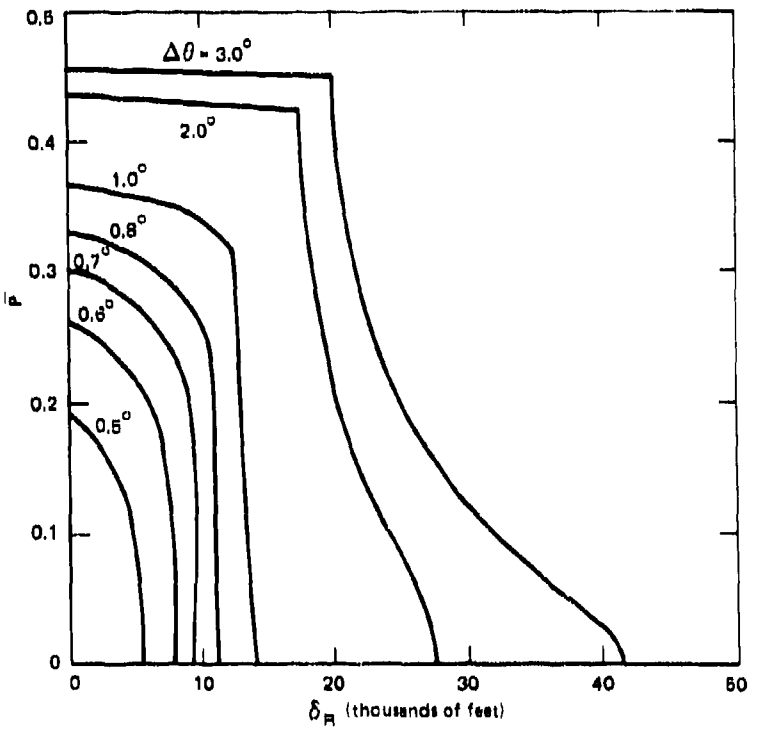

Fig. 5-10 DISPERSION PROBABILITY

Table 5-1

Values of I_3

$K_{S.L.}$	I_3
0	0
0.5	0.25
1.0	0.57
1.5	0.92
2.0	1.33
2.5	1.84
3.0	2.44
3.5	3.20
4.0	4.13
4.5	5.25
5.0	6.60
5.5	8.17
6.0	9.90

Table 5-2

Values of F_w

Altitude (thousands of feet)	J	$K_{S,L.}$					
		1.5	2.0	3.0	4.0	5.0	6.0
160-∞	1	0.007	0.006	0.005	0.004	0.003	0.003
140-160	2	0.005	0.004	0.004	0.002	0.002	0.001
120-140	3	0.010	0.009	0.007	0.006	0.005	0.004
100-120	4	0.025	0.023	0.018	0.013	0.011	0.010
90-100	5	0.021	0.019	0.015	0.011	0.009	0.008
80-90	6	0.030	0.027	0.021	0.017	0.015	0.013
70-80	7	0.045	0.040	0.030	0.024	0.020	0.016
60-70	8	0.064	0.058	0.047	0.035	0.029	0.025
50-60	9	0.086	0.079	0.066	0.053	0.042	0.036
40-50	10	0.109	0.106	0.092	0.077	0.066	0.063
30-40	11	0.147	0.143	0.126	0.110	0.100	0.097
25-30	12	0.089	0.086	0.078	0.071	0.068	0.066
20-25	13	0.103	0.100	0.092	0.086	0.085	0.086
15-20	14	0.086	0.090	0.097	0.105	0.114	0.117
10-15	15	0.089	0.080	0.110	0.142	0.158	0.168
5-10	16	0.058	0.070	0.101	0.130	0.146	0.155
S.L.-5	17	0.047	0.060	0.092	0.114	0.127	0.132

Note. These data are applicable to a 1962 Standard Atmosphere. However, they may be used for any atmosphere by changing the altitude limits for each band. For example, the J = 8 data apply to the altitude band from an altitude corresponding to $P/P_{S.L.}$ = 0.0714 (60 000 feet for the 1962 Standard Atmosphere) to an altitude corresponding to $P/P_{S.L.}$ = 0.0443 (70 000 feet for the 1962 Standard Atmosphere).

Table 5-3

Values of I_5

$K_{S.L.}$	I_5
0	0
0.5	0.50
1.0	1.05
1.5	1.85
2.0	3.00
2.5	4.90
3.0	7.55
3.5	11.30
4.0	17.30
4.5	27.00
5.0	41.00
5.5	61.00
6.0	92.50

Table 5-4

Values of F_ρ

Altitude (feet x 1000)	j	$K_{S,L}$ 1.5	2.0	3.0	4.0	5.0	6.0
160-∞	1	0.004	0.012	0.009	0.006	0.004	0.004
140-160	2	0.014	0.014	0.009	0.006	0.005	0.004
120-140	3	0.027	0.023	0.017	0.012	0.008	0.007
100-120	4	0.053	0.046	0.035	0.025	0.019	0.017
90-100	5	0.045	0.039	0.028	0.021	0.015	0.013
80-90	6	0.055	0.050	0.039	0.029	0.025	0.022
70-80	7	0.069	0.067	0.058	0.045	0.034	0.030
60-70	8	0.088	0.085	0.077	0.065	0.056	0.051
50-60	9	0.118	0.111	0.099	0.090	0.087	0.086
40-50	10	0.142	0.138	0.130	0.123	0.120	0.118
30-40	11	0.140	0.146	0.154	0.157	0.158	0.156
25-30	12	0.072	0.076	0.083	0.088	0.092	0.095
20-25	13	0.068	0.074	0.082	0.090	0.098	0.102
15-20	14	0.044	0.048	0.064	0.078	0.087	0.091
10-15	15	0.030	0.032	0.051	0.066	0.076	0.080
5-10	16	0.019	0.022	0.037	0.053	0.061	0.065
0-5	17	0.012	0.017	0.028	0.046	0.055	0.059

Note: See note to Table 5-2.

6. TRAJECTORY SIMULATION

THE JOHNS HOPKINS UNIVERSITY
APPLIED PHYSICS LABORATORY
SILVER SPRING MARYLAND

SUMMARY

The discussion of the motion of ballistic missiles would be incomplete without some comment on the "work horse" of all trajectory analysts – trajectory simulations. It is beyond the scope of this report to discuss any simulation in detail. However, for the uninitiated, a few brief comments are presented regarding the basic ingredients of all simulations, the relative operational cost of several types of simulations, and some characteristics of a six-degree-of-freedom simulation currently in use at APL.

A trajectory simulation is a computer program by which the time history of the vehicle motion may be determined. Given a set of initial conditions and the particular quantities for which a time history is desired (outputs), the reentry body simulation consists of five major parts (see sketch, page 328):

1. Equations of motion,
2. Earth characteristics,
3. Atmospheric characteristics,
4. Mass characteristics,
5. Aerodynamic characteristics.

Each of the major parts may be very simple or very complex. The equations given in Section 4.3 provide the basis for a very simple simulation in which the equations of motion are reduced to a single degree of freedom (motion along a constant flight path angle), the earth is flat and nonrotating, the acceleration of gravity is zero, the atmosphere obeys the hydrostatic equation, the wind is zero, and the vehicle mass and aerodynamic characteristics are defined by a single parameter (β). However, the usefulness of this simulation is limited to those studies for which approximate time histories of a very few trajectory parameters are sufficient. For many types of work this simple simulation is not adequate.

Increasing the complexity (and cost) over the one-degree-of-freedom (1 DOF) problem, a three-degree-of-freedom (3DOF) trajectory simulation may be used. Usually the 3DOF designation refers to degrees of freedom in the three orthogonal linear dimensions. In this case the simulation is also called a "point mass" simulation. The only mass and aerodynamic characteristics used are the body weight and axial force characteristics. Any atmosphere and earth model may be used. This simulation is reasonably uncomplicated but has sufficient accuracy for most types of flight test analyses, for defining targeting data, and for evaluating most types of range partials (sensitivity of impact dispersion to various anomalies).

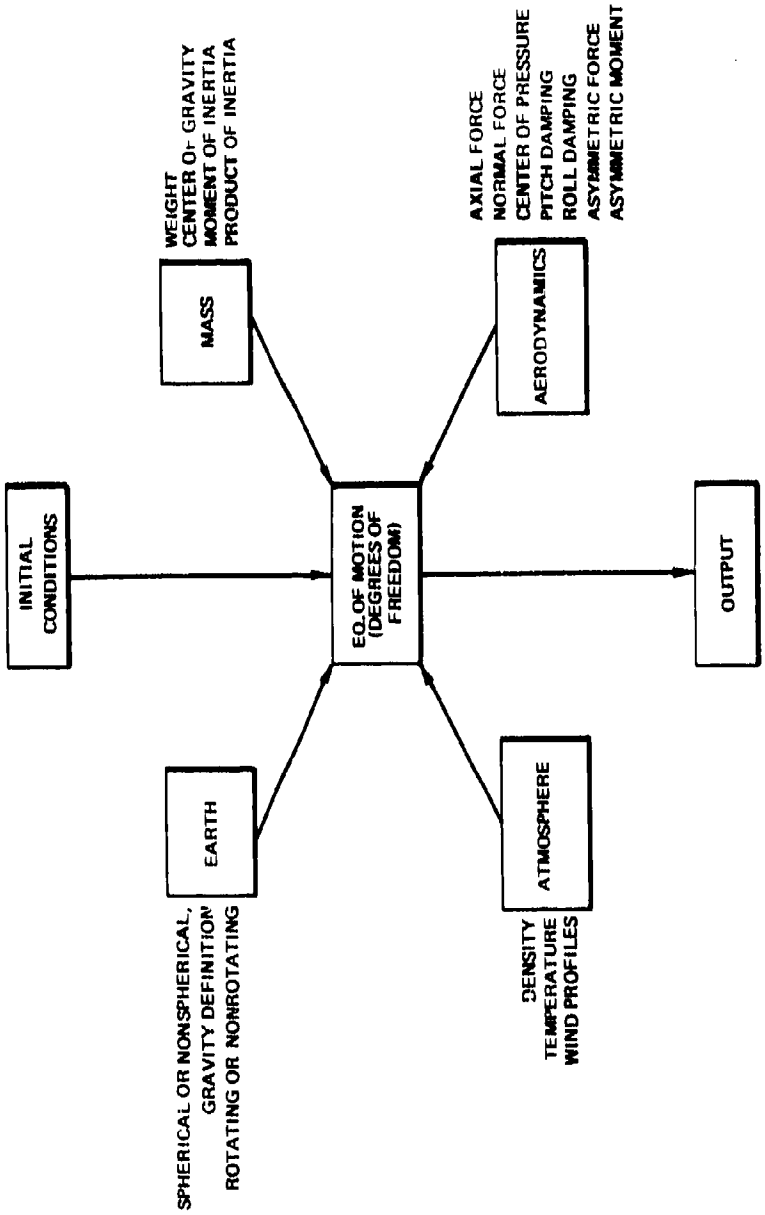
INITIAL CONDITIONS
EQ. OF MOTION (DEGREES OF FREEDOM)
OUTPUT
MASS
WEIGHT
CENTER OF GRAVITY
MOMENT OF INERTIA
PRODUCT OF INERTIA
AERODYNAMICS
AXIAL FORCE
NORMAL FORCE
CENTER OF PRESSURE
PITCH DAMPING
ROLL DAMPING
ASYMMETRIC FORCE
ASYMMETRIC MOMENT
EARTH
SPHERICAL OR NONSPHERICAL,
GRAVITY DEFINITION
ROTATING OR NONROTATING
ATMOSPHERE
DENSITY
TEMPERATURE
WIND PROFILES

For evaluating the detailed dynamic behavior of missile motion and for calculating precise impact locations, a six-degree-of-freedom (6DOF, three linear and three rotational) program is required. In this simulation, the body mass characteristics are defined by weight, center of gravity location (specified by three coordinates), moments of inertia, and products of inertia. The aerodynamic terms include the axial force, normal force, center of pressure location, pitch (or yaw) damping, roll damping, and asymmetric force and moment terms as required for a specific study. This type of simulation is the only one (of the ones discussed) that accurately accounts for angle of attack effects. Any atmosphere and earth model may be used.

There are many modifications to these three basic simulations. For a given study the analyst will select the type of simulation based on a trade-off between accuracy and cost. For a typical reentry trajectory, the approximate machine cost of running the three simulations discussed above is as follows:

1DOF Negligible,

3DOF $1 per trajectory,

6DOF $30 per trajectory.

As an illustration of a typical 6DOF reentry body simulation, one of the simulations currently in use at APL is described briefly.

6.1 Initial Conditions

1. Geometric altitude,
2. Missile velocity and flight path angle relative to rotating earth,
3. α and β components of $\bar{\alpha}$ (see Fig. 4-11),
4. Initial roll orientation of the body axes with respect to the inertial axes,
5. Body rates (roll, pitch, yaw).

6.2 Missile Mass Characteristics

1. Weight,
2. X, Y, Z coordinates of the center of gravity,
3. Moments of inertia (about X, Y, Z axes),
4. Products of inertia (about X, Y, Z axes).

Provision is made for two sets of characteristics so that the trajectory for a two-stage reentry body may be computed. Provision is also made for varying the weight and the two lateral coordinates of the center of gravity as a function of altitude. This option is used for studies in which body shape changes as a result of aerodynamic heating.

6.3 Aerodynamic Characteristics

Some of the aerodynamic data are in an aerodynamic subroutine of the program and some are inputs. The subroutine provides the axial force coefficient, normal force coefficient, center of pressure location, pitch (or yaw) moment damping coefficient, and roll moment damping coefficient. The axial force is a function of Mach number, angle of attack, altitude, and velocity. The center of pressure, pitch damping, and normal force data are functions of Mach number and angle of attack. The roll damping coefficient is a function of velocity and altitude. Provision is made for using two sets of data corresponding to the two sets of mass data.

The aerodynamic inputs include the asymmetric pitching, yawing, and rolling moment coefficients as a function of altitude and multiplying factors as a function of altitude for varying the aerodynamic data included in the aerodynamic subroutine.

6.4 Atmosphere Characteristics

The 1962 Standard Atmosphere is built into the simulation but any variation of density, temperature, wind, and wind direction with altitude may be used.

6.5 Earth Model

The WGS/60 ellipsoidal rotating earth model is used.

6.6 Equations of Motion

The six equations of motion (in body axes) used are the three rotational degrees of freedom given in Eqs. (4.5-1), (4.5-2), and (4.5-3), and the three linear degrees of freedom given in Eqs. (4.4-4), (4.4-5), and (4.4-6). The aerodynamic forces and moments are computed in the body axis system. Accelerations are then computed in the inertial axes, and velocities and translations are computed by integration.

6.7 Output

Various output quantities are available. The output format currently programmed provides the following time histories:

1. Three components of acceleration (body axes),
2. Total angle of attack,
3. Pitch, yaw, and roll rates (body axes),
4. Mach number,
5. Velocity (relative to rotating earth),
6. Dynamic pressure,
7. Flight path angle (relative to rotating earth),
8. Altitude (geometric),
9. Downrange and crossrange coordinates of the trajectory.

The final latitude and longitude are also listed.

Several options are available regarding the printout time interval. The integration time step is variable (with a minimum of 0.0001 second), and readouts may be obtained at every time step, any multiple of the time step, every second, or any multiple of a second.

For a 3DOF simulation only the first and second initial conditions, the first mass characteristic, the axial force coefficient (as a function of Mach number and altitude only), and the three linear degrees of freedom are used. Hence the computer cost is lowered by an order of magnitude compared with the cost of using the 6DOF program.

7. FLIGHT DYNAMICS DATA ANALYSIS

SYMBOLS FOR SECTION 7

Symbol	Definition	Typical Units
A	axial force	pounds
A	amplification factor	-
a	semimajor axis of the dispersion ellipse	feet
b	semiminor axis of the dispersion ellipse	feet
C_A	axial force coefficient, A/qS	-
C_N	normal force coefficient, N/qS	-
C_{N_α}	slope of the normal force coefficient, $\partial C_N/\partial\alpha$	per radian
C_{m_q}	pitch damping coefficient, $\partial C_m/\partial(qd/V)$	-
D	damping parameter (see Fig. 7-11)	-
F	resultant transverse force	pounds
$\bar{g}$	resultant transverse acceleration, $\sqrt{g_Y^2 + g_Z^2}$	g
g_X	longitudinal acceleration	g
g_Y	lateral acceleration	g
g_Z	normal acceleration	g
h	altitude	feet
I_X	roll inertia	slug-ft^2
I_Y	pitch inertia	slug-ft^2
K	parameter defined in Eq. (4.3-6)	-

Symbol	Definition	Typical Units
m	mass	slugs
N	normal force	pounds
P	atmospheric pressure	lb/ft^2
p	roll rate	deg/sec or rad/sec
q	pitch rate	deg/sec or rad/sec
r	yaw rate	deg/sec or rad/sec
q or $\bar{q}$	dynamic pressure	lb/ft^2
S	reference area	ft^2
V	velocity	ft/sec
W	weight	pounds
X, Y, Z	body coordinates with origin at center of gravity. X coordinate is parallel to the body centerline, positive forward; Y coordinate is perpendicular to body centerline, positive to the right looking forward; Z coordinate forms a right-hand system with X and Y, positive direction is down when looking forward.	-
$X_{c.g.}$	distance from nose to center of gravity	feet
$X_{c.p.}$	distance from nose to center of pressure	feet
α	angle of attack in X-Z plane	degrees
β	angle of yaw in X-Y plane	degrees
β	ballistic coefficient, $W/C_A S$	lb/ft^2
$\bar{\alpha}$	total trim angle of attack	degrees
γ	flight path angle	degrees
ΔX	$= X_{c.p.} - X_{c.g.}$	feet
$\Delta\psi$	change in trim maneuver plane due to roll rate	degrees
λ	resonance index (see Fig. 7-11)	-

Symbol	Definition	Typical Units
ψ	orientation of trim maneuver plane, positive measured clockwise from Y axis looking forward	degrees
ω_A	aerodynamic frequency (see Fig. 7-10)	deg/sec

Subscripts

c. p.	center of pressure
c. g.	center of gravity
E	conditions at beginning of reentry (400 000 feet)
o	conditions when p = 0
X, Y, Z	component in the X, Y, or Z direction, respectively

A dot over a symbol means the first derivative with respect to time. Two dots mean the second derivative with respect to time.

THE JOHNS HOPKINS UNIVERSITY
APPLIED PHYSICS LABORATORY
SILVER SPRING MARYLAND

SUMMARY

A detailed discussion is presented of the procedures currently used at APL in the analysis of vehicle motion during reentry. This discussion includes comments on:

1. The basic data available,
2. Basic data processing,
3. Conversion to engineering quantities,
4. Special analyses for dispersion and "roll lock-in."

Examples are given of:

1. Typical flight test records,
2. A method of extracting range time from these records,
3. Typical body rate and acceleration traces,
4. Work sheets for computing angle of attack, aerodynamic pitch frequency, and several quantities related to roll resonance.

7.1 Available Data

The flight data most commonly available for dynamics analysis are the pitch, yaw, and roll rates and the normal, lateral, and longitudinal accelerations at the reentry body center of gravity. In addition, the weather data in the reentry area are required for a detailed reentry dispersion analysis. These data include the atmospheric pressure and temperature, and the wind speed and direction as a function of altitude. Of course, the mass characteristics of the reentry body are required. These include the weight, center of gravity location (three coordinates), and the moments and products of inertia. The initial conditions of the reentry trajectory are also required. These conditions are frequently specified at 400 000 feet altitude, which is an altitude well above the sensible atmosphere, and include the velocity, flight path angle, latitude and longitude, flight path azimuth, and roll rate. Additional initial conditions must be specified if the reentry body motion at very high altitudes is being examined or if the precise impact point must be determined. These quantities include the initial angle of attack, side slip angle, roll angle, pitch rate, and yaw rate.

Although in general all of these data are required for a precise analysis of the reentry dynamics, it occasionally happens that some part of the data is not available. When this situation arises, the analysis sometimes may be continued without seriously compromising its accuracy by substituting nominal values for the missing data. As an example, the weather data may be unavailable, but it may be possible to substitute weather data (except for winds) that were determined during previous tests in that part of the world (and during that time of the year) and still obtain satisfactory results. Or it may be possible to choose one of the available standard atmospheres and obtain a satisfactory result.

Should the acceleration at the reentry body center of gravity be unavailable, accelerations measured at other locations may be used to calculate the acceleration at the

center of gravity. An accelerometer positioned at a point away from the center of gravity will be influenced by the body angular rates and accelerations; the data from such an accelerometer may be corrected to yield the acceleration at the center of gravity by means of the following equations:

$$g_X = \ddot{X}_{\text{measured } g} - \frac{Z}{32.2}(\dot{q} + rp) - \frac{Y}{32.2}(pq - \dot{r}) + \frac{X}{32.2}(q^2 + r^2) \quad (7\text{-}1)$$

$$g_Y = \ddot{Y}_{\text{measured } g} - \frac{Z}{32.2}(rq - \dot{p}) + \frac{Y}{32.2}(r^2 + p^2) - \frac{X}{32.2}(\dot{r} + pq) \quad (7\text{-}2)$$

$$g_Z = \ddot{Z}_{\text{measured } g} + \frac{Z}{32.2}(p^2 + q^2) - \frac{Y}{32.2}(\dot{p} + qr) - \frac{X}{32.2}(pr - \dot{q}) \quad (7\text{-}3)$$

7.2 Data Sources

Redundant receiving stations are frequently used to ensure reception of telemetry from a reentry body. Ground stations, shipboard stations, and airborne stations may be used. The quality of the data received at any one of these stations may vary widely depending upon the geometry of the trajectory relative to the station location. As is now commonly known, a body reentering the atmosphere develops a plasma sheath that impedes RF transmission. The quality of the signal received through this sheath varies greatly with the aspect of the body relative to the station. Reentry bodies with a low ballistic coefficient (essentially a low weight to drag ratio) may have a plasma sheath of such impedance that transmission of the reentry data acquired during this "plasma blackout" must be delayed.

It may be necessary to examine the signal received by several stations in order to acquire the data needed for a reentry analysis.

7.3 Data Format

Flight test data, as currently processed at APL, are in the form of either DITAR records or DITAP records.

In both cases the flight functions are digitized by dividing the calibrated range of the sensing instrument into 255 intervals. A value of the function may then be represented by a number of counts or bits ranging from 0 to 255. In the case of the DITAP records, the count level is plotted as a function of time, and the record is an analog display of the function. An example of the data format is shown in Fig. 7-1. Timing marks are applied to the DITAP records according to the scheme in Fig. 7-2. In the case of the DITAR records, the bits are plotted in a condensed form that permits many telemetry functions to be displayed on one record. Two traces are required for each function, one trace to count from 0 to 15 and the second trace to count in increments of 16 from 0 to 240. By adding the counts from both traces, any number from 0 to 255 can be represented. An example of the data format for DITAR records is shown in Fig. 7-3. An example of the timing marks on the DITAR records is shown in Fig. 7-4. The series of marks on the margin of the record may be interpreted as time of day.

The DITAR data format presents the data very compactly, and although a two point calibration is attached, it is sometimes difficult to establish the zero point from which one should begin counting the bits. From certain physical considerations, a value for one point on the flight records can sometimes be established, and this point can be used to confirm that the correct zero bit level has been chosen.

The following is an example of these techniques for confirming the bit level. The pitch and yaw rate gyro data, before reentry, will have a sinusoidal shape. Except for the effect of principal axis misalignment, which is usually small, the sine wave will be centered about zero rate. From the calibration tables used to convert to engineering units, the number of counts for zero rate can be determined, and this then fixes one point on the rate gyro data curve. Subsequent values can be determined simply by counting bits. Furthermore, the frequency of the pitch and yaw rate gyro sine wave is related

to the roll rate by means of Eq. (4.4-21) when the body is unaffected by the atmosphere. Therefore the exoatmospheric roll rate can be fixed by determining the frequency of the pitch rate gyro output, and subsequent values can be determined by counting. The count level for the accelerations may be established by noting that the exoatmospheric accelerations are zero. The bit level, therefore, must be the one that corresponds to zero acceleration. Subsequent bit levels can be established by counting.

In the case of the longitudinal acceleration data, advantage can also be taken of the two ranges of instruments that are frequently used. One accelerometer is sensitive enough to detect the low level of acceleration at the beginning of reentry, and the second is sturdy enough to measure the peak g. The less sensitive instrument may be expected to go off scale at some point in the reentry. The count level is 255 at the point where the range of the instrument was just exceeded. The acceleration at this point may be determined easily from the calibration and, of course, the less sensitive instrument should also be recording this level of acceleration so that, by means of the calibration, the count level for the less sensitive instrument is established.

Future plans call for a computerized conversion of the data from counts to engineering units as well as for machine plotting of the data in engineering units.

The flight data most commonly used for dynamics analysis are the roll rate and the three accelerations. Typical examples of these functions (as well as the pitch rate) are shown in Figs. 7-5 to 7-8.

7.4 Data Processing

Further data processing depends upon a knowledge of the flight Mach number history. The flight Mach number could be calculated based on the longitudinal deceleration if the altitude were known; however, the altitude history generally is not available. The recourse, then,

is to determine the flight Mach number from a computer simulation. The results of the simulation must be checked against the flight data to ensure an adequate simulation of the reentry trajectory. The easiest check that can be made is a comparison of the longitudinal acceleration history as predicted by the simulation with the flight data results. The velocity history of the body is obtained by integrating the acceleration history. If the simulated longitudinal acceleration history is verified by the flight data, and the transverse accelerations are small enough that the longitudinal acceleration represents the total acceleration, then the simulated velocity history (hence Mach number history) will be correct. For the purpose of matching the simulation results to the flight acceleration, it is convenient to compare the results based on the time after the occurrence of the peak g. The time from peak g to impact is a good check on the calculated Mach number history.

If the acceleration from a nominal simulation does not agree with flight results, the factors in the flight that are not nominal (such as the aerodynamic asymmetries) must be included in the simulation in order to produce a match between the flight results and the simulation. Occasionally it is necessary to modify some of the aerodynamic coefficients in order to produce an acceptable match.

At points where the altitude is known (generally the only point is at impact) the Mach number may be calculated based on the following equations.

By definition of the axial force coefficient:

$$C_A \bar{q} S = A \tag{7-4}$$

or

$$\frac{C_A \bar{q} S}{W} = \frac{A}{W} = -g_X . \tag{7-5}$$

We may introduce the definition of dynamic pressure to give:

$$\frac{C_A(\gamma/2)PM^2S}{W} = -g_X \qquad (7\text{-}6)$$

so that

$$C_A M^2 = \frac{-g_X W}{(\gamma/2)PS} \quad . \qquad (7\text{-}7)$$

The axial force coefficient, C_A, is principally a function of Mach number (and also a slowly varying function of angle of attack and altitude). For a particular angle of attack and altitude, we can plot $C_A M^2$ versus Mach number based on predicted aerodynamic coefficients. We may then use flight data to calculate a value of $C_A M^2$ from Eq. (7-7), enter a plot of $C_A M^2$ versus Mach number, and determine the Mach number. As mentioned previously, this scheme can usually be applied only at the impact point since the altitude (which determines P and has some effect on C_A) is not known at other points along the trajectory.

With the Mach number history established by matching the simulation longitudinal acceleration to the flight results, the angle of attack may be computed as follows.

The maneuver acceleration is related to the transverse force by Newton's second law:

$$\frac{F}{W} = \bar{g} \qquad \text{where } \bar{g} = \sqrt{g_Z^2 + g_Y^2} \quad . \qquad (7\text{-}8)$$

Expressing the transverse force in terms of the normal force coefficient, we have:

$$\frac{C_{N_\alpha}\bar{\alpha}qS}{W} = \bar{g} \quad . \qquad (7\text{-}9)$$

From a similar development considering the longitudinal acceleration we have:

$$\frac{C_A \bar{q} S}{W} = -g_X \quad . \tag{7-10}$$

The above equations are combined to give:

$$\bar{\alpha} = \frac{\bar{g}}{-g_X} \frac{C_A}{C_{N_\alpha}} \tag{7-11}$$

The use of Eq. (7-11) with the flight values for the accelerations and the established (wind tunnel test, etc.) values for the aerodynamic coefficients permits determination of trim angle of attack as a function of time.

For routine flight test analysis, the envelopes of the normal and lateral accelerations are usually all that is extracted from the flight records, and the mean value of the envelope at a particular point in time is used to calculate the trim angle of attack. A sample work sheet that shows a convenient technique for calculating trim angle of attack is shown in Fig. 7-9.

An alternate technique for computing angle of attack is based on the rate gyro data. For small angles of attack:

$$\alpha = \frac{r + \dot{\beta}}{p} \tag{7-12}$$

$$\beta = \frac{q - \dot{\alpha}}{p} \tag{7-13}$$

$$\bar{\alpha} = \sqrt{\alpha^2 + \beta^2} \quad . \tag{7-14}$$

For the times of interest, $\dot{\alpha}$ and $\dot{\beta}$ are frequently negligible so that α and β may be obtained directly from rate gyro data. The significant advantage of this technique – that neither the Mach number history nor the

aerodynamic coefficients must be known – is obvious. The drawback is the required accuracy of the rate gyro data. Rate gyros have a tendency to drift so that the rates indicated may be somewhat in error. At low angles of attack in particular this bias may introduce a considerable error into results obtained with the above equation.

The trim maneuver plane (i.e., the plane of the transverse force acting on the body) is simply calculated from:

$$\psi = \tan^{-1} \frac{g_Z}{g_Y} \quad . \tag{7-15}$$

The aerodynamic frequency is computed from Eq. (4.4-36):

$$\omega_A = \sqrt{\frac{C_{N_\alpha} \Delta X \bar{q} S}{I_Y}} \quad \text{rad/sec} \; . \tag{7-16}$$

Note that C_{N_α} must be in "per radian" units. We may rewrite this expression in terms of the flight data by substituting for $\bar{q}S$ from Eq. (7-10):

$$\omega_A = \sqrt{\frac{-C_{N_\alpha}}{C_A} \frac{\Delta X g_X}{I_Y} w} \quad . \tag{7-17}$$

Flight values of g_X and the established values for the aerodynamic coefficients permit calculation of the aerodynamic frequency. A sample work sheet which describes a convenient format for calculating ω_A is shown in Fig. 7-10.

Depending upon the closeness of the aerodynamic frequency to the roll rate, the trim angle of attack may be amplified to a value different from the result that would be attained by a nonrolling body, as has been discussed in

Section 4.5. For some purposes in reentry flight analysis, it is convenient to have a knowledge of the amplification factor. A sample work sheet that indicates the data necessary to calculate the amplification factor is shown in Fig. 7-11. The ratio of roll rate to aerodynamic frequency also affects the direction of the trim transverse force. A technique for calculating the change in direction of this force $\Delta\psi$ is described in Fig. 7-12.

7.5 Data Analysis

A convenient technique for demonstrating the closeness of the reentry body to resonance is to plot both the roll rate and the aerodynamic frequency as a function of time on the same graph. As discussed in Section 4.5, when the roll rate is close to the aerodynamic frequency, the body is near resonance. Near resonance the previously mentioned amplification factors may be large, and large values of trim angle of attack may develop. It is possible that the large transverse forces associated with resonance (in combination with a center of pressure/center of gravity offset) may cause the roll rate to follow the aerodynamic frequency. This effect, known as "roll lock-in," may be easily detected from the plot of roll rate and aerodynamic frequency versus time.

Roll lock-in is usually considered to be an undesirable phenomenon because of the large lateral loads, localized heating, and high roll rate associated with it (which may be sufficient to cause structural damage and which will cause some impact dispersion due to the abnormally high drag encountered).

Of course, the roll rate may vary so that the rate reaches zero (a condition that usually leads to large impact dispersion), and the aforementioned plot of roll rate versus aerodynamic frequency displays this condition also.

A technique for estimating the dispersion that results when a reentry body spins through zero roll rate

is described in Ref. 7-1. The semimajor axis of the dispersion ellipse can be estimated from:

$$a = \frac{59.1}{\sin^2 \gamma_o} \left(\frac{h_o}{V_o}\right) \frac{\bar{g}_o}{\sqrt{-\dot{p}_o}} \qquad \text{feet} \qquad (7\text{-}18)$$

and the semiminor axis is:

$$b = -a \sin \gamma \qquad \text{feet} .$$

If a simulation for the basic trajectory is available, γ_o, h_o, and V_o are obtained for the time when the flight record indicates zero roll rate. (However, it usually is not necessary to simulate the roll or transverse acceleration behavior in this simulation.) Values of $\bar{g}_o$ and $\dot{p}_o$ are obtained directly from the telemetry records. If a simulation is not available, γ_o, h_o and V_o may be estimated as follows:

1. Assume $\gamma_o = \gamma_E$.
2. Compute $K_o = \dfrac{-P_o}{\beta \sin \gamma_o}$ at the time of $p = 0$ using Eq. (4.3-22) and the g_X telemetry trace.
3. For $\gamma_o = \gamma_E$ and $\beta = \dfrac{W}{C_A S}$, compute P_o and thus h_o.
4. Compute V_o using Eq. (4.3-5).

REFERENCE

7-1 B. F. Fuess, "Impact Dispersion Due to Mass and Aerodynamic Asymmetries," J. Spacecraft and Rockets, Vol. 2, No. 10, October 1967, pp. 1402-1403.

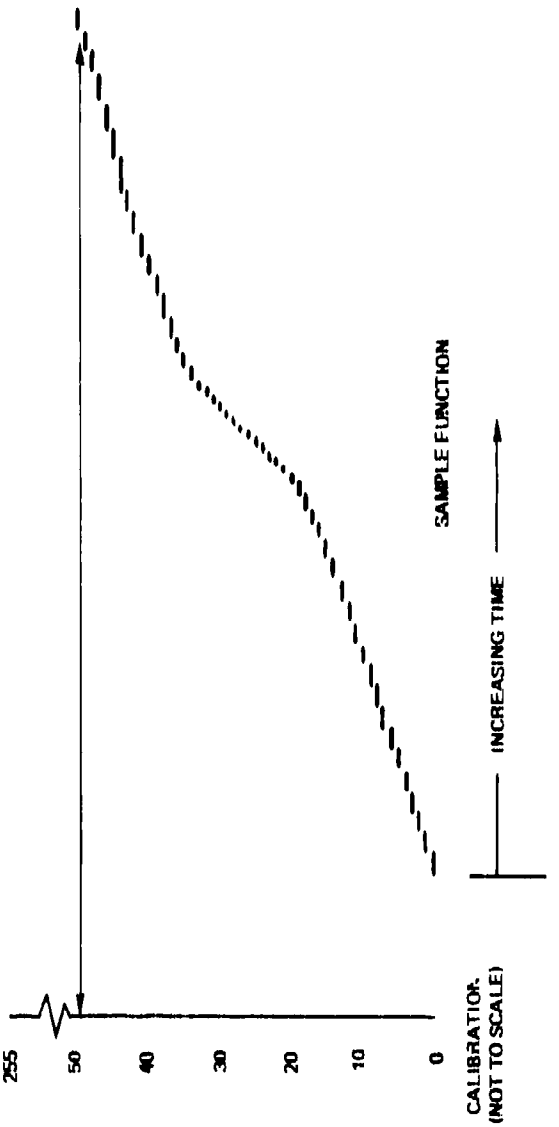

AT ANY POINT IN TIME, THE TOTAL COUNT MAY BE DETERMINED FROM A CALIBRATION SUCH AS THE ONE ON THE LEFT, OR BY COUNTING THE DISCRETE STEPS OF THE FUNCTION. IN THIS EXAMPLE, AS TIME INCREASES, THE NUMBER OF COUNTS (BITS) INCREASES FROM ZERO TO 50.

Fig. 7-1 BIT PRESENTATION SCHEME, DITAP FLIGHT RECORDS

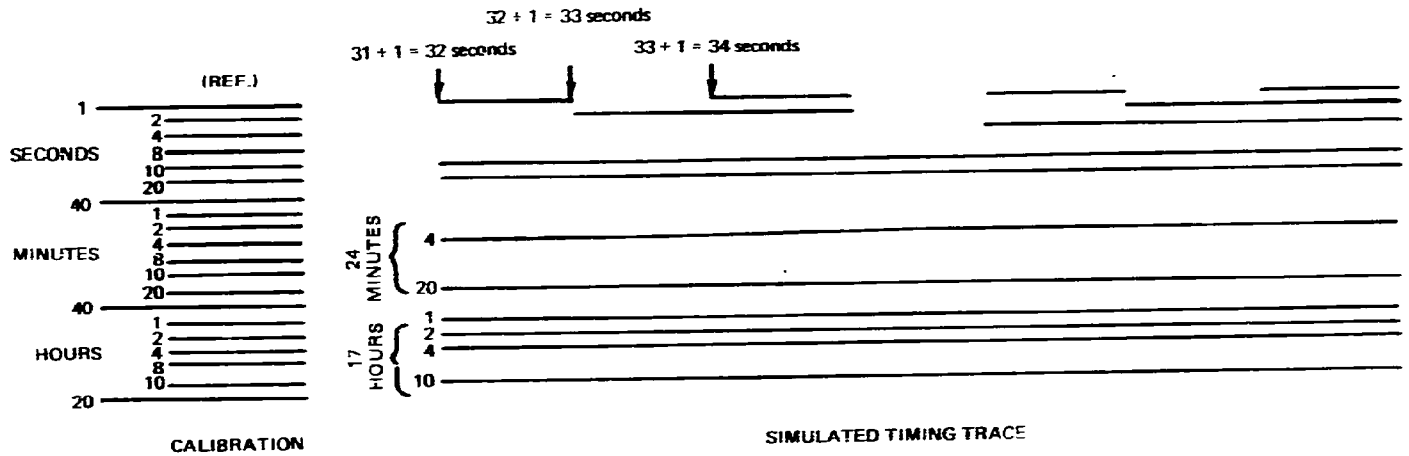

THE TIMING TRACES HAVE THE POTENTIAL VALUES INDICATED BY THE CALIBRATION ON THE LEFT. A MARK INDICATES A "ONE" AND A BLANK INDICATES A "ZERO". TO READ TIME, THE "ONE" PULSES ARE SUMMED, AND THE GREENWICH MEAN TIME IS THEN 1 SECOND PLUS THE SUM. SEE EXAMPLE ABOVE.

Fig. 7-2 TIMING TRACES, DITAP FLIGHT RECORDS

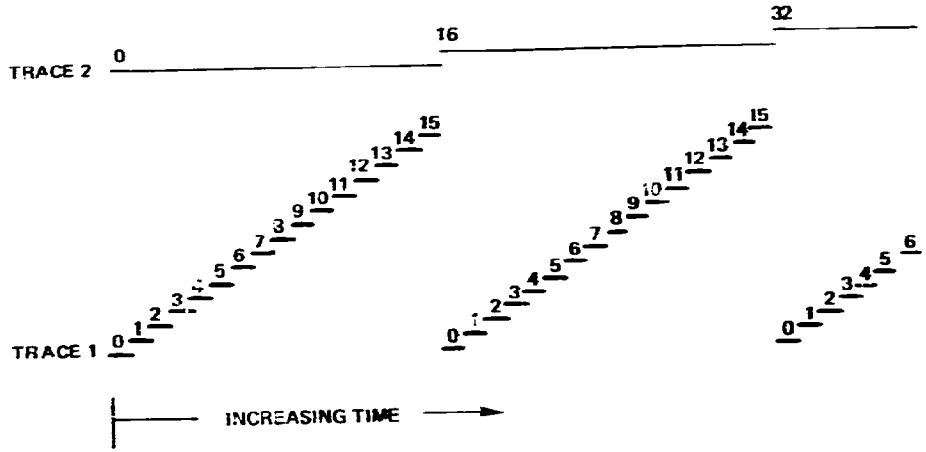

AT ANY POINT IN TIME, THE TOTAL COUNT IS THE SUM OF THE COUNTS FROM THE TWO TRACES. IN THIS EXAMPLE, AS TIME INCREASES THE NUMBER OF COUNTS (BITS) INCREASES FROM ZERO TO 38.

Fig. 7-3 BIT PRESENTATION SCHEME, DITAR FLIGHT RECORDS

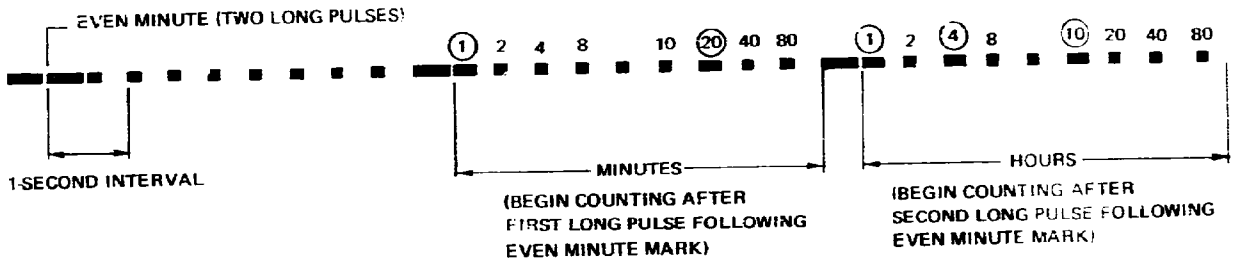

THE TIMING PULSES HAVE THE POTENTIAL VALUES INDICATED ABOVE. A DOUBLE WIDTH PULSE INDICATES A "ONE" AND A NOMINAL WIDTH PULSE INDICATES A "ZERO". TO READ TIME, THE "ONE" PULSES SHOULD BE SUMMED. IN THE EXAMPLE ABOVE, THE GREENWICH MEAN TIME AT THE EVEN MINUTE MARK IS 15:21:00.

Fig. 7-4 TIMING TRACES, DITAR FLIGHT RECORDS

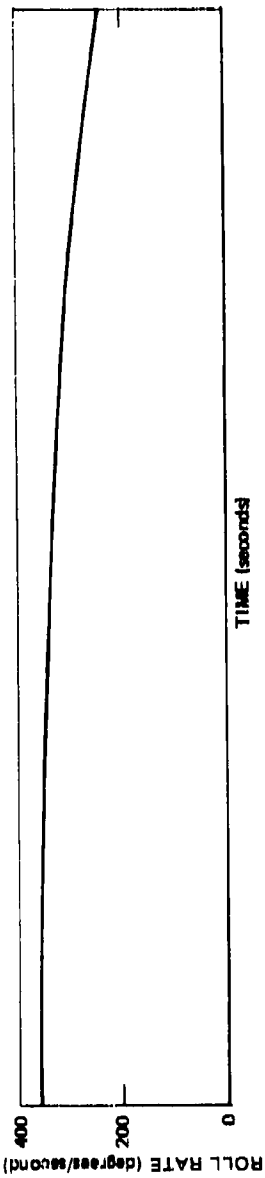

Fig. 7-5 SAMPLE ROLL RATE HISTORY

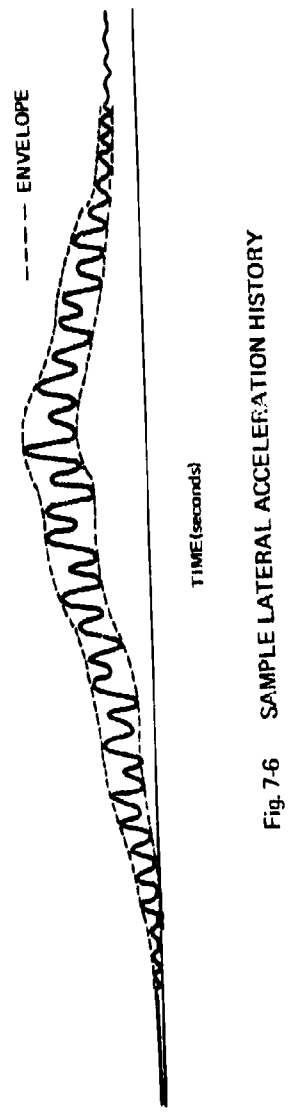

Fig. 7-6 SAMPLE LATERAL ACCELERATION HISTORY

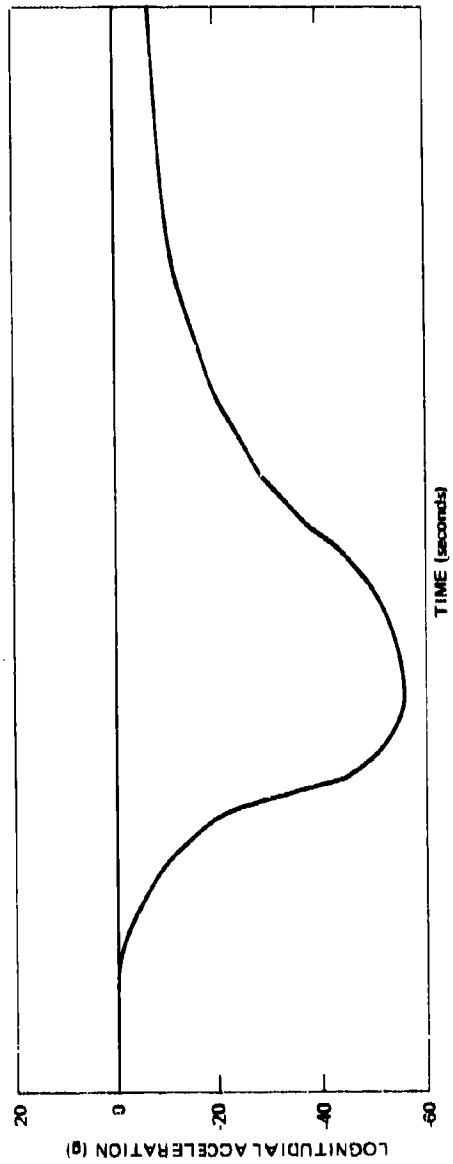

Fig. 7-7 SAMPLE LONGITUDINAL ACCELERATION HISTORY

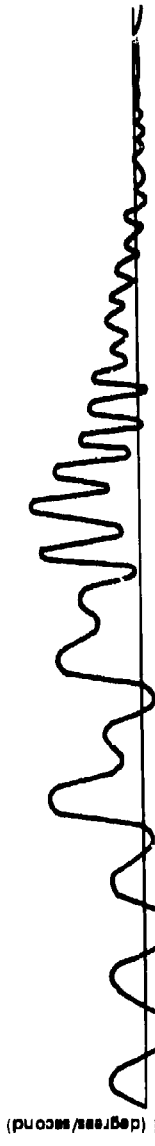

Fig. 7-8 SAMPLE PITCH RATE HISTORY

(13)	$\bar{\alpha} = \frac{(9)}{(12)}$	IMPROVED VALUE FOR ANGLE OF ATTACK
(12)	C_{N_α}	NEW VALUE FOR NORMAL FORCE COEFFICIENT SLOPE, REQUIRED IF ESTIMATE OF ANGLE OF ATTACK IN (10) WAS NOT ACCURATE
(11)	$\bar{\alpha} = \frac{(9)}{(10)}$	ANGLE OF ATTACK (DEGREES)
(10)	C_{N_α}	NORMAL FORCE COEFFICIENT SLOPE FROM LISTING OF AERO DYNAMIC CHARACTERISTICS (PER DEGREE) ESTIMATE OF ANGLE OF ATTACK REQUIRED
(9)	$C_N = (6) \times (8)$	NORMAL FORCE COEFFICIENT CALCULATED FROM FLIGHT DATA (DIMENSIONLESS)
(8)	C_A	AXIAL FORCE COEFFICIENT FROM LISTING OF AERODYNAMIC CHARACTERISTICS (DIMENSIONLESS)
(7)	MACH NUMBER	OBTAINED FROM COMPUTER SIMULATION. USE TIME OF PEAK LONGITUDINAL DECELERATION TO MATCH FLIGHT DATA TO SIMULATION (DIMENSIONLESS)
(6)	$\frac{(4)}{(5)}$	
(5)	g_X	LONGITUDINAL DECELERATION (g)
(4)	$\sqrt{(2)^2 + (3)^2}$	
(3)	g_Z	NORMAL ACCELERATION (g)
(2)	g_Y	LATERAL ACCELERATION (g)
(1)	TIME BEFORE IMPACT	

$$\bar{\alpha} = \frac{\sqrt{g_Y^2 + g_Z^2}}{-g_X} \frac{C_A}{C_{N_\alpha}} \text{ (degrees)}$$

Fig. 7-9 ANGLE OF ATTACK WORK SHEET

(14)	(12) × (13) ω_A	AERODYNAMIC FREQUENCY (DEGREES/SECOND)
(13)	K′	$K' = 57.3\sqrt{\frac{57.3W}{12 I_Y}}$
(12)	$\sqrt{(11)}$	
(11)	(10) × (7)	
(10)	(8) − (9)	
(9)	$X_{c.g.}$	CENTER OF GRAVITY OBTAINED FROM PREFLIGHT DATA (INCHES)
(8)	$X_{c.p.}$	CENTER OF PRESSURE OBTAINED FROM LISTING OF AERODYNAMIC CHARACTERISTICS (INCHES)
(7)	(6) × (3)	
(6)	(4) ÷ (5)	
(5)	C_A	AXIAL FORCE COEFFICIENT OBTAINED FROM LISTING OF AERODYNAMIC CHARACTERISTICS (DIMENSIONLESS)
(4)	C_{N_α}	NORMAL FORCE COEFFICIENT SLOPE OBTAINED FROM LISTING OF AERODYNAMIC CHARACTERISTICS (PER DEGREE)
(3)	g_X	FLIGHT TEST. LONGITUDINAL DECELERATION (g)
(2)	MACH NUMBER	OBTAINED FROM COMPUTER SIMULATION. USE TIME OF PEAK LONGITUDINAL DECELERATION TO MATCH FLIGHT DATA TO SIMULATION (DIMENSIONLESS)
(1)	TIME BEFORE IMPACT	

$$\omega_A = 57.3\sqrt{\frac{W}{I_Y}\frac{57.3}{12}}\sqrt{\frac{C_{N_\alpha}}{C_A}(X_{c.p.} - X_{c.g.})(g_X)}$$

Fig. 7-10 AERODYNAMIC PITCH FREQUENCY (WEATHERCOCK FREQUENCY) WORK SHEET

(21)	$A = \frac{1}{\sqrt{(20)}}$	AMPLIFICATION FACTOR
(20)	(18) + (19)	
(19)	$(17)^2$ (8)	
(18)	$[1 - (8)]^2$	
(17)	$D = \frac{(11)(16)}{(6)\sqrt{1 - \frac{I_X}{I_Y}}}$	
(16)	(13) − (15)	
(15)	(14) $\frac{d^2}{I_Y}$	
(14)	C_{m_q}	PITCH DAMPING COEFFICIENT OBTAINED FROM LISTING OF AERODYNAMIC CHARACTERISTICS (DIMENSIONLESS)
(13)	$\frac{(12)}{m}(1 - \frac{I_X}{I_Y})$	
(12)	C_{N_α}	NORMAL FORCE COEFFICIENT SLOPE OBTAINED FROM LISTING OF AERODYNAMIC CHARACTERISTICS (PER RADIAN)
(11)	$\frac{(10)\,W}{(3)(9)}$	
(10)	$-g_X$	LONGITUDINAL DECELERATION FROM FLIGHT DATA (g)
(9)	C_A	AXIAL FORCE COEFFICIENT OBTAINED FROM LISTING OF AERODYNAMIC CHARACTERISTICS (DIMENSIONLESS)
(8)	$\lambda^2 = \frac{(5)}{(7)}$	
(7)	$(6)^2$	
(6)	AERODYNAMIC FREQUENCY	OBTAINED FROM PREVIOUS CALCULATION
(5)	$(4)^2 (1 - \frac{I_X}{I_Y})$	I_X (ROLL INERTIA) AND I_Y (PITCH INERTIA) OBTAINED FROM PREFLIGHT DATA (degrees/second)
(4)	ROLL RATE	FLIGHT DATA (degrees/second)
(3)	VELOCITY	OBTAINED FROM COMPUTER SIMULATION (feet/second)
(2)	MACH NUMBER	OBTAINED FROM COMPUTER SIMULATION, TIME OF PEAK LONGITUDINAL DECELERATION TO MATCH FLIGHT DATA TO SIMULATION (DIMENSIONLESS)
(1)	TIME BEFORE IMPACT	

$$A = \frac{1}{\sqrt{(1-\lambda^2)^2 + D^2\lambda^2}} \qquad \lambda^2 \approx \frac{p^2}{\omega_A{}^2}\left(1 - \frac{I_X}{I_Y}\right) \qquad D = \frac{(-g_X)W}{VC_A} \cdot \frac{\left[\frac{C_{N_\alpha}}{m}\left(1 - \frac{I_X}{I_Y}\right) - \frac{C_{m_q}d^2}{I_Y}\right]}{\omega_A\sqrt{1 - \frac{I_X}{I_Y}}}$$

Fig. 7-11 AMPLIFICATION FACTOR WORK SHEET

(7)	$\triangle\psi$	SET SIGN OF $\triangle\psi$ TO BE OPPOSITE TO THAT OF THE ROLL RATE
(6)	$\lvert\triangle\psi\rvert$	= SIN^{-1} (5)
(5)	SIN $\triangle\psi$	= (2)(3)(4)
(4)	A	= (COL. (21) FIG. 7-11)
(3)	λ	= (VCOL. (8) FIG. 7-11)
(2)	D	= (COL (17) FIG. 7-11)
(1)	TIME BEFORE IMPACT	

SIN $\triangle\psi$ = - | $\pm$D λ | A

Fig. 7-12 ROTATION OF MANEUVER PLANE WORK SHEET

8. CONSTANTS AND CONVERSION EQUATIONS

Conversion Equations

Degrees Centigrade = $\frac{5}{9}$ (degrees Fahrenheit - 32)

Degrees Rankine = degrees Fahrenheit + 460

Degrees Kelvin = degrees Centigrade + 273

Time (in hours) at zero meridian = local time (in hours) + $\frac{\text{local longitude (in degrees)}}{15}$

where

West longitude is positive

East longitude is negative

Conversion Constants

1 radian = 57.3°

1 meter = 3.28 feet

1 nmi = 6080 feet

1 gram/cubic centimeter = 1.94 slugs/ft^3

1 kilogram/cubic meter = 1.94×10^{-3} slugs/ft^3

1 millibar = 2.09 lb/ft^2

1 knot = 1.69 ft/sec

Constants

Acceleration of gravity at sea level = $g = 32.17$ ft/sec^2

Ratio of specific heats = $\gamma = 1.4$

Gas constant for dry air = 1716 ft^2/sec^2 - degrees Rankine

Gas constant for water vapor = 2759 ft^2/sec^2 - degrees Rankine

Radius of earth = R_e = 3441 nmi = 2.09×10^7 feet

Rotational velocity of earth = $\omega_e = 0.729 \times 10^{-4}$ rad/sec

Napierian base = $e = 2.718$

$\pi = 3.142$

INDEX

A

B

W